STRENGTHENING OF PRESTRESSED CONCRETE BEAMS USING COMBINED EXTERNALLY BONDED AND PRESTRESSED NEAR SURFACE MOUNTED TECHNIQUE

M. OBAYDULLAH

FACULTY OF ENGINEERING
UNIVERSITY OF MALAYA
KUALA LUMPUR

2020

STRENGTHENING OF PRESTRESSED CONCRETE BEAMS USING COMBINED EXTERNALLY BONDED AND PRESTRESSED NEAR SURFACE MOUNTED TECHNIQUE

M. OBAYDULLAH

THESIS SUBMITTED IN FULFILMENT OF THE REQUIREMENTS FOR THE DEGREE OF DOCTOR OF PHILOSOPHY

FACULTY OF ENGINEERING
UNIVERSITY OF MALAYA
KUALA LUMPUR

2020

UNIVERSITY OF MALAYA

ORIGINAL LITERARY WORK DECLARATION

Name of Candidate: M. OBAYDULLAH

Matric No: KHA120104

Name of Degree: Doctor of Philosophy

Title of Thesis: STRENGTHENING OF PRESTRESSED CONCRETE BEAMS USING COMBINED EXTERNALLY BONDED AND PRESTRESSED NEAR SURFACE MOUNTED TECHNIQUE

Field of Study: Structural Engineering and Materials

I do solemnly and sincerely declare that:

(1) I am the sole author/writer of this Work;
(2) This Work is original;
(3) Any use of any work in which copyright exists was done by way of fair dealing and for permitted purposes and any excerpt or extract from, or reference to or reproduction of any copyright work has been disclosed expressly and sufficiently and the title of the Work and its authorship have been acknowledged in this Work;
(4) I do not have any actual knowledge nor do I ought reasonably to know that the making of this work constitutes an infringement of any copyright work;
(5) I hereby assign all and every rights in the copyright to this Work to the University of Malaya ("UM"), who henceforth shall be owner of the copyright in this Work and that any reproduction or use in any form or by any means whatsoever is prohibited without the written consent of UM having been first had and obtained;
(6) I am fully aware that if in the course of making this Work I have infringed any copyright whether intentionally or otherwise, I may be subject to legal action or any other action as may be determined by UM.

Candidate's Signature Date:

Subscribed and solemnly declared before,

Witness's Signature Date:

Name:

Designation:

ABSTRACT

Prestressed concrete beams are now widely used in the construction field. However, there is a lack of studies on the strengthening of prestressed beams. Externally bonded reinforcement (EBR) and near surface mounted (NSM) strengthening have been used to a certain extent to strengthen prestressed beams. However, EBR is prone to premature debonding failure, while NSM reduces but does not completely eliminate premature debonding. Prestressed NSM (PNSM) strengthening is new area of research. In this research work the possibility of using both steel strands and CFRP bars with PNSM strengthening is investigated. A new strengthening technique, the combined EBR with prestressed NSM (CEBPNSM) technique is also proposed in this research work to overcome the limitations of EBR and NSM.

In this study, a total of thirty two prestressed beams were strengthened in order to investigate the structural performance of steel strands and CFRP bars as PNSM reinforcement, as well as the performance of the newly proposed CEBPNSM technique. The beam specimens were divided into six groups according to the type of strengthening conducted on the beams. The first group was strengthened with NSM CFRP bars. The second group was strengthened with NSM steel strands. The third group was strengthened with NSM CFRP bars and EBR CFRP sheet. The fourth group was strengthened with NSM steel strands and EBR CFRP sheet. The fifth group was strengthened with NSM CFRP bars and EBR CFRP plate. The sixth group was strengthened with NSM steel strands and EBR CFRP plate.

The prestress levels in the PNSM and CEBPNSM strengthened beams were also varied from 30% to 70% of the tensile capacity of the NSM strengthening materials to study the effect on the prestressed beam.

A numerical model was also developed using finite element modeling (FEM) to simulate the structural behavior of the strengthened beams and validate the experimental results.

The results of this study showed that both steel strands and CFRP bars were effective as PNSM reinforcement, although steel strands displayed better ductility and serviceability. This study also found that the CEBPNSM strengthening technique improved the structural performance of the prestressed beam significantly more than other strengthening techniques. The ultimate capacity of the CEBPNSM strengthened beams increased by 67% to 81%, depending on variations in the strengthening materials and prestress levels. The serviceability, deflection, and failure mode of the CEBPNSM beams also improved considerably. Increasing the prestress level in the PNSM and CEBPNSM strengthened beams resulted in corresponding increases in flexural performance and load capacity, especially at the service stage. The highest level of prestress (70%) provided the greatest enhancement in flexural performance. The load deflection behavior and damage patterns generated by the FEM model were compared with the experimental results and found to be in good agreement.

ABSTRAK

Rasuk konkrit prategasan digunakan secara meluas di dalam sektor pembinaan. Walau bagaimanapun, kajian mengenai kekuatan unsur struktur prategasan sangat minimal. Teknik pengukuhan Ikatan Luaran (EBR) dan kekuatan teknik pemasangan berhampiran permukaan digunakan pada tahap tertentu untuk menguatkan rasuk konkrit rategasan. Walau bagaimanapun, EBR terdedah kepada kegagalan nyahikatan pramatang dimana pengukuhan NSM akan mengurangkan tetapi tidak akan menghilangkan nyahikatan pramaatang sepenuhnya. Pengukuhan NSM (PNSM) adalah bidang penyelidikan baru yang sedang diperkembangkan. Prategasan CFRP sebagai tetulang NSM telah dijumpai untuk meningkatkan prestasi lenturan. Teknik penguatan baru,antara gabungan EBR dan prategasan NSM (CEBPNSM), dicadangkan untuk mengatasi keterbatasan EBR dan NSM.

Dalam kajian ini, sebanyak tiga puluh dua rasuk prategasan telah diperkuatkan untuk menguji prestasi struktur teknik CEBPNSM, serta prestasi helaian keluli prategasan sebagai tetulang NSM. Bongkah spesimen dibahagikan kepada enam kumpulan mengikut jenis penguatan yang dilakukan pada rasuk. Kumpulan pertama diperkukuhkan dengan bar NSM CFRP. Kumpulan kedua diperkukuh dengan helaian keluli NSM. Kumpulan ketiga diperkukuhkan dengan bar NSM CFRP dan lembaran EBR CFRP. Kumpulan keempat diperkukuhkan dengan helai keluli NSM dan lembaran EBR CFRP. Kumpulan kelima diperkuat dengan bar NSM CFRP dan plat EBR CFRP. Kumpulan keenam diperkukuh dengan lembaran keluli NSM dan plat EBR CFRP. Tahap prategasan dalam tetulang NSM telah berubah dari 30% hingga 70% dari kemampuan tegangan bahan penguat NSM.

Model numerik telah dibangunkan menggunakan kaedah unsur terhingga (FEM) untuk mensimulasikan tingkah laku struktur rasuk yang diperkukuhkan dan mengesahkan keputusan ujikaji.

Keputusan kajian ini mendapati bahawa teknik pengukuhan CEBPNSM dapat meningkatkan prestasi struktur dengan ketara daripada teknik penguatan yang lain. Kapasiti utama CEBPNSM menguatkan rasuk meningkat sebanyak 67% hingga 81%, bergantung kepada variasi dalam bahan pengukuhan dan tahap prategasan. Kebolehfungsian, pesongan, dan mod kegagalan rasuk CEBPNSM juga bertambah baik. Peningkatkan tahap prestress dalam pengukuhan NSM menghasilkan kenaikan dalam prestasi lenturan dan kapasiti beban, terutamanya pada peringkat perkhidmatan. Tahap prategasan tertinggi (70%) memberikan peningkatan yang paling besar dalam prestasi lenturan. Tingkah laku pesongan beban dan corak kerosakan yang dijana oleh model FEM dibandingkan dengan hasil eksperimen dan didapati ianya bersesuaian.

ACKNOWLEDGEMENTS

In the Name of Allah, The Beneficent, The Merciful, I would like to express my utmost gratitude and thanks to the Almighty Allah (s.w.t) for the help and guidance that he has given me through all these years. May Allah bless His Beloved Prophet Muhammad (p. b. u. h.) with the best of blessings, for he is the best model for every aspect of human life.

I would like to express my sincere appreciation and gratitude to my supervisors, Professor Ir. Dr. Mohd Zamin Jumaat and Associate Professor Dr. Johnson Alengaram for their excellent supervision, guidance, encouragement and financial support in carrying out this research work. I am deeply indebted to them.

My sincere and great appreciation goes to University Malaya High Impact Research Grant under Grant Account No: UMC/HIR/MOHE/ENG/36 (D000036-160001) for funding this research work.

I would also like to thank all of the post graduate students of UM for their help, support, and encouragement, and for standing beside me like family throughout the whole course of this research.

TABLE OF CONTENTS

LIST OF FIGURES

LIST OF TABLES

LIST OF ABBREVIATIONS

ACI	:	American Concrete Institute
CEBNSM	:	Combined Externally Bonded and Near Surface Mounted
CEBPNSM	:	Combined Externally Bonded and Prestressed Near Surface Mounted
CFRP	:	Carbon Fiber Reinforced Polymer
C	:	CFRP bar
EBR	:	External Bonded Reinforcement
F	:	Prestressed Force
FEA	:	Finite Element Analysis
FEM	:	Finite Element Modeling
FRP	:	Fiber Reinforced Polymer
LVDT	:	Linear Variable Displacement Transducer
NSM	:	Near Surface Mounting
PNSM	:	Prestressed Near Surface Mounting
PC	:	Prestressed Concrete
Pl	:	EBR CFRP Plate
RC	:	Reinforced Concrete
S	:	Steel strand
Sh	:	EBR CFRP Sheet

CHAPTER 1: INTRODUCTION

1.1 Background

Prestressed concrete has been widely used all over the world since the 1950s, especially in long span bridges. Due to damage, aging, and higher volumes of usage, these prestressed concrete structures often require extensive rehabilitation, including strengthening, at some point in their life cycle to continue being used safely. To extend the serviceability of these structures through rehabilitation is a more economical, efficient and sustainable solution than constructing new structures. The importance of this study lies in the necessity to find new and more efficient and effective ways to improve the structural performance of these existing structures. Strengthening of members is one form of rehabilitation and thus exploring more efficient methods of strengthening is an important field of research (Toutanji et al., 2006).

Various materials and techniques have been developed over the last few decades for strengthening structural members. Steel and carbon fiber reinforced polymer (CFRP) bars, plates and sheets are the most frequently used strengthening materials. The two most common strengthening techniques used for structural strengthening are the externally bonded reinforcement (EBR) technique and the near surface mounted (NSM) technique. Prestressing of strengthening materials is another strengthening technique that is used in conjunction with other strengthening techniques, such as EBR and NSM.

1.2 Problem Statement

The EBR strengthening technique bonds strengthening materials, such as steel or CFRP plates, to the external faces of structures to achieve the desired strengthening effect. However, major disadvantages of EBR strengthening are environmental damage and the likelihood of failure due to premature debonding. Premature debonding in EBR strengthening is mainly due to the high interfacial shear stresses between the strengthening material and the concrete substrate at the end points of the strengthening material. Researchers have found that the thickness of the strengthening material is a major factor in controlling debonding behavior (Lousdad et al., 2010). Various researchers have proposed different measures to counter the debonding problem of EBR strengthening, such as using softer adhesives or stiffer strengthening materials (Al-Emrani et al., 2007, Haghani et al., 2008 and Bouchikhi et al., 2010), and using adhesive fillets or tapering the ends of the strengthening material (Tsai & Morton, 1995). Many studies have found that the design strains in the strengthening material are inversely proportional to the thickness of the strengthening material. Reduced thickness decreases stress concentrations at the ends of the strengthening material (Garden et al., 1997; Oehlers, 1992; Ziraba et al., 1994; Hassanen and Raoof, 2001; Lu et al., 2007; Maruyama & Ueda, 2001; Shehata et al., 2001; Teng et al., 2003). Reducing the thickness of the EBR strengthening material is thus an effective method to reduce debonding failure.

The NSM technique was developed to overcome the disadvantages of EBR strengthening. The NSM strengthening technique inserts and bonds reinforcing material, such as steel or CFRP bars, into grooves cut into the concrete cover. NSM strengthening reduces premature debonding problems and environmental damage, and also improves the composite action of the strengthened member compared to EBR (De Lorenzis et al., 2002; De Lorenzis and Teng, 2007; El-Hacha and Rizkalla, 2004; Rosenboom and Rizkalla, 2006; Teng et al., 2003; Coelho et al., 2015; Hollaway, 2010; Asplund, 1949). Current research has focused on the use of CFRP materials with the NSM technique to strengthen structures. Various studies have found that the flexural strength and performance of NSM strengthened members were significantly enhanced, although debonding was not completely eliminated (Jung et al., 2005; Al-Mahmoud et al., 2009; Bilotta et al., 2015; Sharaky et al., 2015). A major disadvantage of NSM strengthening is that strengthening is often limited by the lack of necessary space due to the limited width of the beam to be strengthened. The width of the beam may be insufficient for the necessary edge clearance and clear spacing between adjacent NSM grooves (De Lorenzis, 2002; Blaschko, 2003; Parretti and Nanni, 2004).

Recently, a strengthening technique which combines the EBR and NSM techniques has been investigated by a few researchers (Darain, 2016; Rahman, 2016; Amarasinghe and Gamage, 2015; Traplsi, 2013; Lim, 2009). This combined EBR and NSM technique is advantageous as it allows the required amount of strengthening reinforcement to be shared between the two systems, reducing the thickness of the EBR strengthening material, as well as reducing the size and number of NSM reinforcements, compared to if each technique had been used on its own. The reduced thickness of the EBR strengthening material will consequently reduce the stress concentration at the ends of the bonded material, improving bond behavior and reducing the likelihood of premature debonding failure. The reduced size and number of NSM reinforcements can reduce the size of the required groove, allowing for sufficient space for edge clearance and groove clear spacing. Furthermore, the NSM groove itself improves overall bond performance due to the additional adhesive used in the groove and the increase in contact surface area between the strengthening materials and the concrete substrate. Stress is equivalent to load divided by the corresponding surface area, thus an increase in surface area will decrease stress, reducing the possibility of debonding failure. This new combined technique takes into consideration the limitations of both the EBR and the NSM techniques and by combining them, the two techniques complement each other and reciprocally reduce each other’s limitations. Rahman (2016) investigated this combined technique using steel bars, steel plates, CFRP plates and CFRP fabric to strengthen RC beams. Darain (2016) used steel bars, CFRP bars, CFRP strips and CFRP fabric to strengthen RC beams using this combined technique. Both studies found that flexural strength and serviceability were improved and debonding behavior was reduced.

Another strengthening technique that has developed over the last few decades is prestressed strengthening. Prestressed strengthening improves the flexural behavior of structural members under service loads especially in bridges and beams with long spans where serviceability and deflection need improvement (El-Hacha and Soudki, 2013). Externally post-tensioned steel strands attached to the sides of beams are one form of prestressed strengthening that has been in use for many years. Prestressed strengthening provides an active rather than passive strengthening system. Prestress forces are transferred from the prestressed strengthening material to the structural member, producing compressive and tensile stresses in the beam, which actively oppose the effects of loading (El-Hacha et al., 2001; Casadei et al., 2006). Prestressed strengthening systems can provide various advantages to strengthened structures such as improved serviceability; reduced deflections, crack widths and internal steel reinforcement strains; delayed initiation of cracking; compressive stresses that resist fatigue failure and oppose dead and live loads; increase of yield load to a higher portion of ultimate capacity; increased live load capacity, shear capacity and fatigue strength; replacement of prestress forces that have been lost; and more efficient use of concrete and strengthening material (El-Hacha et al., 2001).

Prestressed NSM (PNSM) strengthening is a relatively newer practice and area of research. A number of studies investigating the use of prestressed NSM CFRP to strengthen RC beams have found improved flexural behavior at service and ultimate conditions, including higher first crack load, yield load, and ultimate load; and smaller midpoint deflection and crack widths. However, the ductility of the strengthened beams was reduced with increasing prestress force leading to brittle failure at smaller deflections. The reduction in ductility was due to the prestressing of the CFRP, which caused a large portion of the strain capacity of the CFRP to be used. Failure in the strengthened beams occurred mostly by rupture of the CFRP and the deformability of the beams was greatly reduced (Badawi and Soudki, 2009; Nordin and Taljsten, 2006; Peng et al., 2014; El-Hacha and Gaafar, 2011; Badawi and Soudki, 2006; Choi et al., 2010; Oudah and El-Hacha, 2013; Aslam and Jumaat, 2015). El-Hacha and Soudki (2013) concluded that prestressed NSM CFRP strengthening led to less energy dissipation and increased tension reinforcement ratio, which both reduced ductility. Bond behavior and concrete tensile strength also influence ductility, according to Peng et al. (2014). Choi et al. (2010) found that prestressed NSM CFRP strengthening reduced deformability with increasing prestressing level. Casadei et al. (2006) who used prestressed NSM CFRP to strengthen a pre-damaged prestressed concrete I-girder in a pilot research project found that prestressed NSM CFRP strengthening performed better than EBR CFRP.

Ductility is the ratio of deflection at ultimate load to deflection at yield load while deformability is the ratio of deflection at complete failure to deflection at yield load (El-Hacha and Soudki, 2013). Greater deformability is beneficial as there is a gradual progression towards complete failure rather than the sudden failure of structures with low deformability, which can be catastrophic. The gradual progression towards complete failure that structures with high deformability display, allows such structures to exhibit warning signs of imminent total failure such as widening crack widths and greater deflection (Choi et al. 2010). Thus, deformability is an important safety factor as sudden catastrophic failure can lead to excessive damage and loss of life. A major limitation of CFRP strengthening materials is their low ductility due to the linear elastic strain properties of CFRP. After reaching ultimate capacity, CFRP materials have almost no ductility, which results in brittle failure modes where the structural member falls back on the residual steel reinforcement. Furthermore, prestressing of CFRP materials results in a pre-strain in the materials, which further reduces their ductility (Peng et al. 2014).

1.3 Scope

This study will investigate the use of prestressed steel strands as a viable alternative to CFRP for NSM strengthening reinforcement. Compared to CFRP, steel materials have superior ductility due to the elastoplastic nature of steel. This allows steel reinforced structures to fail in a gradual manner after maximum loading. This characteristic of steel is one of the reasons why steel is widely used for construction purposes. Reinforced concrete and prestressed concrete both use steel for internal reinforcement in the form of steel reinforcement bars and steel prestressing strands. Steel has also been used as a strengthening material in the form of externally bonded reinforcement, externally post-tensioned reinforcement, as well as internally bonded as NSM reinforcement. Beams strengthened with steel display high deformability which is highly advantageous in real life situations as it allows catastrophic failure to be easily avoided. Steel is also readily available, economical, and has better bonding performance compared to CFRP (De Lorenzis et al., 2002; Darain et al., 2015; Hosen et al., 2014). The main disadvantage of steel is its tendency to corrode over time. Steel corrosion occurs mainly due to exposure. However, with adequate cover and proper maintenance, steel does have long term durability. In the NSM technique, steel bars used as NSM reinforcement are protected from exposure by the epoxy-filled groove in which the steel is embedded. Epoxy has superior properties that allow the required cover for the NSM steel to be reduced. The satisfactory performance of this epoxy cover can be seen from the few studies that have been done using NSM steel. Darain et al. (2015) studied the flexural performance of RC beams strengthened with NSM CFRP and NSM steel. The study found that although the ultimate strength capacity of the NSM steel strengthened beams was less than the NSM CFRP strengthened beams, the NSM steel displayed better bonding capacity and ductile behavior, which eventually prevented premature failure in the NSM steel strengthened beams, unlike the beams strengthened with NSM CFRP. Hosen et al. (2016) had similar findings in his study on NSM steel and NSM CFRP as flexural reinforcement placed on the sides of the RC beam specimens, concluding that NSM steel was more effective in terms of ductility. There has been limited research on the use of prestressed steel as NSM reinforcement. Zhang et al. (2011) investigated the use of prestressed helical ribbed steel wire as NSM reinforcement on RC beams and found that the prestressed NSM steel effectively delayed the development of cracks, reduced deformation, and increased stiffness.

In this study, strengthening will be conducted on prestressed concrete (PC) beams. Prestressed concrete, like reinforced concrete, has been widely used in the construction field for many decades. Prestressed concrete is used in a wide range of structures, like bridges and buildings, where its high strength and ductility can improve structural capacity and serviceability; as well as allow longer spans, and reduce structural thicknesses and material consumption compared to conventional reinforced concrete. PC structures also face problems of structural deficiency due to damage, aging, increased service loads and revised code requirements. Recent reports have found that many PC bridges, especially those built a few decades back, are structurally deficient and are in need of significant rehabilitation, including strengthening (Klaiber et al., 2003; Rosenboom and Rizkalla 2006). Various strengthening materials and techniques have been used and studied in the strengthening of PC beams, such as steel rods, steel plates, CFRP strips, CFRP bars, using external bonding, near surface mounting and external post-tensioning (Klaiber et al., 2003; Larson et al., 2005; Rosenboom and Rizkalla 2006; Pantelides et al., 2010). However, there is limited research on the use of prestressed NSM strengthening on prestressed beams. To the best of this researcher's knowledge, only one pilot study has been done by Casadei et al. (2006) who investigated the use of prestressed NSM CFRP strengthening on prestressed concrete I-girders. To the best of the researcher's knowledge, no studies have been conducted on the use of prestressed NSM steel strengthening on prestressed concrete beams.

This study also proposes a new strengthening technique which combines the EBR strengthening technique with the prestressed NSM strengthening technique, which in this study is referred to as the CEBPNSM strengthening technique, to further enhance the performance of strengthened beams. The addition of prestress force to the NSM reinforcement in this combination technique provides a strengthening system that actively opposes the effects of dead and live loading. This reduces stresses in the strengthening system by producing opposing stresses in the composite beam, which enhance and prolong the effectiveness of the strengthening system and the composite beam as a whole. The various advantages of prestressed strengthening further enhance this combination technique, such as improved serviceability in terms of reduced deflection, closing of existing cracks, higher crack initiation load, and smaller crack widths; increase of yield load to a higher portion of ultimate capacity; increased ultimate capacity; replacement of prestress forces that have been lost; and more efficient use of concrete and strengthening material (El-Hacha et al., 2001; Obaydullah et al., 2016). Furthermore, the addition of prestressing to the combination technique further reduces the likelihood of, or may even prevent, premature debonding failure. The prestress forces transferred from the prestressed NSM reinforcement to the beam create opposing stresses in the beam, namely tensile stresses at the top face of the beam and compressive stresses at the bottom face of the beam, which produce a cambering effect in the beam. This cambering effect is the main reason for the enhancement in performance brought about by prestressing. This cambering effect caused by prestressing also reduces the interfacial stresses in the EBR and NSM reinforcement in the combination technique, reducing the possibility of debonding failure.

In this study, a number of prestressed beams were strengthened using different strengthening techniques in order to investigate the structural performance of the proposed new strengthening technique that combines EBR and prestressed NSM (CEBPNSM), as well as the performance of prestressed steel strands as NSM reinforcement. A number of different materials were used in this investigation, namely steel strands, CFRP bars, CFRP plate and CFRP sheet. The prestressed beam specimens were divided into six groups according to the type of strengthening conducted on the beams. The first group was strengthened with prestressed NSM CFRP bars. The second group with prestressed NSM steel strands. The third group with a combination of prestressed NSM CFRP bars and EBR CFRP sheet. The fourth group was strengthened with a combination of prestressed NSM steel strands and EBR CFRP sheet. The fifth group was strengthened with a combination of prestressed NSM CFRP bars and EBR CFRP plate. The sixth group was strengthened with a combination of prestressed NSM steel strands and EBR CFRP plate. Besides the beams specimens in these groups, one beam was left unstrengthened as a control beam and three beams were strengthened with only EBR. In order to effectively investigate the effect of prestressing on the PNSM and CEBPNSM strengthening techniques, the prestress level in the NSM reinforcement in the strengthened beams was varied from 30% to 70% of the tensile capacity of the NSM strengthening material. All beams were tested under monotonic loading until failure and the performance of the beams was measured in terms of first crack load, crack width, crack pattern, yield load, concrete strain, steel strain, NSM strain, EBR strain, deflection, ultimate load, and failure mode. The experimental results were further validated using finite element modeling (FEM) to simulate the structural behavior of the beam specimens. The ultimate aim of this study is to develop effective and feasible new strengthening solutions to improve the structural performance of concrete structures, especially prestressed concrete structures, which overcome the limitations of previous strengthening techniques, by investigating the newly proposed CEBPNSM strengthening technique, investigating prestressed steel strands as a viable alternative NSM strengthening material, and investigating the effect of varying the prestress level in PNSM and CEBPNSM strengthening.

1.4 Research Questions

Thus, based on the review of previous research as mentioned in the previous section of this chapter, it is important to answer the following research questions:

i. Can prestressed NSM steel strands become a feasible alternative strengthening material to NSM CFRP bars?

ii. Is the newly proposed CEBPNSM a viable and effective strengthening technique?

iii. How is the performance of the CEBPNSM technique influenced by various strengthening materials (steel strand, CFRP bar, CFRP sheet and CFRP plate)?

iv. How is the performance of the CEBPNSM technique influenced by varying the prestress level in the prestressed NSM reinforcement?

1.5 Objectives

The current study aims to investigate and develop effective strengthening solutions for the flexural strengthening of prestressed concrete beams. The objectives of this research are as follows:

i. To investigate the structural behavior of prestressed beams strengthened using the NSM technique with prestressed steel strands and prestressed CFRP bars.

ii. To propose a new strengthening technique which combines EBR with prestressed NSM to enhance the flexural performance of prestressed beams.

iii. To assess the structural performance of the proposed strengthening technique which combines EBR and prestressed NSM.

iv. To evaluate the effect of varying the level of prestress force in the prestressed NSM reinforcement on the prestressed beams strengthened using PNSM and CEBPNSM.

v. To simulate the structural behavior of the strengthened prestressed beams using finite element modeling and validate the experimental results.

1.6 Significance

Investigating the efficiency of the proposed new CEBPNSM technique as a viable alternative strengthening option is a relevant and timely endeavor. The CEBPNSM strengthening technique could become an effective strengthening technique that greatly enhances the performance of structures in need of strengthening. This new technique may overcome the limitations of previous strengthening techniques, such as premature debonding failure and reinforcement restrictions, which could significantly extend the lifespan of structures, improve serviceability and safety concerns, and ensure full use of structural capacity. The CEBPNSM technique could thus provide a strengthening technique that more effectively meets the needs of the construction industry. Ultimately, the use of strengthening is a more economical, efficient and sustainable solution than constructing new structures.

Investigating the effectiveness of using prestressed steel strands as NSM strengthening material could provide valuable insight into its viability as an alternative to CFRP. Prestressed steel strands as NSM strengthening material could improve structural performance without compromising the ductility and deformability of strengthened structures, which could significantly enhance safety by preventing sudden catastrophic failure. Prestressed steel strands could also provide a more economical option for NSM strengthening compared to CFRP.

Investigating the effect of various strengthening techniques, namely EBR, NSM, PNSM and CEBPNSM, and various strengthening materials, namely steel strands, CFRP bars, CFRP plates and CFRP sheet, on prestressed concrete beams could provide valuable insight into the behavior and performance of prestressed concrete structures when strengthened. Furthermore, investigating the use of prestressed NSM reinforcement with various prestress levels could lead to a better understanding of the effect of adding prestress to prestressed concrete elements. Prestressed concrete is widely used in construction, thus the findings from this investigation could prove valuable for practical strengthening applications in actual prestressed concrete construction in the future.

1.7 Research Methodology

In order to achieve the objectives of this research, certain methodological approaches were followed. Firstly, an extensive review of literature was carried out on existing strengthening techniques and materials, in order to assess the current state of research, identify areas that require further research and place the present research work in a wider context of related work. Secondly, a thorough experimental investigation was conducted in order to examine, evaluate and collect data on the structural performance of the strengthening techniques and materials under investigation in this study. The experimental investigation consisted of an evaluation of the materials to be used, preparation of the beam specimens (beam fabrication and strengthening), testing of the beam specimens under monotonic four point loading until failure, and collection of experimental data. Thirdly, a numerical model was developed using a finite element software, ABAQUS, for comparison with and validation of the experimental results. Fourthly, the experimental and numerical results were analyzed and discussed in detail in order to compare and validate the results, draw conclusions and offer recommendations. Fifthly, the research work was published in peer-reviewed journals and in this thesis for dissemination of the research findings, validation by other researchers and contribution to the field of structural engineering.

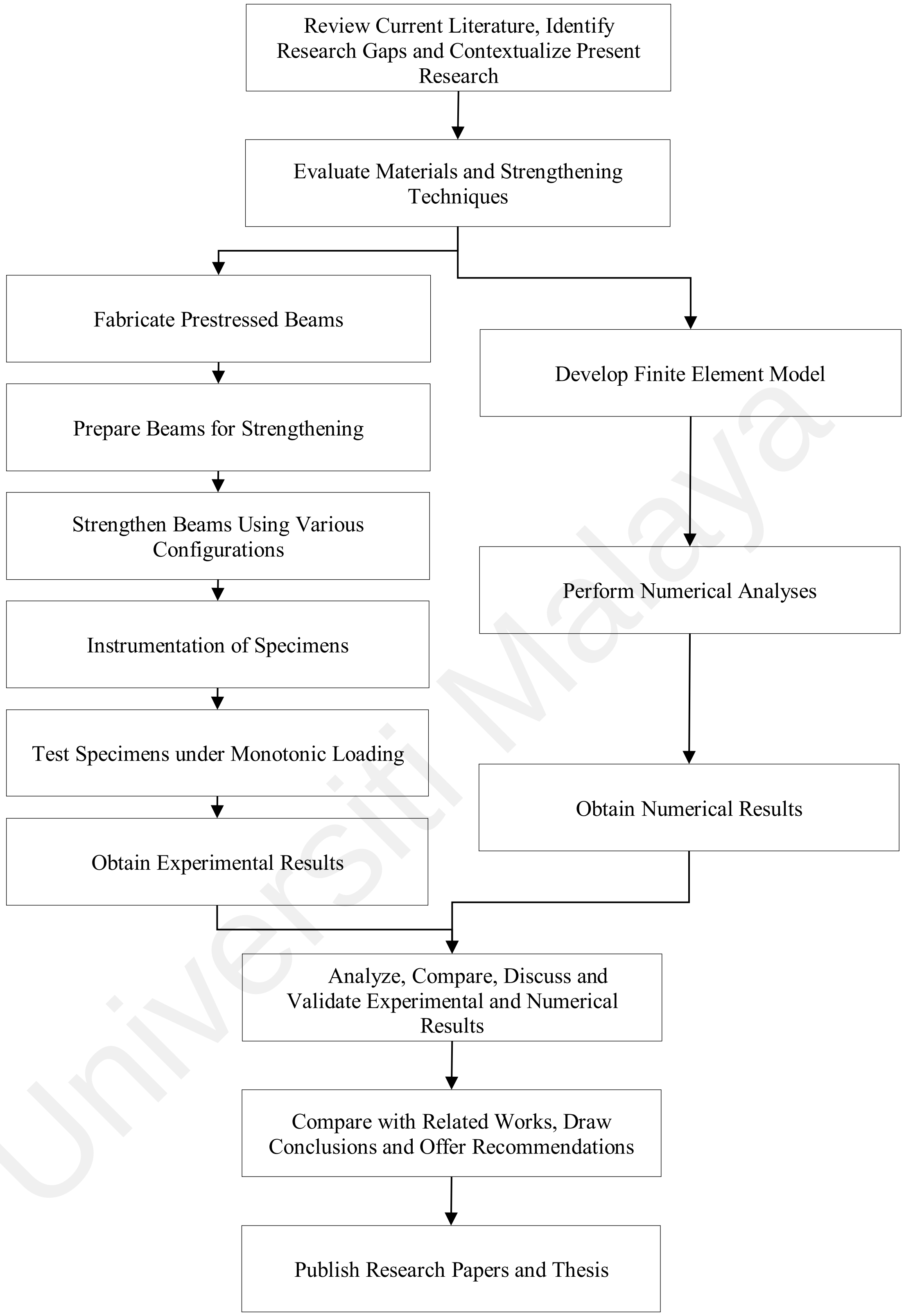

Figure 1.1: Research Methodology

1.8 Thesis Outline

This thesis is divided into five sections, namely i) introduction, ii) literature review, iii) methodology, iv) results and discussions, and v) conclusion and recommendations. The contents of each of the chapters in this thesis are summarized below.

The first chapter is a brief introduction to the research work comprising of the background, problem statement, scope, research questions, objectives, significance, research methodology and thesis outline.

The second chapter presents a concise yet thorough review of relevant recent literature concerning current strengthening techniques and materials, their characteristics, performance, limitations, and significant advancements. From this review, certain areas that require further research were identified and the how the present study addresses these gaps in research is discussed. A review of numerical studies of strengthened beams based on finite element modeling is also presented in this chapter.

The third chapter describes the methodology of the experimental investigation and numerical modeling. The experimental test matrix is presented with details of the different beam specimens. This chapter also describes the beam specifications, beam fabrication, material properties, procedures followed for strengthening the beams using various techniques and materials, instrumentation of specimens, and test setup. The finite element modeling strategy and simulation technique are also described in this chapter.

The fourth chapter presents the results of the study. The experimental and numerical data are described, analyzed, discussed, compared and validated with reference to previous research works. This includes the structural performance of the prestressed beam specimens in terms of first crack load, crack width, crack pattern, yield load, concrete strain, steel strain, NSM strain, EBR strain, deflection, ultimate load, and failure mode. A parametric study was performed with the experimental results in terms of strengthening material and prestress level. The results from the finite element model were critically analyzed and compared with the experimental results for validation purposes.

The fifth chapter summarizes the main findings of this research work, concludes the thesis and offers recommendations for future research.

CHAPTER 2: LITERATURE REVEIW

The construction of concrete structures began in the late 19th century and by mid-20th century large scale reinforced concrete and prestressed concrete structures were being constructed in many countries all over the world. The use of RC and PC structures has become a vital part of modern transportation and building. However, structural engineering now faces significant challenges to improve the sustainability of construction. Sustainability in construction refers to the effective consumption of materials, economical use of resources and leaving of quality resources for future generations. One way the structural engineering community is improving the sustainability of the built environment is by extending the lifespan of existing structures rather than constructing new structures. Existing structures often face serviceability issues due to aging, damage, design and construction flaws, increased loading from higher volumes of usage and upgraded structural design requirements. To extend the service life of these structures, extensive rehabilitation including structural strengthening, may be required at some point in their life cycle.

Structural strengthening is the process of upgrading structures to improve performance under existing loads or to increases the strength of structural members to carry additional loads. Structural strengthening may be required to increase load capacity, withstand seismic loads, support additional live and dead loads not included in the original design, to relive stresses generated by design or construction errors, or to restore the original load capacity of damaged structural elements. Figure 2.1 graphically illustrates the need for structural strengthening in certain situations. Research in structural strengthening has focused on the development of new and existing strengthening techniques and materials to more efficiently and effectively improve the structural performance of existing structures

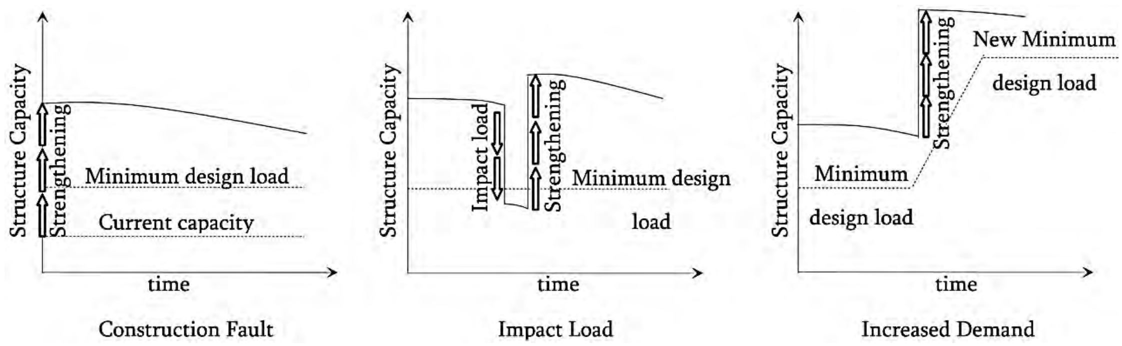

Figure 2.1: Reasons for strengthening of existing structure (Badawi, 2007)

Various structural strengthening techniques and materials have been developed over the last few decades. Steel and carbon fiber reinforced polymer (CFRP) are the most frequently used strengthening materials. Two of the most common structural strengthening techniques are the externally bonded reinforcement (EBR) technique and the near surface mounted (NSM) technique. Prestressing of strengthening materials is another strengthening technique that is used in conjunction with other strengthening techniques, such as EBR and NSM. A new strengthening technique that is still under development is the combined externally bonded and near surface mounted (CEBNSM) technique.

This chapter presents a review of current research on the structural strengthening of RC and PC beams using several strengthening techniques, namely the EBR, NSM, PNSM and CEBPNSM techniques. A review of research developing numerical models for structural strengthening is also presented. A number of conclusions are drawn from the review of current research to highlight the position of the present research work undertaken in this study and how it addresses certain limitations found in the existing research on structural strengthening.

2.1 Methods of Strengthening

There are many methods for strengthening, such as: section enlargement, steel plate bonding, and external post tensioning method, epoxy bonded (EB) system, unbounded anchored system and near-surface mounted (NSM) system. General methods for strengthening are summarized in (Table 2.1). The basic concept of strengthening is to improve the strength and stiffness of concrete members by adding reinforcement to the concrete surface.

Table 2.1:Methods of strengthening

Methods	Description
(a) Section Enlargement	"Bonded" reinforced concrete is added to an existing structural member in the form of an overlay or a jacket.
(b) Steel plate bonding	Steel plates are glued to the concrete surface by epoxy adhesive to create a composite system and improve flexural strength.
(c) External post tensioning system	Active external forces are applied to the structural member using post-tensioned cables to improve flexural strength.
(d) Externally bonded reinforcement (EBR) system	FRP composites are bonded to the concrete surface by using epoxy adhesive to improve the flexural strength. FRP material could be in the form of sheets or plates.
(e) Near-surface mounted (NSM) system	FRP bars or plates are inserted into a groove on the concrete surface and bonded to the concrete using epoxy adhesive.
(f) Combination of EBR and NSM (CEBNSM) technique	This is a combination of EBR and NSM system.

However, the cross-section enlargement is not applicable in the congested area or limited available areas, and it added huge loads on the structures. The external steel plates and post-tensioning tendon are seriously affected by severe weather conditions and require special protection.

2.2 EBR Strengthening Technique

Externally bonded reinforcement (EBR) technique increases the flexural capacity by introducing steel plate or unidirectional fiber reinforced polymer plate or fabric at the maximum tensile region of RC beam. At first, during the 60's, this EBR technique was launched to strengthen concrete structures with steel plate to glue with epoxy and/or anchor which was popular due to economical aspect. Despite limited manufacturing technology, this epoxy bonded steel plate was popular within Europe for the last three decades (Beber et al., 2001). However, due to heavy self-weight, extreme corrosiveness, and installation difficulties, researchers introduced FRP which is lightweight, non-corrosive and easy to install. This was a scientific breakthrough in literature; the ultimate flexure capacity increment was reported as 160% (Meier & Kaiser, 1991; Ritchie et al., 1991). However, the percentage increase had been limited to 40% due to ductility and serviceability limitations. The use of Fiber Reinforced Polymer (FRP) to strengthen reinforced concrete (RC) structures has grown in popularity and established itself as an acceptable engineering practice in recent years. In particular, using FRP as external reinforcement is a widely used technique for structural rehabilitation.

Oehlers (1992) investigated the structural characteristics of RC beam specimens glued in the tension face by steel plates. The test variables were the several shear span lengths under monotonic loading condition. The experimental outcomes showed that peeling cracks of the specimens depends on the moment to shear ratio, bond length of steel plate's extension does not influence the shear capacity; and the shear cracks at the curtailment location are the key factors to influence the premature failure of the specimens.

El Maaddawy and Soudki (2005) examined the serviceability of corroded RC beam specimens repaired with EBR method utilizing CFRP laminates. The specimens were damaged by several levels of corrosion. This research outcome demonstrated that CFRP laminates increased the strength of corroded specimens compared with the virgin specimen but suggestively decreased the deflection capability.

Esfahani et al. (2007) investigated the flexural performance of RC specimens strengthened with EBR-CFRP sheets. The experimental variables were reinforcing steel ratio, CFRP sheet number of layers, width and length. It was concluded that low reinforcing steel ratio with CFRP sheets increased the higher flexural capacity compared with the maximum reinforcing steel ratio specimens. However, the large reinforcing steel ratio with CFRP sheets specimens' capacity were very consistent with ACI 404.2R-08 (2008) and ISIS Canada (2012) guidelines.

Akbarzadeh and Maghsoudi (2010) investigated the experimental and analytical behavior of RC high strength continuous beam specimens strengthened by EBR-FRP sheets. The outcomes exhibited that the increasing number of layer of CFRP sheets improved ultimate strength but decreased moment redistribution, ductility and ultimate stain of sheets. Conversely, the GFRP sheets decreased the loss of moment redistribution and ductility but did not meaningfully improve the ultimate strength.

Attari et al. (2012) investigated experimental and analytical behaviour of RC beam specimens repaired by EBR method with CFRP, GFRP and combination of CFRP and GFRP as hybrid sheets. Experimental variables were the type of FRP, number of layers and end-anchorage. Their results found that the hybrid sheets were cost effective for enhancing the strength and ductility compared with the mono CFRP or GFRP sheets but the failure modes were flexural and peeling off.

Dong et al. (2013) examined the flexural and shear behaviour of RC beam specimens by EBR-FRP sheets. Different strengthening arrangements with CFRP and GFRP were used in this study. The specimens strengthened with flexural-shear sheets exhibited more effectiveness over the flexural strengthened specimens. All flexural strengthened specimens failed by debonding of the FRP sheets.

Hawileh et al. (2014) investigated the experimental and analytical characteristics of RC beam specimens strengthened flexurally by EBR method utilizing GFRP, CFRP and hybrid (together with CFRP and GFRP) sheets. The experimental outcomes showed that hybrid sheets strengthened specimens were enhanced the ductility higher than the CFRP or GFRP strengthened specimens.

Spadea et al. (2015) studied the effectiveness of RC beam specimens strengthened in flexure and shear by EBR method using FRP laminates. Different type of anchorages (internal and end) and U-mechanically anchored steel were used for strengthening of specimens. Most of the specimens failed by debonding but anchorages increased strength and ductility of the specimens.

Gao et al. (2016) investigated the flexural characteristics of preloaded RC beam specimens strengthened by EBR technique utilizing prestressed CFRP laminates. The test variable parameters were a different level of pre-tensioned forced, CFRP reinforcement ratio and sustained load. The experimental and numerical results showed that the ultimate load was reduced over the sustained load more than 40 % of the ultimate load of control specimen and intermediate crack debonding failure mode was occurred in the mechanical end-anchored strengthened specimens.

Tanarslan (2017) assessed the flexural performance of RC beam specimens strengthened by EBR technique using the ultra-high performance fibre reinforced concrete (UHPFRC) laminates. The experimental outcomes have shown that UHPFRC strengthened specimens enhanced the ultimate capacity and the debonding failure mode of the specimens was eliminated by anchorage.

Nayak et al. (2018) examined the flexural behaviour of RC beam specimens strengthened with EBR-GFRP sheets experimentally and theoretically. They found from the results that, increasing the number of GFRP sheets layer enhanced the flexural strength but the failure modes of the specimens changed from flexure to brittle and most of the EBR-GFRP specimens failed by debonding.

2.3 External bonding with prestressing

Strengthening of RC structures with prestressed FRP materials under monotonic loading has been investigated by a number of researchers. Usually, three modes of failure are expected in RC beams strengthened with externally pre-stressed bonded FRP materials: a crushing of the concrete, a rupture of the FRP, or de-bonding of FRP resulting in a sudden drop in the load that constitutes a brittle failure regardless if the tension steel reinforcement has yielded or not (Meier and Kaiser, 1991; Meier et al., 1992; Garden and Hollaway, 1998).

Triantafillou and Deskovic (1991) reported an analysis of the problem of providing the maximum achievable pre-stress level without experiencing a de-bonding failure in the end zone. They found that a higher pre-stress level can be achieved by increasing the length of bond. It was also concluded that for pre-stressed FRP strengthened RC beams, an additional mechanical anchor at the ends would increase the potential of using pre-stressing technique for externally bonded FRP materials.

Later, Triantafillou et al.(1992) verified their analytical model by performing an experimental test. A reasonable agreement was achieved between their model and the obtained experimental results. It was also found that excellent flexural behavior was obtained in terms of strength, stiffness, and ductility. A similar study was conducted by Quantrill and Hollaway (1998). Two different span lengths (1.0 m and 2.3 m) of RC beams were studied with two levels of pre-stressed CFRP plate (ranging from 17.5% - 41.7% of the CFRP plate tensile strength). The losses after pre-stressing were monitored and the lengths over which the force was transferred to the CFRP plate were found to be 150mm and 200mm for 1.0 m and 2.3 m span beams, respectively. Pre-stressing the plate before bonding it to the beam increased the flexural stiffness, the cracking, the yield and the ultimate loads. The results also showed that a beam strengthened with pre-stressed CFRP plate exhibited a similar or slightly increased level of ductility compared to non-pre-stressed strengthened beams. This conclusion might be dependent on the type of failure.

Wight et al. (2001) studied the flexural strengthening of RC beams using pre-stressed sheets mechanically anchored at the ends. A pre-stressing level of 200MPa in the CFRP sheet was examined. They reported that pre-stressing of CFRP sheets to strengthen RC structures was an effective and practical method. It was also concluded that pre-stressed CFRP sheets could remarkably improve the serviceability of RC structures. For a further research, it was recommended that a higher pre-stressing level needs to be investigated.

Tehrani et al. 2019 studied both experimental and analytical studies on the behavior of reinforced concrete (RC) beams strengthened in flexure using prestressed carbon-fiber-reinforced polymer (CFRP) plates via the externally bonded reinforcement on grooves (EBROG) method. It was observed that prestressing CFRP plates attached via EBROG method was able to postpone the debonding and increase the strength efficiency of the FRP plates. A maximum enhancement of 20% in ultimate load-carrying capacity was measured in prestressed beams strengthened via the EBROG technique relative to the non-prestressed ones.

2.4 Limitation of external bonding system

Due to the desirable properties of FRP, numerous studies have looked at many aspects of using externally applied FRP for structural strengthening. However, one of the key concerns with externally bonded FRP is premature loss of bond between the concrete substrate and the externally bonded FRP laminate. Premature debonding in the present context means loss of bond before the FRP laminate can reach its expected capacity based on a perfect bond.

To strengthen the structure, the FRP must transfer its resistance contribution to the concrete section via shear stresses through the epoxy adhesive and the epoxy adhesive-concrete interface. Therefore, a sufficient bond between the epoxy adhesive and the concrete is critical for the strengthening of the structure. If the bond between the concrete and epoxy adhesive remains intact, stress can be transferred from concrete to FRP, and vice versa, and full composite action between the FRP and the unstrengthened RC beam will prevail. If premature debonding occurs, the composite action is lost, thus the RC beam cannot reach the theoretical ultimate capacity of the composite beam.

If an FRP-plated beam retains its composite action, there are two possible failure modes (Saxena et al., 2008) : (1) compressive concrete crushing prior to, or after, tensile steel yielding and (2) flexural failure due to rupture of the FRP. When premature debonding occurs between the FRP plate and concrete, the composite action of the beam is lost. The loss of composite action is characterized by the following four failure modes: (1) concrete cover separation (2) plate end debonding, (3) Shear crack induced debonding and (4) intermediate crack (IC) debonding (Table 2.2)

Plate end debonding is caused by high normal and shear stresses developed at the laminate ends during loading. When the stresses exceed the strength of the weakest element, failure occurs. Upon failure, the FRP will deboned from the concrete, usually within the concrete, at one end of the beam/slab leading to failure of the specimen. Concrete cover separation is caused by a crack developing at the laminate end propagating upwards to the level of the steel tensile reinforcement and horizontally along the reinforcement. The extension of the crack along the tensile reinforcement leads to concrete cover separation and the failure of the specimen. This type of failure typically occurs in members with relatively thinner cover, larger internal reinforcing bars and a stronger FRP-concrete interface. Failure of the concrete cover is initiated by the formation of a crack at or near the plate end due to high interfacial shear and normal stresses caused by the abrupt termination of the plate.

Intermediate Crack (IC) debonding occurs when flexural or flexural-shear cracks develop in an RC beam or slab, releasing tensile stress to the adjacent FRP. High strain in the FRP plate is necessary to accommodate the high local interfacial stress across the crack. This high strain causes the propagation of cracks along the FRP-concrete interface. This high strain causes the propagation of cracks along the FRP-concrete interface. The growth of these cracks toward the region of less moment leads to premature debonding of FRP in the form of IC debonding. The cracks commonly occur in the concrete below the concrete-epoxy interface because the tensile strength of the epoxy adhesive is much higher than that of the concrete. The vertical displacement on either side of a flexural-shear crack can also cause a peeling force on one side of the crack which also contributes to IC debonding. However, the peeling force is considered less significant than the widening of cracks in causing IC debonding (Chen & Teng, 2001).

Table 2.2: Failure modes of EBR strengthened RC beam (Obaidat, 2011; Smith & Teng, 2002a)

Failures	Failure types	Failure Modes
Case I Full composite action	Concrete Crushing	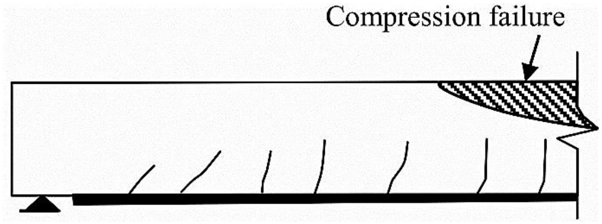

Failures	Failure types	Failure Modes
	FRP rupture	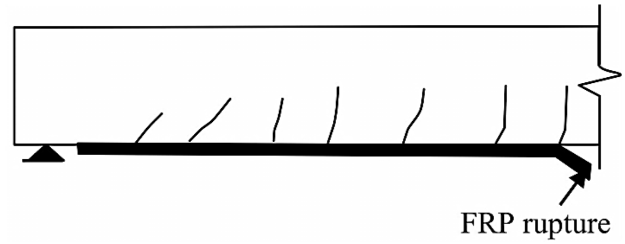
<u>Case II</u> Premature failure	End cover separation	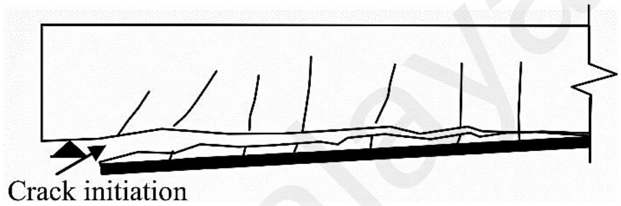
	End interfacial delaminati on	
	Shear crack induced debonding	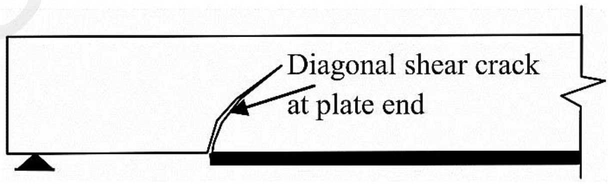
	Flexural crack induced (IC) debonding	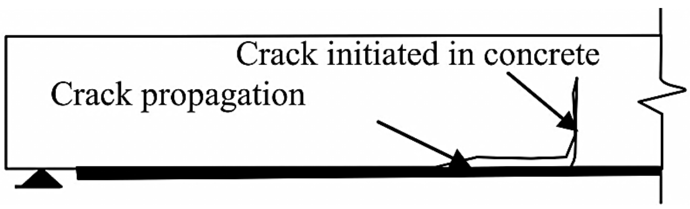
	Flexural-shear crack induced IC debonding	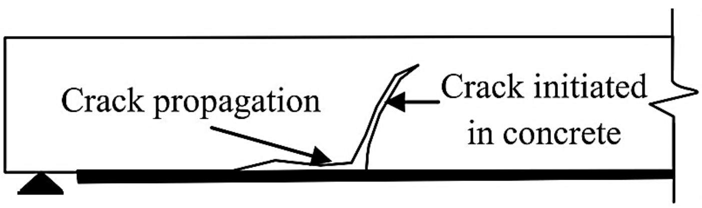

2.5 Eliminating premature de-bonding in external bonding method

Plate end debonding can be prevented using the FRP anchorage system. It also enhances the ultimate load capacity by providing a vertical stiffness against peeling off stresses. Compared to the un-anchorage strengthened RC beam, the plate end FRP anchorage showed superior ductility ratios and increased ultimate capacity in Figure 2.2 (Breña & Macri, 2004; Ritchie et al., 1990).

FRP anchorage sheet is also used along the beam length to delay the Intermediate crack debonding. Chicoine (1997) tested FRP strengthened beams which failed due to debonding at their end. After this result, he developed two different configurations with FRP anchorage to prevent the premature failures (Figure 2.2). The 1st arrangement consisted of U-shaped FRP anchorage which was fixed at the end of two main FRP laminate. In the other configuration, unidirectional transverse strips were used along the FRP laminate. The first and second configurations enhanced the flexural capacity of the strengthened RC beam by 32.0% and 46.0% respectively compared to the un-strengthened beam. The second configuration changed the failure mode from debonding to flexure failure (rupture of FRP laminate). A similar observation was also reported by (Kotynia et al., 2008; Ritchie et al., 1990; Spadea et al., 1998)

The splitting of concrete cover can be prevented using the FRP anchor with transverse reinforcement. The FRP U-wrap is an efficient device which can be clamped at plate end. The area of this transverse clamping reinforcement A_f can be ascertained using the following equation 2.1 (Reed et al., 2005).

$$\boldsymbol{A_{fanchor}} = \frac{(\boldsymbol{A_f f_{fu}})_{\boldsymbol{longitudinal}}}{(\boldsymbol{E_f \kappa_v \epsilon_{fu}})_{\boldsymbol{anchor}}} \qquad (2.1)$$

Leung, 2006 found in his study that the FRP anchorage away from the plate end sometimes demonstrated better performance and the use of the plate end anchorage was not so successful always.

Kotynia et al. (2008) did not extend the FRP U-shaped anchorage sheet to the end of the FRP laminates. The study found that the debonding initiated just after the end of the continuous FRP anchorage laminates and propagated towards the plate ends at load level similar to the failure load of the un-anchorage beam (Figure 2.2).

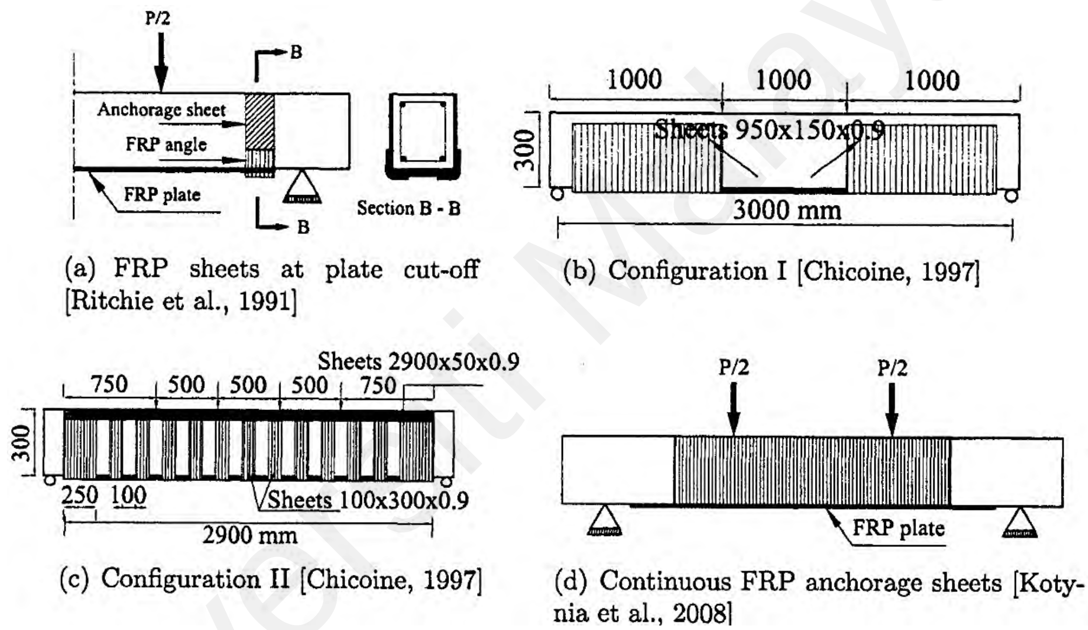

Figure 2.2: Various anchorage schemes for FRP strengthened RC beams(Kotynia et al., 2008)

The basic reasons behind anchorage usage in externally bonded reinforcement techniques are: a) to delay or avoid interfacial crack initiation; b) to enhance the interfacial shear stress reassignment; c) to develop a shear transfer process if the bond length is not available beyond the critical section. Based on this anchorage behavior, Grelle and Sneed (2013) categorized type I, II, and III anchorage device (Figure 2.3).

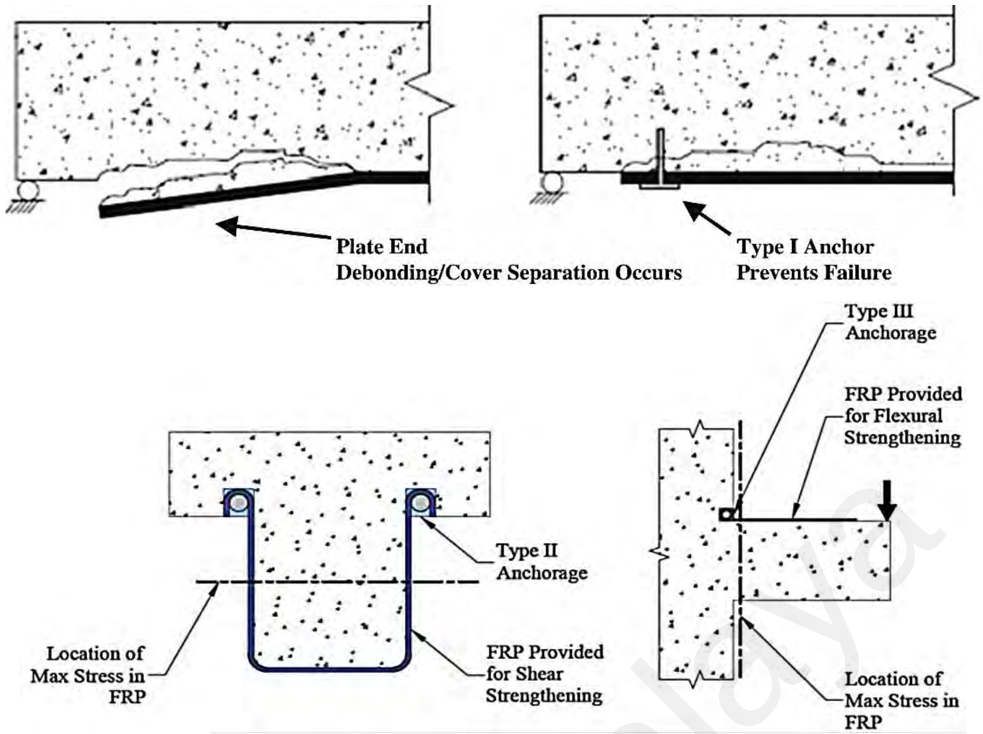

Figure 2.3: Type I, II and III anchorage device (Grelle & Sneed, 2013)

Type I anchorage will prevent the plate end interfacial debonding or concrete cover separation. A typical example of this anchorage is the mechanical anchor provided at the FRP laminate end. Type II anchorage improves the interfacial shear stress transfer mechanism. It is needed when the effective bond length is more than the transfer length because of the geometric configuration of the structural member. Type III is used where no bond length is available beyond the critical section. This condition applies when the critical design section is located at a sheet or plate end, or near an abrupt change in fiber direction, such as at the location of an interface between two orthogonal structural members. U-anchor is used to represent the type II and III anchorage (Figure 2.3). The author suggested performing an independent full scale anchor test data to incorporate the anchorage system in the design code.

Kalfat et al. (2011) reviewed several anchorage devices to achieve superior fiber utilization to delay or prevent debonding failure. Known anchorage devices for FRP-to-concrete applications comprise FRP U-jackets, FRP spike anchors, patch anchors, nailed metal plates, near-surface mounted rods, mechanical fastening, concrete embedment, and mechanical substrate strengthening. FRP U-jackets are non-invasive and their easy installation procedure makes ideal choice for flexurally strengthened RC beams. It was obtained that inclined U-jackets were 74% more effective than vertically orientated U-jacket anchors, and the subsequent anchorage efficiency was k_{fab} =1.36. FRP anchors demonstrated 46% more efficiency than vertically positioned U-jackets and marginally less efficiency than inclined U-jackets.

2.6 NSM Strengthening Technique

NSM strengthening is a promising technique for enhancing the service life and performance of concrete structures in need of rehabilitation (Teng et al., 2003; Hollaway L, 2010; Coelho et al., 2015). The NSM strengthening system was first used in Sweden in the 1940s to strengthen a deck slab of a bridge using steel bars placed inside grooves cut into the concrete cover and filled with cement mortar by Asplund, 1949. More recently, there has been a surge of interest in the use of FRP materials with the NSM technique. Numerous studies have been conducted on the use of NSM FRP to strengthen structures. Jung et al. (2005) compared NSM CFRP strengthened beams with externally bonded CFRP strengthened beams. Al-Mahmoud et al. (2009) investigated the flexural response of NSM CFRP strengthened RC beams under four-point loading. Bilotta et al. (2015) and Sharaky et al. (2015) examined the efficiency of RC beams flexurally strengthened with EBR plates and NSM CFRP strips.

De Lorenzis et al. (2001b) and De Lorenzis L. (2002) performed research on flexural and shear strengthening of RC beam specimens by NSM technique applying FRP bars. The experimental variables were the type of specimens and ratio of reinforcing steel. The prevalent failure mode was debonding for strengthened T-beams and rectangular beams comprising the low ratio of reinforcing steel. Higher ratio of reinforcing steel in rectangular beams failed by crushing of extreme fiber concrete. Therefore, posttensioning NSM technique was proposed for avoiding the end debonding of the beams.

El-Hacha et al. (2004) conducted an experimental study of RC T-beam specimens strengthened by NSM and EBR techniques using FRP for evaluating the flexural performance. Eight T-beam specimens comprising one specimen was the reference and other specimens were strengthened by NSM and EBR techniques. The experimental variables were the strengthening techniques and FRP types. All specimens were tested beneath the displacement control and the rate of displacement was 0.18 mm/s. The NSM technique with FRP achieved the full composite action among the FRP strips and concrete surface. The flexural capacity of the strengthened specimens notably increased and it was superior than the EBR strengthened specimens.

Rosenboom et al. (2006) studied the static and fatigue behavior of prestressed RC girder specimens strengthened with NSM technique using different configurations of CFRP. The NSM bars or strips strengthened specimens were tested beneath static loading until failure; their ultimate strength increased by 20% compared with the un-strengthened specimen. The NSM with CFRP strengthened specimens revealed upright characteristics with slight degradation and decreased crack width beneath fatigue loading and carried loads up to two million cycles.

Barros and Fortes (2005) and Barros et al. (2006) conducted experimental studies for structural strengthening by NSM technique utilizing the CFRP laminates as a strengthening reinforcement. The experimental variables were several reinforcing steel ratio and depth of cross-section of the specimens and number of CFRP laminates. The ultimate load and ductility were significantly enhanced by the NSM-CFRP laminates. Furthermore, the serviceability limit state study exhibited that the enhancement of rigidity of the specimens was about 28% over the control specimen.

Choi et al. (2010) investigated the influence of partially bonded CFRP bars on the RC T-beam specimens flexurally strengthened by NSM technique. One specimen was control and other five specimens were strengthened by NSM and tested underneath the static loading, employing a displacement rate of 1.0 mm/min. One specimen was strengthened with fully bonded CFRP bars and other specimens were strengthened with unbonded length of CFRP bars were 1300 mm, 1500 mm, 1700 mm and 2100 mm at mid-span, correspondingly. They found that the mode of failure of the partially bonded strengthened specimens was concrete crushing at the extreme fiber compression zone.

Almusallam et al. (2013) investigated the flexure characteristics of RC beam specimens strengthened by NSM method experimentally and numerically applying steel and GFRP bars. Sixteen specimens having width of 150 mm, depth of 200 mm, total span length of 2200 mm and effective span length of 2000 mm were investigated. The experimental variables were NSM bars form (steel and GFRP), number and diameter of NSM bars. They reported that most of the strengthened specimens were failed by extreme fiber concrete crushing after yielding of reinforcing steel bars. Singh et al., 2014; Bilotta et al., 2015 & Sena-Cruz et al. (2012) also found similar findings.

Triantafyllou et al. (2018) examined experimentally and analytically, the flexural behavior of corroded RC beam specimens strengthened by EBR and NSM techniques using FRP laminates. The NSM-FRP strips strengthened specimens exhibited higher load-bearing capacity over the EBR-FRP laminate strengthened specimens. The corroded specimens with NSM and EBR-FPR were failed by debonding.

Dias et al. (2018) investigated the flexural performance of RC beam specimens strengthened with NSM technique utilizing CFRP laminates. The experimental variable was CFRP laminates reinforcement ratio. The load-bearing capacity increased and ductility level reduced with the increasing CFRP percentage. Most of the NSM-CFRP laminates strengthened specimens were failed by debonding.

Patel et al. (2019) assessed the flexural responses of RC beam specimens strengthened by NSM technique with different types of FRP bars. The test variables were FRP bars type (GFRP, Fe-415 and BFRP) and end-anchorage. The strengthened specimens failed by end-debonding.

These studies have found that flexural strength and performance of NSM strengthened members were significantly enhanced, although debonding was not completely eliminated.

2.7 NSM strengthened beams using steel:

Steel materials have superior ductility compared to FRP due to the elastoplastic nature of steel which results in gradual failure of structures after maximum loading. Steel is widely used in the construction field partially due to this characteristic. It is used as internal reinforcement in RC structures and prestressing strands in prestressed concrete. As a strengthening material, steel has been used as externally bonded reinforcement, externally post-tensioned reinforcement, as well as internally bonded as NSM reinforcement. The high deformability of steel strengthened beams is highly advantageous in real life situations as it allows catastrophic failure to be easily avoided. The main problem with the use of steel as strengthening reinforcement is the tendency of steel to corrode over time. However, steel is a readily available material and less costly compared to FRP. Although steel may be prone to corrosion when exposed, with adequate cover and proper maintenance it has been shown to have long term durability. Steel also displays greater ductility and better bonding performance compared to FRP (De Lorenzis et al., 2002). Using the NSM technique, steel bars are protected from exposure by the epoxy-filled NSM groove in which the steel is embedded. Due to the superior properties of epoxy, the required cover for the NSM steel can be reduced. The adequacy of this epoxy cover can be seen from the few studies that have been done using NSM steel. Darain et al. (2015) conducted a study on the flexural performance of RC beams strengthened with NSM CFRP and NSM steel. The study concluded that although the ultimate strength capacity of the NSM steel strengthened beams was less than the NSM CFRP strengthened beams, the NSM steel displayed better bonding capacity and ductile behavior, which eventually prevented premature failure in the NSM steel strengthened beams, unlike the beams strengthened with NSM CFRP. Hosen (2019) had similar findings in his study on NSM steel and CFRP as flexural reinforcement mounted on the sides of the RC beam specimens, concluding that NSM steel was more effective in terms of ductility. Zhang et al. (2011) investigated the use of prestressed helical ribbed steel wire as NSM reinforcement and found that the NSM prestressed steel effectively delayed the development of cracks, reduced deformation and increased stiffness in RC beams. Sun et al. (2011) demonstrated a comparative study of RC beam specimens strengthened by NSM technique using CFRP and steel bars, and steel fiber reinforced polymer composite bars (SFCB). The experimental variables were the type of NSM bars and dimensions of the NSM grooves. The NSM-steel bars strengthened specimens were failed by flexure whereas the NSM-CFRP and SFCB strengthened specimens failed by debonding of concrete with less ductility.

2.8 Prestressed NSM strengthening of RC beams:

Prestressed strengthening is an additional strengthening technique which can be used with EBR and NSM to improve the effectiveness of strengthening and enhance the overall flexural response of strengthened structures. Prestressed strengthening provides an active strengthening system where prestress force is transferred from the strengthening reinforcement to the structural member, inducing a cambering effect, which is the reason behind much of the enhanced structural behavior of prestressed strengthened structures. Various other advantages of prestressed strengthening include improved serviceability, less deflection, smaller cracks, lower internal strains, delayed crack formation, replacement of lost prestress and better utilization of strengthening materials and concrete.

A number of studies have investigated the use of prestressed NSM CFRP to strengthen RC beams. These studies have found overall improvement in flexural behavior at service and ultimate conditions, including higher yield load, ultimate load, and first crack load; and smaller midpoint deflection and crack width of strengthened beams. The strengthened beams mostly failed by rupture of the FRP (Badawi et al., 2009; Peng et al., 2014; El-Hacha & Gaafar, 2011; Aslam et al., 2015).

Nordin and Taljsten (2006) tested fifteen RC beams under four point loading to investigate the use of prestressed NSM CFRP for flexural strengthening. Among the beam specimens three variables were changed: the bond length, the modulus of elasticity, and the prestressing force in the CFRP quadratic rods. Prestressing level was varied between 10–27% of the ultimate tensile strength of the rods. The results of the tests showed that cracking, yield and ultimate loads increased significantly, while deflection and crack widths decreased. All of the strengthened beams failed by CFRP rupture. Varying the bond length did not significantly affect failure loads. However, a higher modulus of elasticity of the CFRP rod resulted in stiffer beams with higher yielding loads. Higher prestress levels increased the cracking and yielding loads, but reduced ductility at failure as a large part of the possible strain in the CFRP was used during prestressing, resulting in failure at smaller deflections.

Badawi and Soudki (2009) tested four RC beams to study the effectiveness of strengthening with prestressed NSM CFRP rods. Two levels of prestressing force were used, 40% and 60% of the ultimate strength of the rods. The test results found a remarkable improvement in the cracking, yield and ultimate loads, and significant reduction in the deflections and crack widths for the prestressed strengthened beams. The prestressed strengthened beams failed by fiber rupture. Increasing the level of the prestressing force resulted in improved serviceability in terms of reduced crack widths and deflections, but decreased ductility.

El-Hacha and Gaafar (2011) investigated the use of prestressed NSM CFRP bars to strengthen RC beams by testing five beams under static loading. Three prestressing levels, 20%, 40% and 60% of the ultimate tensile strength of the bars, were tested. The results of the tests showed that increasing the prestressing level greatly improved serviceability and ultimate strength but reduced ductility. Failure of the prestressed strengthened beams occurred due to CFRP rupture after yielding of the tension steel reinforcement with no debonding.

Choi et al (2010) investigated the flexural behavior of RC T-beams strengthened with prestressed near-surface-mounted NSM CFRP. The specific objective was to study the effect of partial unbonding of the CFRP reinforcement on the beam flexural behavior to increase the deformability. A total of eight RC T-beams were tested under four-point monotonic loading. The main variables were the level of prestressing force in the CFRP bars and the unbonded length at the midspan of the beam. The test results showed that all of the prestressed strengthened beams effectively improved the ultimate load-carrying capacity and the serviceability performance compared to the unstrengthened beam. The partially bonded prestressed beams exhibited an enhancement of the deformability compared to the fully bonded beams while minimizing the reduction of the load-carrying capacity. Partial unbonding was more effective to improve the deformability at higher levels of prestressing force. The general behavior of the partially bonded beams was reasonably well predicted by an analytical model developed previously by the writers.

Hajihashemi et. al. (2011) conducted a study on five RC beams to investigate prestressed NSM CFRP strengthening. Among these five beams, three were strengthened with NSM CFRP strips prestressed to 5%, 20% and 30% of their nominal ultimate strain capacity, while the remaining beams were a control beam and non-prestressed NSM CFRP strengthened beam. The tests concluded that the prestressed strengthened beams were more effective at improving cracking and yielding loads, with improved crack distribution and width, as well as higher ultimate load carrying capacity and lower deflections. Higher levels of prestressing corresponded to greater improvement in serviceability and ultimate load but reduced ductility.

Peng et. al. (2014) tested seven RC beams to investigate the behavior of prestressed NSM CFRP strengthening. Six beams were strengthened with CFRP, of which one was strengthened with non-prestressed NSM CFRP strips, and one with an externally bonded prestressed CFRP plate. The remaining four were strengthened with prestressed NSM CFRP strips with varying bond lengths, anchorage, number of NSM grooves, and strip thickness. The prestressing force used was 1000Mpa, approximately 50% of the tensile strength of the CFRP strips. The test results showed that strengthening with prestressed NSM CFRP strips significantly improved load carrying behavior of the beams. Peng et. al. also concluded that increasing bond length and using end anchorage could prevent debonding failure.

Rezazadeh et. al. (2014) fabricated five RC beams which were tested under monotonic four-point loading to investigate the benefits of prestressing NSM CFRP for strengthening RC beams that may not fulfill SLS conditions namely the deflection limit. Prestressing force levels of 20%, 30%, and 40% of the nominal tensile strength of the

CFRP strips were used. The results of the tests showed that increasing the prestressing level greatly improved serviceability in terms of cracking and yielding loads, as well as the load at deflection limit, but ductility was reduced.

Hong and Park (2016) investigated the effects of prestress levels and transverse grooves on the flexural behavior of eight RC beams under four point bending. Prestressing force levels of 10%, 20%, 30% and 50% of the nominal tensile strength of the NSM CFRP strips were used. The results found that increasing the prestress level increased cracking, yielding and ultimate loads and reduced deflection. Increasing the prestress level further delayed concrete cover separation and improved the composite behavior of the beam and NSM strengthening. Failure of the prestressed strengthened beams was by concrete cover separation. The use of transverse grooves had no significant effect on failure mode, cracking and yield loads and corresponding deflections, but did improve ultimate load and deflection. Based on their research, Hong and Park (2016) recommended 50% prestressing level for optimal energy absorption.

Lee et. al. (2017) conducted a study on eight RC beams to investigate the effectiveness of prestressed NSM CFRP strengthening. Several variables were examined, namely prestressing method (pre-tensioning and post-tensioning), type of filler (epoxy and mortar), surface treatment of the CFRP bar (grind and sand-coating), and number of bars (one bar and two bars). The CFRP bars were prestressed to approximately 50% of their tensile strength. Overall, the study found that prestressed NSM CFRP strengthening enhanced the flexural behavior of the RC beams in terms of concrete cracking, steel yielding, and ultimate loads. Post-tensioning provided greater enhancement of beam performance compared to pre-tensioning due to the anchorage systems placed in the beams which minimized bar slip and loss of prestress force. Epoxy as a groove filler provided better strengthening performance compared to mortar due to the higher bond strength, which led to less prestress force loss. Sand-coating as surface treatment for the CFRP bars enhanced beam performance more than grind surface treatment as the sand coating promoted higher bond strength between the filler and the CFRP bar. two bars over one bar.

Jung et al. (2017) tested RC beams strengthened with prestressed NSM CFRP using beams applying an external anchor system with the prestressing force of 20% of the ultimate CFRP strength using both CFRP bars and plates, and compared the test results to non-prestressed beams. Jung et al. concluded that the prestressed beams increased the cracking load and the stiffness of the beam and could prevent the premature debonding failure.

2.9 Limitations of the NSM technique

Although debonding failures are a less likely problem with NSM FRP compared to externally bonded FRP, they may still significantly limit the efficiency of this technology. The likelihood of debonding failure depends on several parameters, among which the internal steel reinforcement ratio, the FRP reinforcement ratio, the cross-sectional shape and surface configuration of the NSM reinforcement, and the tensile strengths of both the epoxy and the concrete. Some researchers (De Lorenzis, 2002; Taljsten et al., 2003) extended the NSM FRP reinforcement over the beam supports to simulate anchorage in adjacent members. Despite this anchorage, de-bonding failures can still occur (De Lorenzis, 2002). However, Taljsten et al. (2003) reported that one beam failed by FRP rupture where the reinforcement was extended over the supports, as opposed to the failure by debonding observed in an identical beam where the NSM reinforcement did not extend over the supports. Blaschko and Zilch (1999) reported the results of tests on two beams strengthened with NSM FRP. The first beam failed by concrete cover separation starting from the cut-off section but the second beam, which was provided with a steel U-jacket bonded to the cut-off section, failed by rupture of the FRP strips.

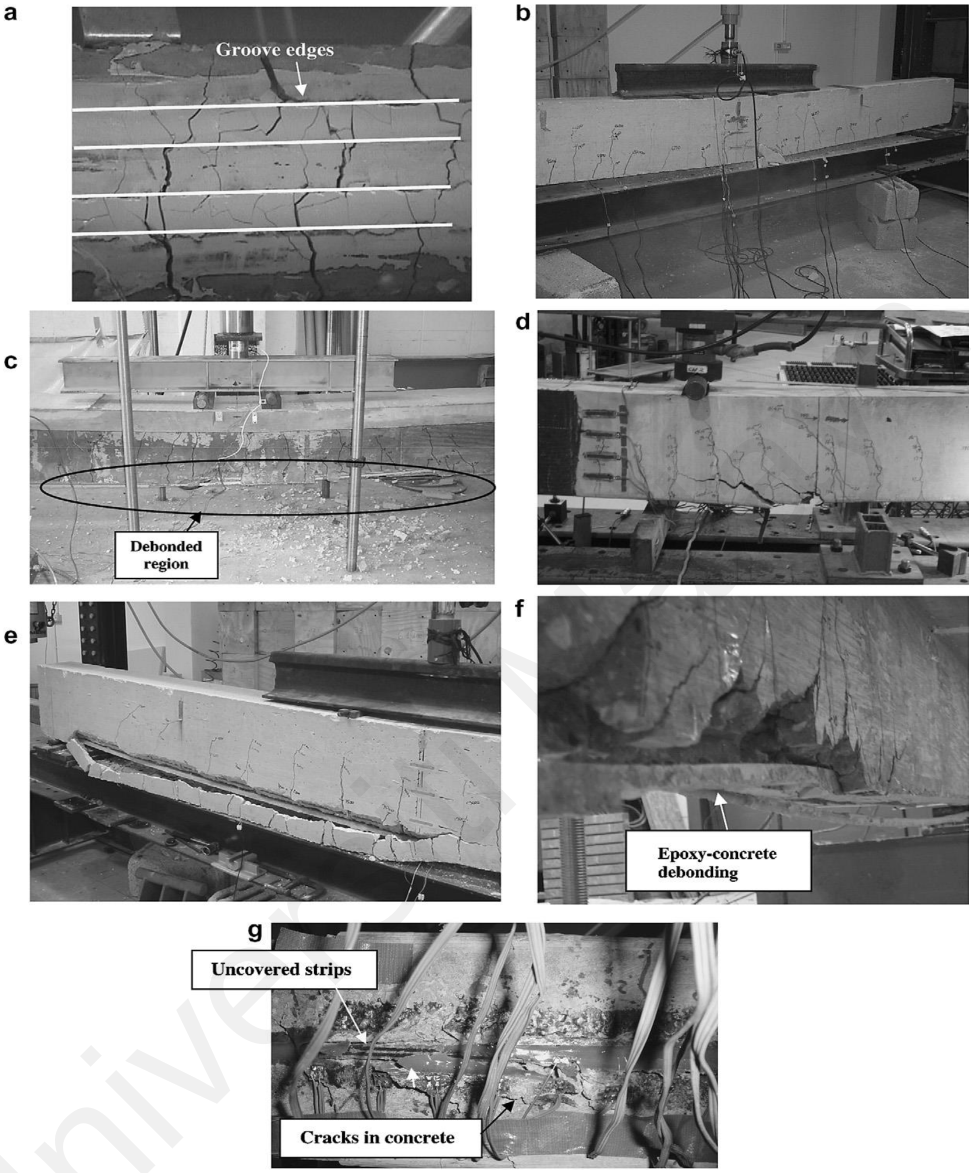

Figure 2.4: Failure mode of NSM technique (Lorenzis & Teng, 2007)

De Lorenzis and Teng (2007) observed seven debonding failure modes for RC beams flexurally-strengthened with NSM bars and strips. These seven modes are shown in Figure 2.4.

(a) Debonding at the bar-epoxy interface.

(b) Separation of concrete cover between two cracks in the maximum moment region.

(c) Separation of concrete cover over a large length of the beam.

(d) Separation of concrete cover starting from a cutoff section.

(e) Separation of concrete cover along the edge.

(f) Secondary loss of bond between epoxy and concrete.

(g) Secondary splitting of the epoxy cover.

The mechanics of debonding in beams strengthened with NSM systems is still not fully understood. Descriptions of failure modes in existing literature are often not sufficiently detailed to provide an understanding of the progression of the failure process. Based on the available experimental evidence in research works, the possible failure modes of beams flexurally strengthened with NSM FRP reinforcement are shown in Figure 2.4. The interaction between the main failure modes and the secondary failure modes are still unclear and deserve further investigation.

De Lorenzis and Teng (2007) have pointed out that a large number of parameters can affect the flexural behavior of RC beams with NSM FRP reinforcement, and thus further experimental and theoretical work is required, particularly to clarify the debonding failure mechanisms in the NSM reinforced beam. Also, the relationship between concrete cover separation and other modes of debonding that occur to the NSM FRP concrete joint, such as fracture at the epoxy and concrete interface and splitting of the epoxy cover, needs further research. Additionally, investigating the behavior of pre-damaged beams strengthened with NSM FRP would be significant especially in the practical field, as cracking and damage to the concrete cover may have a significant effect on the debonding failure process. De Lorenzis and Teng (2007) have also recommended that the relationship between bond failure mechanisms and debonding failure mechanisms in flexurally-strengthened beams be clarified through detailed experimentation and theoretical modeling. In such an investigation the interaction between flexural or flexural-shear cracking and bond stresses must be clarified for the development of numerical and analytical models to predict debonding failure.

2.10 Prestressed strengthening of prestressed concrete beams:

A limited number of studies have been conducted on prestressed strengthening of PC beams. Casadei et al. (2006) conducted a pilot research project on pre-damaged prestressed concrete I-girders to investigate the efficiency of prestressed NSM CFRP strengthening in restoring flexural strength and service performance. Three prestressed I-girders with longitudinal reinforcement tendons prestressed to 75% of yield strength were tested. Two beams were intentionally damaged and then repaired using EBR CFRP laminate for one beam and prestressed NSM CFRP bars for the other. The CFRP bars were prestressed to around 33% of their ultimate strength, which was calculated to restore the original level of prestress in the beam. The tests found that although both repair methods restored the ultimate capacity of the damaged beams, the prestressed NSM CFRP strengthened beam performed in a more ductile manner compared to the EBR CFRP strengthened beam. Prestressed NSM CFRP also improved performance in terms of symmetric behavior across the beam cross section at both service and ultimate conditions.

Kim et al. (2008) investigated the flexure behavior of prestressed concrete beams strengthened with prestressed CFRP sheets, focusing on ductility and cracking behavior. Structural ductility of a beam strengthened with CFRP sheets is critical, considering the abrupt and brittle failure of CFRP sheets themselves. Cracking may also affect serviceability of a strengthened beam and may be especially important for durability. Midscale prestressed concrete beams of 3.6 m in length are constructed and a significant loss of prestress is simulated by reducing the reinforcement ratio to observe the strengthening effects. The prestressed CFRP sheets result in less localized damage in the strengthened beam and the level of the prestress in the sheets significantly contributes to the ductility and cracking behavior of the strengthened beams. Consequently, the recommended level of prestress to the CFRP sheets is 20% of the ultimate design strain with adequate anchorages.

Reza Aram et al. (2008) tested four short PC beams to investigate the use of prestressed EBR CFRP strips for strengthening. However, no significant improvement in flexural behavior or strength was found, and the beams failed by premature debonding. The researchers concluded that prestressed strengthening may be more effective in long span beams than short beams.

Obaydullah et al. (2016) conducted an experimental study on strengthening prestressed beams using prestressed NSM steel strands. A total of seven prestressed beams were constructed for static testing, with one unstrengthened control beam, one beam strengthened with a non-prestressed NSM steel strand, and five beams strengthened with NSM steel strands prestressed to varying levels of their nominal tensile strength. Based on the results, applying prestress force provides an increase in load carrying capacity with corresponding higher concrete cracking and steel yielding initiations when compared to beams strengthened with no added prestress force. The influence of various prestress levels on the deflection of the tested beams was also assessed, and the relevant results were presented and discussed. The test results showed that the strengthened prestressed beam with a 70% prestressed steel strand performed better compared to the other strengthened beams.

2.11 Combination of Different Strengthening Techniques

Combining EBR and NSM (CEBNSM) is a recent advancement in structural strengthening which can enhance the effectiveness of strengthening and overcome some of the limitations of both techniques. A number of researchers have investigated the use of this technique on RC beams. Traplsi (2013) conducted an experimental program with four r.c. T beams strengthened with combined steel NSM and EBR GFRP fabric. All the beams were tested monotonically to failure. All the strengthened beams were failed by premature GFRP debonding and NSM delamination. The ultimate load of the combined strengthened specimens was increased from 53% to 156% over the control beam.

Lim (2009) examined the effectiveness of flexural strengthened RC T-beams with the combination of NSM and EBR techniques using CFRP strips (Figure 2.5). A total of nine T-beams were tested in two groups. The first group of specimens was strengthened with NS CFRP strips and the second group of specimens was strengthened with combined techniques used as a T shape CFRP strips. The test variables were spacing and number of NSM strips and the width and number of EBR strips. The experimental outcomes demonstrated that the combination of NSM and EBR strengthened specimens significantly improved the flexural capacity and stiffness over the NSM-CFRP strips strengthened specimens. The maximum enhanced flexural capacity was about 347% compared with the control specimen. Failure was initiated in the specimens strengthened with combined techniques by the debonding of EBR strips which succeeded the NSM strips partial separation along the longitudinal direction. Diagonal cracks appeared and propagated as the load increased. However, abrupt concrete cover separation failure has occurred in the shear region. The ultimate tensile strains measured in the NSM and EBR strips of the specimens strengthened with combined techniques were found to be about 8200-11600 $\mu\varepsilon$ and 7000-8900 $\mu\varepsilon$, respectively. Therefore, the combined strengthening techniques have a decent combination to defend the applied load and redistribute the total stress subjected to the EBR and NSM strips in the specimens.

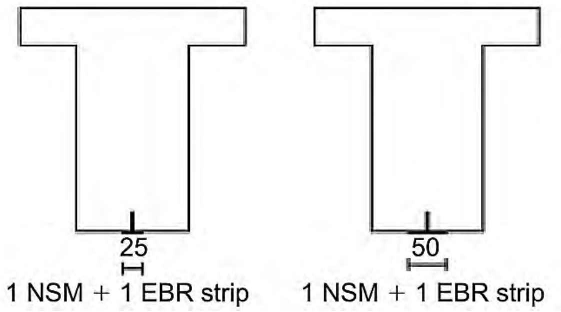

Figure 2.5: Rectangular and T-shaped CFRP strip (Lim, 2009)

Mostofinejad and Shameli (2013) studied the flexural responses of RC beam specimens strengthened by grooving method (GM) with the distinctive systems of externally bonded reinforcement on grooves (EBROG) and externally bonded reinforcement in grooves (EBRIG) which is the substitute of the traditional EBR technique. The test variables were strengthening techniques (NSM, EBR, EBROG and EBRIG) and the number of EBR sheets (1, 2 and 3). Thirty two beam specimens were divided into six groups; the first group comprised of control specimens, the second group contained of specimens strengthened by EBR technique without surface preparation, the third group confined of specimens strengthened by EBR technique with surface preparation, the fourth group comprised of specimens strengthened with NSM technique, the fifth group covered of specimens strengthened with EBROG method and the final group contained of specimens strengthened with EBRIG method using FRP sheets as shown in Figure 2.6. It was revealed that EBROG and EBRIG methods increased ultimate strength over the EBR and NSM techniques using multiple layers of FRP sheets. EBR, NSM, EBROG and EBRIG strengthened specimens were prematurely failed except EBROG and EBRIG methods with monolayer of sheet.

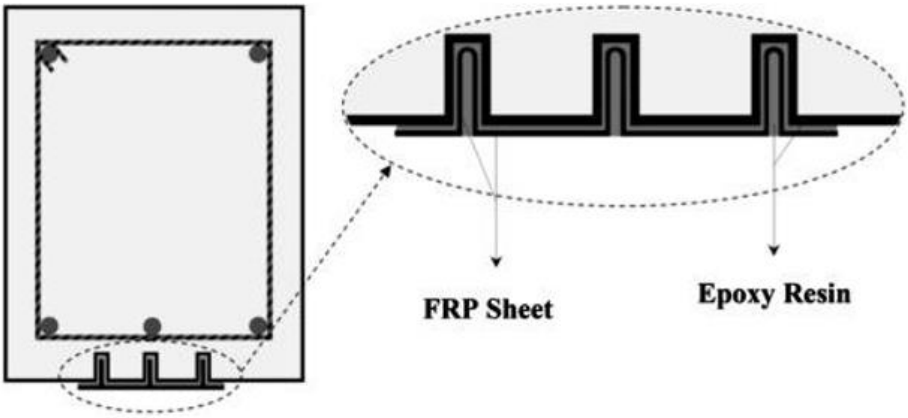

Figure 2.6: EBRIG method of strengthening (Mostofinejad & Shameli, 2013)

Rahman et al. (2015) addressed RC beam specimens flexurally strengthened with hybrid bonding technique using steel bars into the NSM grooves and plate in the tension face as an EBR. The experimental variables were the number of bars into NSM grooves and geometrical dimensions of the EBR plate. The ultimate load of the hybrid strengthened specimens were increased from 27% to 65% over the control specimen and all the strengthened specimens failed by the concrete cover separation (Figure 2.7). Moreover, increasing the number of NSM grooves adversely affected the effectiveness of this technique and ductility was reduced subsequently.

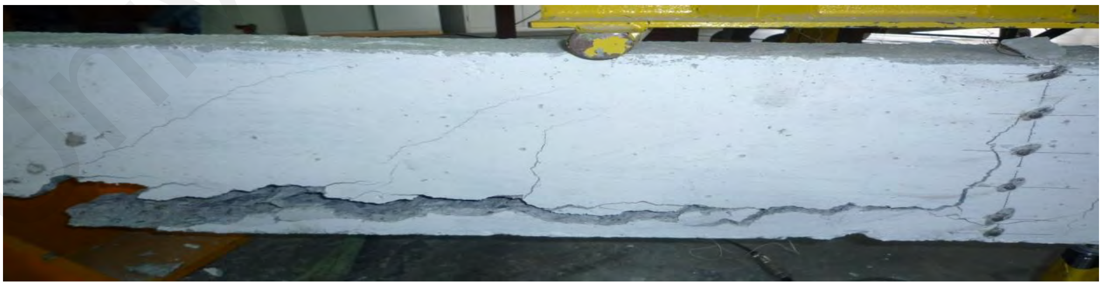

Figure 2.7: Typical failure mode for hybrid strengthened beam (Rahman et al. 2015)

Darain et al. (2016) investigated the experimental and analytical simulation of RC beam specimens strengthened with the combined externally bonded and near surface mounted (CEBNSM) technique utilizing CFRP bar and fabrics. The test variables were the diameter of the NSM bars and the number of fabrics layers in the EBR. The results exhibited that the CEBNSM strengthened specimens increased the ultimate load bearing capacity from 71% to 105% compared with the reference specimen. The premature end debonding was not fully eliminated (Figure 2.8).

Figure 2.8: Premature end debonding for CEBNSM strengthened beam (Darain et al. 2016)

Mathew et al. (2018) has carried out an experimental investigation on the behaviour of Reinforced Concrete Beams flexurally strengthened with combined EBR and NSMR. Experimental investigation aims at finding the failure load, deflection and ductility of RC beams which uses steel plates and steel bars as strengthening tools. The results exhibited that the combined strengthened specimens increased the ultimate load bearing capacity from 59% to 120% compared with the reference specimen. The premature end debonding was not fully eliminated.

These studies have found that flexural strength and performance of CEBNSM strengthened members were significantly enhanced, although premature debonding was not completely eliminated.

2.12 Finite Element Modeling on Strengthened Beams

Finite element analysis of FRP strengthened RC beams attracts attention of the researchers in the recent decades. Experimental analyses of the FRP strengthened structures are extremely costly and several uncertainties (construction error, mishandling, material property discrepancy) are involved during experiments which make the experimental results questionable. FEM provides an alternative approach to simulate the actual behavior of a strengthened structure under variable loading. Several researchers performed finite element analysis to confirm their experimental findings.

Hu et al., 2004 developed an FE model using ABAQUS to predict the ultimate capacity of FRP strengthened RC beams. Proper constitutive models were used to model the nonlinearities of the concrete, steel and FRP. Short and long beams are studied with low and high steel ratio to study the influence of beam length, reinforcement ratio and fiber orientation under uniformly distributed load. Only ¼ th of the beam was modeled where symmetric boundary condition was applied along two symmetric planes. The numerical results showed that beams with low steel ratio significantly affected with the length of beam. However, the high steel ratio did not exhibit such relation with beam length. The beam with high steel ratio displayed more cracks at the mid-span region, whereas the low steel ratio beams showed more cracks at the support area.

De Lorenzis et al., 2004 presented the mechanics of bond of NSM FRP bar with concrete using current and previous test results. They also developed a three-dimensional FEM model and calibrated with experimental results. The test variables of experimental test series were bar type, groove size, bonded length, and groove-filling material. The NSM reinforcement was modelled having two interfaces: the bar-epoxy and the epoxy-concrete interface which differed from the regular internal steel bar bond with concrete. The epoxy concrete interface was modeled with a Coulomb frictional model. On principle, the interface element has a relation with the traction and displacement. The concrete, epoxy, and FRP bar were all modeled with solid elements. After calibrating the FEM model with some of the experimental beams, it was capable to simulate the failure mode, ultimate load and the load-deflection behavior. Even this model gave the bond-slip behavior as output rather than an input.

Soliman et al., 2010 assessed flexural performance of RC beam strengthened by NSM-FRP bars. Displacement controlled nonlinear three-dimension FEM analysis was performed in ADINA software to observe the flexure behavior of the tested beam. Concrete, CFRP, and epoxy layers were modeled using eight node brick elements and steel bars were simulated with two node truss element. The general multi-axial stress–strain relations are derived from the nonlinear uniaxial stress–strain relation. After comparing the experimental and numerical findings, a parametric study was done which included the factors of internal steel reinforcement ratio, concrete compressive strength, bonded length and area, and the Young's modulus of NSM–FRP bars. Worthy agreement was established between experiment and analysis in terms of load–deflection and load–strain relationships, ultimate capacities, and modes of failure. Due to the full bond consideration between the adhesive and the FRP, the numerical model demonstrated 5% higher debonding strain compared to the experimental one.

Hawileh, 2011 developed three-dimensional nonlinear FEM model through ANSYS finite element software based on the experimental result of Al-Mahmoud et al., 2009. The nonlinear model predicts load-deflection and failure mode by measuring the effect of carrying capacity and response of NSM-CFRP strengthened RC beam under four-point bending test. Figure 2.9 showed the modelling strategy which counted the nonlinear constitutive concrete material property, yielding of steel reinforcement, cracking of the filler materials, bond slip of the steel and NSM reinforcements with the adjacent concrete surfaces, and bond at the interface between the filling materials and concrete. This experiment validated the numerical results with other researcher's experimental result. Validated model was used for further study of the effect of NSM bar type and size.

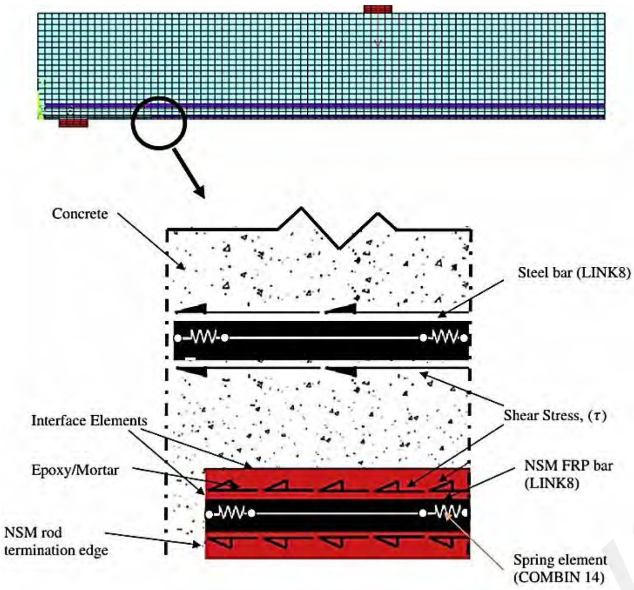

Figure 2.9: Detail modelling strategy of NSM bar and main reinforcement (Hawileh, 2011)

Zhang and Teng, 2013 described the interaction forces between RC beam and NSM bar. ABAQUS software had been used for FEM analysis. Maintaining the geometry, a quarter of the beam was modeled using eight-node brick element to save the computational cost. Both the analytical and FEM studies confirm the high interaction forces at bar end region due to the debonding failure. The authors described this approach as a generic solution which could be applicable to circular and elliptical shaped NSM bars.

Almusallam, 2013 tested NSM- Steel & GFRP flexure strengthened RC beams under monotonic load and nonlinear FEM analysis was conducted using LS-DYNA finite element program. Only half of the strengthened RC beam were modeled considering the overall beam geometry. Concrete and epoxy adhesive were modeled using 8-node solid hexahedron elements. The software can control the undesirable hourglass modes by applying three dimensional algorithms. The problem solving issue was dependent on explicit time integration algorithms and the displacement controlled operation fixed a pace rate of 1 mm/min to match with the experimental rate. The FE simulated failure mode was nicely matched with the experimental failures. The load-deflection curves were also in good agreement with a little variation (8% to 11%) of ultimate strength prediction.

Darain, 2016 experimentally investigated the structural behavior of CEBNSM strengthened beams. Finite element method (FEM) was also used to simulate the structural behavior of the strengthened beams using ABAQUS. The results simulated by the FEM model satisfactorily agreed with the load-deflection and strain values of the CEBNSM strengthened RC beams. The simulated damage pattern of the beams also matched well with the experimental beams (Figure 2.10).

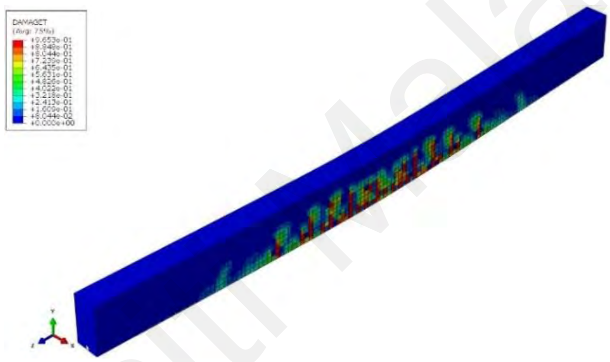

Figure 2.10: Typical tension damage behavior of CEBNSM beam (Darain, 2016)

2.13 Summary of Research Findings from Literature Review

Based on the review of existing literature presented above, the following conclusions can be drawn on the present condition of research on the strengthening of PC beams:

i. A very limited number of studies have been conducted on prestressed strengthening of prestressed concrete beams.

ii. Prestressing of the strengthening material engages a greater portion of the tensile capacity of the material, which increases the efficiency of the material in withstanding service and ultimate loads. Prestressed NSM strengthening improves serviceability in terms of reduced crack widths and deflection, and higher crack, yield and ultimate loads.

iii. Prestressed CFRP bars have been widely used as NSM strengthening on RC beams. However, very limited research has been done on the strengthening of PC beams using the prestressed NSM technique with CFRP bars.

iv. Steel offers a viable alternative strengthening material to CFRP. The main problem with the use of steel as strengthening reinforcement is the tendency of steel to corrode over time when there is a lack of adequate cover. However, steel is a readily available material and much more economical. Although steel may be prone to corrosion when exposed, with adequate cover and proper maintenance it has been shown to have long term durability. Steel also displays greater ductility and good bonding performance. Using the NSM technique, steel bars are protected from exposure by the epoxy-filled NSM groove in which the steel is embedded. However, there is limited research on the use of steel as an NSM strengthening material.

v. No research was found on the strengthening of PC beam using PNSM with steel strands.

vi. The effect of varying the level of prestress when using the PNSM technique to strengthen PC beams has also not yet been explored.

vii. When using the NSM method, it is often found that the width of the beam may be insufficient for the necessary amount of strengthening reinforcement due to the required edge clearance and clear spacing between two adjacent NSM grooves.

viii. EBR strengthening allows the use of greater amounts of strengthening material but is prone to premature debonding failure when the amount of EBR reinforcement exceeds certain limits.

ix. Most of the EBR and NSM strengthened beams were found to have failed by debonding while the PNSM strengthened beams failed flexurally.

x. To overcome the limitations of both the NSM and EBR techniques, while exploiting their advantages, researchers have proposed the use of a combined technique, the CEBNSM technique.

xi. The CEBNSM technique is a very recent development in research on strengthening techniques. These studies have found that the flexural strength and performance of CEBNSM strengthened beams were significantly enhanced, although premature debonding was not completely eliminated.

xii. At present, FEM models on various structural strengthening techniques have been developed by different researchers. FEM can be an effective tool to verify or predict the behavior of structural elements under applied load. A few researchers have developed FEM models for the CEBNSM technique.

This present study further develops the CEBNSM strengthening technique with the addition of PNSM to propose an innovative new strengthening technique, namely the CEBPNSM technique, which combines EBR with PNSM. The aim of this study is to develop the CEBPNSM technique as an efficient new strengthening solution to overcome the limitations of NSM, EBR and CEBNSM, and provide a possible solution for structures that require higher levels of strengthening. A FEM model was also developed using ABAQUS to verify the flexural responses of the strengthened specimens.

CHAPTER 3: RESEARCH METHODOLOGY

3.1 Introduction

This chapter will describe the experimental program and the numerical modeling procedures. The first section describes the experimental program. This consists of a description of the six groups of strengthened beams, as shown in Table 3.1. The specific dimensions and reinforcements of the prestressed concrete beams are also described, as well as the exact procedures followed in fabricating the prestressed beams. The properties of the various materials used to prepare and strengthen the PC beam specimens, namely concrete, steel reinforcing bars, steel prestressing strands, CFRP bars, CFRP plates, CFRP sheet and epoxy adhesive, are also presented in this section. The procedures followed in strengthening the beams using various strengthening techniques, namely EBR, NSM, PNSM, CEBNSM and CEBPNSM, are explained in detail. The prestressing setup used to prestress the PNSM reinforcement is presented here. The test setup and loading conditions are described, as well as the various instruments used, and the instrumentation and data collection procedures.

The second section describes the numerical modeling procedures. This consists of a description of how the numerical model was developed using the finite element software ABAQUS. The constitutive models for the various materials used and their properties are described. The discretization of the beam specimens into a finite number of elements and the creation of the 3D models of the beam specimens by meshing the finite elements according to the constitutive models of the various materials were also presented. The boundary conditions and loading conditions were also described.

3.2 Experimental Program

An experimental program was devised to investigate the structural performance of prestressed beams strengthened using various strengthening techniques, namely EBR, NSM, PNSM, CEBNSM and CEBPNSM, in order to achieve the objectives of this study.

3.2.1 Test Matrix

A total of thirty-two prestressed beams were tested based on the test matrix provided in Table 3.1. For comparison purposes, one control beam was left unstrengthened and three beams were strengthened using EBR strengthening, one with EBR CFRP sheet, one with EBR CFRP plate and one with EBR CFRP plate with end anchors. The remaining twenty-eight beams were divided into six groups for strengthening.

Group A contained a total of six prestressed beams. One prestressed beam was strengthened using an NSM CFRP bar with no prestressing force. The remaining five specimens were strengthened with PNSM CFRP bars prestressed to 30%, 40%, 50%, 60% and 70% of the tensile capacity of the CFRP bars. Each strengthened beam used one strengthening bar.

Group B also consisted of six prestressed beams. One prestressed beam was strengthened using an NSM steel strand with no prestressing force. The remaining five specimens were strengthened with PNSM steel strands prestressed to 30%, 40%, 50%, 60% and 70% of the tensile capacity of the strands. Each strengthened beam used one strengthening strand.

Group C had four prestressed beams. One beam was strengthened using the CEBNSM technique with one CFRP bar and a CFRP sheet. The remaining three beams were strengthened using the CEBPNSM technique with a combination of CFRP bar and CFRP sheet, and the levels of prestress used were 50%, 60% and 70% of the tensile capacity of the CFRP bar. Each strengthened beam used one CFRP bar and one CFRP sheet.

Group D also contained four prestressed beams. One beam was strengthened using the CEBNSM technique with one steel strand and a CFRP sheet. The remaining three beams were strengthened using the CEBPNSM technique with a combination of steel strand and CFRP sheet, and the levels of prestress used were 50%, 60% and 70% of the tensile capacity of the steel strand. Each strengthened beam used one steel strand and one CFRP sheet.

Group E had four prestressed beams. One beam was strengthened using the CEBNSM technique with one CFRP bar and a CFRP plate with end anchorage. The remaining three beams were strengthened using the CEBPNSM technique with a combination of CFRP bar and CFRP plate with end anchors, and the levels of prestress used were 50%, 60% and 70% of the tensile capacity of the CFRP bar. Each strengthened beam used one CFRP bar and one CFRP plate.

Group F also consisted of four prestressed beams. One beam was strengthened using the CEBNSM technique with one steel strand and a CFRP plate with end anchorage. The remaining three beams were strengthened using the CEBPNSM technique with a combination of steel strand and CFRP plate with end anchors, and the levels of prestress used were 50%, 60% and 70% of the tensile capacity of the steel strand. Each strengthened beam used one steel strand and one CFRP plate.

Table 3.1 Test Matrix

No.	Specimen ID	NSM Strengthening Material		Prestressing Force on NSM	EBR Strengthening Material	
		Type	Diameter (mm)	(% of Tensile Capacity)	Type	Dimensions (mm)
1	UB	Unstrengthened Beam		-	-	-
2	EBR-Sh	-	-	-	CFRP Sheet	2900×100×0.17
3	EBR-Pl	-	-	-	CFRP Plate	2900×50×1.2
4	EBR-Pl-A	-	-	-	CFRP Plate	2900×50×1.2
	Group A: Beams Strengthened with NSM CFRP Bars					
5	NSM-C-0%F	CFRP Bar	10	0%	-	-
6	NSM-C-30%F	CFRP Bar	10	30%	-	-
7	NSM-C-40%F	CFRP Bar	10	40%	-	-
8	NSM-C-50%F	CFRP Bar	10	50%	-	-
9	NSM-C-60%F	CFRP Bar	10	60%	-	-
10	NSM-C-70%F	CFRP Bar	10	70%	-	-
	Group B: Beams Strengthened with NSM Steel Strands					
11	NSM-S-0%F	Steel Strand	9.6	0%	-	-
12	NSM-S-30%F	Steel Strand	9.6	30%	-	-
13	NSM-S-40%F	Steel Strand	9.6	40%	-	-
14	NSM-S-50%F	Steel Strand	9.6	50%	-	-
15	NSM-S-60%F	Steel Strand	9.6	60%	-	-
16	NSM-S-70%F	Steel Strand	9.6	70%	-	-
	Group C: Beams Strengthened with NSM CFRP Bars and EBR CFRP Sheet					
17	NSM-C-0%F-Sh	CFRP Bar	10	0%	CFRP Sheet	2900×100×0.17
18	NSM-C-50%F-Sh	CFRP Bar	10	50%	CFRP Sheet	2900×100×0.17
19	NSM-C-60%F-Sh	CFRP Bar	10	60%	CFRP Sheet	2900×100×0.17
20	NSM-C-70%F-Sh	CFRP Bar	10	70%	CFRP Sheet	2900×100×0.17
	Group D: Beams Strengthened with NSM Steel Strands and EBR CFRP Sheet					
21	NSM-S-0%F-Sh	Steel Strand	9.6	0%	CFRP Sheet	2900×100×0.17
22	NSM-S-50%F-Sh	Steel Strand	9.6	50%	CFRP Sheet	2900×100×0.17
23	NSM-S-60%F-Sh	Steel Strand	9.6	60%	CFRP Sheet	2900×100×0.17
24	NSM-S-70%F-Sh	Steel Strand	9.6	70%	CFRP Sheet	2900×100×0.17
	Group E: Beams Strengthened with NSM CFRP Bars and EBR CFRP Plates					
25	NSM-C-0%F-Pl-A	CFRP Bar	10	0%	CFRP Plate	2900×50×1.2
26	NSM-C-50%F-Pl-A	CFRP Bar	10	50%	CFRP Plate	2900×50×1.2
27	NSM-C-60%F-Pl-A	CFRP Bar	10	60%	CFRP Plate	2900×50×1.2
28	NSM-C-70%F-Pl-A	CFRP Bar	10	70%	CFRP Plate	2900×50×1.2
	Group F: Beams Strengthened with NSM Steel Strands and EBR CFRP Plates					
29	NSM-S-0%F-Pl-A	Steel Strand	9.6	0%	CFRP Plate	2900×50×1.2
30	NSM-S-50%F-Pl-A	Steel Strand	9.6	50%	CFRP Plate	2900×50×1.2
31	NSM-S-60%F-Pl-A	Steel Strand	9.6	60%	CFRP Plate	2900×50×1.2
32	NSM-S-70%F-Pl-A	Steel Strand	9.6	70%	CFRP Plate	2900×50×1.2

Note: UB = Unstrengthened beam, NSM = NSM strengthening technique, S = Strengthened with steel strand, C = CFRP bar, F = Percentage prestressing force applied, Pl = CFRP Plate, Sh = CFRP sheet, EBR = EBR strengthening technique, A = End anchored

3.2.2 Beam Specifications

The beam dimensions were 150 mm width, 300 mm height, and 3300 mm length, with 3000 mm as the effective span and a shear span of 1250 mm. The beams were designed with top and shear reinforcement to avoid shear failure before failure of the strengthening system. Conventional deformed steel bars, 10 mm in diameter, were used to construct the beams. Two steel bars were used as longitudinal top reinforcement and two steel bars were used as bottom reinforcement. The steel bars for shear reinforcement were distributed along the shear zone of the beams with 75 mm spacing center to center. All the beams were cast with three seven-wire prestressing strands, 12.9 mm in diameter. Two strands were used in the tension zone and one in the compression zone.

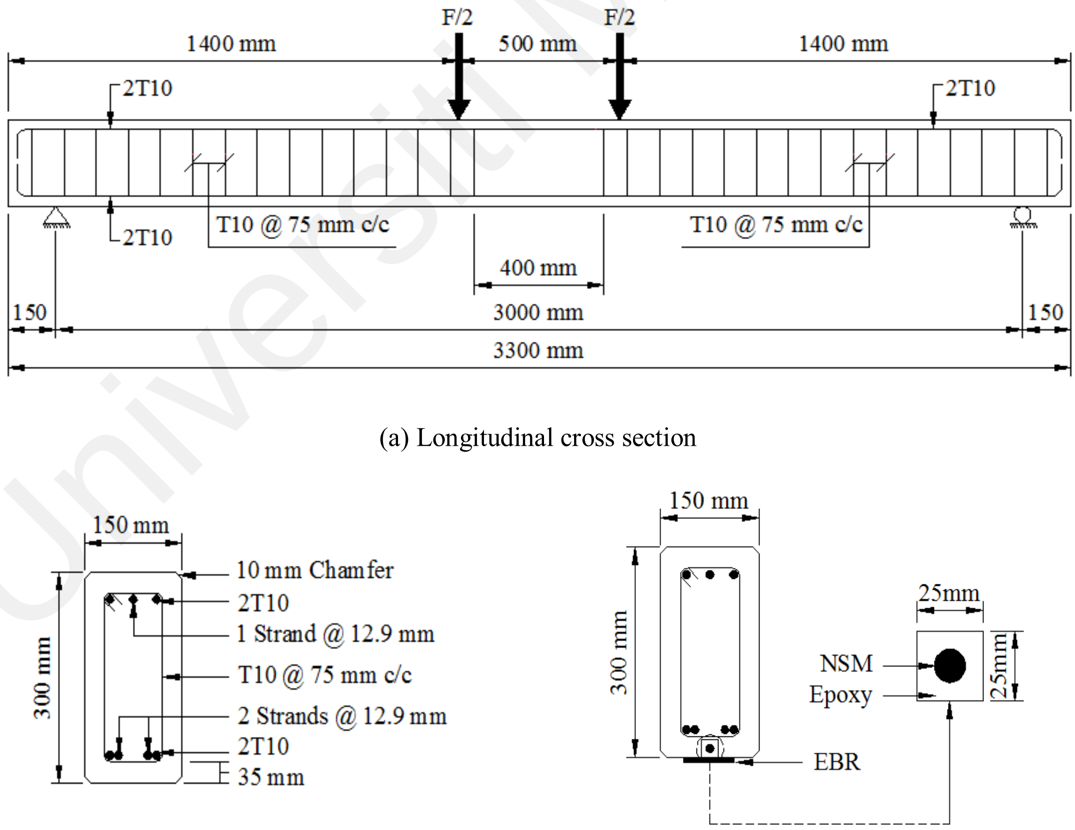

(b) Cross section of unstrengthened beam (c) Cross section of strengthened beam

Figure 3.1: Specimen Details

3.2.3 Beam Fabrication

All the prestressed beams were cast in the casting yard of Eastern Pretech Sdn Bhd, a reputable precast concrete company located in Kajang, Selangor, Malaysia. This was done in order to utilize the prestressing facilities and to ensure the quality of the prestressed beams was consistent in terms of prestressing force and material properties. The beams were carefully transported by factory lorry from the casting yard to the university laboratory and were found to be in good condition on arrival.

All thirty two prestressed beams were cast in a single pretensioning casting bed in one casting. The prestressed beams were produced using the long line pretensioning system developed by Hoyer, which is the usual system used by factories to mass produce pretensioned elements. The casting bed was basically a 120 meters long steel frame with two bulkheads, which were fixed at either end of the bed. One end served as the dead end with anchorage for the prestressing strands. The other end was the live end and was fitted with hydraulic jacks for tensioning the strands. The steel side walls of the casting mold were adjustable for varying beam width.

For the fabrication of the prestressed concrete beams used in this study, the steel bars as specified in the previous section were formed into steel cages according to the design and dimensions shown in Figure 3.1. After all thirty two steel cages were formed, they were placed in the casting bed. One steel side wall of the casting mold was fixed in place by welding to the steel floor of the casting bed between the two bulkheads. The steel cages were placed along the length of this steel side wall and then wooden dividers were placed between the steel cages to make each separate beam mold. The three prestressing strands were then passed through the steel cages and dividers. The prestressing strands were positioned according to the beam design shown in Figure 3.1. The prestressing strands were then anchored to the bulkheads with steel wedges and attached to the hydraulic jacks. The strands were tensioned by the hydraulic jacks and were stretched with constant eccentricity. Pressure gauges calibrated to the hydraulic jacks indicated the magnitude of force applied to the prestressing strands. All three strands were prestressed to 75% of their tensile capacity. To achieve this level of prestress, 139.5kN of force was applied to each of the strands. The elongation lengths of the strands were also manually measured to confirm that the prestressing force had been accurately applied. The steel wedge anchors in the bulkheads held the prestressing force after the force had been applied by the jacks, preventing the transfer of the force to the beams until the time of release.

After the strands had been prestressed, two 5mm strain gauges were mounted at the midspan of each of the beams on each strand in the tension zone to allow the strain in the tension reinforcement to be measured. Before installing the strain gauges, the two steel strands were cleaned properly using acetone to remove any dirt or dust that may have been present. After the strain gauges were attached, they were wired and care was taken to avoid any point of contact between the wires and the steel strands as this would have prevented the strain gauges from giving any reading. A multi-meter was used to check that the strain gauges were functioning after wiring. The strain gauges were then covered with silicone to protect them from moisture and damage during and after the concrete casting of the beams.

Then the other steel side wall of the casting frame was positioned alongside the prepared steel cages and fixed in place by welding. Both steel side walls had been prepared and lubricated beforehand by the casting yard. The molds were now complete and the beams were ready for concreting. High early strength concrete was mixed by the factory and used to cast the beams. The beams were cast sequentially one by one. The concrete was poured and simultaneously compacted using a vibration machine. Twelve cubes and three prisms were cast from the same batch of fresh concrete, in order to determine the compressive strength and flexural strength of the concrete. The next day after twenty four hours, when the concrete had hardened and reached the required minimum design compressive strength for prestress transfer, the prestress strands were simultaneously released using the hydraulic jacks, transferring the prestress force to the concrete beams. The prestressed beams were then demolded, the prestressing strands connecting the beams were cut and the beams separated. The prestressed beams were transported to the university lab seven days later. The whole beam fabrication process is shown in Figure 3.2 and Figure 3.3.

(a) Placing steel cages in casting mold

(b) Mold preparation

(c) Fixing strain gauges on strands

(d) Prestressing strands with steel wedge anchors

Figure 3.2: Fabrication of Prestressed Beams at Casting Yard

(a) Preparing concrete prisms and cubes

(b) Pouring concrete

(c) Concrete casting

(d) Compacting concrete with vibration

(e) After casting

(f) Demolding

Figure 3.3: Casting of Prestressed Beams at Casting Yard

3.2.4 Material Properties

The main materials used to fabricate the prestressed beam specimens were concrete, steel bars and prestressing steel strands. Additional materials used during strengthening of the beam specimens were carbon fiber reinforced polymer (CFRP) bars, CFRP plates, CFRP sheet and epoxy adhesive. Certain mechanical properties of the concrete and reinforcing steel bars used to fabricate the beams were determined in the laboratory. The properties of the CFRP bars, CFRP plates, CFRP sheet, prestressing steel strands and epoxy were obtained from their respective manufacturers. The mechanical properties of all the various materials used to construct the beam specimens are given in the following sections.

3.2.4.1 Concrete

High early strength concrete was mixed by the factory and used to cast the beams. The concrete mix was designed to obtain a characteristic concrete compressive strength of 50 MPa at 28 days. Crushed granite was used as coarse aggregate with a maximum size of 20 mm. Natural sand and crushed rock fines were used as fine aggregate. The water to cement ratio was 0.36. A superplasticizer, Glenium Ace 389, was also added to the concrete as a liquid admixture to improve early strength development and reduce curing time. Three concrete prisms and twelve concrete cubes were cast at the same time as beam casting for concrete testing purposes. The dimensions of the cubes were 100 mm × 100 mm × 100 mm. The prisms were 500 mm × 100 mm × 100 mm. The minimum concrete strength at the time of prestress transfer (when prestressing force was released and transferred to the beams) was 35MPa. This value was calculated based on design specifications of the prestressed beams and the level of force used to prestress the beams. This minimum concrete strength was required to ensure the beams were able to withstand the transfer of prestress force without damage to the concrete and without loss of bond between the concrete and steel prestressing strands. This minimum strength requirement was confirmed by testing three concrete cube specimens before transferring the prestress force. The 28 day concrete compressive strength was 50.1 MPa, an average value obtained by testing three concrete cube specimens. The flexural strength at 28 days was 5.5 MPa, a value obtained from testing the three concrete prisms. Concrete compressive strength was also tested at 7 days and 14 days. The concrete cube and prism test results are given in Appendix A.

3.2.4.2 Steel Bars

Deformed steel bars, 10 mm in diameter, were used for both the internal longitudinal reinforcement and as well as the shear reinforcement in the beams Figure 3.4. The deformed bars were tested in the laboratory for tensile strength to confirm the tensile properties supplied by the manufacturer. The yield strength of the steel bars was confirmed to be 516 MPa, and the ultimate strength was 587 MPa. The modulus of elasticity of the bars was 200 GPa, as provided by the manufacturer.

Figure 3.4: Steel bar used for specimen preparation

3.2.4.3 Steel Prestressing Strands

Seven-wire low relaxation Grade 270 prestressing strands were used for both the internal prestressed strands and the NSM reinforcement. The diameters of the internal prestressed strands were 12.9 mm. The strands used for NSM reinforcement were 9.6

mm in diameter. According to product specifications provided by the manufacturer, the tensile strength for both the 12.9 mm and 9.6 mm diameter seven-wire prestressing strands was 1860 MPa, and the modulus of elasticity was 195 GPa.

Figure 3.5: Steel prestressing strand used for specimen preparation

3.2.4.4 CFRP Bars

Pultruded CFRP bars with a circular cross section of 10 mm diameter were used as NSM reinforcement to strengthen some of the beams. According to product data provided by the manufacturer, the tensile strength of the bars was 1760 MPa and the modulus of elasticity was 135 GPa. The ultimate strain at breaking point was 1.7% and the density was 1.65 g/cm^3. The CFRP bars were sand-coated by the manufacturer to enhance bond performance.

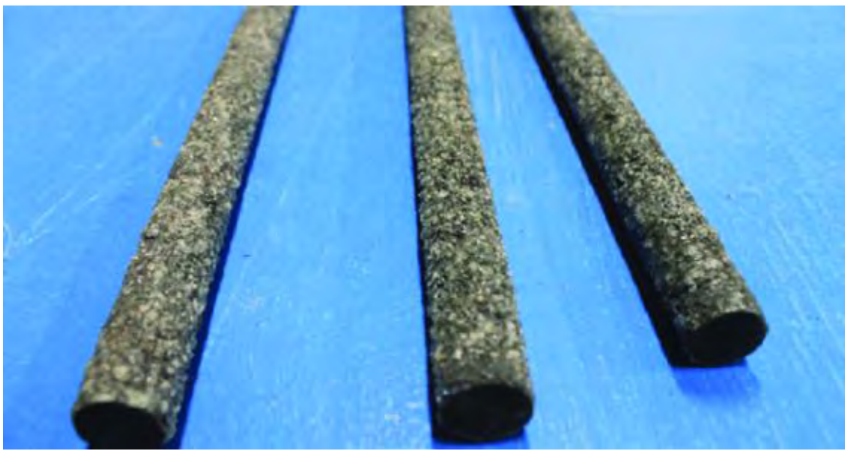

Figure 3.6: CFRP bars used for strengthening of beams

3.2.4.5 CFRP Sheet

SikaWrap 301C woven unidirectional carbon fiber sheet was used as a flexural strengthening material, as well as end anchorage material in preparing some of the beam specimens. Sikawrap 301C is designed for structural strengthening applications. The CFRP sheet came as a roll of fabric, 100 m in length and 500 mm in width. The required amounts of CFRP sheet were measured and carefully cut from the roll as needed using scissors. According to the manufacturer's product specifications, the thickness of the sheet was 0.167 mm and its density was 1.8 g/cm^3. The tensile strength and modulus of elasticity of the sheet were 4900 MPa and 230 GPa, respectively. The ultimate strain at break was 1.7%.

Figure 3.7: CFRP sheet used for strengthening of beams

3.2.4.6 CFRP Plates

Sika CarboDur S1012 pultruded CFRP plates was used as flexural strengthening material for some of the beam specimens. These plates are designed for structural strengthening purposes. The plates came in the form of a large roll, with a length 50 m and a width of 100 mm. The thickness of the plates were 1.2 mm. The required amounts of CFRP plate were cut from this roll as needed using a sharp bladed cutter. According to the manufacturer's specifications, the tensile strength of the CFRP plates was 2800

MPa and the modulus of elasticity was 160 GPa. The density of the plates was 1.6 g/cm^3 and the ultimate strain was 1.7%.

Figure 3.8: Roll of CFRP plate used for strengthening of beams

3.2.4.7 Epoxy Adhesives

Two different epoxy adhesives were used during strengthening of the beam specimens, namely Sikadur® 30 and Sikadur® 330. Sikadur® 30 was used for bonding the NSM steel strands, NSM CFRP bars, and EBR CFRP plates to the concrete substrate. Sikadur® 330 was used for bonding the CFRP sheet to the concrete substrate. These epoxy adhesives were chosen for their excellent mechanical properties, which include their high strength, high elastic modulus, high creep resistance, and very good bond strength.

Sikadur® 30 is a two component structural adhesive based on a combination of epoxy resins and special filler. It is designed for bonding structural reinforcement, particularly in structural strengthening works, to a variety of substrates such as concrete and timber. The two components, namely component A (white) and component B (black), are mixed in a ratio of 3:1. An electric low speed drill fitted with a mixing spindle is used to mix the epoxy at low speed to avoid entrapping air. The epoxy is mixed until a smooth consistency and uniform grey color is achieved. After mixing, the density of the epoxy is 1.65 kg/liter (at 23°C). The epoxy must be used immediately after mixing as it hardens quickly. The curing time for the epoxy to reach full strength is seven days. After being fully cured, the compressive strength of the epoxy is 95 MPa and the tensile strength is 31 MPa. The shear strength is 19 MPa and the modulus of elasticity is 11.2 GPa. The bond strength for steel was 21 MPa and for concrete was 4 MPa. These properties are according to the manufacturer's product data.

Sikadur® 330 is a two component epoxy based impregnating resin and adhesive. It is mainly used for applying CFRP sheet as reinforcement using the dry lay-up process. The two components, component A (white paste) and component B (grey paste), are mixed at low speed in a ratio of 4:1 by weight until a uniform light grey paste has formed. The density and viscosity of the epoxy after mixing (at 23°C) is 1.3 kg/liter and 6000 mPas, respectively. The pot life of the mixed epoxy is approximately one hour at 23°C, so it must be used immediately after mixing. The curing time for the epoxy to reach full strength is seven days. After seven days, the tensile strength of the epoxy is 30 MPa and the modulus of elasticity is 3.8 GPa. The elongation at break (ultimate strain) is 0.9% and the bond strength for concrete is 4 MPa. These properties have been provided by the manufacturer.

Figure 3.9: Mixing of epoxy adhesive

3.2.5 Strengthening Procedures

Strengthening of the beams was carried out after the beams were fully cured after twenty eight days. Five strengthening techniques were used in this research, namely the NSM technique, prestressed NSM technique, EBR technique, CEBNSM technique and CEBPNSM technique. Steel strands, 9.6 mm in diameter, and CFRP bars, 10 mm in diameter, were used for the NSM strengthening technique and the prestressed NSM technique. The effective length of the steel strands and the CFRP bars was 2900 mm. CFRP plates, 2900 mm × 50 mm × 1.2 mm, and CFRP sheet, 2900 mm × 100 mm × 0.167 mm, were used for the EBR strengthening technique. For the CEBNSM and CEBPNSM techniques, steel strands or CFRP bars were combined with CFRP plates or CFRP sheet. Epoxy adhesives were used to bond the strengthening materials to the concrete substrate of the beam specimens. All of the beams were inverted during strengthening. The specific procedures followed for each of the strengthening techniques are described in detail in the following sections.

3.2.5.1 Near Surface Mounted (NSM) Technique

The NSM technique basically involved cutting a groove into the concrete surface of the beam to be strengthened and then inserting and bonding the selected strengthening material into the groove. Two beam specimens were strengthened using only the NSM technique. However, the NSM technique was also used as part of the PNSM technique, CEBNSM technique and CEBPNSM technique. Thus, the following procedures were carried out on most of the beam specimens in this study.

Each beam specimen strengthened using the NSM technique had a single groove cut along the length of the soffit of the beam, spaced an equal distance from both sides. The depth and the width of the groove were both 25 mm, which was about 2.5 times the dimeter of the NSM strengthening material. NSM groove dimensions generally vary from 2 to 3 times the diameter of the selected reinforcement. Controlling factors for groove dimension include concrete cover, number of grooves, edge clearance and groove clear spacing. The groove must be large enough to accommodate the strengthening material and an adequate amount of epoxy adhesive for proper bonding to take place. However, care must be taken that the groove does not cut into existing internal reinforcements, and that there is adequate spacing between grooves and the edges of the beam. The groove dimensions of 25 mm width and depth were selected as appropriate for adequate concrete cover and epoxy bonding in the beam specimens in this study.

The NSM groove was cut along the whole length of the beam soffit, from one end to the other. A special concrete cutting system was developed in the lab to facilitate the ease, speed, accuracy and workmanship with which the NSM grooves were cut. Two parallel lines, 25 mm apart, indicating the groove to be cut, were first carefully marked on the concrete surface and then the beam was placed in the frame of the concrete cutting system. The diamond blade of the cutter was carefully adjusted to cut to the desired depth (25mm) and then concrete was cut along the parallel lines marked on the beam. The concrete between the two cut lines was then cut up with the cutter and any remaining concrete was removed with a hammer and hand chisel, creating a roughened inner surface for the groove. Throughout the cutting process, a hosepipe was connected to the diamond blade to provide a constant flow of water. The water dampened the dust generated from cutting the concrete and cooled the cutting blade, preventing overheating. The groove was cleaned using a wire brush, high pressure air jet and vacuum to remove any debris, dust, and foreign particles. Acetone was used to wipe the groove to remove any grease and remaining particles. The final groove was clean and dry, with a rough inner surface free of any laitance, contaminants or other bond inhibiting materials. These steps were taken to ensure the quality of the bond between the epoxy adhesive and the concrete.

The strengthening material (steel prestressing strand or CFRP bar) and the epoxy adhesive were then prepared for placement in the NSM groove. The steel strands were cleaned with acetone to remove any possible contaminants. Sikadur® 30 was used as the epoxy adhesive for NSM strengthening. The epoxy adhesive was mixed according to the manufacturer’s instructions. The prepared groove was then two-thirds filled with epoxy using a spatula. The prepared NSM reinforcement was gently pressed into the epoxy filled groove until the epoxy flowed around and covered the reinforcement. The NSM reinforcement was placed to ensure a minimum of 10 mm clear cover from the soffit of the beam. More epoxy was used to fill the groove and the surface was levelled. The NSM strengthening was allowed to cure for seven days to achieve full strength. Testing or any further strengthening was carried out after this curing period.

(a) Cutting groove with diamond cutter blade

(b) Removing dirt from groove by air jet

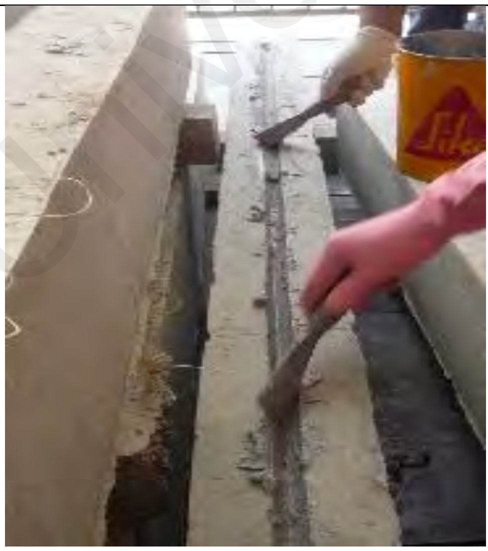

(c) Applying epoxy in groove

(d) Pressing NSM into epoxy in groove

Figure 3.10: NSM strengthening procedures

3.2.5.2 Prestressed Near Surface Mounted (PNSM) Technique

The PNSM technique was basically the NSM technique with the addition of prestress force to the NSM reinforcement. The PNSM reinforcement was prestressed before inserting in the groove and bonding with epoxy adhesive. A total of ten beams were strengthened using the PNSM technique, five with steel strands and five with CFRP bars.

A special prestressing setup was used to facilitate the safe release of prestressing force in the strengthening material. This setup consisted of a heavy steel frame, clamp, anchors, adjuster screw (for beam leveling and positioning), and a hydraulic jack, which was used to prestress the strengthening material. After the groove was prepared, the inverted beam was placed in the frame of the prestressing setup. The strengthening material (steel strand or CFRP bar) was placed above the groove, attached to the hydraulic jack and fixed to the prestressing frame with anchors. At this stage, the length of the strand or bar was kept longer than the length of the beam to facilitate prestressing. The hydraulic jack was then used to tension the strengthening material to the desired level of prestress. The level of prestress in the strengthening reinforcement was varied from 30% to 70% of their tensile capacity. A pressure gauge calibrated to the hydraulic jack indicated the magnitude of force applied to the reinforcement. Once the desired level of force was reached, the clamp was tightened to lock the system. The elongation length of the strengthening reinforcement was also manually measured to confirm the applied force.

After the application of prestressing force to the strengthening material, the groove was two-thirds filled with epoxy (Sikadur® 30). The position of the beam was then adjusted using the adjuster screw to slightly raise the level of the beam in the steel frame. The beam was gradually raised until the prestressed strengthening material was positioned in the epoxy filled groove. As the prestressed reinforcement was placed in the groove in this manner, it lightly pressed into the epoxy, forcing the epoxy to flow around and cover the strengthening material. The prestressed NSM reinforcement was placed to ensure a minimum of 10 mm clear cover from the soffit of the beam. Additional epoxy was used to fill the groove and then the surface was levelled.

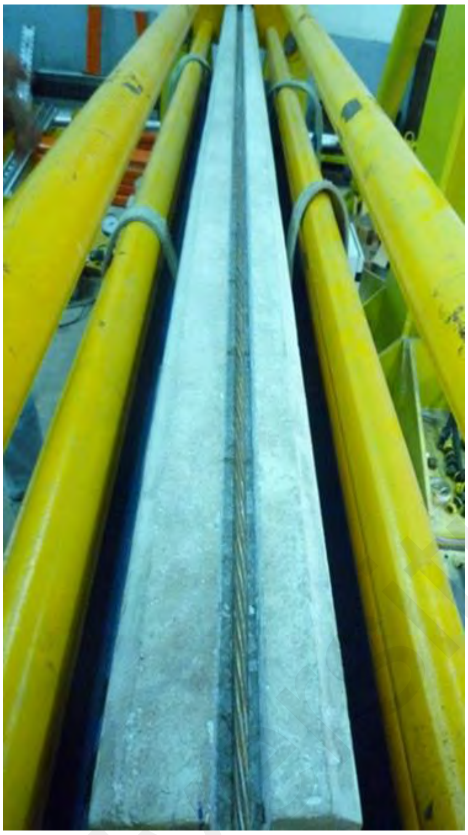

(a) During prestressing of NSM

(b) After prestressing

(c) Live end with hydraulic jack

(d) Dead end anchor

Figure 3.11: NSM prestressing setup

The epoxy was allowed to cure for at least six days before the prestressing force was released (Badawi, 2007). To release the prestressing force, the clamp and hydraulic jack were slowly loosened to gradually transfer the prestressing force to the beams through the epoxy. Using the pressure gauge, about 20% of the prestressing force was released at a time until the prestressing force was fully released. The anchors were finally removed, and the strengthening reinforcement was cut along the beam sides. The specimen was allowed to cure for one more day (seven days in total) before testing or any further strengthening work.

3.2.5.3 Externally Bonded Reinforcement (EBR) Technique

The EBR strengthening technique was basically involved the bonding of a strengthening plate or sheet to the external face of the soffit of the beam using an epoxy adhesive. Three of the prestressed beam specimens were strengthened using the EBR technique. One beam was strengthened using externally bonded CFRP sheet, one beam was strengthened using externally bonded CFRP plate without end anchors and one beam was strengthened using externally bonded CFRP plate with end anchors (to prevent plate debonding).

The concrete surface to which EBR strengthening material (CFRP plate or CFRP sheet) was applied required special mechanical preparation to ensure proper bonding between the concrete substrate and the strengthening material. The concrete surface was ground using a concrete grinder with diamond blade and abrasive blast cleaning equipment to remove cement laitance, any loose and friable materials and to expose the texture of the coarse aggregate in the concrete so as to achieve a profiled and open textured surface. The prepared surface was brushed, vacuumed, air blasted, and wiped with acetone to remove any remaining contaminants such as dust, foreign particles, cement laitance, oil, grease, etc., which could adversely affect or inhibit the bond between the strengthening material and the concrete. The final open textured surface was clean, dry, sound, and free of any damaged concrete, loose particles, contaminants or any other bond inhibiting materials.

EBR strengthening with CFRP sheet was carried out following the standard dry lay-up practice to bond the CFRP sheet to the prepared concrete surface of the beam. The epoxy adhesive Sikadur®330 was used as both substrate primer and impregnation resin for the CFRP sheet. The epoxy adhesive was prepared according to the manufacturer's instructions. The prepared concrete surface was then primed and saturated with the epoxy to seal the concrete and promote bonding. Proper care was taken to fill up any small voids in the concrete surface while spreading the epoxy with a spatula to ensure the quality of the bond between the concrete substrate, the epoxy and the CFRP sheet. The amount of epoxy spread over the surface was around 1.5 kg/m^2 as recommended by the manufacturer. The dry CFRP sheet, which had been cut to the required size beforehand, was then placed directly on the epoxy saturated concrete surface with the CFRP fibers placed in the longitudinal direction. The sheet was gently and firmly smoothed onto the concrete in the same direction as the fibers using a special plastic impregnation roller provided by the manufacturer. This was done until the adhesive was squeezed out through the fibers and the sheet was completely saturated with epoxy. Any air bubbles were squeezed out using the roller to ensure good bonding. The epoxy was allowed to cure for at least seven days before testing.

In the case of EBR strengthening with CFRP plate, the epoxy adhesive Sikadur®30 was used to bond the strengthening material to the surface of the concrete beam. The concrete surface was prepared as explained above. The surfaces of the CFRP plate were wiped clean with acetone to remove any dust or grease, and allowed to completely dry. The epoxy adhesive was prepared according to the manufacturer's instructions. The epoxy was applied onto the prepared surfaces and spread so that it was approximately 1 mm thick on the sides and 2 mm thick in the middle, as per the manufacturer's instruction. Proper care was taken to fill up any small voids in the concrete surface to ensure good bonding between the epoxy, concrete substrate and CFRP plate. The CFRP plate was then placed onto the epoxy covered concrete surface. A special hard rubber roller provided by the manufacturer was used to press the plate firmly onto the substrate until the epoxy was forced out on both sides of the plate. This excess adhesive was removed and disposed of before allowing the epoxy to cure. The epoxy was allowed to cure for at least seven days before testing or further strengthening work, as recommended by the manufacturer.

The EBR strengthened beam with CFRP plate without end anchorage was found to fail prematurely due to plate end debonding. Additional end anchorage was used to prevent end debonding of the CFRP plate in the EBR strengthened beam. CFRP sheet, 250 mm in width, was used to wrap the ends of the CFRP plate strengthened beam in a U-shape (Badawi, 2007). This end anchorage was placed 100mm from the location of the support. The CFRP U-wrap was affixed to the strengthened beam using the same procedures used for EBR strengthening with CFRP sheet. This involved the proper preparation of the concrete surfaces to which the CFRP U-wrap would be attached and the use of epoxy adhesive for bonding. The arrangement of the CFRP U-wrap end anchors is shown in the figure below.

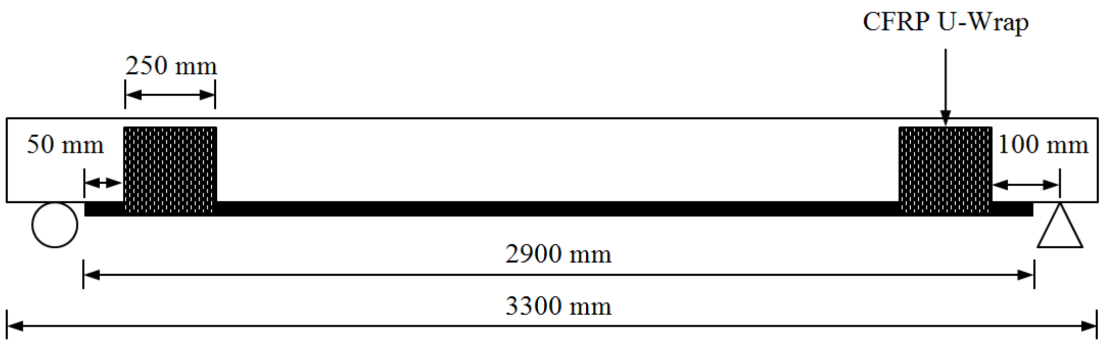

Figure 3.12: CFRP U-Wrap as end anchorage to prevent plate debonding

3.2.5.4 Combination of EBR and NSM (CEBNSM) Technique

The CEBNSM technique, as indicated by its name, is simply a combination of the EBR and NSM techniques. Four prestressed beams were strengthened with the CEBNSM technique. One beam was strengthened with EBR CFRP plate and NSM steel strand. Another beam was with EBR CFRP plate and NSM CFRP bar. Another was with EBR CFRP sheet and NSM steel strand. The last was with EBR CFRP sheet and NSM CFRP bar. (Please refer to Table 3.1 Test Matrix – these are beams NSM-S-0%F-Pl-A, NSM-C-0%F-Pl-A, NSM-S-0%F-Sh and NSM-C-0%F-Sh, respectively. These beams had 0% prestress force.) The beams with CFRP plate as EBR reinforcement also had CFRP U-wrap end anchorage to prevent end debonding.

For the CEBNSM technique, the beam was first strengthened using the NSM technique and then the EBR technique, following the strengthening procedures that have been outlined in the previous sections. After the NSM strengthening had been completed, the beam was allowed to cure for seven days as per the instructions of the manufacturer. The EBR strengthening was carried out after this curing period. The EBR reinforcement was placed over the cured NSM reinforcement. The concrete surface preparation and epoxy application for the EBR reinforcement followed the same procedures as explained previously for the EBR technique. The surface of the cured epoxy of the NSM reinforcement was lightly grinded to level out the surface of the beam soffit and produce a rough surface for good bonding. After the EBR reinforcement was completed, the CEBNSM strengthened beams were not disturbed for at least seven days to allow proper curing to take place. CFRP U-wrap end anchorage was affixed to the beams with CFRP plate reinforcement after this curing period. Testing was carried out on the strengthened beams after they were fully cured.

(a) Beam strengthened with a combination of NSM steel strand and CFRP sheet

(b) Beam strengthened with a combination of NSM steel strand and CFRP plate and with end anchorage

(c) Beam strengthened with a combination of NSM CFRP bar and CFRP plate (before CFRP plate installation)

(d) Beam strengthened with a combination of NSM CFRP bar and CFRP plate

Figure 3.13: Beams strengthened with CEBNSM technique

3.2.5.5 Combination of EBR and PNSM (CEBPNSM) Technique

The CEBPNSM technique combines the EBR technique with the PNSM technique. Twelve prestressed beams were strengthened using CEBPNSM technique. These twelve beams can be divided into four groups based on the strengthening materials used, namely (i) steel strand and CFRP plate, (ii) CFRP bar and CFRP plate, (iii) steel strand and CFRP sheet, and (iv) CFRP bar and CFRP sheet. Each group had three specimens with 50%, 60% or 70% prestress force in the NSM reinforcement. The beams with EBR CFRP plate were end anchored to prevent end debonding

In the CEBPNSM technique the same procedures were followed as in the CEBNSM technique with the addition of prestressing of the NSM reinforcement. The prestressing of the NSM reinforcement was carried out following the procedures detailed for the PNSM technique. After PNSM strengthening, the beams were strengthened with EBR reinforcement and end anchorage was applied to the beams with CFRP plates. Appropriate curing times were allowed between the various strengthening techniques and the final CEBPNSM strengthened beams were allowed to cure for at least seven days to achieve full strength before testing.

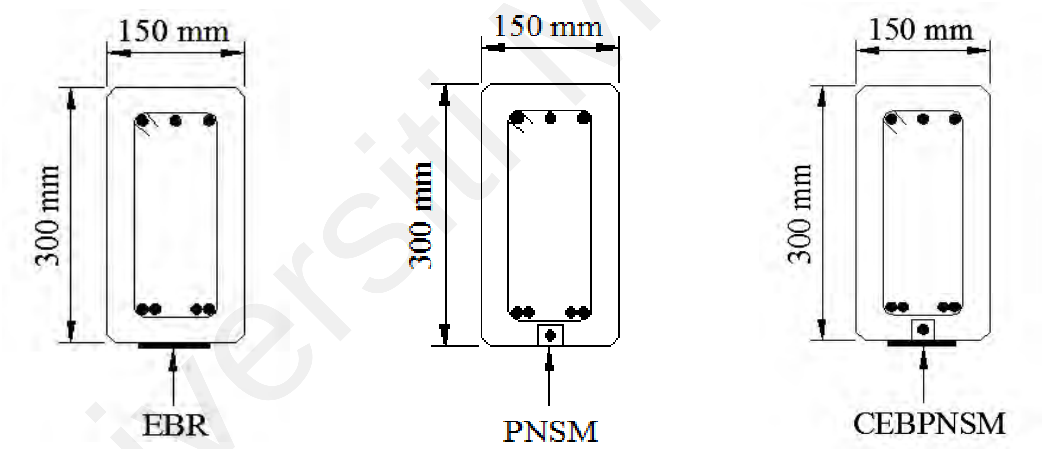

Figure 3.14: CEBPNSM strengthening system

3.2.6 Instrumentation

A number of instruments were used to capture and record accurate and reliable data on the structural behavior of the beam specimens during testing. These instruments were used to measure deflection, strain and cracking.

A Linear Variable Differential Transducer (LVDT) with a working transverse range of 100 mm was used to measure the deflection of the beam at midspan. The LVDT was positioned, with the help of a magnetic stand, under the beam at midspan such that it touched the soffit of the strengthened beam. The LVDT was manufactured by TML. In addition to the LVDT, the deflection at midspan was also measured manually using a conventional ruler, especially after failure initiation of the beams to avoid damaging the LVDT. This data is useful for understanding the ductility and deformability of the tested beams.

Electrical resistance strain gauges were used to measure the strains in the internal prestressed strands, NSM reinforcement, EBR reinforcement and concrete. The strain gauges were manufactured by TML and Kyowa Electronic Instruments. Strain gauges of 5 mm length were attached to the middle of the internal strands and the NSM reinforcement to record the strain profile. The NSM CFRP bars were lightly grinded at the center to smoothen the surface before attaching the strain gauges. Acetone was used to wipe the surfaces of the steel strands and the grinded CFRP bars, and then liquid super glue was used to attach the strain gauges. After the glue had set, the strain gauges were wired, the connection checked with a multi-meter, and silicon was applied on the strain gauges to protect them from moisture. Two 30 mm strain gauges were placed at the middle of the top face of the concrete beam to measure the concrete compressive strains. The concrete surface where the strain gauges were to be attached was lightly grinded and cleaned with acetone. Then the strain gauges were fixed in place using fast setting adhesive. Strain gauges of 30 mm length were also attached, using liquid super glue, to the middle of the bottom face of the EBR reinforcement to measure tensile strains in the EBR material.

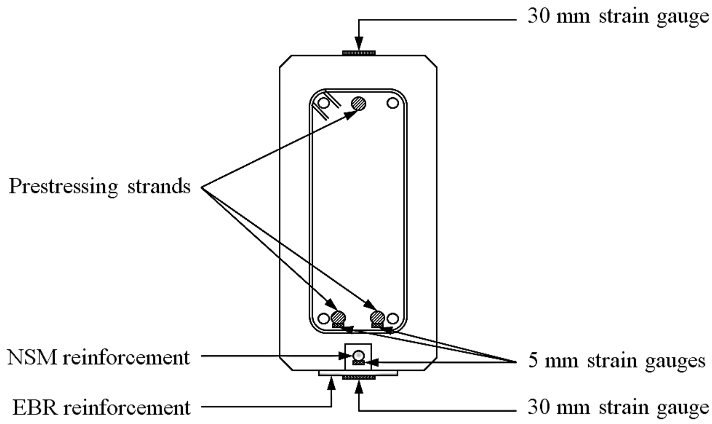

Figure 3.15: Placement of strain gauges

A portable data logger was used to scan and record the load, displacement and strain readings from their respective instruments, specifically the digital controller of the testing machine, the LVDT, and the strain gauges. The instruments were connected to the data logger by wiring. The instruments were scanned and the data recorded at a time interval of one second. The data logger was manufactured by TML and the model number was TDS-530.

Figure 3.16: Data logger

Figure 3.17: Digital microscope with laptop

A Dino-lite digital microscope was used to measure crack widths during testing. The microscope was manufactured by AnMo Electronics. This device can be used to measure crack widths with an accuracy of up to 0.001 mm. The microscope was operated with a software, DinoCapture 2.0, which was installed on a laptop. The microscope's adjustable lens allowed sharp pictures of the cracks to be taken which were transferred in real time to the laptop. The images were later processed by the software to accurately estimate the widths of the cracks. All crack widths were measured along the level of the tension reinforcement in the beams. However, the spacing of the cracks along the beam length was measured manually using a conventional ruler. Crack propagation was visually traced and marked with a marker on sides of the beam specimen.

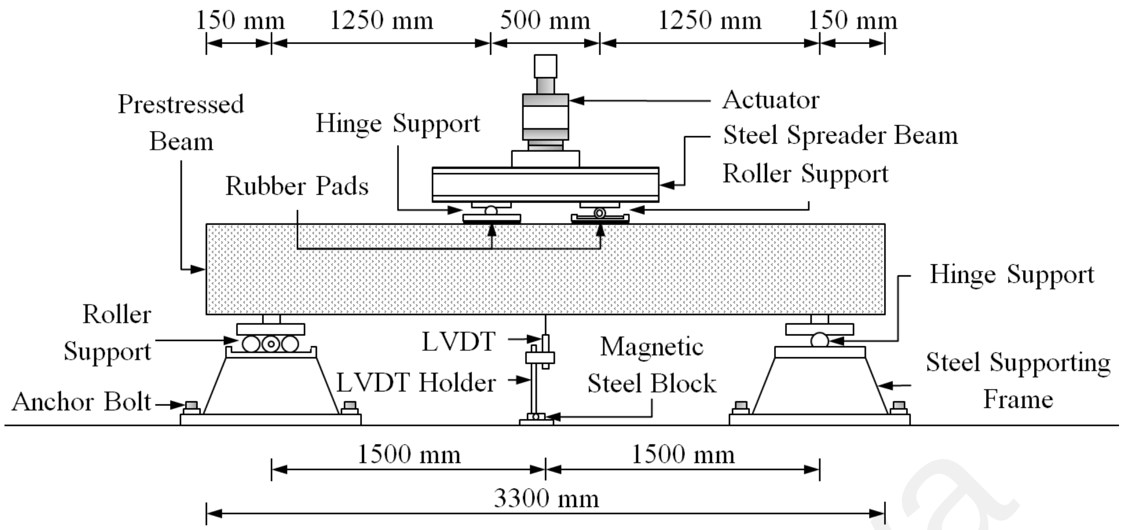

Figure 3.18: Schematic of test setup

3.2.7 Test Setup

All beam specimens were tested under monotonic load conditions using four point loading. The beams were placed on steel frames with roller and hinge support, and simply supported for an effective span of 3000 mm. The tests were conducted with a closed-loop hydraulic Instron Universal testing machine of 500 kN capacity. The monotonic load was directed through the hydraulic actuator of the testing machine and reacted against the steel supporting frames, which were anchored to the laboratory's solid floor. The load was distributed equally by a steel spreader beam which transferred the applied load to the beam through two steel supports with rubber pads. The distance between the two loading points of the spreader beam was 500 mm. During testing the actuator was loaded at a low rate so that readings from the data logger and crack measurement could be done easily. Loading was controlled in two ways during testing. Firstly, applied force was controlled until close to the yield capacity of the beams, and, secondly, displacement was controlled from yield until failure of the specimens. The rate of the actuator was set to 5kN/min during load control and 1.5 mm/min during displacement control. Loading was controlled in these two ways in order to complete the tests efficiently and obtain a full history of the flexural behavior of the beam specimens. Test data was recorded at regular intervals by taking the readings from the data logger, and measuring crack widths, crack spacing and deflection. The beam specimens were tested until complete failure, which was indicated by a rapid drop in loading and a sudden large increase in deflection.

Figure 3.19: Photo of test setup

3.3 Finite Element Modelling

Finite element modelling is a process of approximation for continuum problems that are separated into a finite number of interrelated portions or elements. A certain number of parameters are used to specify the behavior of each finite element, which has a displacement function associated with it. All the interrelated elements are linked to each other, directly or indirectly, through common interfaces, with nodes, borderlines, and/or surfaces. The solution to the system will be finite if the system behaves as a complete system. This occurs when all the elements follow the same rule as the standard discrete problem. The conduct of a specific node in a structure can be discovered through the stress-strain relationship of the material that makes up the structure. The conduct of each node is described by a set of equations which form a series of algebraic equations that are ideally rendered in matrix notation.

For this research, a 3D finite element model (FEM) was constructed to conduct a numerical analysis to authenticate the experimental results. ABAQUS, a commercial software, was employed to create the model and study the beams. The FEM model was utilized to examine the failure mode, ultimate load and load-deflection behavior of selected beams.

3.3.1 General Modelling Procedure

There are two methods utilized in FEM, specifically a) the force or flexibility method and b) the displacement or stiffness method. For the first approach, the forces are considered to be unknown and the governing equations are formed using the equilibrium with the rest of the associated equations. In the second approach, the displacement at the node is considered to be unknown. The element linked via a common node prior to loading will stay linked after loading with deformation. Thus, the equilibrium equation as well as the relating force to displacement are used to determine the governing equation in terms of the displacement. The following steps should be implemented to obtain the solution of any FEM problem:

Step 1: Discretize and Select the Element Types

Firstly, the structure must be divided into an equivalent system of many finite elements with connected nodes, and the most suitable element types must be selected for each constitutive material. There are different types of elements, such as the primary line element (bar or truss and beam element), two-dimensional element (triangular and quadrilateral), and tetra-hedral and hexahedral brick elements. On the condition that the geometry or loading are symmetric about an axis, the axisymmetric element can be used. This is formed through revolving a triangle or quadrilateral about a fixed axis.

Step 2: Select a Displacement Function

An appropriate displacement function is selected for each element. In the case of a two-dimensional element, this function is the relationship between the coordinates of its plane (e.g. the x-y plane).

Step 3: Define the Strain/Displacement and Stress/Strain Relationships

In the process of determining the equation for each finite element, the stress-strain or strain-displacement relationships are significant. For example, in the x direction there is a strain ε_x which is related to the displacement u in equation 3.1.

$$\boldsymbol{\varepsilon_x = \frac{du}{dx}} \tag{3.1}$$

Step 4: Derive the Element Stiffness Matrix and Equations

The direct equilibrium method determines the nodal force and displacement using the stiffness matrix and the corresponding element equation. Alternatively, an easier technique is to develop the stiffness matrix and equations for two- and three-dimensional elements through a work or energy method. Common methods that are utilized for forming the element equations include the principle of virtual work (using virtual displacements), the principle of minimum potential energy, and Castigliano's theorem. Weighted residuals (popularly known as the Galerkin's method) is another method for deducting the element equations. This method constructs results that are close to the energy method. This is particularly advantageous when a functional such as potential energy is not easily obtainable. The weighted residuals method enables the finite element method to be used directly for any differential equation.

The elementary stiffness matrix (equation 3.2) is as shown below (equation 3.3)

$$\begin{Bmatrix} f_1 \\ f_2 \\ f_3 \\ \vdots \\ f_n \end{Bmatrix} = \begin{bmatrix} k_{11} & k_{12} & k_{13} & \dots & k_{1n} \\ k_{21} & k_{22} & k_{23} & \dots & k_{2n} \\ k_{31} & k_{32} & k_{33} & \dots & k_{3n} \\ \vdots & & & & \vdots \\ k_{n1} & & & \dots & k_{nn} \end{bmatrix} \begin{Bmatrix} d_1 \\ d_2 \\ d_3 \\ \vdots \\ d_n \end{Bmatrix} \tag{3.2}$$

$$\{f\} = [k]\{d\} \tag{3.3}$$

where {f} is the vector of element nodal forces, [k] is the element stiffness matrix, and {d} is the vector of unknown element nodal degrees of freedom or generalized displacements, n.

Step 5: Assemble the Element Equations to Obtain the Global or Total Equations and Introduce Boundary Conditions.

The superposition method (direct stiffness method) allows the combination of the discrete element equations formulated in step 4, which are derived from the nodal force equilibrium to obtain the overall equations for the whole structure. Equation 3.4 represents the concluding accumulated or global equation in the matrix format.

$$\{\boldsymbol{F}\} = [\boldsymbol{K}]\{\mathrm{d}\} \tag{3.4}$$

Step 6: Solve for the Unknown Degrees of Freedom (or Generalized Displacements).

Equation 3.4 is altered through adjusting the boundary conditions, forming equation 3.5. It presents a new set of equations in their corresponding matrix form

$$\begin{Bmatrix} \boldsymbol{F_1} \\ \boldsymbol{F_2} \\ \boldsymbol{F_n} \end{Bmatrix} = \begin{bmatrix} \boldsymbol{K_{11}} & \boldsymbol{K_{12}} & \boldsymbol{K_{1n}} \\ \boldsymbol{K_{21}} & \boldsymbol{K_{22}} & \boldsymbol{K_{2n}} \\ \boldsymbol{K_{n1}} & \boldsymbol{K_{n2}} & \boldsymbol{K_{nn}} \end{bmatrix} \begin{Bmatrix} \boldsymbol{d_1} \\ \boldsymbol{d_2} \\ \boldsymbol{d_n} \end{Bmatrix} \tag{3.5}$$

where n is the total number of unknown nodal degrees of freedom of the structure. An elimination method like Gauss's method or an iterative method like Gauss-Seidel's method could be used to find the d's.

Step 7: Solve for the Element Strains and Stresses

The problem of structural stress-analysis requires the significant secondary numbers of strain and stress (or moment and shear force) to find it's solution.

Step 8: Interpret the Results

Ultimately, the goal is to comprehend and examine the outcomes for use in the design/analysis process. It is necessary to determine the location maximum stress and deformation when analyzing or designing a structure.

3.3.2 FEM Model Construction

The numerical model in this study used FEM to construct three dimensional models to examine and analyze the control and selected strengthened PC beam specimens. ABAQUS® was the FEM software utilized in this study. The numerical results were validated with the experimental data with regards to load-deflection behavior, damage behavior and ultimate load capacity to gauge the accuracy of the FEM model.

With regards to the geometric attributes, material characteristics and boundary conditions, the FEM models of the PC beams were constructed to be as similar as possible to the experimental simply supported PC beams. The perfect inelastic damage behavior of concrete with regards to simultaneous tension and compression was simulated employing the concrete damage plasticity model. Concrete interaction in relation with the reinforcement, tension stiffening and strain-softening were described by the decreasing branch of the concrete stress-strain curve when exposed to tension. For the CFRP strengthening materials the elastic–brittle failure behavior in tension was considered, as well as the zero strength and stiffness in compression. The interfaces between the CFRP, epoxy and concrete, and between the steel reinforcement and concrete were examined. ABAQUS provided the environment for simulating consistent constitutive models pertinent to the reinforcement and concrete. The following sections contain a brief discussion on the input material properties and constitutive models.

3.3.2.1 Material Properties and Constitutive Laws

(a) ***Concrete***

ABAQUS provides a number of processes for simulating concrete damage behavior, such as the smeared crack model, brittle crack model, and the damaged plasticity model. The current research chose to apply the damaged plasticity model because of the greater probability of convergence in contrast with the other models. Also, it appropriately characterizes the inelastic behavior of concrete in tension and compression and the damage characteristics. The predominant failure mechanisms assumed by this model are tensile cracking and compressive crushing. Crack propagation is modelled using continuum damage mechanics and stiffness degradation.

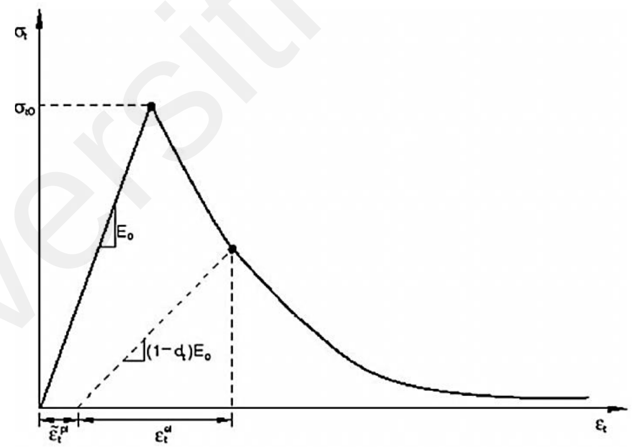

Figure 3.20: Response of concrete to uniaxial loading in tension (Abaqus documentation)

The stress-strain behavior of concrete exposed to uniaxial tension is depicted in Figure 3.20. This proceeds on a linear elastic path up to the point of the failure stress σ_{t0}. After ultimate strength, the descending concrete stress-strain graph is due to the concrete softening response as cracking initiates. This encourages strain localization within the concrete structure.

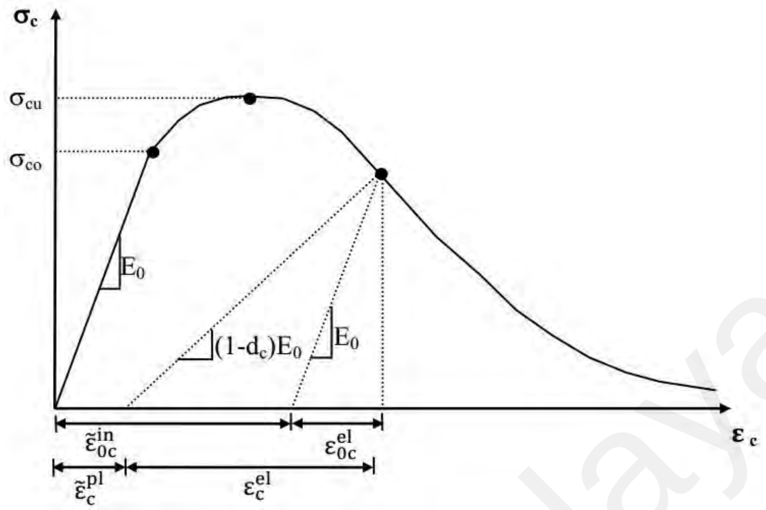

Figure 3.21: Response of concrete to uniaxial loading in compression (ABAQUS documentation)

The axial compression behavior of concrete is displayed in Figure 3.21 in which the stress-strain response is linear to the point of initial yield σ_{c0}. Between the initial yield and the ultimate stress σ_{cu}, there is a stress hardening with a strain softening response that defines the plastic stage. It is assumed that the uniaxial stress-strain relationship could be modified into stress versus plastic-strain curves (Equation 3.6 and 3.7).

$$\boldsymbol{\sigma_t = \sigma_t\left(\tilde{\varepsilon}_t^{pl}, \dot{\tilde{\varepsilon}}_t^{pl}, \theta, f_i\right)} \tag{3.6}$$

$$\sigma_c = \sigma_t\left(\tilde{\varepsilon}_c^{pl}, \dot{\tilde{\varepsilon}}_c^{pl}, \theta, f_i\right) \tag{3.7}$$

Where the subscripts t and c denote tension and compression, respectively; $\tilde{\varepsilon}_t^{pl}$ and $\tilde{\varepsilon}_c^{pl}$ are the equivalent plastic strains, $\dot{\tilde{\varepsilon}}_t^{pl}$ and $\dot{\tilde{\varepsilon}}_c^{pl}$ are the equivalent plastic strain rates, θ is the temperature, and $f_i, (i = 1, 2, \ldots)$ are other predefined field variables.

The elastic stiffness degradation is described by the damage variables d_t and d_c, surmising that that both variables are related to the plastic strains, temperature, and field variables as shown in equations 3.8 and 3.9.

$$\mathbf{d_t = d_t(\tilde{\varepsilon}_t^{pl}, \theta, f_i); \quad 0 \le d_t \le 1} \tag{3.8}$$

$$d_c = d_c(\tilde{\varepsilon}_c^{pl}, \theta, f_i); \quad 0 \le d_c \le 1 \tag{3.9}$$

The damage variables can select out the values between zero, which represents undamaged material, to one, which refers to completely damaged material, within ABAQUS. Considering the undamaged material elastic stiffness to be E_0, the stress-strain relationships that result from uniaxial tension and compression are shown in equations 3.10 and 3.11.

$$\boldsymbol{\sigma_t = (1 - d_t)E_0(\varepsilon_t - \tilde{\varepsilon}_t^{pl})} \tag{3.10}$$

$$\sigma_c = (1 - d_c)E_0(\varepsilon_c - \tilde{\varepsilon}_c^{pl}) \tag{3.11}$$

A number of parameters are required to build the damaged plasticity model, such as plastic damage parameters, Poisson's ratio, elastic modulus, and the description of tensile and compressive behavior. The five plastic damage parameters are the dilation angle, the flow potential eccentricity, the ratio of initial equiaxial compressive yield stress to initial uniaxial compressive yield stress, the ratio of the second stress invariant on the tensile meridian to that on the compressive meridian and the viscosity parameter that describes viscoplastic regularization.

The tension stiffening method may be followed to find the significant interface relation between rebar and concrete. This allows the simulation of the load transfer over the cracks through the rebar. Likewise, this enables the simulation of the strain-softening behavior of cracked concrete by the model. The tension stiffening in concrete may be defined using two methods: a) post failure stress-strain relation and b) fracture energy cracking criterion. The fracture energy process put forward by Hillerborg et al. (1976) is preferred over the post failure stress-strain relation, as the latter poses the problem of mesh sensitivity. In this method, it is presumed that the total energy (G_F) needed for opening wide a unit area of crack is a material property as shown in Figure 3.22.

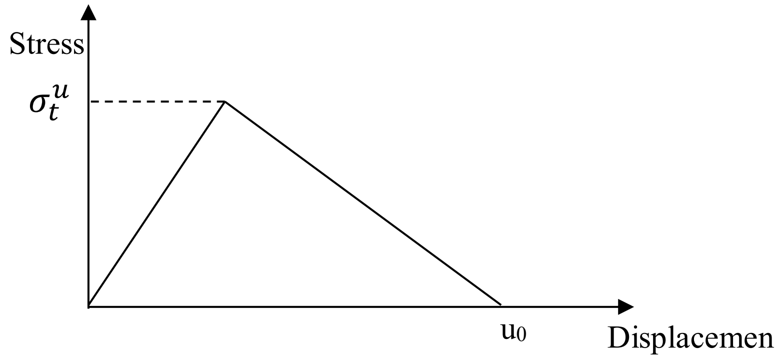

Figure 3.22: Fracture energy cracking model (ABAQUS documentation)

The concrete compressive strain ε_o at peak stress f_c' normally ranges between 0.002 to 0.003, when uniaxial compression is applied. According to the ACI Committee 318 (Committee, 2011) there is a suggested demonstrative value and this study includes it as ε_o = 0.003. Poisson's ratio ν_c of concrete is 0.15 – 0.22, when uniaxial compressive stress is applied. However, a demonstrative value of 0.19 or 0.20 was utilized by Nilson in 1982. For the present modelling, Poisson's ratio of concrete was taken to be ν_c = 0.20. This study regarded the uniaxial tensile strength of concrete f_t' to be 4.5, as displayed in equation 3.12 (Hu et al., 2004).

$$f_t' = 0.33\sqrt{f_c'} \text{ MPa} \tag{3.12}$$

As shown in equation 3.13, the modulus of elasticity of concrete E_c is greatly dependent on the compressive strength, and the empirical formula may be used to calculate it (Committee, 2011).

$$E_c = 4700\sqrt{f_c'} \text{ MPa} \tag{3.13}$$

When there are multiaxial combinations, the failure strengths of concrete are noted to have different forms. Additionally, when multiple stress conditions are applied, the maximum strength envelope is seen to be mainly independent from the load path (Kupfer et al., 1969). For the purpose of modelling the concrete failure surface a Mohr-Coulomb genre compression surface as well as a crack detection surface are utilized in

ABAQUS, as shown in Figure 3.23. The concrete beam was modeled using C3D8R, an 8-node linear solid element.

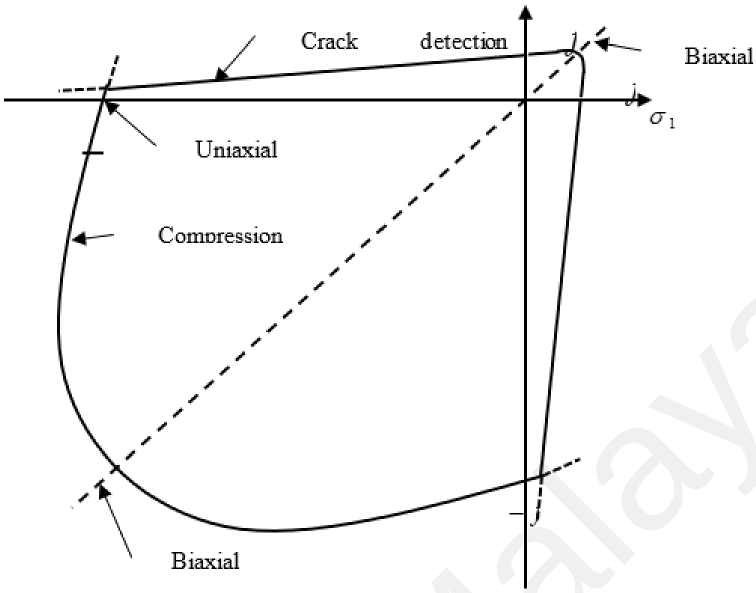

Figure 3.23: Plane stress concrete failure surface (ABAQUS documentation)

(b) ***Steel Reinforcements***

Figure 3.24 displays the steel reinforcement stress–strain curve, which was assumed to be elasto-plastic. A number of parameters are required to define the stress-strain relation including the modulus of elasticity (E_s), Poisson's ratio (υ) and yield stress (f_y). The modulus of elasticity was defined as 200 GPa while Poisson's ratio of internal steel was 0.3, for the present research. Within ABAQUS, the steel reinforcements were taken to be uniaxial equivalent material and the influence of any bond-slip between concrete and steel was not taken into account. The actual experimental beam specifications were taken into account while modeling the constitutive behavior of the reinforcements, including the cross-sectional area, position, spacing and orientation of the reinforcements. All the steel reinforcements were modelled using T3D2, a 2-node straight truss element, and each element was placed inside the concrete beam as in the experimental specimens.

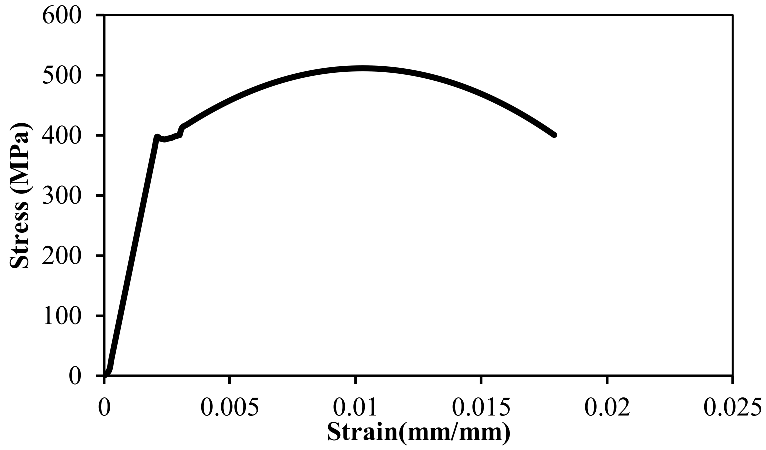

Figure 3.24: Elasto-plastic model for reinforcement

(c) ***CFRP***

The CFRP materials were considered linear elastic until failure. It was assumed that the CFRP materials had no ductile behavior after ultimate, and failure occurred when the strain in the CFRP material (ε_{pu}) reached the rupture stress (f_{pu}), as shown in Figure 3.25. Although CFRP is an orthotropic material, no significant difference was found when this isotropic linear elastic assumption was used to model the CFRP strengthened beams.

In forming the model, the values defined for the material properties of the CFRP bar, sheet and plate were as given in the experimental section. The uniaxial stiffness of the of the CFRP primarily carried tensile strains, with no observable lateral or shear resistance. The externally bonded CFRP sheet or plate formed a relatively thin layer on the soffit of the beam specimens. Thus, they were modelled using C3D8R, an 8-node linear solid element, which was attached directly to the bottom surface of the beams. The CFRP bar was modelled using T3D2, a 2-node straight truss element, which was placed inside the beam at the soffit as in the experimental specimens.

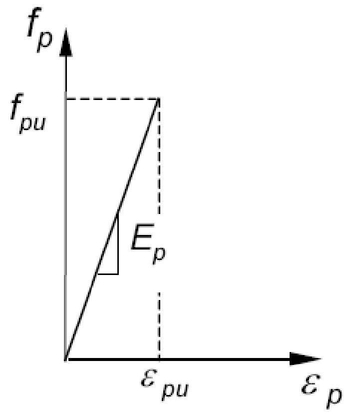

Figure 3.25: Stress-strain diagram of CFRP

3.3.2.2 Bond Interface

Three interfaces were analyzed in this research, namely, the steel and concrete interface, the CFRP bar and epoxy interface, and the concrete and epoxy interface. In this research, every interface bond was surmised to be perfectly bonded. The interface bonds were modeled using ABAQUS's tie and embedded constraints feature. Also, it was assumed that the steel reinforcement was embedded inside the concrete and the CFRP bar was embedded in the epoxy. Tie constraints were utilized to constrain the epoxy to the concrete. In contrast with the experimental results, the perfect bond model displays a certain amount of overestimation of the ultimate load and stiffness. Nevertheless, this method is advantageous with regards to convergence and computational capability (Darain et al. 2016; Lee et al. 2017).

3.3.2.3 Model Geometry

For the purpose of simulating the real behavior of the tested PC beams, constitutive 3D models of the PC beams were constructed using the selected types of finite elements based on the material properties described in the previous section. To model concrete, 8-node reduced integration solid hexahedron elements were employed. The elements possessed three degrees of freedom at every node. Gaussian quadrature was used to perform single point volume integration. The greatest benefit of utilizing solid elements with one-point integration is that the computation time is considerably less, although the zero energy modes must be controlled. Unwanted hourglass modes usually possess periods that are characteristically are a lot smaller compared to the periods of the structural response, and also are frequently detected as oscillatory. Viscous damping or small elastic stiffness can be used to prevent the development of irregular modes and undesirable hour glassing, while having a negligible impact on the stable global modes. ABAQUS provides three-dimensional algorithms for controlling the hourglass modes, and these are normally used. The solid 8-node linear brick element, C3D8R, was used for concrete material with decreased integration and hourglass control.

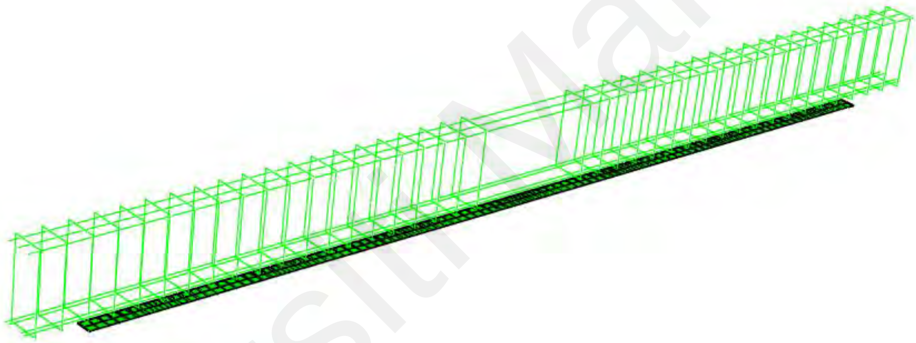

Figure 3.26: 3D non-linear finite element model of reinforcements

As presented in Figure 3.26, 2-node straight truss elements were employed for modelling the longitudinal and strengthening steel reinforcement, and utilized for linear interpolation of position and displacement. The truss elements possess three degrees of freedom at each node, which translate into *x*, *y*, and *z* directions. The truss elements possess only axial stiffness, while beam stiffness is related to the deformation of the axis of the beam. It was assumed that there were perfect bonds between the steel bars and the encompassing concrete for the numerical analysis.

A convergence of results is achieved when an adequate number of elements are used in the model. The interconnected elements of the model form a mesh and previous studies have found that too fine or too coarse a mesh density can hinder convergence and produce errors. A fine mesh provided accurate results, but an even finer mesh gave almost the same results but severely increased the computation time, with the danger of computer memory overflow. Thus, a proper meshing size was defined to discretize the concrete, steel, CFRP and epoxy in order to transfer loading from one to another appropriately and ensure the accuracy of the numerical simulations. The meshed form of the CEBPNSM model is shown in Figure 3.27.

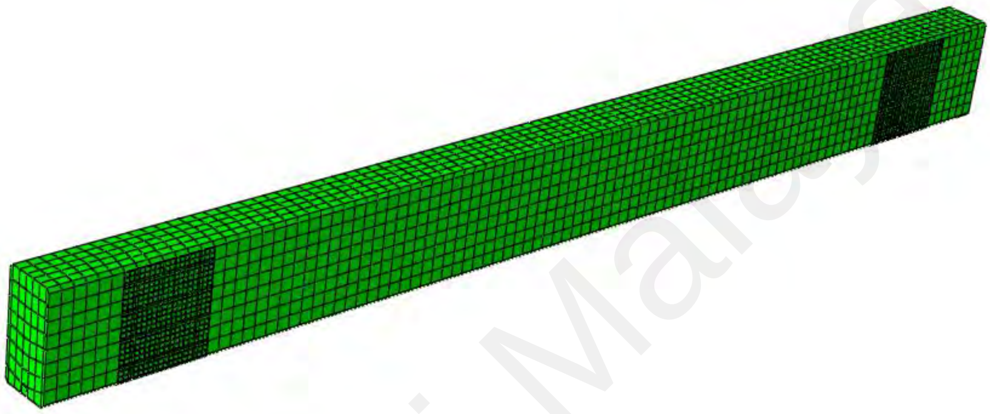

Figure 3.27: 3D finite element mesh of strengthened specimen

3.3.2.4 Loading Simulation

ABAQUS allows concentrated nodal forces or moments to be implemented on the displacement or rotation of the degrees of freedom. For FEM the model, dispersed constant pressure forces were employed on the beams through two load pads (Figure 3.28), to simulate the monotonic experimental loading of the beams. The actual experiment involved the application of four-point bending loads on the control and strengthened beams. The load control mode was sustained at 5 kN/minute until the yield point of the tested beam. After the applied load passed the yield point the load control mode was altered to the displacement control mode at the rate of 1.5 mm/minute up to the point at which the experimental beams failed. In ABAQUS, an appropriate amplitude was selected within a specified time domain to simulate the exact loading application.

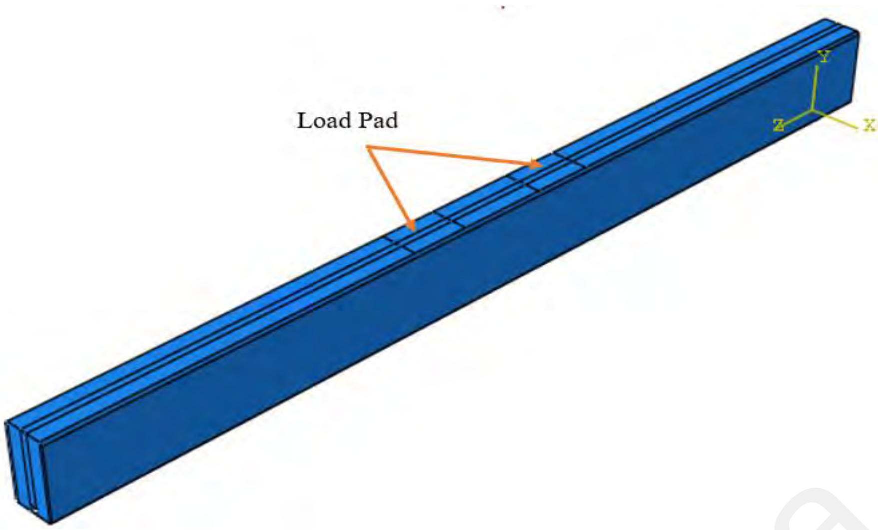

Figure 3.28: Applied loading on the FEM beam model

3.3.2.5 Modeling of Prestress Forces

For the purpose of simulating the internal prestressing of the PC beams and the prestressed strengthening, two steps were implemented. Firstly, the prestressing forces within the internal prestressed strands were simulated by adding a 1395 MPa stress to the specific steel reinforcements. This corresponds to 75% of the tensile strength within the principal internal strands. Secondly, the prestressing force within the strengthening CFRP bar or steel strand was applied in the model according to the level of prestress used in each specific beam specimen.

CHAPTER 4: RESULTS AND DISCUSSIONS

The extensive data obtained from the experimental investigation are presented and analyzed in this chapter. Several parameters were considered to assess the performance of the strengthening techniques, namely flexural capacities, failure modes, deflection behavior, cracking characteristics, strain profiles of the different components of the experimental specimens, ductility, stiffness, energy absorption, prestress loss and effect of prestressing. The simulated results obtained from the FEM model are also presented in this chapter and compared with the experimental results. The results generated by the FEM model were in terms of flexural capacity, load-deflection behavior and damage patterns. The following sections elaborately discuss the experimental and FEM results of the different strengthening techniques investigated in this research.

The first two sections offer a brief discussion of the experimental and FEM results obtained for the control beam and EBR strengthened beams, as these beams were mainly for comparison purposes. The third and fourth section present an extensive discussion of the experimental and FEM results obtained for the PNSM strengthening technique with CFRP bars and with steel strands. The following four sections are an extensive discussion of the CEBPNSM technique, in terms of the experimental and numerical results obtained in this research on the use of various combinations of strengthening material with the CEBPNSM strengthening technique. A final section offers a summary of the findings of this research, with a brief assessment of how the objectives of this research were achieved.

4.1 Unstrengthened Control Beam

4.1.1 Flexural Behavior

One unstrengthened prestressed concrete beam, the control beam (UB), was tested as a reference beam for comparison with the strengthened beams. The control beam was identical to all the strengthened beams in terms of size, concrete grade, internal reinforcement, and other beam properties except that it was not strengthened in any way. The control beam was also tested under identical loading conditions as the strengthened beams, namely monotonic four-point loading.

The experimental load and deflection results of the control beam are given in Table 4.1. The first crack appeared at 63 kN, yield occurred at 110 kN, and the ultimate load capacity of the control beam was 127 kN. Serviceability is an important design consideration which indicates the fitness of a structure for its intended use. This service load was determined as the load corresponding to the deflection that is equal to span/480, as provided in ACI 318-11. This service deflection was calculated to be 6.25 mm for the beams used in this research. The corresponding service load in the control beam was found to be 83 kN.

Table 4.1: Experimental load and deflection results of control beam

Beam specimen	First crack (P_{cr})		Service (P_s) (kN)	Yield (P_y)		Ultimate (P_{ult})	
	Load (kN)	Deflection (mm)		Load (kN)	Deflection (mm)	Load (kN)	Deflection (mm)
UB	63	3.1	83	110	19.8	127	45.6

The load deflection curve of the control beam is shown in Figure 4.1. The control beam displayed the typical linear elastic followed by plastic load-deflection behavior expected from concrete beams. From load initiation until first crack, there was a stiff linear elastic response. After first crack deflection increased slightly due to cracking, although the beam response was still mostly linear elastic, until yielding of the internal steel. After yield, the control beam entered the plastic deformation stage with rapidly increasing deflection and plateauing of loading around the ultimate capacity. At ultimate, the concrete began to crush in the main compression zone at the top surface of the beam and the load-deflection curve began to slope slightly downward reflecting the softening of the beam at this stage. The control beam eventually failed flexurally by typical concrete compression failure. The failure mode of the control beam can be seen in Figure 4.2.

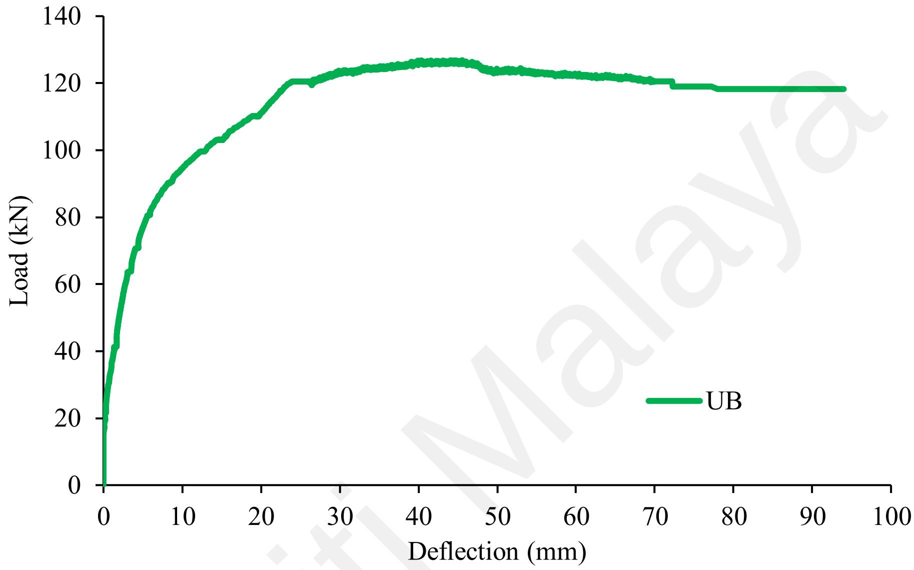

Figure 4.1: Load-deflection curve of control beam (UB)

The cracking behavior of the beam was typical of a reinforced concrete beam, with a typical flexural crack pattern (Figure 4.2). The first crack appeared around the midspan at about 50% of the beam's ultimate capacity. The high first crack load compared to a conventional RC beam is due to the existing prestress force in the beam. As the load increased, more vertical flexural cracks formed along the midspan and grew deeper from the soffit towards the top of the beam. The cracks were more concentrated at areas close to the midspan and reduced gradually in the areas near the supports. New crack formation continued until yielding of the tensile reinforcement after which no new cracks formed, but the existing cracks grew wider and deeper until failure. The maximum measured concrete compressive strain for the control beam was 0.00289 and the maximum tensile steel strain was 0.00612, indicating that the full concrete compressive strength and steel yield strength were utilized.

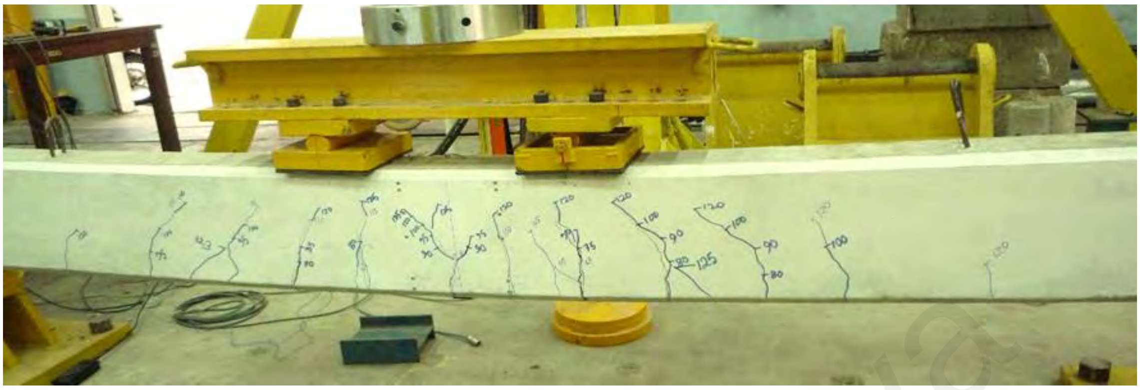

Figure 4.2: Failure mode of control beam

4.1.2 Assessment of FEM

A comparison of the experimental and FEM results for the control beam is given in Table 4.2. The error between the experimental and numerical results reached a maximum of 3% for ultimate load and 2% for the corresponding deflections. Thus, the differences between the experimental results and FEM output is within the acceptable limit of 10% (Darain, 2016). The agreement between the predicted load carrying capacity from the numerical FEM model and the experimental results is satisfactory.

Table 4.2: Experimental and FEM results at ultimate for control beam

Beam specimen	Experimental		FEM		FEM/Experimental	
	Load (P_{exp}) (kN)	Deflection (Δ_{exp}) (mm)	Load (P_{FEM}) (kN)	Deflection (Δ_{FEM}) (mm)	Load (P_{FEM}/P_{exp})	Deflection ($\Delta_{FEM}/\Delta_{exp}$)
UB	127	45.6	131	46.5	1.03	1.02

The load-deflection relationships for the numerical model and the experimental results are shown in Figure 4.3. It can be clearly observed that the correlation is reasonably good between the numerical results and experimental data.

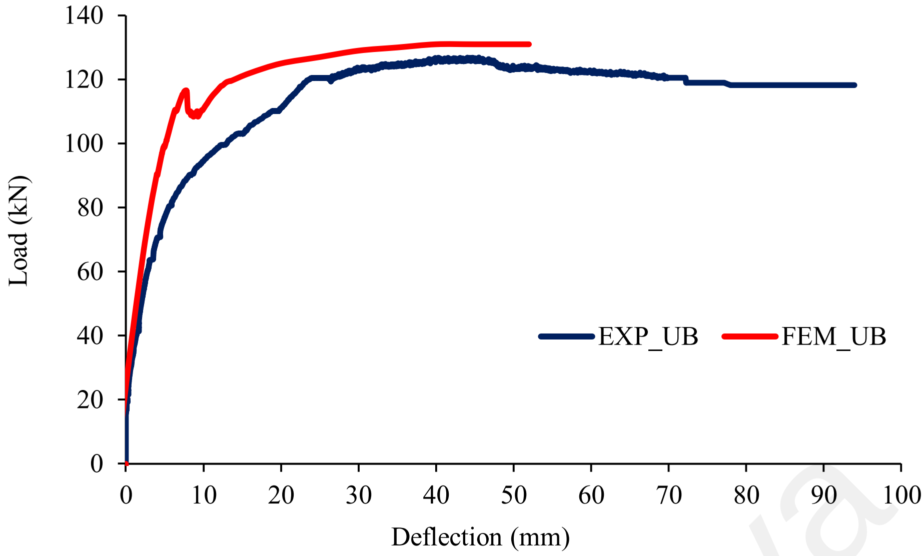

Figure 4.3: FEM load-deflection for control beam

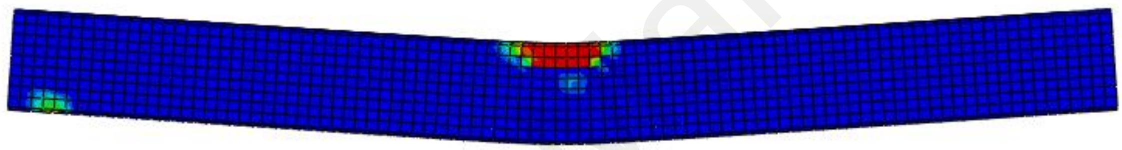

(a) Compressive damage behavior

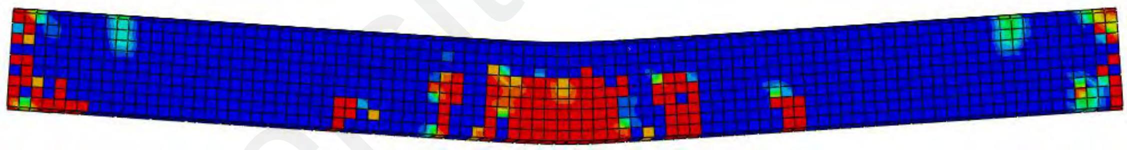

(b) Tensile damage behavior

Figure 4.4: FEM damage behavior of control beam

The compressive damage behavior and tensile damage behavior generated by the FEM model for the control beam are shown in Figure 4.4. ABAQUS requires the compressive damage and tensile damage of a beam to be displayed separately as shown in the figure. The typical failure mode for concrete beams is by concrete crushing at the top fibers of the beam after yielding of the tension reinforcement, which was the failure mode seen in the experimental control beam. The numerical damage behavior of the control beam was similar to the experimental failure mode.

4.2 EBR Strengthened Beams

4.2.1 Flexural Capacities

Three beams in this study were strengthened using the EBR strengthening technique with CFRP sheet or CFRP plate, for the purpose of comparison with the CEBPNSM technique. One beam was strengthened with EBR CFRP sheet, one beam with EBR CFRP plate without end anchors and one beam with EBR CFRP plate with end anchors. Plate debonding was observed in the EBR CFRP plate strengthened beam without end anchors, which is why another beam was tested using EBR CFRP plate with end anchors. The end anchorage used was CFRP sheets U-wrapped around the ends of the CFRP plate strengthened beam (Badawi, 2007), as has been explained in more detail in the methodology chapter. End anchorage was successfully able to prevent plate end debonding in the EBR CFRP plate strengthened beam. Thus, for all of the CEBPNSM and CEBNSM beams strengthened with a combination of EBR CFRP plate and NSM reinforcement, end anchorage in the form of CFRP U-wrap was used in order to prevent plate debonding. This use of end anchors was effective as can be seen from the flexural failure modes of the CEBNSM and CEBPNSM strengthened beams where CFRP plate was used as one of the strengthening reinforcements.

Table 4.3 presents the experimental load and deflection results of the EBR strengthened beams. As can be seen from the results, the improvement in first crack load was comparable for the three EBR beams, although the CFRP plate strengthened beams showed slightly higher first crack loads. More interestingly, the use of CFRP plate as EBR reinforcement was able to significantly reduce deflection at first crack by about 40% for both of the EBR CFRP plate strengthened beams, in comparison to the control beam. This was due to the high stiffness properties of the CFRP plate. This reduction in deflection at the first crack stage was also the most probable reason for the significant increase in the service load of the EBR CFRP plate strengthened beams when compared to the control beam and EBR CFRP sheet strengthened beam. The service deflection of 6.25 mm (span/480) in these beams occurred significantly later at a higher load. However, at yield the deflection and load capacity of the three EBR strengthened beams were was almost similar, although the EBR CFRP plate strengthened beam with end anchors reached a slightly higher yield load than the other two EBR beams. All three of the EBR strengthened beams significantly reduced the deflection at yield, by around 55% on average, compared to the control beam. The deflection at yield of the EBR CFRP plate strengthened beam without end anchors was slightly less than the EBR CFRP sheet strengthened beam although the yield load was similar, probably due to the high stiffness of CFRP plate. However, the end anchored EBR CFRP plate beam showed a slightly higher yield deflection than the other two beams, which may be attributed to the increased yield load achieved by the end anchored EBR CFRP plate beam. At ultimate, a similar pattern was seen in the deflection and load capacities of the three EBR beams. All three EBR strengthened beams were able to significantly increase the ultimate load capacity of the beams in comparison to the control beam. The EBR CFRP plate strengthened beam with end anchors was able to increase the ultimate capacity of the beam the most among these three beams, by 39% in comparison to the control beam. The end anchored beam reached a higher ultimate load capacity than the EBR CFRP plate beam without anchors due to the CFRP U-wrap anchorage preventing debonding and as the anchors themselves acted as an additional strengthening material. The EBR CFRP plate strengthened beams also displayed reduced deflection at ultimate in comparison to the control beam, despite the significantly increased corresponding ultimate load. This can be attributed to stiffness properties of CFRP plate.

Table 4.3: **Experimental load and deflection results of EBR beams**

Beam specimen	First crack (P_{cr})		Service (P_s) (kN)	Yield (P_y)		Ultimate (P_{ult})	
	Load (kN)	Deflection (mm)		Load (kN)	Deflection (mm)	Load (kN)	Deflection (mm)
UB	63	3.1	83	110	19.8	127	45.6
EBR-Sh	70 (10%)	3.2	93 (11%)	118 (7%)	9.7	165 (30%)	48.6
EBR-Pl	71 (12%)	1.9	111 (33%)	118 (6%)	7.9	166 (30%)	27.4
EBR-Pl-A	71 (13%)	1.9	114 (37%)	125 (13%)	9.0	176 (39%)	31.2
Note: Parentheses represent percentage increase over control beam							

4.2.2 Failure Modes

The failure modes of the EBR strengthened beams are shown in Figure 4.5. The beam strengthened with EBR CFRP sheet failed by concrete crushing after which the CFRP sheet debonded from the beam. Sometime after the internal steel yielded, concrete crushing began at the top face of the beam in the maximum compression zone. At this point, the CFRP sheet, which was under high tensile strain especially in the maximum flexural zone, lost full compatibility with the concrete surface and the CFRP sheet suddenly and swiftly debonded from the beam with a loud explosive sound. Concrete crushing continued to occur after this and testing was eventually discontinued. As concrete crushing occurred before debonding of the CFRP fabric, the strengthened beam is considered to have behaved in a fully composite manner and reached its full strength. This is confirmed by the maximum measured compressive strain in the concrete just before failure, which was 0.00290. This indicates that the full compressive strength of the concrete was utilized.

As previously stated, failure of the EBR CFRP plate strengthened beam occurred by plate debonding. The debonding of the CFRP plate took place after yielding of the internal steel reinforcement. At this stage, the flexural cracks extending from the interface between the CFRP plate and the beam towards the maximum compression zone were widening, and the CFRP plate was placed under increasingly greater tensile strains, especially at the maximum flexural zone. At this point, the CFRP plate was unable to maintain full compatibility with the beam and abruptly debonded from the beam soffit with a sudden loud sound. Concrete crushing followed and testing was stopped. The maximum concrete compressive strain measured before failure was 0.00301. However, the debonding of the CFRP plate occurred before concrete crushing was observed, which indicates a loss of full composite action just before the beam could reach its potential full strength.

A further EBR CFRP plate strengthened beam was tested but with CFRP U-wrap end anchors to eliminate debonding, as explained earlier. This beam specimen failed in the more favorable flexural manner of concrete crushing followed by plate debonding. Failure occurred after yielding of the steel reinforcement. Concrete crushing was observed in the maximum compression zone, and deflection increased as the beam began to soften. Soon after this the CFRP plate debonded with a loud sound along the midspan of the beam due to the increasingly high local curvature of the beam in the maximum flexure zone. The maximum concrete compressive strain measured before failure was 0.00299, indicating the full composite action of the beam.

(a) EBR-Sh

(b) EBR-Pl

(c) EBR-Pl-A

Figure 4.5: Failure modes of EBR beams

4.2.3 Load-Deflection Behavior

The load-deflection curves of the EBR strengthened beams are shown in Figure 4.6, with the deflection values at first crack, yield, ultimate and end point of test given in Table 4.3. The beams displayed the typical tri-linear response seen in CFRP strengthened beams (Attari et al. 2012), where there is a steep linear elastic progression in deflection from load initiation to first crack, followed by a slightly less steep but still linear progression of deflection from first crack to yield, and then from yield to ultimate the deflection progresses at an even shallower, but sill linear, slope. At ultimate, the CFRP debonded and was unable to carry any further loading, causing the load to abruptly fall back to the level of the control beam and loading was then carried by the internal steel. As can be seen from Figure 4.6, the EBR plate strengthened beams showed a stiffer response than the EBR sheet strengthened beam, especially from yield to ultimate. From Table 4.3, it can also be seen that the CFRP plate strengthened beams were able to significantly reduce deflection at first crack and ultimate, unlike the CFRP sheet strengthened beam. This was due to the greater stiffness of the CFRP plate than the CFRP sheet. At yield, however, the EBR CFRP sheet and EBR CFRP plate showed comparable reductions in deflection over the control beam. The end anchored beam displayed a slight increase in deflection at yield and ultimate due to the increased yield and ultimate loads compared to the CFRP plate beam without anchors.

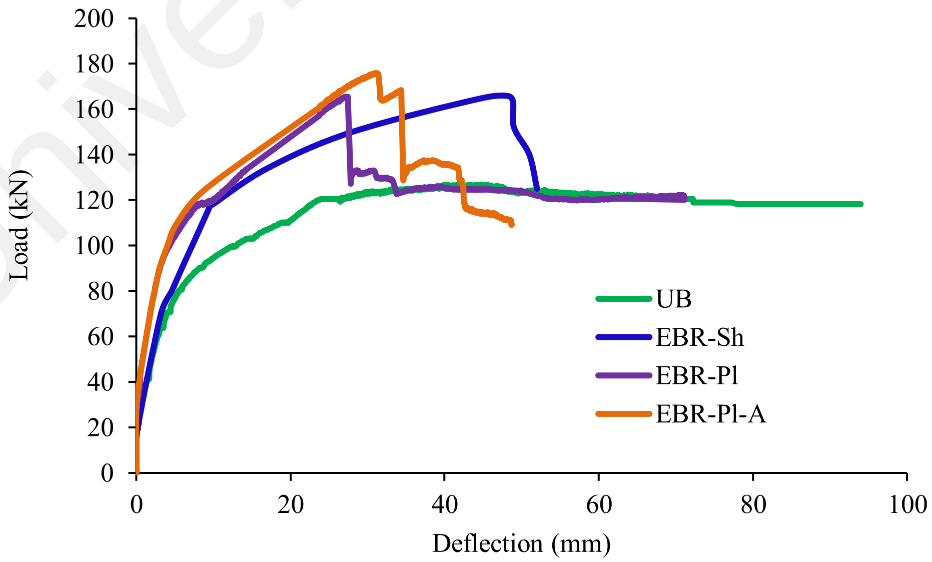

Figure 4.6: Load-deflection curves of EBR beams

4.2.4 Assessment of FEM

Table 4.4: Experimental and FEM results at ultimate for EBR beams

Beam specimen	Experimental		FEM		FEM/Experimental	
	Load (P_{exp}) (kN)	Deflection (Δ_{exp}) (mm)	Load (P_{FEM}) (kN)	Deflection (Δ_{FEM}) (mm)	Load (P_{FEM}/P_{exp})	Deflection ($\Delta_{FEM}/\Delta_{exp}$)
EBR-Sh	165	48.6	167	45.3	1.01	0.93
EBR-Pl-A	176	31.2	171	33.1	0.97	1.06

A comparison of the experimental and FEM results for the beam strengthened with EBR CFRP sheet and the beam strengthened EBR CFRP plate with end anchors is given in Table 4.4. The error between the experimental and numerical results reached a maximum of 3% for the ultimate load and 7% for the corresponding deflection, which was within the acceptable limit of 10% (Darain, 2016). The agreement between the load carrying capacity obtained from the experimental investigation and the values generated by the numerical model for the EBR strengthened beams is satisfactory.

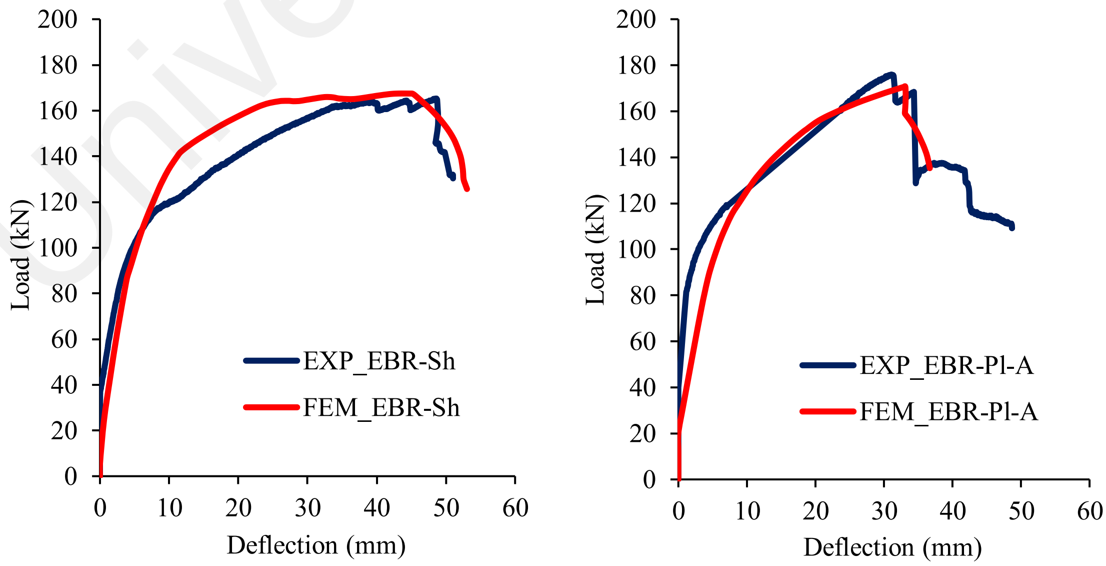

(a) Load vs deflection for EBR-Sh (b) Load vs deflection for EBR-Pl-A

Figure 4.7: FEM load-deflection for EBR beams

The load-deflection relationships produced by the numerical model and the experimental results for the EBR strengthened beams are compared in Figure 4.7. As can be seen from the figure, the correlation between the numerical results and experimental data is reasonably good.

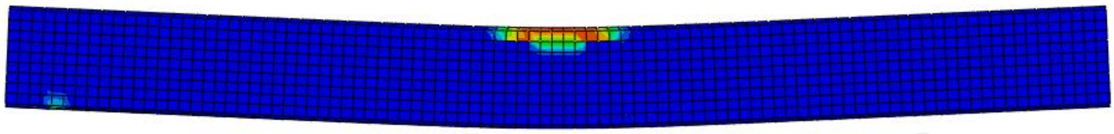

(a) Compressive damage behavior of EBR-Sh

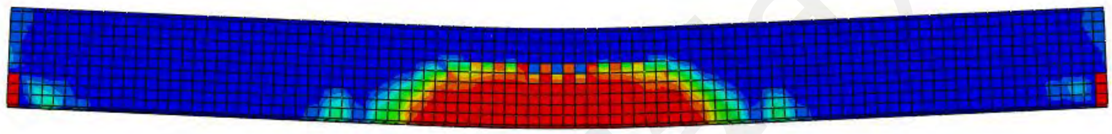

(b) Tensile damage behavior of EBR-Sh

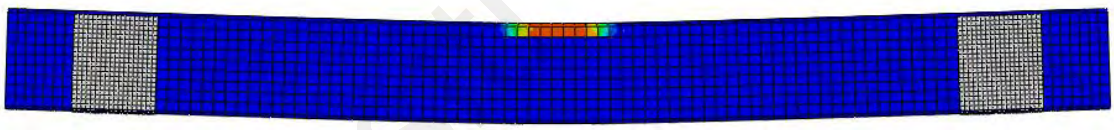

(c) Compressive damage behavior of EBR-Pl-A

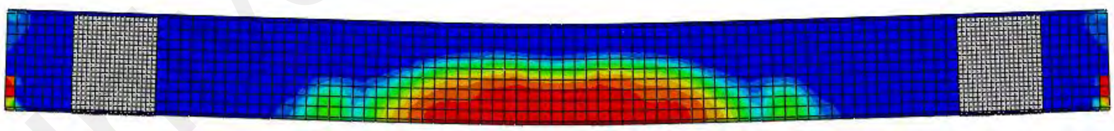

(d) Tensile damage behavior of EBR-Pl-A

Figure 4.8: FEM damage behavior of EBR beams

The simulated compressive damage behavior and tensile damage behavior for both EBR beams were quite similar as shown in Figure 4.8. The compressive damage and tensile damage of the beams are displayed separately in ABAQUS. The model was able to show the typical flexural damage behavior seen in concrete beams with concrete crushing at the top fibers of the beams after yielding of the tension reinforcement, and tensile damage in the maximum flexure zone. The experimental results for the EBR strengthened beams found failure to initiate with concrete crushing at the top face of the beam before CFRP debonding. As the beam softened and deflected more, the CFRP debonded due to high local curvature. The numerical model was able to adequately simulate the concrete damage behavior seen in the experimental EBR beams.

4.3 PNSM Strengthened Beams Using CFRP Bars

4.3.1 Flexural Capacities

The flexural performance of the PNSM strengthened beams using CFRP bars in terms of load carrying capacity at first crack, service, yield and ultimate, and the corresponding deflections are presented in Table 4.5, with the control beam and NSM strengthened beam included for comparison. The load carrying capacity at first crack, service, yield and ultimate improved significantly for the strengthened beams.

The first crack load increased significantly by 23% to 43% for the PNSM CFRP strengthened beams in comparison to the control beam. In comparison to the NSM strengthened beam without prestress, the PNSM CFRP strengthened beams with 30%, 40%, 50%, 60% and 70% prestress improved at first crack load by 15%, 18%, 22%, 28% and 34%, respectively. Delayed crack initiation is highly advantageous as early exposure to environmental elements can cause more damage to structural elements.

As stated in the previous sections, serviceability is an important design consideration and the service range is considered to be from first crack to service load. This service load was determined as the load corresponding to the point of deflection that is equal to the span/480 (Obaydullah et al. 2016), as stated in the ACI 318-11 standard. The service deflection for the tested beams was calculated to be 6.25 mm. The service load improved by 14% to 34% for the PNSM CFRP strengthened beams compared to the control beam. In comparison to the non-prestressed NSM CFRP strengthened beam, the service load increased by 11%, 14%, 18%, 24% and 30% for the 30%, 40%, 50%, 60% and 70% PNSM CFRP strengthened beams, respectively. Improvement at service is an essential concern when strengthening any structural element.

Table 4.5: Experimental load and deflection results of PNSM CFRP beams

Beam specimen	Level of prestress (%)	First crack (P_{cr})		Service (P_s) (kN)	Yield (P_y)		Ultimate (P_{ult})	
		Load (kN)	Deflection (mm)		Load (kN)	Deflection (mm)	Load (kN)	Deflection (mm)
UB	-	63	3.1	83	110	19.8	127	45.6
NSM-C-0%F	0	67 (6%)	3.4	86 (3%)	113 (2%)	11.7	166 (31%)	40.1
NSM-C-30%F	30	77 (23%)	3.6	95 (14%)	122 (10%)	11.6	170 (34%)	38.6
NSM-C-40%F	40	79 (26%)	3.6	98 (17%)	124 (12%)	11.5	174 (37%)	38.1
NSM-C-50%F	50	82 (30%)	3.5	101 (22%)	133 (20%)	11.5	177 (40%)	37.1
NSM-C-60%F	60	86 (36%)	3.4	106 (28%)	140 (27%)	11.5	180 (42%)	36.5
NSM-C-70%F	70	90 (43%)	3.4	111 (34%)	149 (35%)	11.4	186 (46%)	35.1
Note: Parentheses represent percentage increase over control beam								

The yield load of the PNSM CFRP strengthened beams also increased significantly by 14% to 35% over the control. Increasing the level of prestressing force from 30% to 70% in the PNSM CFRP bars caused the yield load to increase significantly by 8% to 31% over the non-prestressed NSM CFRP bar strengthened beam. As prestress force was increased, the yield load moved closer to the ultimate load of the beams, which improved the serviceability and durability of the beam. Other researchers have also found similar results where the yield point moves closer to the ultimate point as the level of prestress is increased in the strengthening reinforcement (El-Hacha et al. 2011; Obaydullah et al. 2016).

The ultimate load increased with strengthening by 34% to 46% for the PNSM CFRP beams compared to the control beam. Compared to the NSM strengthened beam, the PNSM beams were able to enhance ultimate load capacity by 3% to 12%. Higher prestress levels corresponded to higher flexural loads, although the percentage increase in ultimate load over the non-prestressed strengthened beam was less significant than the increases seen in yield and first crack loads. This is similar to the findings of previous researchers such as Nordin et al. 2006, Rezazadeh et al. 2014 and Peng et al. 2014.

The load carrying behavior of the PNSM with CFRP bar strengthened beams in this study are comparable to and agree with the findings of previous research. Overall, it was found that PNSM strengthening with CFRP bars greatly enhanced load capacity at all stages. Increasing the prestress level in the CFRP bar caused a most significant enhancement to be seen in the first crack, service and yield loads. This enhancement of load capacity at the service range is a crucial advantage of applying the PNSM strengthening technique.

4.3.2 Failure Modes

The failure modes of the PNSM and NSM strengthened beams using CFRP bar are shown in Figure 4.9. All the strengthened beams failed by rupture of the CFRP bar in combination with concrete crushing, after yielding of the tensile steel. The concrete at the top fiber of the beams began to crush before the rupture of the CFRP bar. However, complete crushing occurred after the CFRP bar ruptured. When the rupture of the CFRP bar occurred, a loud sound was heard and spalling of part of the epoxy cover at the rupture location was observed. No debonding was observed during the experimental tests. The behavior of the beams at failure indicates that the beams performed in full composite action until failure as is desirable for strengthened structures. Failure by

CFRP rupture is the most common failure mode for beams strengthened with PNSM CFRP as can be seen from previous research. Nordin et al. (2006), Badawi et al. (2007) and El Hacha et al. (2011) found that RC beams strengthened with PNSM CFRP generally failed by CFRP rupture. Shang et al. (2005) found that RC beams strengthened with prestressed CFRP sheet failed by CFRP rupture. Kim et al. (2008) investigated the strengthening of a PC beam with prestressed CFRP sheet and failure also occurred by rupture of CFRP.

(a) NSM-C-0%F

(b) NSM-C-30%F

(c) NSM-C-40%F

(d) NSM-C-50%F

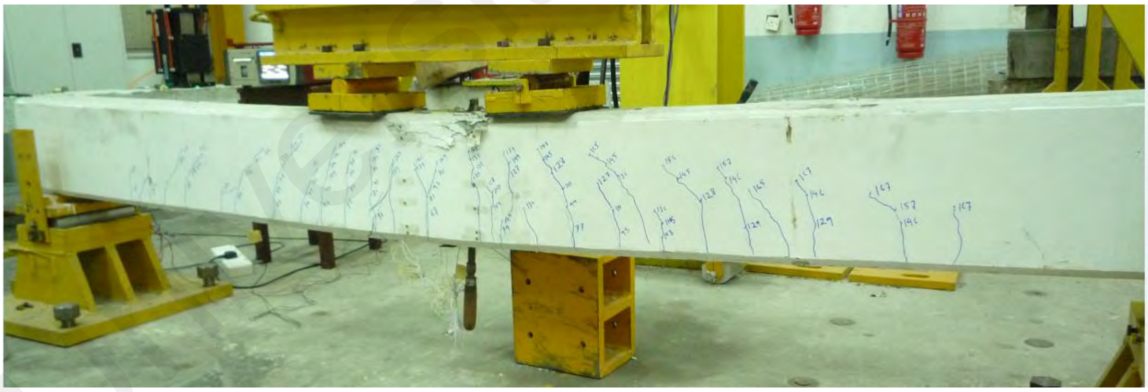

(e) NSM-C-60%F

(f) NSM-C-70%F

Figure 4.9: Failure modes of PNSM CFRP beams

4.3.3 Load-Deflection Behavior

The load-deflection curves for all of the PNSM CFRP bar strengthened beams are presented in Figure 4.10 and the exact deflection values at the crucial load points are given in Table 4.5. The beams displayed a tri-linear response with three nearly linear stages from load initiation to first crack, from first crack to yielding, and from yielding to ultimate; followed by a degradation phase after the ultimate load was reached until the final collapse of the beam, where the response of the beam was more erratic and unpredictable. Increasing the level of prestress force in the CFRP bar caused the load-deflection relationship of the strengthened beam to display steeper and higher, indicating reduced deflection and increased load capacity.

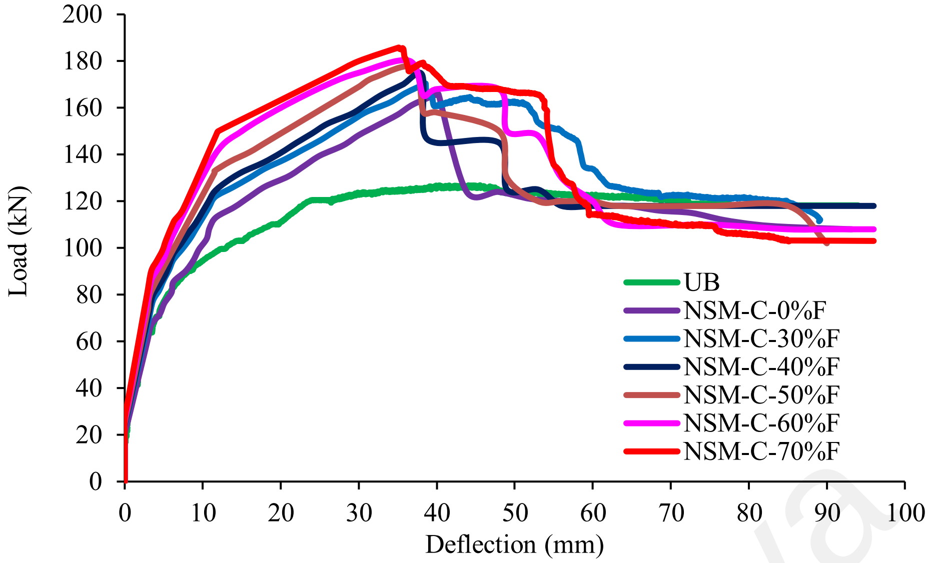

Figure 4.10: Load-deflection curves of PNSM CFRP beams

The first stage from load initiation to first crack was characterized by steep, almost linear slopes with minimal deflection, as the beams were at full functionality with no loss of stiffness. The deflection at first crack was 3.1 mm for the control beam and around 3.5 mm for the strengthened beams. Although the deflection at first crack was within a close range for all the beams, the first crack load increased significantly for the strengthened beams especially the beams strengthened with higher levels of prestress force. This allowed the initial stiffness of the beam to remain much longer with minimal deflection. The steepness of the load-deflection curves for each specimen was slightly reduced at the end of this stage, due to cracking which causes the initial stiffness of the beam to lessen slightly.

At the second stage from first crack to yield, more cracks developed and spread causing some loss in stiffness, thus the load-deflection curves at this stage were characterized by slopes that were less steep with slightly increasing deflection. The load-deflection curves at this stage were still nearly linear due to the typical behavior of CFRP in strengthened beams. The strengthened beams displayed less deflection for similar load levels, with increasing levels of prestress force showing greater reductions in deflection and thus steeper slopes. The deflection at yield for the control beam was 19.8 mm and for the strengthened beams around 11.5 mm, with remarkable increases in yield load for the prestressed NSM CFRP strengthened beams, especially at the higher levels of prestress force. At yield, the tensile strain in the internal tension reinforcement exceeded the yield strain, which caused the reinforcement to weaken and reduced the stiffness of the beam. This caused the load-deflection curves to further deflect after the yield point.

In the third stage from yield to ultimate, the flexural cracks widened and extended from the tension to the compression zone at the midspan of the specimens, further reducing the stiffness of the beams. This caused the rate of deflection of the beams at this stage to greatly increase compared to the previous two stages and the load-deflection curves of the beams to extend at a shallower slope. The linear manner of the load-deflection curves of the NSM CFRP strengthened beams at this stage can also be attributed to the typical stiff behavior of CFRP in strengthened beams. However, increasing the prestress force in the strengthened beams caused progressively steeper load-deflection slopes, indicating reduced deflection. The strengthened specimens displayed ultimate deflections that were less than the control beam by 12%, 15%, 16%, 19%, 20% and 23% for NSM-C-0%F, NSM-C-30%F, NSM-C-40%F, NSM-C-50%F, NSM-C-60%F and NSM-C-70%F specimens, despite the greatly increased ultimate loads. At ultimate point, failure occurred after which the beams were unable to carry any greater loading and the strengthened beams displayed sharp drops in load carrying capacity due to CFRP rupture. This can be seen in the load-deflection curves.

In the final degradation phase, the composite behavior of the beams was lost as failure occurred in both the tensile zone and compression zone with cracks spreading from the soffit to the top fiber of the beam. The widths of the cracks in the extreme tensile zone also widened simultaneously. As the integrity of the beams was lost, the beams displayed large increases in deflection with reduced load levels. The load-deflection curves of the strengthened beams in this phase show sudden sharp drops in load carrying capacity with beam capacity eventually falling back to the level of the control beam. The prestressed strengthened beams displayed greater deflection in the fall from ultimate back to the level of the control beam, with several drops in load, compared to the non-prestressed strengthened beam which displayed a single sharp drop with little deflection. This is similar to the results found by Badawi and Soudki (2009) and Choi et al. (2010). After the load capacity of the strengthened beams fell to the level of the control beam, the behavior of the strengthened beams became similar to the control beam as behavior is then controlled by the main tensile steel reinforcement.

4.3.4 Cracking Behavior

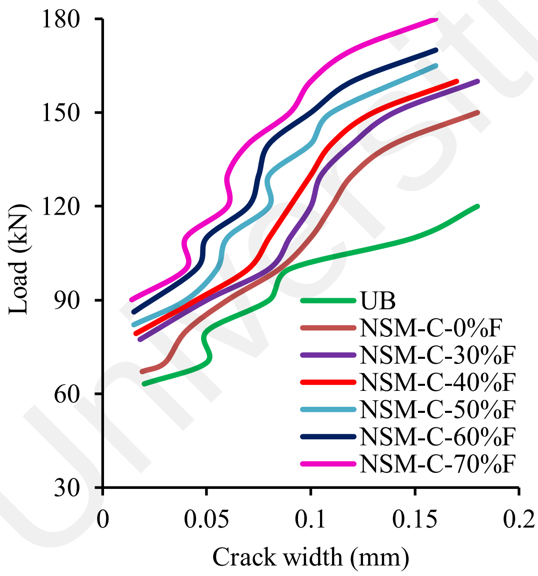

(a) Load vs crack width

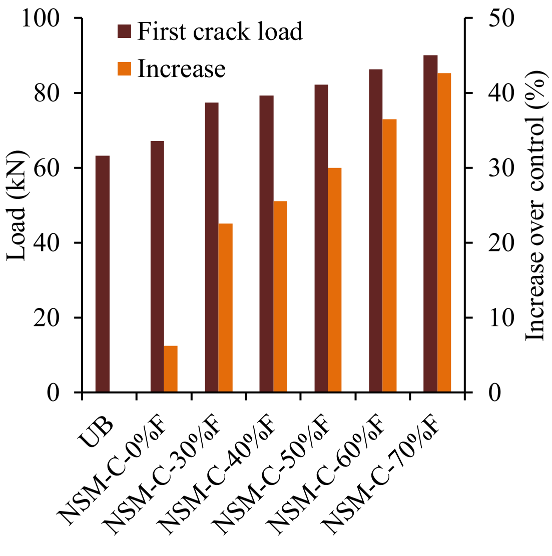

(b) Increase in first crack over control

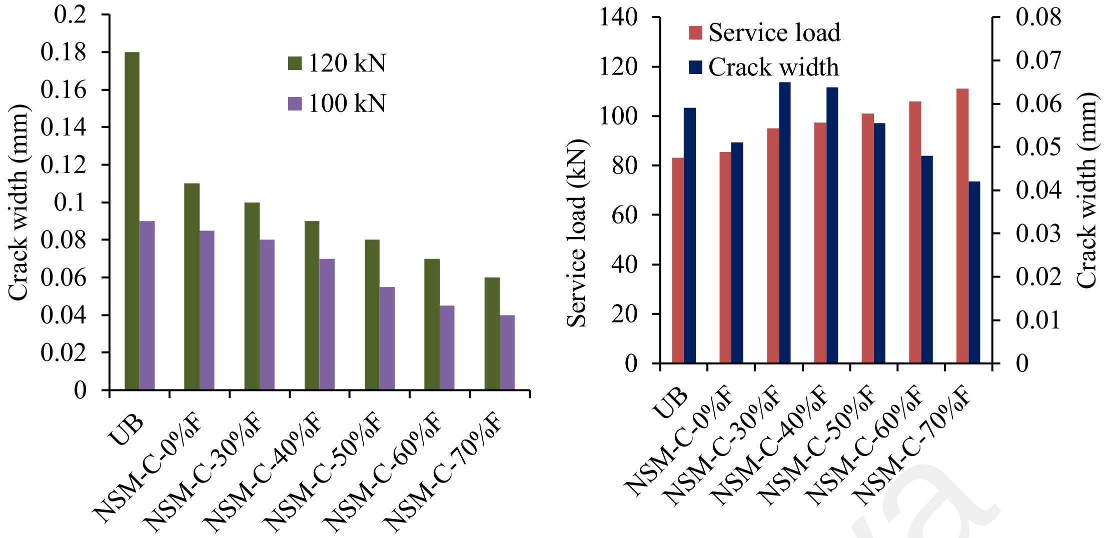

(c) Crack width at 100 kN and 120 kN (d) Crack width at service load

Figure 4.11: Cracking behavior of PNSM CFRP beams

Concrete cracks occur when the tensile stress in the concrete exceeds the tensile strength of the concrete (Hassoun, 1984). Crack formation and propagation also depend in large part on the concrete tensile strength. When the principle tensile stresses in the beam exceeds the concrete tensile strength, flexural cracks occur in the vertical direction (Rafi et al. 2008).

All of the PNSM CFRP bar strengthened beams displayed typical flexural crack patterns, which can be seen in Figure 4.9. No longitudinal cracks were observed at the bottom face of the beam or along the sides of the beam at the level of the internal steel, indicating the full composite action of the strengthened beams. The first crack load, crack width, crack number and crack spacing of the PNSM CFRP strengthened beams all improved in comparison to the control beam.

The first crack loads of the beam specimens and the percentage improvement over the control beam are given in Table 4.5 and graphically presented in Figure 4.11(b). As can be seen from the table and figure, the first crack load improved significantly in the

PNSM CFRP strengthened beams and increasing the level of prestress caused the first crack load to have significant corresponding increases. The NSM CFRP beam (without prestress) showed only a 6.2% increase in first crack load, while the 70% PNSM CFRP beam improved first crack load by 42.6%.

The crack widths of the beams as loading increased can be seen in Figure 4.11 (a). As can be seen from the figure, the PNSM CFRP strengthened beams reduced crack width compared to the control beam and increasing the level of prestress in the PNSM CFRP bar produced corresponding reductions in crack width, for any given load level. In Figure 4.11 (c), it can be seen that at the given load of 100 kN, crack width was greatly reduced by increasing the level of prestress in the PNSM CFRP strengthening. The greatest reduction in crack width was seen in the beam with the highest level of prestress (NSM-C-70%F). Crack width is an important issue at the service stage as large crack widths during service can lead to excessive damage from the environment. The crack widths of the beams at service load are shown in Figure 4.11(d). As can be seen from the figure, the PNSM CFRP beams with higher levels of prestress were able to reduce crack width at service, compared to the control beam and the NSM CFRP beam without prestress. Increasing the level of prestress caused a gradual reduction in crack width, despite the significant increases in service load.

After the first crack occurred and as loading continued, more flexural cracks appeared along the span of the beam. New cracks continued to form until yielding occurred, after which no new cracks formed (Obaydullah et al. 2016; Huda et al. 2017). However, existing cracks continued to grow longer and wider until the eventual complete failure of the beam. While testing the beams, it was observed that the widths of the cracks would sometimes decrease when new cracks formed even though loading was increased (Obaydullah et al. 2016), as can be clearly seen in Figure 4.11 (a). This was due to the redistribution of tensile stresses after new cracks formed along the beam. The PNSM CFRP strengthened beams also displayed more flexural cracks with closer spacing, smaller crack widths and more uniform distribution compared to the control beam (Figure 4.9). The control beam had 15 cracks spaced mostly along the midspan. The strengthened beams had around 25 to 30 cracks each. The higher number of cracks produced closer spacing and smaller crack widths (Rezazadeh et al. 2014; Choi et al. 2010). The cracks were more concentrated nearer the midspan with fewer cracks near the supports.

The improved cracking characteristics of the PNSM CFRP strengthened beams can be attributed to the effect of strengthening with CFRP and using prestress. Both the CFRP bar and the additional prestress improved the stiffness of the beam, and improved stiffness correlates to higher first crack loads and reduced crack widths, both of which are important durability and serviceability concerns. Increasing the level of prestress significantly enhanced these effects. This was due to the prestress effect which produces compressive strains in the tension region of the beam, which balance internal bending forces from applied loads and thus resist crack formation and crack widening. This is especially useful in practical applications to reduce crack widths and close cracks.

4.3.5 Concrete Compressive Strains

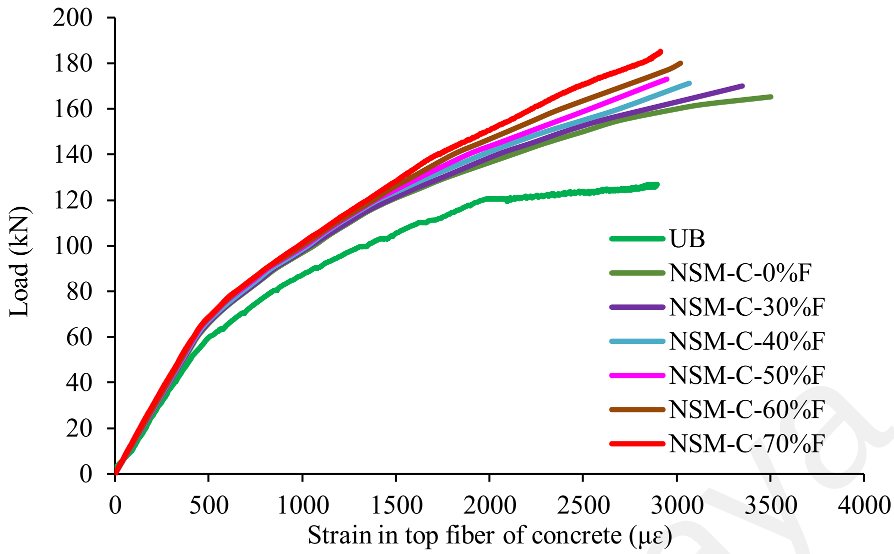

Figure 4.12: Concrete compressive strains in PNSM CFRP beams

The variation of concrete compressive strain at midspan due to loading is shown in Figure 4.12. The concrete compressive strain increased in a linear manner with a steep slope at almost the same rate for all the beams until first crack. After first crack the control beam diverged to a shallower slope with a greater rate of increase in strain while the strengthened beams diverged less and had similar rates of increase in strain until yield. The rate of increment of the compressive strain was higher in this phase due the loss in stiffness after first crack. Overall, the compressive strains in the strengthened beams were significantly less than the strain in the control beam for a given load. Increasing the level of prestress in the PNSM CFRP bar reduced compressive strains in the beams at higher load levels, especially after yield. The reduction in compressive strain was due to the increased stiffness of the prestressed strengthened beams. The maximum compressive strain values were last measured just before ultimate and for all of the beams maximum concrete compressive strain was around 0.003, after which strain could not be measured as concrete crushing damaged the strain gauges. The maximum concrete compressive strain measured in the strengthened beams indicates that the full compressive strength of the concrete was used and confirms the full composite action of the strengthened beams until ultimate.

4.3.6 Tensile Strains in Main Steel Strands

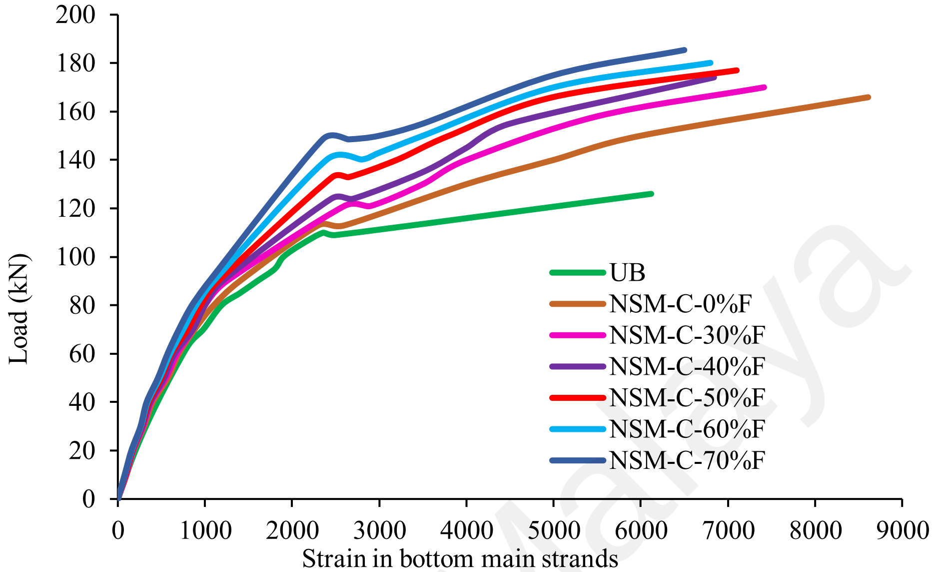

Figure 4.13: Main steel tensile strains of PNSM CFRP beams

The tensile strains in the bottom main strands were measured at midspan during loading of the beams, and the results are shown in Figure 4.13. All of the PNSM CFRP beams displayed similar tensile strain curves, with linear increment in strain up to crack initiation in concrete and then nearly linear at a lower slope until yield of the internal steel reinforcement. After yield, the strain exhibited a less linear curve at a much gentler slope, indicating the increased rate of strain increment in this phase as beam stiffness decreased after yield and cracks widened. The strengthened beams showed significant reductions in tensile strain for a given load level, and increasing the prestressing level in the strengthening bar caused further reductions in strain. This was due to the increase in stiffness from strengthening and prestressing with the CFRP bar. The maximum tensile strain values measured in the main steel strands were 0.00612, 0.00861, 0.007415, 0.006908, 0.007101, 0.0068 and 0.0065 for the control beam, NSM-C-0%F, NSM-C-30%F, NSM-C-40%F, NSM-C-50%F, NSM-C-60%F and NSM-C-70%F respectively, before the strain gauges were damaged by the failure of the beams at ultimate. The control beam had a much lower maximum tensile strain as it failed by concrete crushing at a much lower load level than the strengthened beams. The non-prestressed strengthened beam measured the highest maximum strain before failure compared to the prestressed strengthened beams, which had progressively lower maximum tensile strain values before failure. This is due to the compressive strains induced by prestressed strengthening in the tensile region of the beams, which controlled tensile stresses in the beams.

4.3.7 Tensile Strains in PNSM CFRP Bars

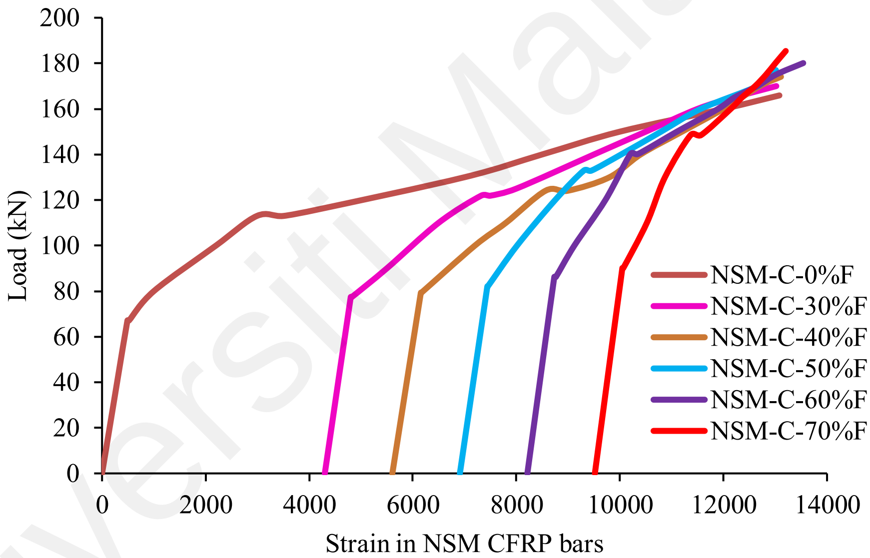

Figure 4.14: PNSM CFRP bar tensile strains

The load versus CFRP tensile strain at midspan is shown in Figure 4.14, where the initial strains due to prestressing are shown at zero load. All the strengthened beams behaved in a similar manner with three distinct phases of strain increment. In the first phase from zero until first crack, all the strengthened beams showed very similar linear rates of strain increment with sharp slopes due to the high stiffness of the beams. After first crack, the strain curves of all of the beams became less steep due to loss of stiffness from concrete cracking. However, beams with higher prestressed strengthening displayed steeper curves than those with less prestressed strengthening, indicating that the rate of strain increment was reduced by prestressed strengthening. After yield, the strain curves again became less steep although the higher prestressed strengthened beams still displayed relatively steep curves compared to the other beams. After yield, the rate of strain increment in the CFRP bars was higher than in the previous two phases as the applied load was now carried in large part by the CFRP bar. The maximum tensile strains measured in the CFRP bars were about 0.013, 0.013, 0.013, 0.013, 0.014 and 0.013 for NSM-C-0%F, NSM-C-30%F, NSM-C-40%F, NSM-C-50%F, NSM-C-60%F and NSM-C-70%F, respectively. These were the strain values just before the beams reached their ultimate point and failure occurred, damaging the strain gauges so no further readings could be taken. The rupture strain for the CFRP bars according to the manufacturer's specification was 13000 micro strain. Some of the beams with higher levels of prestressed strengthening recorded CFRP strain levels higher than the ultimate strain given by the manufacturer. The strains recorded by the strain gauges placed on the NSM CFRP bar at midspan can be affected by the local curvature of the CFRP, which can lead to higher strain values than those found in direct tensile tests, as reported by Rezazadeh et al. [23]. The maximum strains recorded for the CFRP bars indicate that the capacity of the CFRP was fully used and is in agreement with the observed failure mode of these specimens, which was rupture of the CFRP bars with concrete crushing.

4.3.8 Ductility

Ductility is the ability to withstand inelastic deformation before collapse, without significant loss in resistance or strength capability. It is a desirable structural property that allows stress redistribution and provides warning before failure by increasing deflections. Ductility also provides a structure with the capacity to withstand sudden local impact and accidental loading without collapse (robustness), and the ability to dissipate energy under cyclic loading (Morais et al. 2001).

To measure the ductility of a structural member, a ductility index is commonly used [44]. The ductility index is expressed as follows:

$$\mu_{\Delta u} = \frac{\Delta_u}{\Delta_y} \tag{4.1}$$

Where $\mu_{\Delta u}$ is the ductility index at ultimate load, Δ_u and Δ_y are the displacement at ultimate load and yield load, respectively.

The ductility index and the improvement in ductility over the control beam of the PNSM CFRP bar strengthened beams are presented in Figure 4.15. The ductility index of the strengthened beams was significantly improved compared with the control beam. However, the ductility index of the PNSM CFRP bar strengthened beams gradually decreased with increasing level of prestress in the CFRP bar. This is due to the increase in stiffness with increasing prestress level in the strengthened beams.

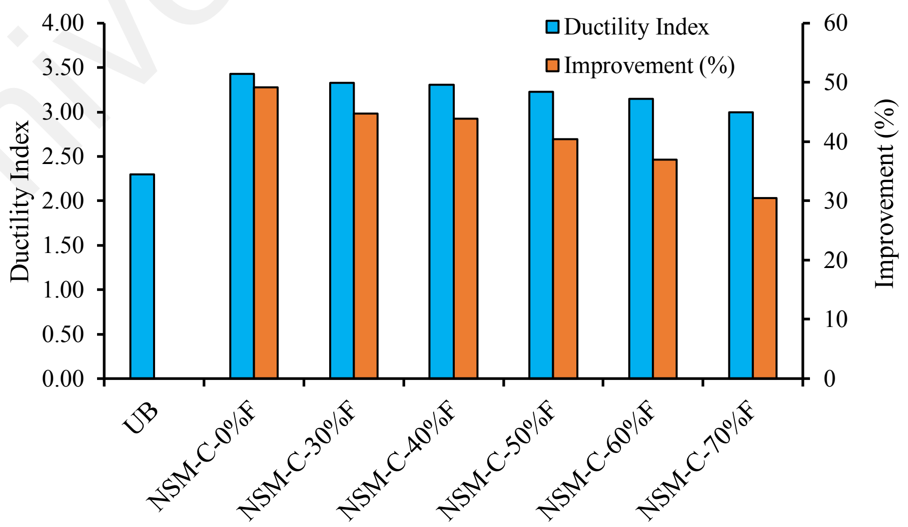

Figure 4.15: Effect of PNSM CFRP bar strengthening on ductility index

4.3.9 Energy Absorption Capacity

Energy absorption is the capacity of materials or structures to dissipate kinetic energy during impact or intense dynamic loading. The greater the ability of the material or structure to resist damage, the higher its energy absorption (Lu et al. 2003). In the case of concrete structures, energy absorption can be an important factor for structural durability in certain situations such as vehicle collisions and earthquakes (Kumar et al. 2017). For concrete beams, energy absorption capacity effects fracture and plastic damage behavior and ductility. The energy absorption capacity of the PNSM CFRP strengthened beam specimens was calculated as the area under their load deflection curves (Omran et al. 2010, Hong et al. 2016, El-Hacha et al. 2013) and the values are presented in Figure 4.16. Strengthening the PC beams with PNSM CFRP bars increased the energy absorption capacity of the specimens, and increasing the prestress level further increased the energy absorption capacity. The beam strengthened with 70% prestress force showed the highest increase (20%) in energy absorption over the control beam. This was due to the prestressed strengthening delaying crack formation and increasing the cracking and service loads of the beam and the balanced failure mode of the strengthened beams (concrete crushing and CFRP rupture simultaneously), which indicates that the full energy capacity of the concrete and CFRP was used (El-Hacha et al. 2013, Obaydullah et al. 2016, Hong et al. 2016). Overall, the strengthened beams displayed high energy absorption capacity due to the increased flexural capacity from CFRP strengthening and prestressed strengthening.

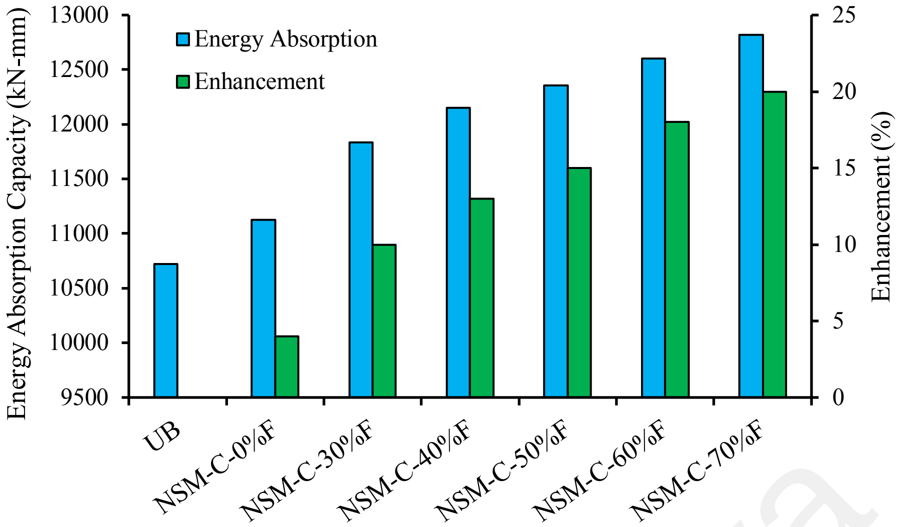

Figure 4.16: Effect of PNSM CFRP bar strengthening on energy absorption

4.3.10 Stiffness

Stiffness or flexural rigidity allows a beam to resist bending or deflection when loading is applied, which increases the strength and durability of the beam. Stiffness is an important structural property that is especially significant at the service stage and is represented by the gradient of the load-deflection curve of a beam. The stiffness of the strengthened beams was calculated at service load, which was defined as the load at the point of deflection equal to the ratio of the effective beam span over 480 (ACI 318-11 standard [46]). The following equation was used to calculate the stiffness of the beams at service:

$$K_{SLS} = (P_{SLS} - P_{CR})/(\delta_{SLS} - \delta_{CR}) \times 1000 \text{ kN/m} \tag{4.2}$$

Where, K_{SLS} is the flexural stiffness of the beams at service load, P_{SLS} is service load, P_{CR} is cracking load, δ_{SLS} is deflection at service load and δ_{CR} is deflection at first crack load respectively.

The stiffness values of the PNSM CFRP beam specimens and the enhancement in stiffness of the strengthened beams over the control beam are shown in Figure 4.17. All the strengthened beams showed improvement in stiffness compared to the control beam and the non-prestressed NSM strengthened beam. Increasing the level of prestress force further enhanced stiffness. The beam with the highest level of prestressed strengthening (70%) had the greatest increase in stiffness; approximately 17% over the control beam and 13% over the beam strengthened without prestress. The increased stiffness of the prestressed strengthened beams delayed the initiation of cracking and reduced deflection. Up until the first crack occurred, the beams retained near full stiffness as all the sections of the beam were uncracked and resisted applied loads (Hong et al. 2016). Immediately after crack initiation, the flexural stiffness of all the beams decreased significantly and again after yield. The rate of loss of stiffness in these two stages (from crack to yield, and yield to ultimate) was nearly constant in each stage, although the loss was greater in the final stage before ultimate as can be seen from the shallower linear gradient of the load-deflection curve. Strengthening improved stiffness due to the additional restraint provided by the CFRP bar. Prestressing the strengthening bar further improved stiffness as the capacity of the CFRP was better utilized and the prestress forces induced compressive and tensile strains in the beam that actively opposed loading, deflection and cracking (El-Hacha et al. 2013).

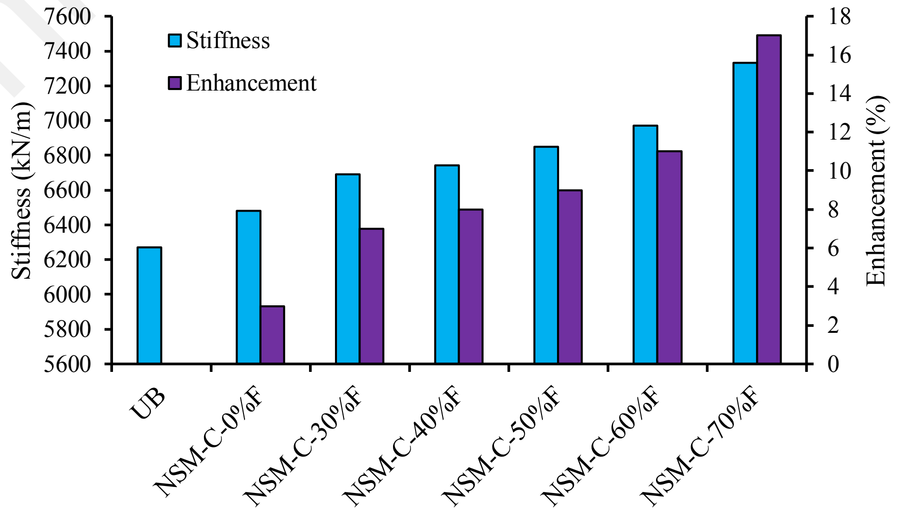

Figure 4.17: Effect of PNSM CFRP bar strengthening on stiffness

4.3.11 Prestress Losses

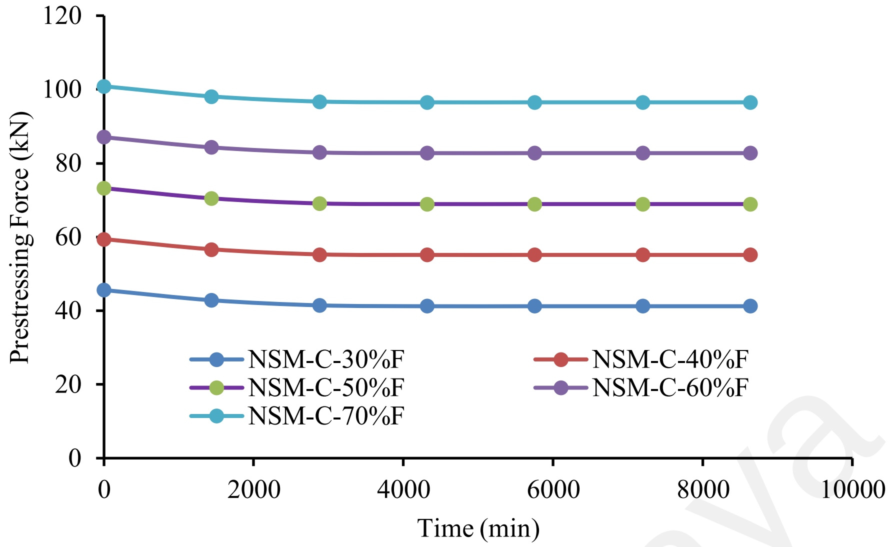

Figure 4.18: Prestress force during curing period in PNSM CFRP bar

Table 4.6: Prestress force and camber effect in the PNSM CFRP beams

Beam specimen	Applied prestress force		Effective prestress force		Negative camber at midspan (mm)
	(kN)	(%)	(kN)	(%)	
NSM-C-30%F	45.6	33	41.2	29.8	0.34
NSM-C-40%F	59.4	43	55.1	39.9	0.40
NSM-C-50%F	73.2	53	68.9	49.9	0.72
NSM-C-60%F	87.0	63	82.5	59.7	0.85
NSM-C-70%F	100.9	73	96.1	69.6	1.20

The prestress force in the PNSM CFRP bar was monitored during prestressing, during the six days curing period, and during release of the prestress. The PNSM CFRP bars were prestressed to approximately 46 kN, 59 kN, 73 kN, 87 kN and 101 kN in the beams NSM-C-30%F, NSM-C- 40%F, NSM-C-50%F, NSM-C-60%F and NSM-C-70%F, respectively. The initial applied prestress force in the CFRP bar was 3% over the target stress level to offset prestress losses due to anchor slip and epoxy creep (Badawi et al. 2009). The specimens were then left to cure for six days before releasing the prestress force. The prestress levels in the PNSM CFRP bars during the curing period are shown in Figure 4.18. The loss in prestress force during this time was at about 4.3 kN to 4.8 kN. This loss was due to adhesive creep and anchor slip (Badawi et al. 2009). Thus, the effective prestress levels at testing were about 30%, 40%, 50%, 60% and 70% of the tensile capacity of the CFRP bar in the respective beam specimens as shown in Table 4.6. After release of the prestressing force, a negative bending moment occurred due to the eccentricity of the prestress force in relation to the neutral axis of the beam, causing a negative camber (upward deflection) in the beam. This cambering effect was measured using an LVDT to monitor the deflection at midspan during the release of the prestress force. The initial cambers of the prestressed beams are given in Table 4.6.

4.3.12 Effect of Increasing Prestress Level

Prestressing the CFRP bar significantly influenced and enhanced the flexural behavior of the beams. Overall, the load bearing capacity of the beams increased significantly at all crucial load stages, as can be seen from Figure 4.19 (a). Higher levels of prestress corresponded to higher load levels, with the 70% prestressed strengthened beam showing the greatest increase in load capacity at all stages. The first crack load, service load, yield load and ultimate load of beam NSM-C-70%F increased by about 23 kN, 26 kN, 35 kN and 20 kN or 34%, 30%, 31% and 12% compared to the beam strengthened without prestress. The load capacity at the service stage (first crack to yield) was especially enhanced by prestressing the CFRP bar.

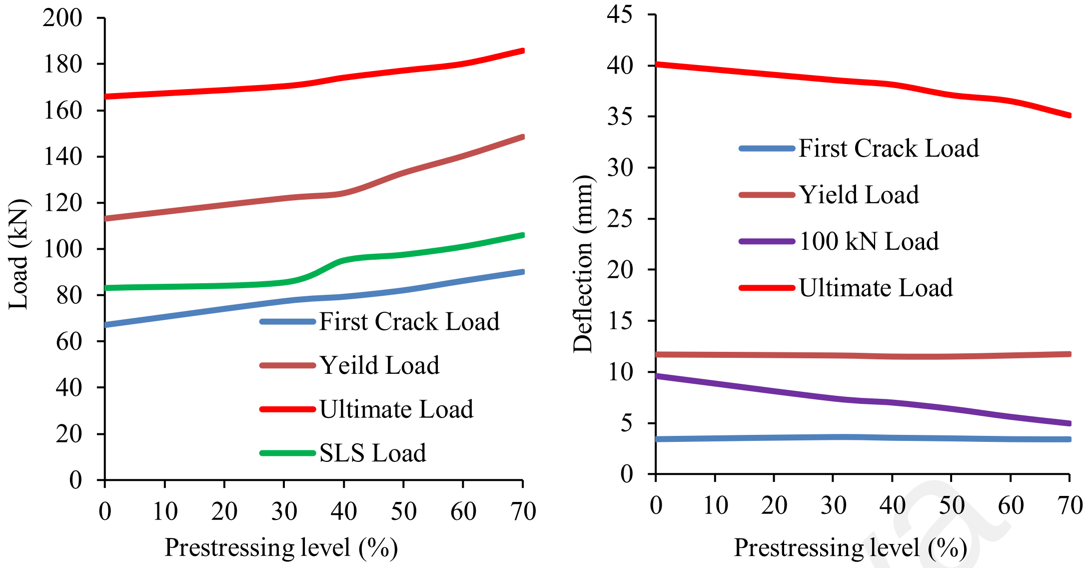

(a) Load vs prestress level

(b) Deflection vs prestress level

Figure 4.19: Effect of prestress level on PNSM CFRP beams

The deflection of the strengthened beams decreased with increasing prestressing level at any given load level. For instance, at an arbitrarily chosen load level of 100 kN, the deflection of the prestressed strengthened beams dropped from 10 mm (NSM-C-0%F) to 5 mm (NSM-C-70%F), as shown in Figure 4.19 (b). The deflection at first crack and yield was similar for all the strengthened specimens despite the large increases in load for the prestressed strengthened beams at these two crucial stages. This indicates that the prestressed strengthening was largely able to control deflection during the service stage. At ultimate, deflection decreased slightly with increasing level of prestressed strengthening despite increased ultimate loads. This was due to the greatly enhanced stiffness of the prestressed strengthened beams. Deflection dropped at ultimate from 40 mm (NSM-C-0%F) to 35 mm (NSM-C-70%F), a drop of 12.5%.

The failure mode of the beams was not affected by prestressing the strengthening CFRP bar. All the prestressed beams failed flexurally by CFRP rupture and simultaneous concrete crushing. This indicates that prestressing the strengthening material even to high levels of prestress did not compromise the full composite action of the strengthened beam and prestressed strengthening may help eliminate premature debonding failure.

Prestressing the strengthening bar also significantly improved the cracking behavior of the beams with higher first crack loads, better crack distribution (more cracks with less spacing) and reduced crack widths (El-Hacha et al. 2011, Obaydullah et al. 2016).

Increasing the level of prestress in the PNSM CFRP bar improved the flexural behavior of the beams due to the increased compressive effect in tension region of the beams, which caused a corresponding increase in the stiffness of the beams, as well as an increase in the camber of the beams (El-Hacha et al. 2011, Obaydullah et al. 2016).

4.3.13 Assessment of FEM

Table 4.7: Experimental and FEM results at ultimate for PNSM CFRP beams

Beam specimens	Level of prestress (%)	Experimental		FEM		FEM/Experimental	
		Load (kN)	Deflection (mm)	Load (kN)	Deflection (mm)	Load (P_{FEM}/P_{exp})	Deflection ($\Delta_{FEM}/\Delta_{exp}$)
UB	-	127	45.6	131	46.5	1.03	1.02
NSM-C-0%F	0	166	40.1	168	37.1	1.02	0.92
NSM-C-50%F	50	177	37.1	182	37.2	1.02	1.00
NSM-C-60%F	60	180	36.5	183	37.2	1.02	1.02
NSM-C-70%F	70	186	35.1	184	37.1	0.99	1.06

A comparison of the experimental and FEM results for ultimate load and ultimate deflection for the control beam, the beam strengthened with NSM CFRP and the beams strengthened with 50%, 60% and 70% PNSM CFRP is given in Table 4.7. The error between the experimental and numerical results reached a maximum of 3% for ultimate load and 8% for the corresponding deflection. Thus, the differences between the experimental results and the FEM output was within the acceptable limit (10%) [20]. The agreement between the load carrying capacity and deflection generated by the numerical model and the experimental ultimate loads and deflections is reasonably good.

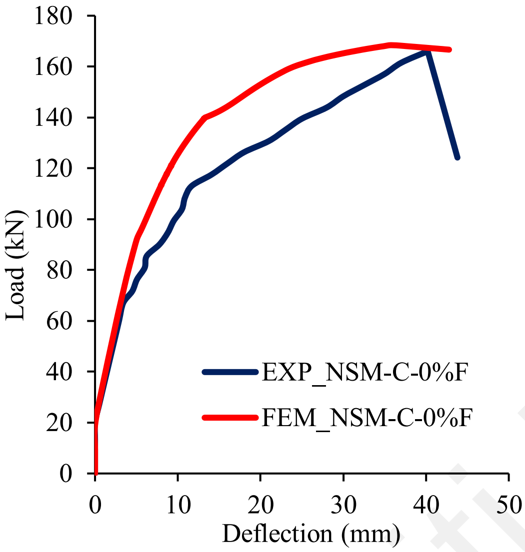

(a) NSM-C-0%F

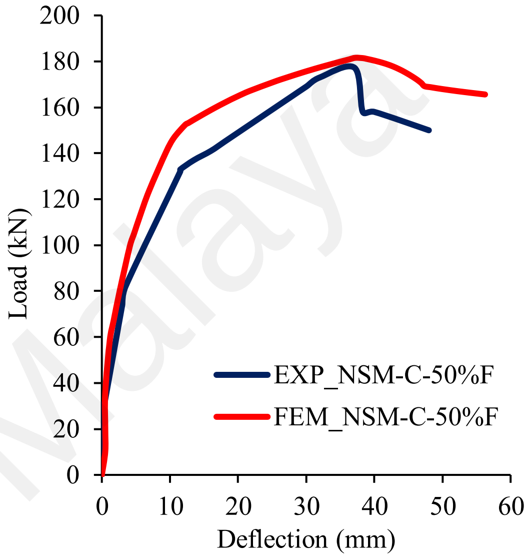

(b) NSM-C-50%F

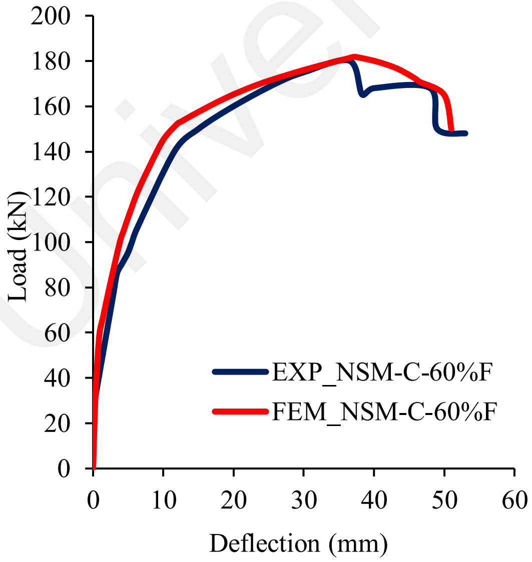

(c) NSM-C-60%F

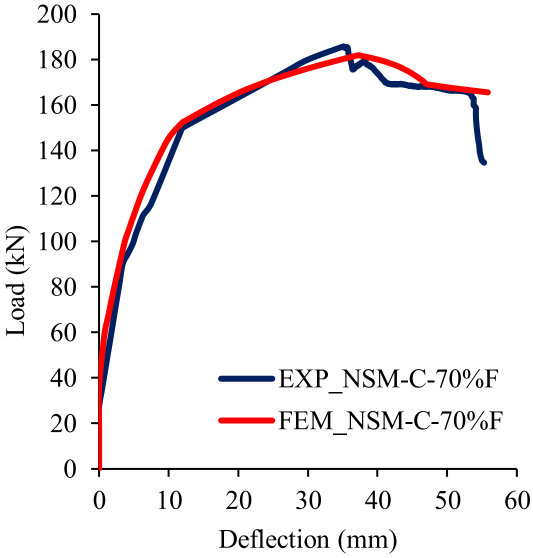

(d) NSM-C-70%F

Figure 4.20: FEM load-deflection for PNSM CFRP beams

The load-deflection relationships simulated by the numerical FEM model for the strengthened beams are shown in Figure 4.20 and compared to the experimental load-deflection curves. The correlation between the numerical output and the experimental results is satisfactory.

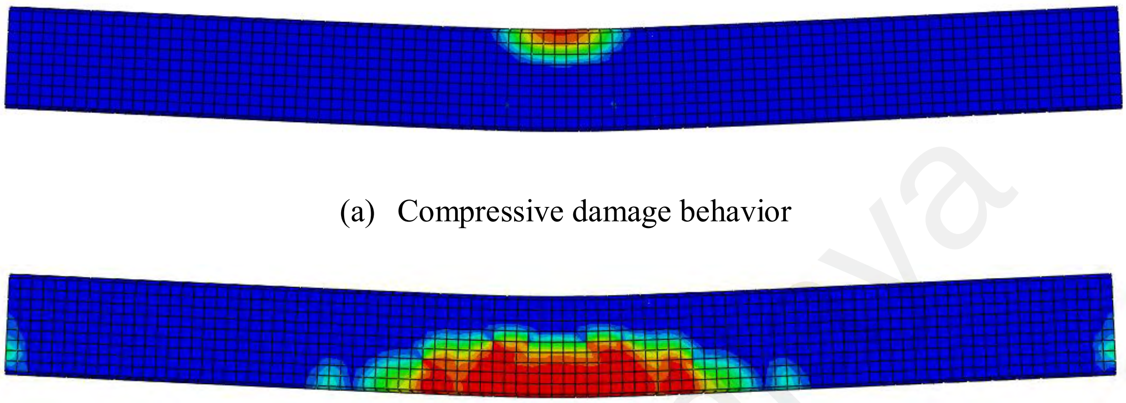

(a) Compressive damage behavior

(b) Tensile damage behavior

Figure 4.21: FEM damage behavior of NSM-C-70%F

The compressive and tensile damage behaviors simulated by the FEM model were similar for all the strengthened beams. Figure 4.21 shows the damage behavior of the 70% PNSM CFRP beam. The compressive and tensile damage behaviors are displayed separately due to ABAQUS requirements. The PNSM CFRP strengthened beams failed by concrete crushing at the top fiber of the beam together with CFRP rupture. The numerical model was able to simulate the concrete damage behavior of the strengthened beams with reasonably good similarity to the concrete failure observed in the experimental specimens.

4.4 PNSM Strengthened Beams Using Steel Strands

4.4.1 Flexural Capacities

Table 4.8 presents a summary of the flexural load capacities and corresponding deflection of all of the PNSM steel strand strengthened beams in terms of first crack load, service load, yield load, and ultimate load. The results of the control beam and a

NSM steel strand strengthened beam are also given for comparison. As shown in Table 4.8, the addition of the steel strand increased the ultimate load capacity by 28%, 30%, 33%, 35%, 37% and 40% for NSM-S-0%F, NSM-S-30%F, NSM-S-40%F, NSM-S-50%F, NSM-S-60%F and NSM-S-70%F, respectively, compared to the control beam. The first crack, service and yield load of the beams also increased significantly after strengthening. The most significant increase was seen at the service stage and yield stage in the PNSM strengthened beam with 70% prestress – the service load increased by 61% and the yield load increased by 57%, over the control beam.

Table 4.8: Experimental load and deflection results of PNSM steel strand beams

Beam specimen	Level of prestress (%)	First crack (P_{cr})		Service (P_s) (kN)	Yield (P_y)		Ultimate (P_{ult})	
		Load (kN)	Deflection (mm)		Load (kN)	Deflection (mm)	Load (kN)	Deflection (mm)
UB	-	63	3.1	83	110	19.8	127	45.6
NSM-S-0%F	0	66 (5%)	3.2	92 (10%)	145 (32%)	23.5	162 (28%)	38.3
NSM-S-30%F	30	77 (21%)	3.4	103 (24%)	154 (39%)	23.2	165 (30%)	36.0
NSM-S-40%F	40	78 (24%)	3.5	111 (33%)	164 (48%)	19.9	169 (33%)	36.8
NSM-S-50%F	50	81 (28%)	3.1	111 (34%)	169 (53%)	19.1	172 (35%)	35.3
NSM-S-60%F	60	85 (34%)	3.1	118 (42%)	170 (54%)	18.9	174 (37%)	33.7
NSM-S-70%F	70	88 (40%)	2.5	134 (61%)	174 (57%)	18.7	178 (40%)	30.1
Note: Parentheses represent percentage increase over control beam								

Increasing the level of prestress in the PNSM steel strand caused corresponding increases in the first crack, service, yield and ultimate loads. Increasing the prestress level also caused the yield load to rise to a higher proportion of the ultimate load. The yield of the control beam occurred at 87% of its ultimate load. However, in the strengthened beam with 70% prestress force (NSM-S-70%F) yield increased to 97% of the ultimate load. This is in agreement with El-Hacha et al. (2011).

There was also a remarkable increase in the first crack load of the PNSM strengthened beams compared to the control beam and the NSM strengthened beam without prestress. This improvement is a major advantage of using prestressed strengthening as early crack initiation can lead to excessive damage from the environment. Thus, a higher first crack load is highly advantageous.

In comparison to the NSM strengthened beam without prestress, the PNSM strengthened beams, especially at higher levels of prestress, showed remarkable enhancement in load carrying capacity at all stages. The most significant improvement was seen in the PNSM beam with 70% prestress which improved load capacity at first crack and service by 34% and 46%, respectively, over the NSM strengthened beam.

4.4.2 Failure Modes

The failure modes of the strengthened beams are shown in Figure 4.22. All of the strengthened beams had failure modes similar to the control beam, which is to say that failure occurred flexurally by concrete crushing in the main compression zone after yielding of the main steel reinforcement and the strengthening steel strands. This indicates that the strengthened beams experienced full composite action up to failure, as is desirable for all strengthened structures.

(a) NSM-S-0%F

(b) NSM-S-30%F

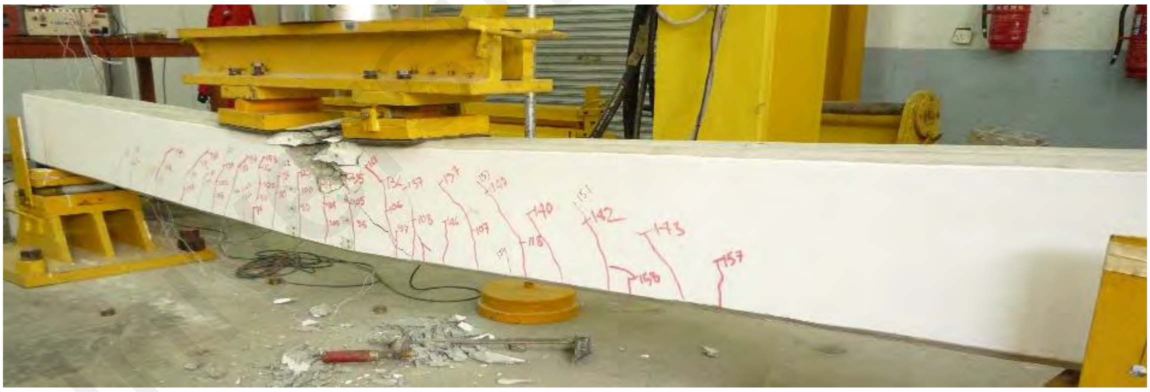

(c) NSM-S-40%F

(d) NSM-S-50%F

(e) NSM-S-60%F

(f) NSM-S-70%F

Figure 4.22: Failure modes of PNSM steel strand beams

4.4.3 Load-Deflection Behavior

The load versus midspan deflection curves of the PNSM steel strand strengthened beams are shown in Figure 4.23. The relation between the load and deflection of the strengthened beams was similar to the control beam. The beams displayed an initial steep linear elastic slope which gradually curves at a lower incline with increasing loads and rates of deflection until ultimate, after which the curve goes slowly downwards with increasing deflection but decreasing load. The linear elastic behavior remains mostly intact until yield, after which the beams enter the plastic deformation phase until complete failure as can be seen from the load-deflection curves in Figure 4.23. The gentle curve of this typical load-deflection behavior is characteristic of concrete beams with steel reinforcement and is indicative of the ductile behavior of the strengthened beams.

Strengthening with PNSM steel strands and increasing the level of the prestress force in the steel strand greatly reduced overall deflection for any given load level and increased the service range, while also increasing the load capacity of the beams. This can be seen from the increasingly higher curves of the PNSM strengthened beams in Figure 4.23. This was due to the increased stiffness of the beam from the addition of the steel strand and prestressing. The higher levels of prestress resulted in greater stiffness and less deflection. Prestressing the strengthening strand also further reduced deflection due to the additional cambering effect in the beams which delayed cracking, controlled crack widths and resisted the tensile stresses caused by loading (Wight et al. 2001). The delay in the formation of the first crack allowed the initial stiffness of the beams to remain active until a much higher load, which reduced deflection at all load levels.

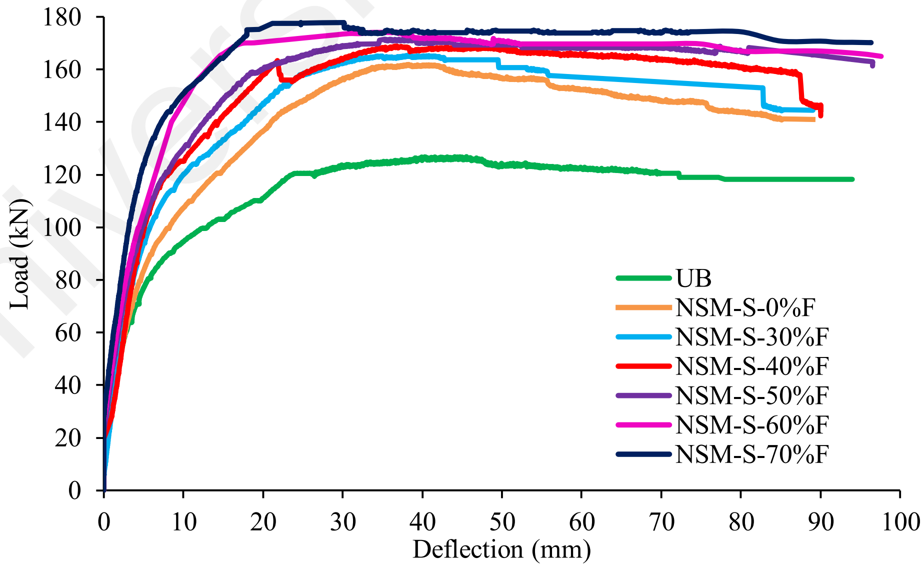

Figure 4.23: Load-deflection curves of PNSM steel strand beams

The exact deflection values of the tested beams at first crack, yield, ultimate and end point of test are given in Table 4.8. Prestressing the steel strand was able to control deflection at first crack and yield by maintaining deflection levels similar to the control beam even with the significant increases in load capacity of the beams at these stages. At ultimate, the PNSM steel strand strengthened beams displayed reduced deflection levels despite much higher ultimate loads than the control beam. Strengthening with a non-prestressed NSM steel strand and using lower levels of prestress (30% and 40%) caused deflection to slightly increase at first crack and yield due to the significant increase in load. However, at the higher levels of prestress (50%, 60% and 70%), it can be seen from Table 4.8 that deflection was controlled and reduced. The beam strengthened with 70% prestress showed the greatest reduction in deflection for any given load level. Beam NSM-S-70%F showed a reduction in deflection at ultimate of about 34% compared to the control beam and about 21% compared to the beam strengthened without prestress (NSM-S-0%F).

4.4.4 Cracking Behavior

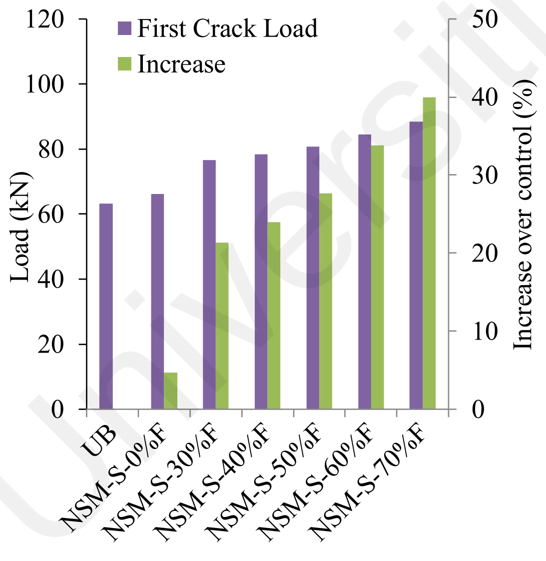

(a) Increase in first crack over control

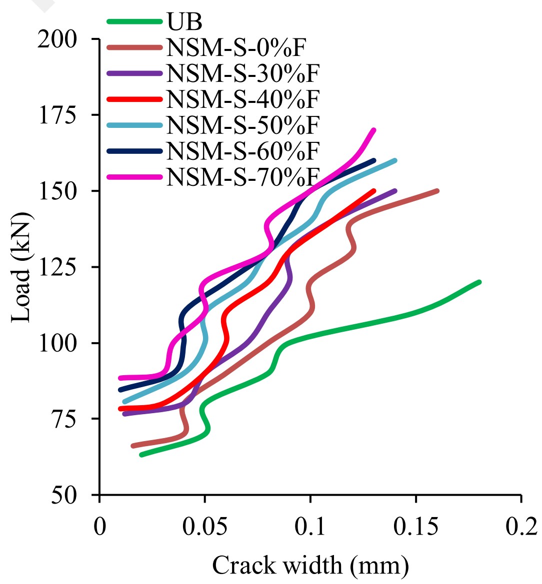

(b) Load vs crack width

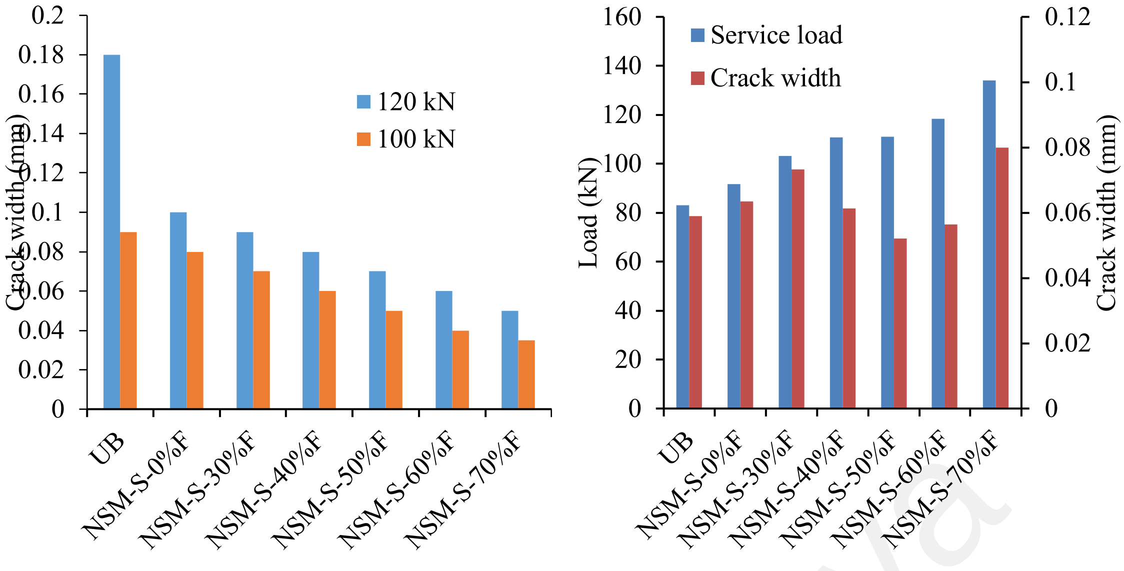

(c) Crack width at 100 kN and 120 kN

(d) Crack width at service load

Figure 4.24: Cracking behavior of PNSM steel strand beams

All of the PNSM steel strand strengthened beams displayed typical flexural crack patterns with greater crack development at the midspan. The fully developed crack patterns of all the strengthened beams at ultimate failure are shown in Figure 4.22. No longitudinal cracks were observed at the soffit of the beams between the epoxy and concrete or at the level of the bottom steel, indicating full composite beam behavior. The cracking behavior of all the strengthened beams improved in terms of first crack load, crack width, crack number and crack spacing compared to the control beam.

The exact values for the first crack load and the percentage increase in first crack load over the control beam for the PNSM steel strand strengthened beams can be seen in Table 4.8. The first crack load increased slightly in the NSM steel strand strengthened beam without prestress, but PNSM strengthening led to significantly higher increases, as can be seen in Figure 4.24 (a). This was due to the effect of the additional prestress force on the beam, which induced more compressive forces that balanced the internal bending forces from the applied loads. Increasing the prestress level in the PNSM strand also increased the first crack load to a higher proportion of the ultimate load.

Cracks occur when the tensile strain in the concrete exceeds the capacity of the concrete (cracking strain) (Hassoun, 1984; Rafi et al. 2008). The first crack usually develops into a critical crack with a relatively large width. For all of the beams, the first flexural crack developed in the midspan section between the two load points, starting from the soffit and extending towards the compression zone. The width of this crack was measured throughout testing at the lateral side of each specimen at the level of bottom longitudinal bar. The measured crack width of the beams at different load levels can be seen in Figure 4.24 (b). The measured crack width at any given load level was reduced by strengthening with PNSM strands and increasing the prestress level in the PNSM strand further reduced crack width compared to the control beam and NSM beam. As can be seen from Figure 4.24 (c), crack width at two random load levels, 100 kN and 120 kN, was significantly reduced by strengthening. Crack width is an important issue at the service stage. The crack widths of the beams at service load are shown in Figure 4.24 (d). As can be seen from the figure, the PNSM steel strand beams were mostly able to control crack width at service to levels similar to the control beam and the NSM steel beam without prestress, despite the significant increase in loads.

During testing it was observed that the crack width would sometimes decrease when new cracks formed, although loading was increased. This was due to the redistribution of stresses along the concrete beam. This phenomenon can be clearly seen in Figure 4.24 (b) from the wavy lines of the crack width graphs and was observed in all tested beams. New crack formation continued in the strengthened beams with increasing loading until yielding of the tensile reinforcement. The strengthened beams displayed more vertical flexural cracks with closer spacing, narrower crack widths and more uniform distribution compared to the control specimen. The control beam had 15 cracks spaced mostly along the midspan. The beam strengthened without prestress had 20 cracks and the beams with prestressed strengthening, 30%, 40%, 50%, 60% and 70%, had 24, 24, 25, 25, and 30 cracks, respectively. The increasing number of cracks resulted in increasingly closer spacing and smaller crack widths. The cracks were more concentrated nearer the midspan with fewer cracks near the supports. The flexural cracks continued to propagate with formation of some shear cracks at higher load levels, but shear failure was effectively controlled by the internal shear reinforcement. After yielding, no new cracks formed. However, existing cracks continued to increase with some of the major cracks at midspan forming branched crack patterns extending towards the top of the beam. Further loading after ultimate point led to greater deflection and increasing crack widths and depths.

Cracking behavior is an important aspect in the serviceability of concrete structures (Nawy 2005). The load at first crack is important because after first crack the initial integrity of the beam is lost and stiffness is reduced. If the first crack occurs early, the beam usually shows greater deflection and larger crack widths. Larger crack widths are especially problematic in field situations where the environmental elements can penetrate through large cracks and damage the reinforcing bars, leading to deterioration of a structure. Thus, higher first crack load and smaller crack widths are desirable to improve the durability of structures. Strengthening and especially prestressed strengthening, increases the first crack load, and causes more cracks to be distributed more evenly along the beam. The higher number of cracks and smaller spacing between cracks leads to reduced crack width. Increasing the level of prestress in the beam further increases these beneficial effects. In the practical field, in addition to repairing cracks using conventional sealing materials, structures with pre-existing cracks can be strengthened with prestressed strengthening materials to keep cracks closed or reduce crack widths.

4.4.5 Concrete Compressive Strains

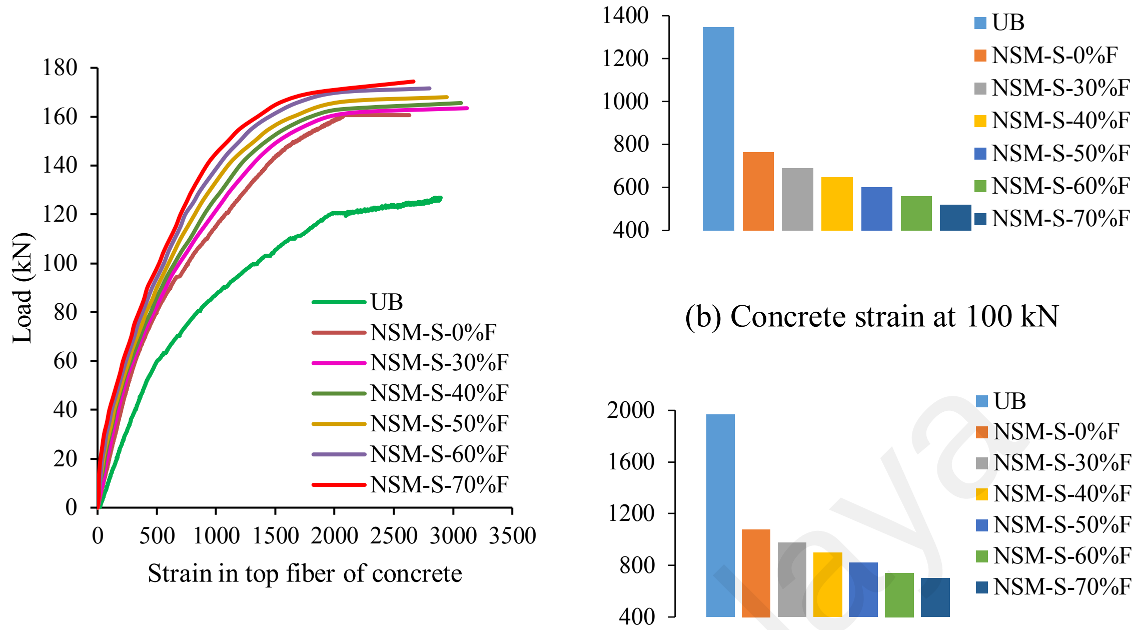

(a) Load vs concrete strain

(b) Concrete strain at 100 kN

(c) Concrete strain at 120 kN

Figure 4.25: Concrete compressive strain in PNSM steel strand beams

Figure 4.25 presents the measured compressive strain at the top fiber of the beam specimens. The concrete compressive strain increased in a linear manner until first crack and then almost linear at a shallower slope until yield for all the beam specimens. The maximum strain value was measured just before crushing of the concrete initiated, after which the strain gauge was damaged and unable to measure compressive strains. The beam strengthened with the non-prestressed NSM strand had a maximum concrete compressive strain of 0.002631. For the beams strengthened with PNSM, the maximum strain values measured were 0.003117, 0.003067, 0.002947, 0.002801 and 0.002666 for beams NSM-S-30%F, NSM-S-40%F, NSM-S-50%F, NSM-S-60%F and NSM-S-70%F, respectively. From Figure 4.25, it can be seen that concrete compressive strain decreased with strengthening and with increasing prestress force for any given load level. Compared with the control beam at the arbitrary load level of 100 kN [Figure 4.25(b)], concrete compressive strain was reduced by about 43%, 49%, 52%, 55%, 58%

and 61%, in the strengthened beams with 0%, 30%, 40%, 50%, 60% and 70% additional prestress force. A similar trend in strain reduction was seen at the higher arbitrary load level of 120 kN for the strengthened beams, as shown in Figure 4.25(c). Higher levels of prestress result in greater stiffness and consequent reduction of concrete compressive strain at the top fiber of the beam specimens.

4.4.6 Tensile Strains in Main Steel Strands

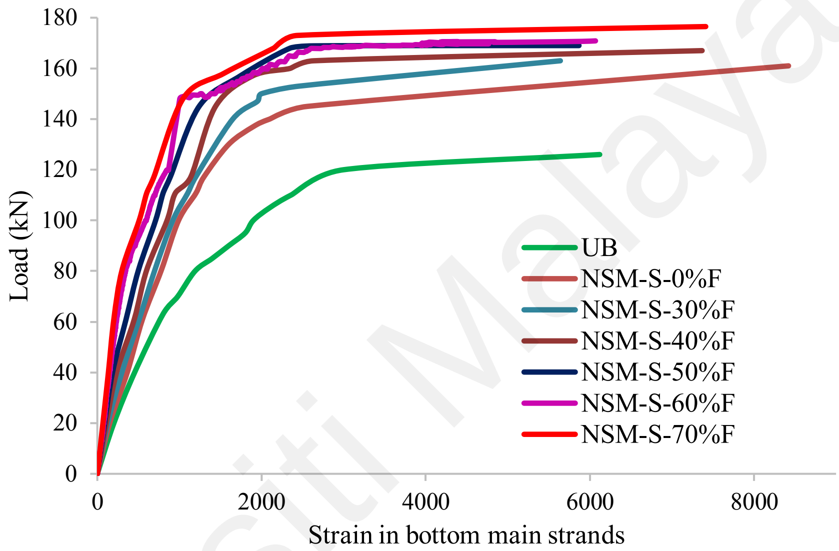

Figure 4.26: Main steel tensile strains in PNSM steel strand beams

Figure 4.26 presents the variations in tensile strain with increasing load level in the bottom main strands of the PNSM steel strand beams during testing. The strain was measured at midpoint where the strain was greatest. As can be seen from the diagram, all specimens displayed the typical linear elastic to plastic variation in tensile strain characteristic of steel. The main steel tensile strains of the strengthened beams were significantly reduced compared to the control beam at all load levels. Comparing the strain levels of the beam specimens at the arbitrary load levels of 100kN and 120kN, it can be seen that tensile strain decreased with increasing levels of prestress force in the PNSM strengthening strand. This is due to the increased stiffness of the beams. Higher levels of prestress resulted in greater stiffness and consequently greater reduction in tensile strain.

4.4.7 Tensile strains in PNSM Steel Strands

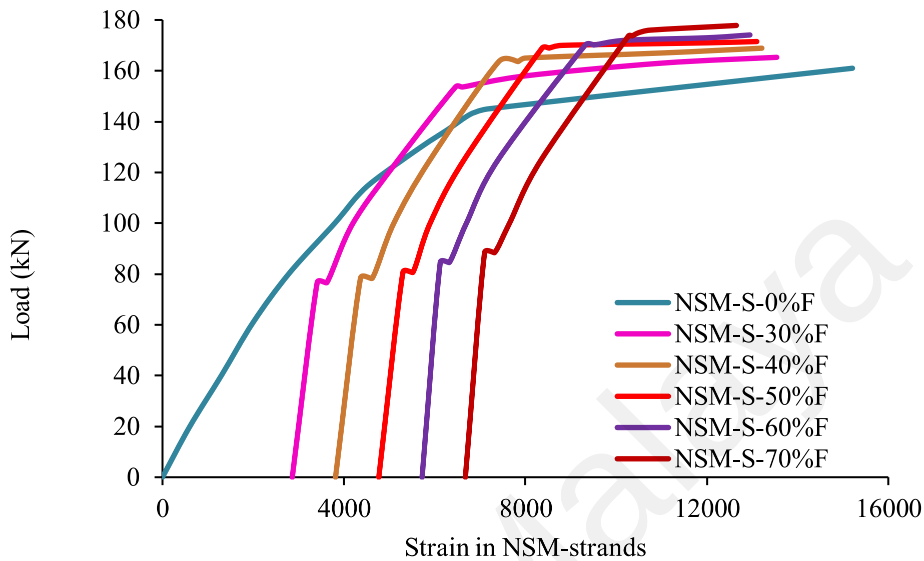

Figure 4.27: PNSM steel strand tensile strains

Figure 4.27 presents the variation in tensile strain with increasing load level in the PNSM strands of the strengthened beam specimens during testing. The strain was measured at midpoint where the strain is greatest. Prestressing caused an initial strain in the PNSM steel strands. This initial strain was calculated from the effective prestressing force and the load-tensile strain curves of the PNSM strands were accordingly displaced at zero loading, as can be seen in Figure 4.27. At first crack, tensile stresses shifted from the concrete beam section to the tensile reinforcements, which caused an abrupt increase in the tensile strain in these reinforcements. This can be seen as a small deflection at first crack load in the tensile strain graphs for the bottom main strands and the PNSM strands. As can also be seen from the graphs, the PNSM steel strands and the internal main steel strands underwent yielding at about the same time. This occurred due to the strain sharing properties of composite strengthened beams and indicates the composite action of the PNSM steel strand strengthened beams. From the tensile strain curves of the PNSM steel strands, it can be seen that prestressing caused the strain curves to become steep, indicating that the rate of strain increment in the steel strand was greatly reduced until yield compared to the non-prestressed steel strand. Prestressing also caused yield to occur at higher load and strain values, due to the increased stiffness of the beams. The maximum strain values before failure of the PNSM strands were reduced, due to the existing strain from prestressing reducing the final strain capacity of the strand. Overall, prestressing resulted in greater stiffness and consequently reduced tensile strain increment and higher yield point.

4.4.8 Ductility and Deformability

Ductility is the ability of a material, section or structure to withstand inelastic deformation before collapse, without significant loss in resistance or strength capability. It is a desirable structural property that allows stress redistribution and provides warning before failure by increasing deflections. The capacity of a reinforced member to gradually deform at the plastic stage is essential for various reinforced concrete design approaches. Ductility also provides a structure with the capacity to withstand sudden local impact and accidental loading without collapse (robustness), and the ability to dissipate energy under cyclic (e.g. seismic) loading (Morais et al. 2001).

The ductile behavior of a structural member after ultimate point until complete failure is specifically referred to as the deformability of the member. A higher deformability is beneficial for gradual progression towards complete failure with clear warning signs such as widening crack widths and greater deflection. Low deformability can result in sudden failure without warning (Choi et al. 2010). Deformability is an important safety factor as sudden catastrophic failures can lead to loss of life and excessive damage.

Many studies have found that increasing the reinforcement of a beam can decrease the ductile behavior of the beam due to increased stiffness (Rasheed et al. 2010). CFRP displays almost no ductility after ultimate point resulting in brittle failure modes where the structural member falls back on the residual strength of the steel reinforcement. However, beams reinforced with additional steel continue to show ductile behavior after ultimate point (deformability), comparable to the ductile behavior of unstrengthened reinforced concrete beams, resulting in gradual failure where the beam can continue to bear similar levels of loading with increased deflections. This difference is due to the different structural properties of CFRP and steel. CFRP displays linear elastic behavior until failure without the capacity to yield, while steel has the ability to yield after which it can continue to bear loading but at a lower rate with higher deflection.

To measure the ductility and deformability of a structural member, a ductility index and deformability index are commonly used (Hawileh et al. 2014). The ductility index and deformability index are expressed as follows:

$$\mu_{\Delta u} = \frac{\Delta_u}{\Delta_y} \tag{4.3}$$

$$\mu_{\Delta f} = \frac{\Delta_f}{\Delta_y} \tag{4.4}$$

Where $\mu_{\Delta u}$ is the ductility index at ultimate load, $\mu_{\Delta f}$ is the deformability index at failure load, Δ_u, Δ_f and Δ_y are the displacement at ultimate load, complete failure and yield load, respectively. Table 4.9 presents a comparison of the ductility and deformability indexes of the strengthened beam specimens with the control specimen.

The ductility index at ultimate load decreased with strengthening reinforcement. This is due to the increased stiffness of the strengthened beams. However, the deformability of the strengthened beams was almost similar to the unstrengthened beam, especially at higher levels of prestress. This deformable behavior after ultimate of the PNSM steel strand strengthened beams also indicates that the PNSM steel strand continued to work in a composite manner with the beam even after ultimate was reached and the residual capacity of the steel strands continued to be utilized until complete failure.

Table 4.9: Ductility and deformability of PNSM steel strand beams

Beam specimen	Ductility index $\mu_{\Delta u}$	Ratio over control beam	Deformability index $\mu_{\Delta f}$	Ratio over control beam
UB	2.30	1.00	4.74	1.00
NSM-S-0%F	1.63	0.71	3.80	0.80
NSM-S-30%F	1.55	0.68	3.85	0.81
NSM-S-40%F	1.85	0.80	4.52	0.95
NSM-S-50%F	1.85	0.80	5.07	1.07
NSM-S-60%F	1.78	0.78	5.16	1.09
NSM-S-70%F	1.61	0.70	5.15	1.09

This confirms that strengthening beams with steel is beneficial for the ductility of the beams both before and after ultimate. The greater stiffness and consequently lower ductility of the steel strengthened beam before ultimate results in greater strength capacity. The ductile behavior of the steel strengthened beams after ultimate is beneficial for gradual failure behavior.

Prestressing the strengthening strand did not very significantly change the ductility of the beam compared to the non-prestressed strengthened beam. However, the deformability index of the non-prestressed strengthened beam slightly decreased compared to the control beam, whereas for the beams strengthened with higher levels of prestress (50%, 60% and 70%), the deformability indexes were slightly higher than that of the control beam. These results imply that prestressed beams strengthened with steel strands will have the ability to meet the ductility and deformability requirements of reinforced concrete structures.

4.4.9 Energy Absorption Capacity

Energy absorption is an important characteristic for the evaluation of impact damage behavior and durability of the overall structural element. The energy absorption capacity was calculated as the area under the load–deflection curve. The energy absorption capacities for all the PNSM steel strand specimens are shown in Table 4.10. All the strengthened beams had higher energy absorption values compared to the control beam.

The strengthened beam without additional prestress, NSM-S-0%F, exhibited an increase in energy absorption of about 16% over the control beam. The specimens strengthened with additional prestressing force, NSM-S-30%F, NSM-S-40%F, NSM-S-50%F, NSM-S-60%F and NSM-S-70%F, exhibited an increase in energy absorption of about 22%, 28%, 42%, 48% and 50%, respectively, over the control beam. The increase in energy absorption of all the strengthened beams is due to delay in crack formation, increased stiffness, and considerable enhancement in yield and ultimate load. The ductile behavior of the strengthened beam specimens after ultimate also contributed to the high energy absorption values. The beam strengthened with the highest level of prestress, 70% prestressing force, showed the largest increase in energy absorption. This large increase in energy absorption is related to the large increase in failure load and greater stiffness after yielding compared to the other beams.

Thus, strengthening with PNSM steel strands significantly enhanced energy absorption capacity. The results of this study are in agreement with previous research. Omran and El-Hacha (2010) concluded in their study that energy absorption increases in prestressed strengthened beams when the prestressing level, tensile reinforcement ratio, or concrete compressive strength are increased, as long as failure is governed by concrete crushing.

Table 4.10: Effect of PNSM steel strand strengthening on energy absorption and stiffness

Beam specimens	Energy dissipation	Increase over control beam	Stiffness at service	Increase over control beam
	E (kN.mm)	(%)	(kN/m)	(%)
UB	10721	-	6269	-
NSM-S-0%F	12443	16%	8306	32%
NSM-S-30%F	13043	22%	9345	49%
NSM-S-40%F	13745	28%	11911	90%
NSM-S-50%F	15237	42%	9761	56%
NSM-S-60%F	15831	48%	10720	71%
NSM-S-70%F	16055	50%	12316	96%

4.4.10 Stiffness

Flexural stiffness is the ability to resist bending or deflection under loading and is also called flexural rigidity. It is an essential concern when considering the serviceability behavior of concrete structures. Increased stiffness influences structural properties such as deflection, ductility and cracking behavior.

The stiffness of the beam specimens can be seen from the slope of the load-deflection graphs (Figure. 4.23). The initial stiffness of the beams is linear until first crack. After first crack, all specimens showed a reduction in stiffness. Most beams that carry service loads are usually at this stage (Nawy E.G. 2005). Hence, it is important to evaluate the increase in stiffness at the service load range due to strengthening of the specimens. The service load range is defined as the load range from first crack load to the load corresponding to the point of deflection that is equal to the span/480. This ratio is provided by the ACI 318-11 standard for roofs or floors constructed supporting or attached to nonstructural elements that are likely to be damaged by large deflections. The service load deflection (span/480) for the beam specimens was found to be 6.25 mm. The stiffness was calculated as the ratio of the applied load at service range to the corresponding deflection. The stiffness values of all the specimens are presented in Table 4.10.

All the strengthened specimens exhibited an increase in stiffness at service over the control beam. Prestressing the steel strand resulted in greater stiffness of the beam, with higher levels of prestress corresponding to greater stiffness. The beam strengthened with 70% prestress (NSM-S-70%F) showed the greatest increase in stiffness at 96.45% over the control beam.

In normal unstrengthened beams, the internal steel reinforcement affects the stiffness of the beam by controlling the growth of cracks. In strengthened beams, the strengthening material provides additional restraint to the initiation and growth of cracks. Prestressing the strengthening material further controls cracking and thus further increases the stiffness of the beam compared to non-prestressed strengthening. In the PNSM steel strand strengthened beams in this study, the overall stiffness of the beams was greatly enhanced by the use of steel strands and by increasing the level of prestress.

4.4.11 Prestress Losses

The prestress forces applied to the steel strands were monitored during prestressing, during the six days curing period and at release. For the strengthened beams NSM-S-30%F, NSM-S-40%F, NSM-S-50%F, NSM-S-60%F and NSM-S-70%F the PNSM strand was prestressed to 30.69 kN, 40.92 kN, 51.15 kN, 61.38 kN and 71.61 kN, respectively. After prestressing, the PNSM strands were locked in place for six days to allow the epoxy to cure before the prestress force was released. The prestress levels in the steel strands over the six-day curing period are shown in Figure 4.28. The prestress loss during this time was negligible at about 0.28kN to 0.46kN. Thus, at the time of testing the beams, the effective prestress levels were 30%, 40%, 50%, 60% and 70% in the respective beam specimens as shown in Table 4.11. The prestressing force was released at a slow rate of about 20% at a time until 100% of the prestress force was released. This was done by controlling the hydraulic jack and adjustor clamp. No crack formation was noticed during and after the release of the prestressing force. After release of the prestressing force, a negative bending moment occurs due to the eccentricity of the prestress force in relation to the neutral axis of the beam, causing a negative camber (upward deflection) in the beam. This cambering effect was measured using an LVDT to monitor the deflection at midspan during the release of the prestress force. The initial cambers of the prestressed beams are shown in Table 4.11. The higher levels of prestress produced greater cambering in the beams.

Table 4.11: Prestress force and camber effect in the PNSM steel strand beams

Beam specimen	Applied prestress force		Effective prestress force		Negative camber at mid-section (mm)
	(kN)	(%)	(kN)	(%)	
NSM-S-30%F	30.7	30	30.4	29.7	0.15
NSM-S-40%F	40.9	40	40.6	39.7	0.25
NSM-S-50%F	51.2	50	50.8	49.7	0.40
NSM-S-60%F	61.4	60	61.0	59.6	0.60
NSM-S-70%F	71.6	70	71.1	69.6	0.75

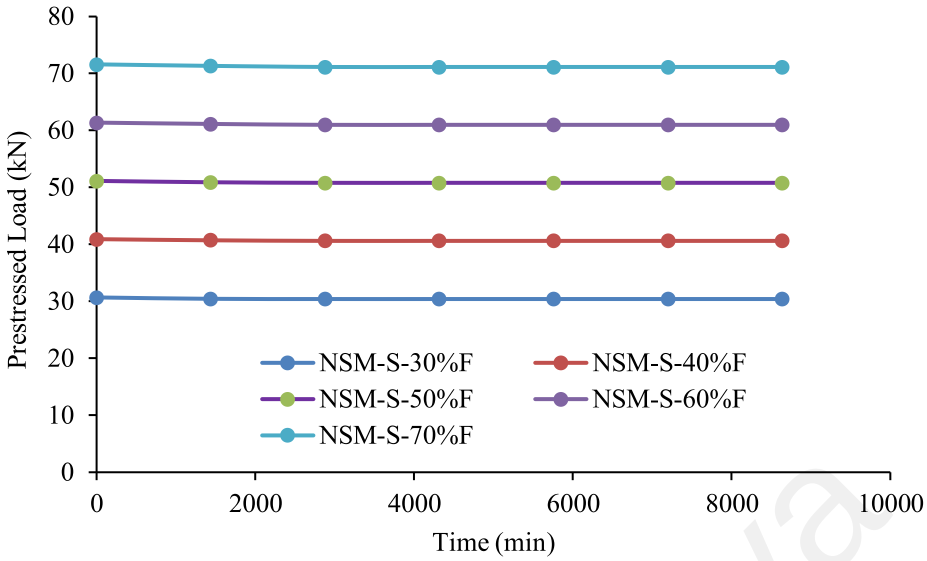

Figure 4.28: Prestress force during curing period in PNSM steel strands

4.4.12 Effect of Increasing Prestress Level

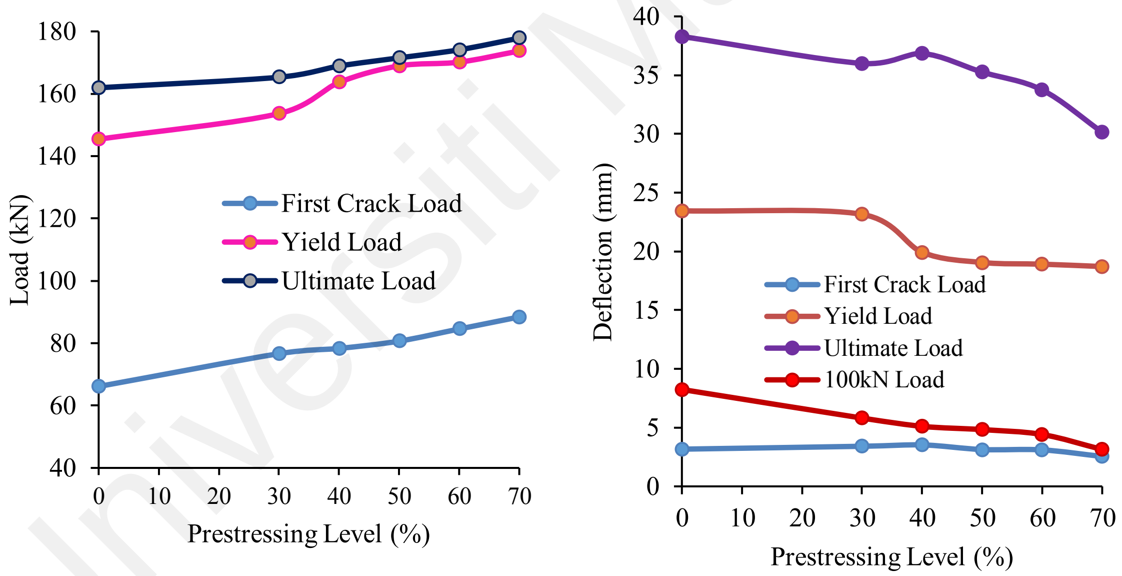

(a) Load vs prestress level (b) Deflection vs prestress level

Figure 4.29: Effect of prestress level on PNSM steel strand beams

To evaluate the effect of prestressing the steel strand on the overall flexural behavior of the strengthened beams, two graphs of the structural performance of the PNSM steel strand beams with various prestress levels (10% - 70%) and the NSM steel strand beam (0%) are shown in Figure 4.29. The first graph [Figure 4.29 (a)] shows the effect of increasing the level of prestress force in the steel strand on the first crack, yield and ultimate loads of the beam specimens. The second graph shows the effect of increasing the prestress level in the strengthening strand on the deflection of the beam specimens at first crack, yield, ultimate and at a randomly chosen load level of 100 kN. The exact load and deflection values of the tested beams at first crack, yield and ultimate are shown in Table 4.8.

Increasing the prestress level in the strengthening strand significantly increased the first crack and yield loads, and slightly increased the ultimate load [Figure 4.29(a)]. Based on the results, prestressing the steel strand to 70% of its tensile capacity produced the best performance in the strengthened beams in terms of first crack, yield and ultimate loads compared to the beams with no prestress and lower levels of prestress in the strengthening strand. The first crack yield and ultimate loads of the 70% prestressed strengthened beam increased by about 34%, 20% and 10% compared to the beam without prestressed strengthening. This indicates that the load-carrying capacity of the beam was significantly improved by increasing the level of prestress in the PNSM strands, especially at the service stage.

Overall, the deflections of the PNSM steel strand beams decreased with increasing levels of prestress for any given load level. At an arbitrary load level of 100 kN, the deflection decreased by 30%, 38%, 41%, 46.5% and 62% for beams NSM-S-30%F, NSM-S-40%F, NSM-S-50%F, NSM-S-60%F and NSM-S-70%F, respectively, compared to beam NSM-S-0%F. The deflection at first crack for the PNSM strengthened beams was comparable to the NSM beam without prestress, indicating that the prestressed strengthening was able to control deflection at this stage despite the significantly increased first crack loads. However, the beam strengthened with the highest level of prestress (70%) was able to reduce deflection at first crack by about

20% compared to the beam strengthened without prestress. The deflections at yield and ultimate load decreased with increasing levels of prestress and compared to the non-prestressed strengthened beam. The decrease in deflection at yield and ultimate load was most significant for the beam strengthened with the 70% prestress, with a 20% and 21% decrease, respectively, over the beam with non-prestressed strengthening. The 40% PNSM beam showed a pronounced decrease in deflection at yield compared to the beam with 30% PNSM beam. This is due to the greater deflection at yield point of the 30% prestressed specimen compared to other specimens which may have occurred due to instrumental error. Overall, it was found that deflection can be significantly reduced by increasing the level of prestressed strengthening, especially at the serviceability stage. Higher levels of prestress can control deflection to a greater degree than lower levels of prestress. From the results of the PNSM steel strand beams, 70% prestressed strengthening was found to be the most effective level of prestress for decreasing deflection at all load stages. This is due to the greater stiffening effect of the higher level of prestress on the beam.

The beams strengthened with prestressed strengthening failed in the same mode as the beam strengthened with no prestress, as well as the control beam, namely flexural failure with concrete crushing at the top fiber of the beam. This is the most desirable mode of failure for a structure as it indicates full composite action between the beam and the strengthening system, and that the full load-bearing capacity of the strengthening material was utilized. PNSM strengthening, even at higher levels of prestress, was able to avoid premature debonding failure. This can be attributed to the prestress effect which creates a negative camber in the beams, which decreases the possibility of debonding as tensile stresses are reduced.

4.4.13 Assessment of FEM

Table 4.12: Experimental and FEM results at ultimate for PNSM steel strand beams

Beam specimens	Level of prestress (%)	Experimental		FEM		FEM/Experimental	
		Load (kN)	Deflection (mm)	Load (kN)	Deflection (mm)	Load (P_{FEM}/P_{exp})	Deflection ($\Delta_{FEM}/\Delta_{exp}$)
UB	-	127	45.6	131	46.5	1.03	1.02
NSM-S-0%F	0	162	38.3	163	39.3	1.00	1.03
NSM-S-50%F	50	172	35.3	168	36.1	0.98	1.02
NSM-S-60%F	60	174	33.7	170	34.0	0.98	1.01
NSM-S-70%F	70	178	30.1	172	31.7	0.97	1.05

Table 4.12 presents a comparison of the experimental and FEM results for ultimate load and deflection for the control beam, the NSM steel strand strengthened beam and the PNSM steel strand strengthened beams with 50%, 60% and 70% prestress. The percentage error between the experimental and numerical results reached a maximum of 3% for ultimate load and 5% for the corresponding deflection, which is within the acceptable limit (10%) [20]. The agreement between the ultimate load capacity and deflection values produced by the FEM model and the experimental results is satisfactory.

The correlation between the load-deflection relationships generated by the numerical model and the experimental load-deflection curves was reasonably good as can be seen in Figure 4.30.

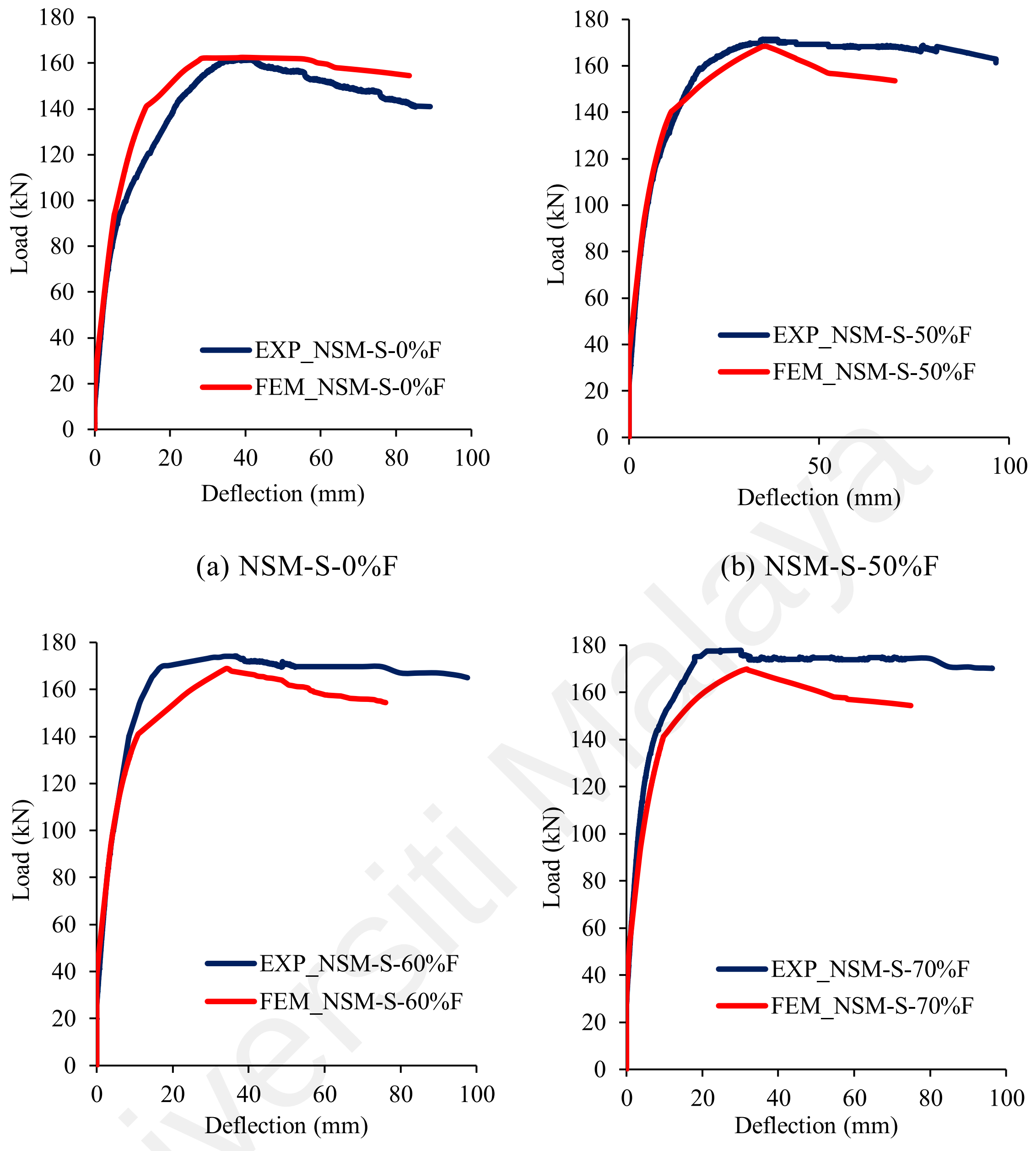

(a) NSM-S-0%F (b) NSM-S-50%F

(c) NSM-S-60%F (d) NSM-S-70%F

Figure 4.30: FEM load-deflection for PNSM steel strand beams

Figure 4.31 shows the pattern of concrete damage generated by the FEM model for the 70% PNSM steel strand beam. All of the FEM simulated beams presented similar patterns of damage behavior, with the greatest damage occurring at the bottom flexural zone and the top midspan compressive zone. This was similar to the experimental results as the experimental failure modes of the PNSM steel strand beams, the NSM steel strand beam and the control beam were all by concrete crushing at the top fiber of the beam after yielding of the tension reinforcement. Also, experimentally the prevailing crack pattern of the strengthened beams was of flexural cracks spaced along span of the beam with greater crack development in the midspan region. Thus, the numerical damage behavior of the beams agreed reasonably well with the experimental failure modes and crack patterns.

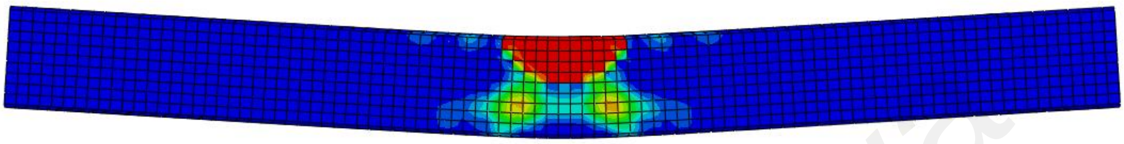

(a) Compressive damage behavior

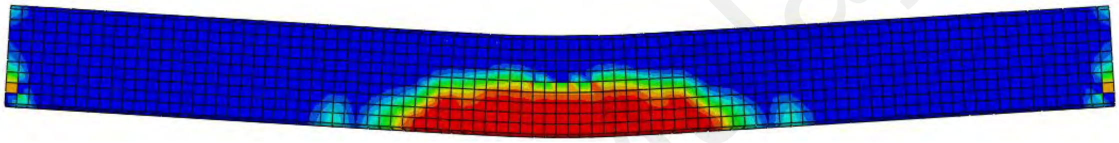

(b) Tensile damage behavior

Figure 4.31: FEM damage behavior of NSM-S-70%F

4.5 CEBPNSM Strengthened Beams Using CFRP Bars and CFRP Sheet

4.5.1 Flexural Capacities

The flexural load capacities of the CEBPNSM strengthened beams using CFRP bars and CFRP sheet in terms of first crack, service, yield and ultimate loads, and the corresponding deflections and percentage increase in loads over the control beam are presented in Table 4.13. The load and deflection results of the control beam, the EBR CFRP sheet strengthened beam and the NSM CFRP bar strengthened beam are also given in Table 4.13 for comparison purposes. In general, CEBPNSM strengthening greatly enhanced the flexural capacity of the beam at all stages and the strengthened beams with higher levels of prestress showed the greatest enhancement.

Table 4.13: Experimental load and deflection results for CEBPNSM beams with CFRP bar and CFRP sheet

Beam specimen	Level of prestress (%)	First crack (P_{cr})		Service load (Ps) (kN)	Yield (P_y)		Ultimate (P_{ult})	
		Load (kN)	Deflection (mm)		Load (kN)	Deflection (mm)	Load (kN)	Deflection (mm)
UB	-	63	3.1	83	110	19.8	127	45.6
EBR-Sh	-	70 (10%)	3.2	93 (11%)	118 (7%)	9.7	165 (30%)	48.6
NSM-C-0%F	0	67 (6%)	3.4	86 (3%)	113 (2%)	11.7	166 (31%)	40.1
NSM-C-0%F-Sh	0	73 (16%)	3.2	87 (5%)	120 (9%)	13.0	204 (61%)	44.2
NSM-C-50%F-Sh	50	88 (40%)	3.2	104 (25%)	140 (27%)	12.9	216 (70%)	41.4
NSM-C-60%F-Sh	60	93 (46%)	3.1	110 (32%)	147 (34%)	12.9	218 (72%)	39.8
NSM-C-70%F-Sh	70	96 (53%)	3.0	116 (40%)	156 (41%)	12.7	224 (76%)	38.1
Note: Parentheses represents percentage increase over control beam								

The first crack load increased significantly in the CEBPNSM strengthened beams by 40%, 46% and 53% for NSM-C-50%F-Sh, NSM-C-60%F-Sh and NSM-C-70%F-Sh, respectively, compared to the control beam [Figure 4.32 (a)]. In comparison, the first crack load increased by only 16% in the CEBNSM strengthened beam (NSM-C-0%F-Sh), 10% in the EBR CFRP sheet strengthened beam, and 6% in the NSM CFRP bar strengthened beam, over the control beam.

The service load of the CEBPNSM strengthened beams was also significantly enhanced by 25%, 32% and 40% for NSM-C-50%F-Sh, NSM-C-60%F-Sh and NSM-C-70%F-Sh, respectively, over the control beam [Figure 4.32 (b)]. In comparison, the CEBNSM beam (NSM-C-0%F-Sh), the EBR CFRP sheet strengthened beam and the

NSM CFRP bar strengthened beam showed increases in service load of 5%, 11% and 3%, over the control beam.

The yield load and ultimate load were also similarly enhanced by the CEBPNSM technique. The yield load increased by 27%, 34% and 41% in the NSM-C-50%F-Sh, NSM-C-60%F-Sh and NSM-C-70%F-Sh beams, respectively, over the control beam [Figure 4.32 (c)]. While the yield load in the CEBNSM beam, the EBR CFRP sheet strengthened beam and the NSM CFRP bar strengthened beam increased by only 9%, 7% and 2%, respectively, over the control beam.

The ultimate load increased by 70%, 72% and 76% in the CEBPNSM strengthened beams, NSM-C-50%F-Sh, NSM-C-60%F-Sh and NSM-C-70%F-Sh, respectively, over the control beam [Figure 4.32 (d)]. The increase in ultimate in the CEBNSM beam, the EBR CFRP sheet strengthened beam and the NSM CFRP bar strengthened beam was only 61%, 30% and 31%.

The greatest increase in flexural load carrying capacity at all stages was seen in the CEBPNSM strengthened beam with the most prestress (NSM-C-70%F-Sh). The most significant increase over the control beam was seen at ultimate where the load increased by 76%. In comparison to the EBR and the NSM strengthened beams, CEBPNSM strengthened beams far outperformed them at all load stages. The significant enhancement in flexural capacity of the CEBPNSM strengthened beams over the control beam, EBR beam and NSM beam can be attributed to the combination of materials, techniques and prestress force. In comparison to the CEBNSM strengthened beam (without prestress), it can be seen that the additional prestress used in the CEBPNSM strengthened beams caused significant increases in load capacity at each stage (Figure 4.33). The most significant increase in load capacity over the CEBNSM beam was seen at service, where the CEBPNSM beams with 50%, 60% and 70%

prestress (NSM-C-50%F-Sh, NSM-C-60%F-Sh and NSM-C-70%F-Sh) showed increases of 15%, 25% and 34%, respectively, over the CEBNSM beam. The CEBPNSM beam with 70% prestress (NSM-C-70%F-Sh) was able to enhance first crack, yield and ultimate loads by 32%, 24% and 10%, respectively, over the CEBNSM beam (NSM-C-0%F-Sh).

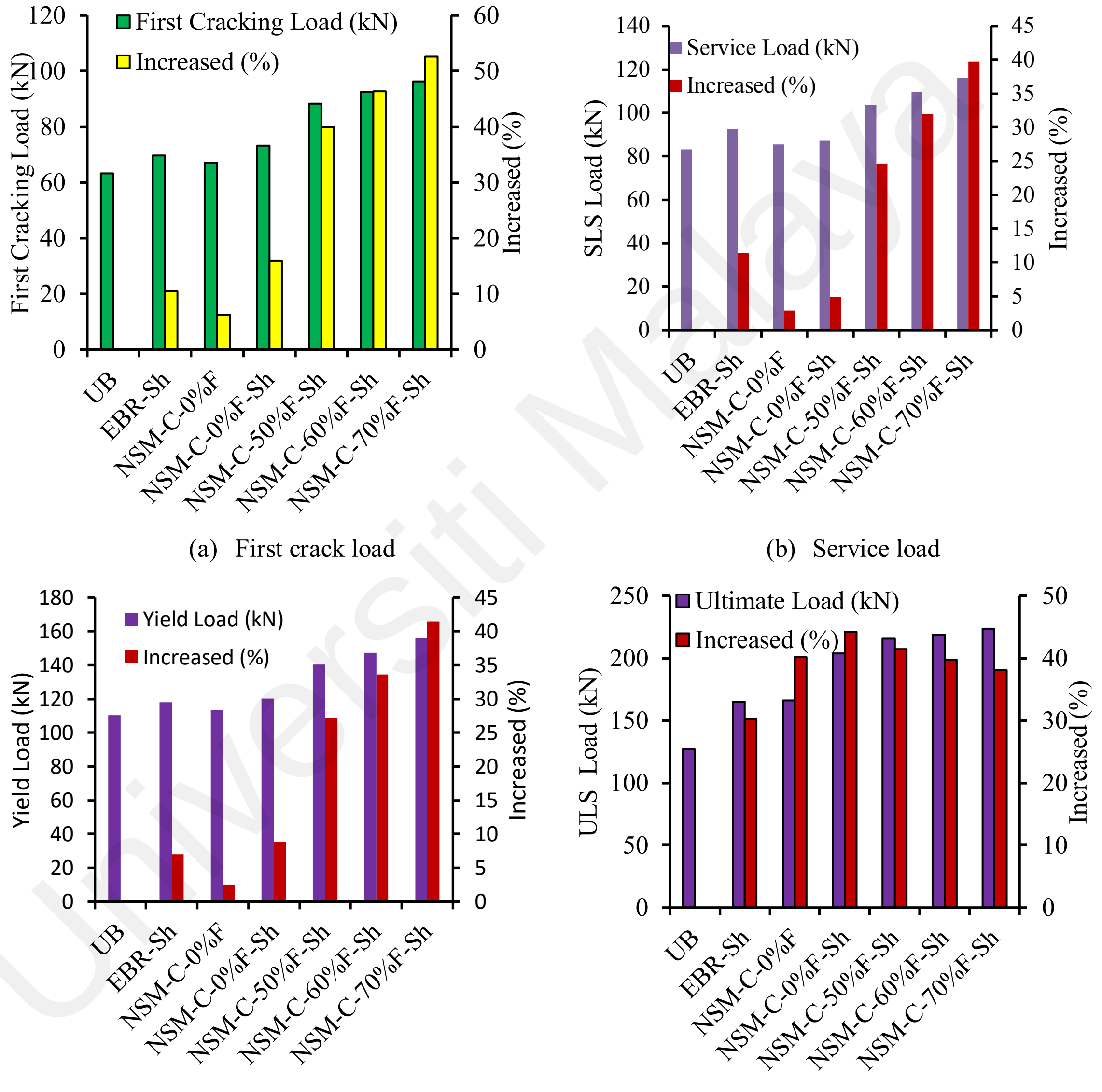

(a) First crack load

(b) Service load

(c) Yield load

(d) Ultimate load

Figure 4.32: Load enhancement over control beam of CEBPNSM beams with CFRP bar and CFRP sheet

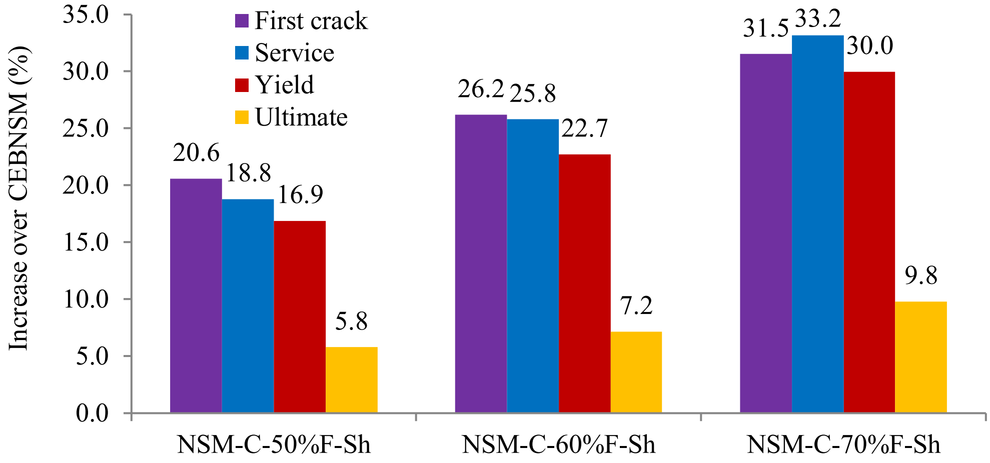

Figure 4.33: Load enhancement over CEBNSM beam of CEBPNSM beams with CFRP bar and CFRP sheet

4.5.2 Failure Modes

Figure 4.34 shows the failure modes of the CEBPNSM beams and the CEBNSM beam strengthened with CFRP bars and CFRP sheet. All the beams failed in a flexural manner by rupture of the CFRP in combination with concrete crushing after the main tension reinforcement yielded, similar to the beams strengthened with PNSM CFRP bars. At ultimate, concrete crushing initiation was observed at the top fiber of the beams and was quickly followed by rupture of the CFRP sheet at midspan where the tensile stress was the greatest. The CFRP sheet ruptured in stages, with initially a small portion of the sheet splitting away from the beam. A loud sound was heard as CFRP rupture initiated, due to the sudden loss of beam stiffness. It is assumed that the CFRP bar also ruptured at this stage, although no observable signs were seen on the outside of the beam. This assumption is based on the load-deflection behavior of the beams (Figure 4.35) where it can be clearly seen that the load capacity of the beams fell back to the level of the internal steel reinforcement, indicating that both the CFRP sheet and CFRP bar were no longer able to carry any loading. No debonding of the NSM CFRP bar or the CFRP sheet was observed during testing. The failure behavior of these strengthened beams indicates that full composite action was achieved and the full strength of the CFRP bar and CFRP sheet were utilized.


(a) NSM-C-0%F-Sh

(b) NSM-C-50%F-Sh
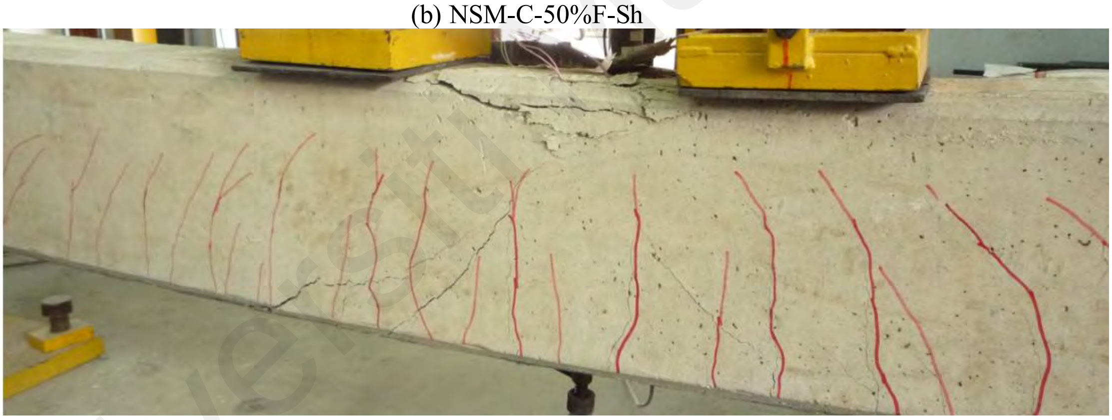
(c) NSM-C-60%F-Sh
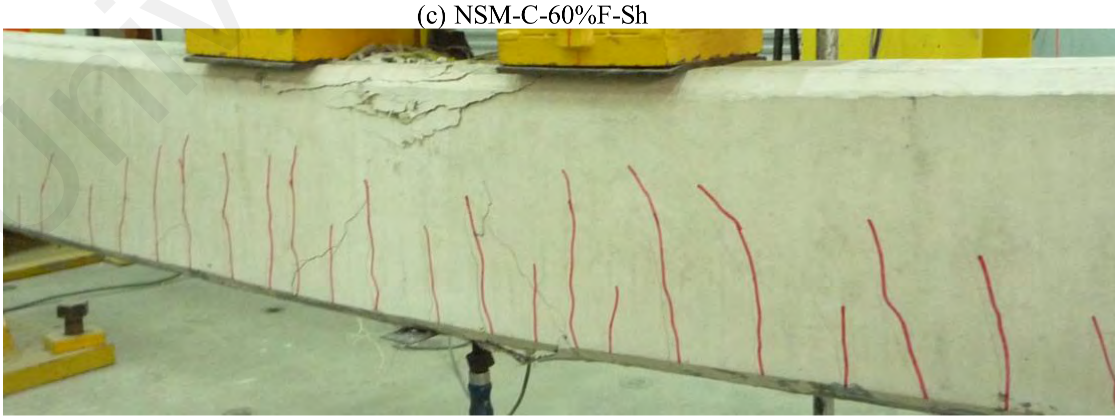
(d) NSM-C-70%F-Sh

Figure 4.34: Failure modes of CEBPNSM beams strengthened with CFRP bars and CFRP sheet

4.5.3 Load-Deflection Behavior

The load-deflection behavior of the beams strengthened using CEBPNSM with CFRP bars and CFRP sheet are presented in Figure 4.35 and the exact deflection values at first crack, yield, and ultimate are given in Table 4.13. The load-deflection behavior of the CEBPNSM strengthened beams was somewhat similar to that of the NSM, EBR and CEBNSM strengthened beams, as can be seen in Figure 4.35, in that the typical tri-linear response of CFRP strengthened beams was observed in all the beams until ultimate, after which the rupture of the CFRP caused the loading to fall back to the level of the internal steel. The first three stages from load initiation to first crack, first crack to yield and yield to ultimate were linear in response, although at each stage the rate of deflection increased as beam stiffness was reduced due to cracking and yielding. This was followed by a degradation phase where the beam response was erratic with large deflections and two large drops in loading as the CFRP bar and CFRP sheet ruptured and load capacity fell back on the main reinforcements. The behavior of the beams was then governed by the remaining strength in the internal steel reinforcements until complete failure with large deflections.

However, the CEBPNSM and CEBNSM strengthened beams had significantly higher load-deflection curves compared to the EBR and NSM strengthened beams, and the control beam. At first crack, the deflections of the combined strengthened beams (CEBPNSM and CEBNSM) were less than the EBR and NSM strengthened beams, and comparable to the control beam, even though first crack load was significantly increased, as can be seen in Table 4.13. Both of these effects can be attributed to the increased amount of strengthening material, which increased stiffness, reduced deflection and greatly improved load capacity at all stages. At yield, the deflection of the combined strengthened beams was greater than the EBR and NSM beams (due to the significantly higher yield loads attained by the combined strengthened beams), although the yield deflection was still significantly less than the control beam. At ultimate, the deflection of the combined strengthened beams was less than the EBR and control beams, but comparable to the NSM strengthened beam.

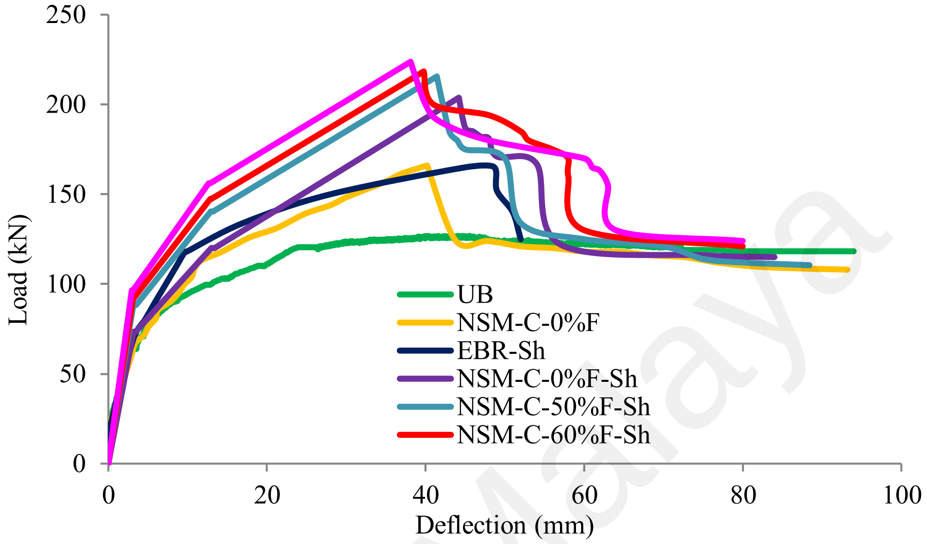

Figure 4.35: Load-deflection curves of CEBPNSM beams strengthened with CFRP bars and CFRP sheet

When comparing the two combined techniques, CEBNSM and CEBPNSM, it can be seen that the CEBPNSM beams had significantly higher and steeper load-deflection curves and increasing the level of prestress caused a corresponding increase in this effect, indicating the reduced deflection and increased flexural capacity of the CEBPSNM beams with higher levels of prestress. At first crack, yield and ultimate, the CEBPNSM beams displayed less deflection than the CEBNSM beam and increasing the level of prestress produced further reductions in deflection, while simultaneously further increasing the flexural loads. This ability of prestress force to control deflection is due to the compressive strain introduced by the prestress force into the tension region of the beams, which inhibits the formation and widening of cracks, and opposes tensile stresses, thus increasing beam stiffness and strength. Among the combined strengthened beams in this group, the CEBPNSM beam with 70% prestress (NSM-C-70%F-Sh) showed the greatest enhancement in load-deflection response and the most reduction in deflection at all load stages.

Overall, CEBPNSM strengthening was able to significantly reduce deflection at any given load level, while greatly increasing load capacity for any given deflection, compared to the other strengthening techniques and the control beam.

4.5.4 Cracking Behavior

The CEBPNSM beams strengthened with CFRP bars and CFRP sheet showed typical flexural crack patterns, as can be seen in Figure 4.34. Overall, first crack load, crack width, crack number and crack spacing showed significant improvement over the control beam. The beam specimens displayed new flexural cracks from first crack until yield, after which no new cracks formed, although the existing cracks continued to widen and grow. The CEBPNSM strengthened beams showed more cracks, with smaller crack widths and crack spacing, and more uniform crack distribution along the midspan compared to the control beam. The average number of cracks observed on the CEBPNSM beams was 26. No longitudinal cracks were seen at the soffit or on the sides of any of the strengthened specimens, which indicates the full composite action between the beams and the strengthening materials.

The CEBPNSM strengthened beams were able to enhance cracking behavior significantly more than the EBR, NSM and CEBNSM strengthened beams. Increasing the level of prestress in the CEBPNSM strengthening caused the enhancements in cracking behavior to become significantly more pronounced. Thus, the CEBPNSM strengthened beam with the highest level of prestress (NSM-C-70%F-Sh) showed the greatest enhancement in cracking behavior. The NSM-C-70%F-Sh increased first crack load by 53% over the control beam, while also reducing first crack deflection, compared to the EBR, NSM and CEBNSM beams, which improved first crack load by 10%, 6%

and 16% over the control, respectively, while slightly increasing first crack deflection (Table 4.13).

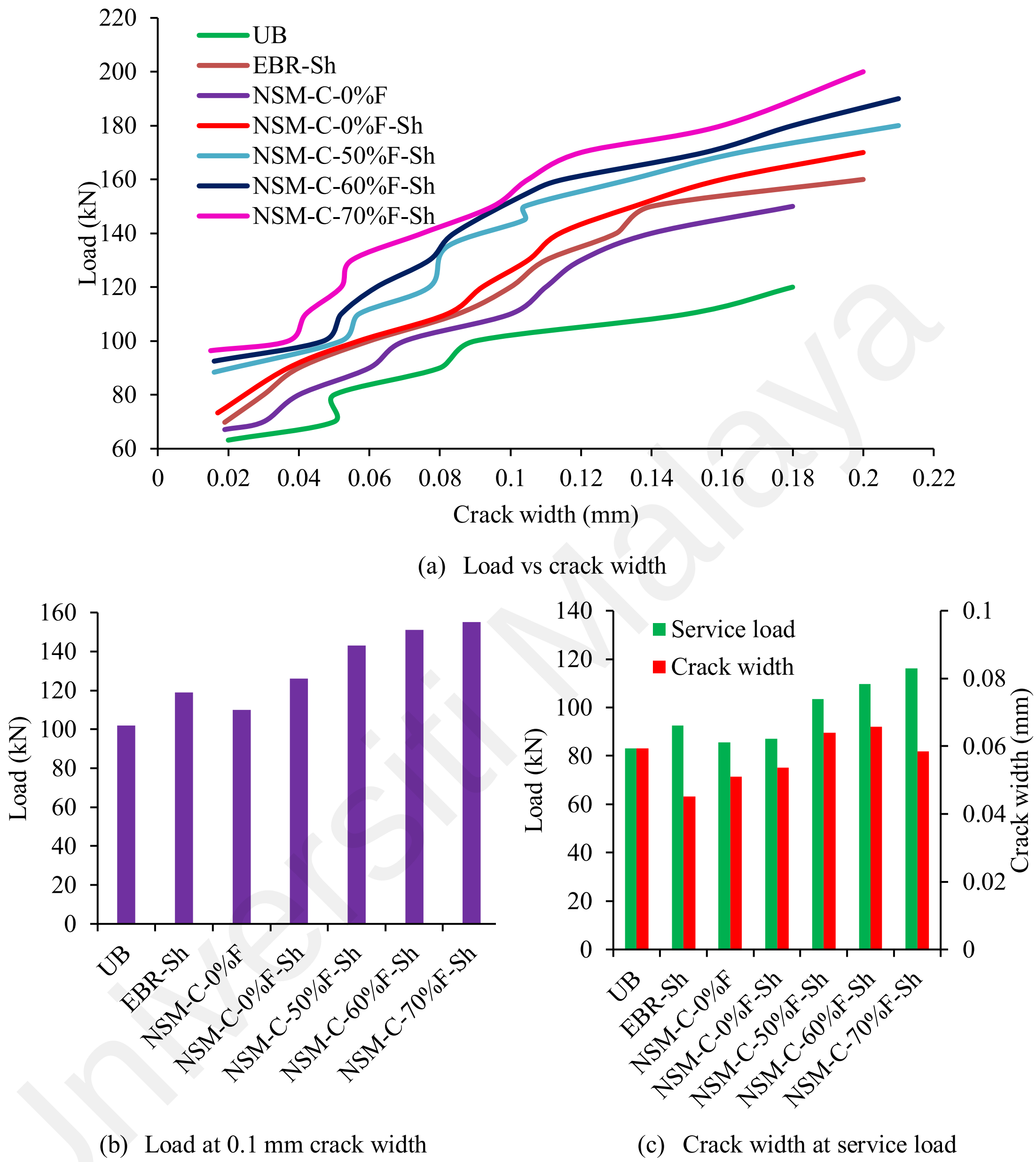

Figure 4.36: Cracking behavior of CEBPNSM beams strengthened with CFRP bar and CFRP sheet

As can be seen in Figure 4.36 (a), the crack width of NSM-C-70%F-Sh was significantly less than the EBR, NSM and CEBNSM beams for any given load level. For a given crack width, such as at 0.1 mm [Figure 4.36 (b)], NSM-C-70%F-Sh was able to greatly increase the load level compared to the other beams. Crack width at service is an important design consideration, and as can be seen in Figure 4.36 (c), NSM-C-70%F-Sh was able to reduce crack width at service in comparison to the control beam, despite the greatly increased service load.

These significant improvements in cracking behavior seen in the CEBPNSM beams can be attributed to the combination of strengthening materials and techniques, and the use of prestress force as an additional strengthening enhancement, all of which improved stiffness and strength, and resisted the formation and widening of cracks. Improved cracking behavior is highly desirable in strengthened structures for better serviceability performance and long term durability.

4.5.5 Concrete Compressive Strains

The concrete compressive strains at the top face of the beams at midspan were measured during testing and relationship between the measured strains and loading is presented in Figure 4.37. Overall, concrete compressive strains decreased with strengthening and with increasing prestress force for any given load level. The CEBPNSM strengthened beam with 70% prestress showed the greatest reduction in concrete compressive strain for a given load among the strengthened beams. This was due to the high level of prestress in the 70% beam which significantly enhanced the stiffness of the beam. The final strains measured in the beam specimens before failure were 0.00289, 0.00350, 0.00290, 0.00300, 0.00310, 0.00310 and 0.00300 in the control, NSM, EBR, CEBNSM, and 50%, 60% and 70% CEBPNSM beams, respectively. These final concrete strain values of the CEBPNSM beams indicate that the full concrete strength of the beams was utilized, which implies that the strengthened beams had full composite action until failure.

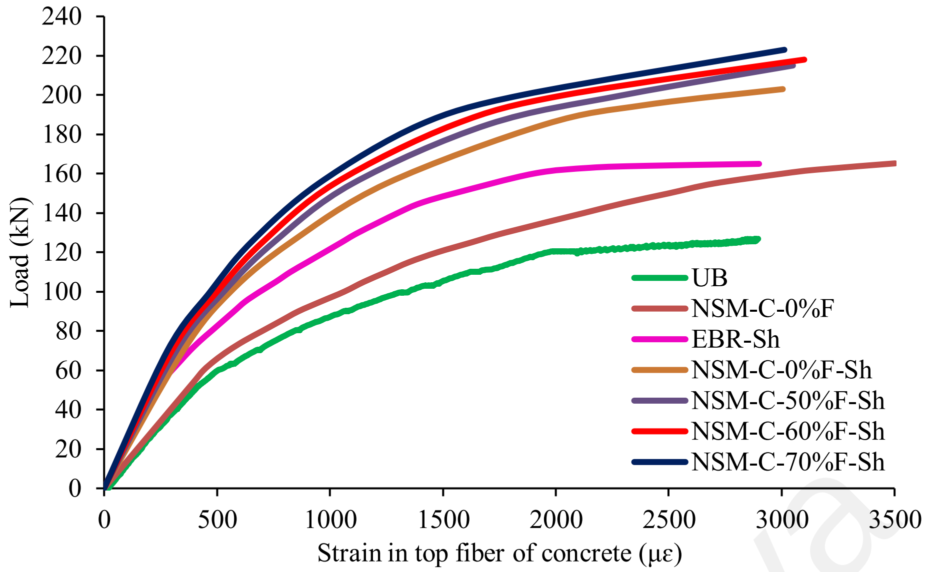

Figure 4.37: Concrete compressive strains in CEBPNSM beams strengthened with CFRP bars and CFRP sheet

4.5.6 Tensile Strains in Main Steel Strands

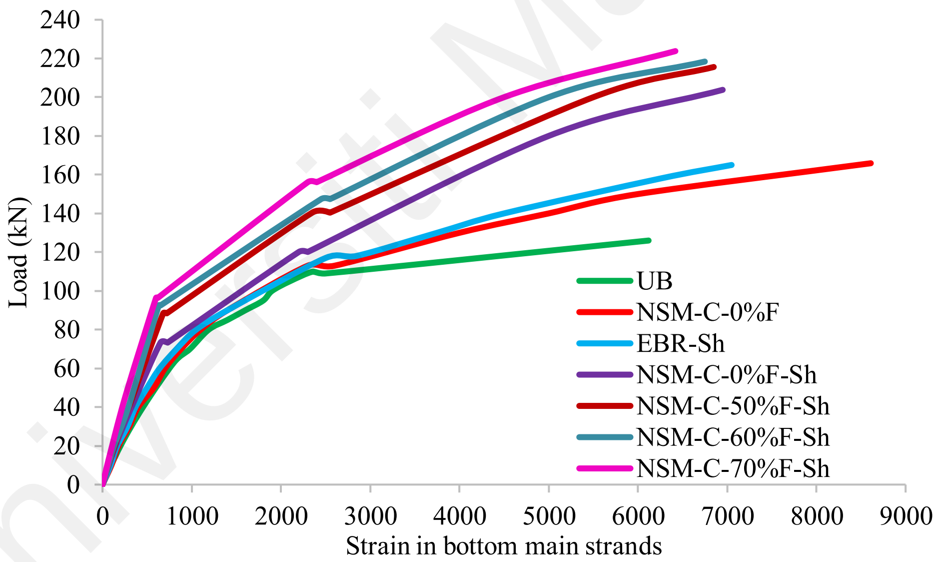

Figure 4.38: Main steel tensile strains in CEBPNSM beams with CFRP bar and CFRP sheet

The relation between loading and the tensile strain in the bottom main strands at midspan of the beam specimens is shown in Figure 4.38. The tensile load-strain curves of the strengthened beams adapted to the CFRP strengthening and displayed more of a tri-linear strain curve than the usual elastic-plastic curve seen in reinforced beams. The strain curves of the strengthened beams became especially steeper at the yield to ultimate stage, compared to the control beam, indicating the increased ability of the main steel to bear loads even after yielding. The CEBPNSM beams showed higher strain curves than the other strengthened beams, and increasing the prestress level further enhanced this effect. This was due to the increases in stiffness which allowed the beams to carry greater loads before reaching similar strain levels. The maximum tensile strain values measured in the bottom main steel strands before the strain gauges were damaged during beam failure were 0.00610, 0.00860, 0.00710, 0.00700, 0.00690, 0.00680 and 0.00640 for the control, NSM, EBR, CEBNSM, and 50%, 60% and 70% CEBPNSM beams, respectively. The CEBPNSM strengthened beams with 50%, 60% and 70% prestress, displayed progressively lower maximum tensile strain values, due to the preexisting compressive strains introduced into the lower half of the beams by prestressing the CFRP bar, which opposed the tensile strains created by loading but also slightly reduced the final strains of the beams due to greatly increased stiffness. This is similar to the findings of El-Hacca and Gafar (2011). The CEBPNSM strengthened beam with the highest level of prestress (70%) displayed the steepest load-strain curve, indicating that tensile steel strains were controlled to much higher load levels.

4.5.7 Tensile Strains in NSM CFRP Bars

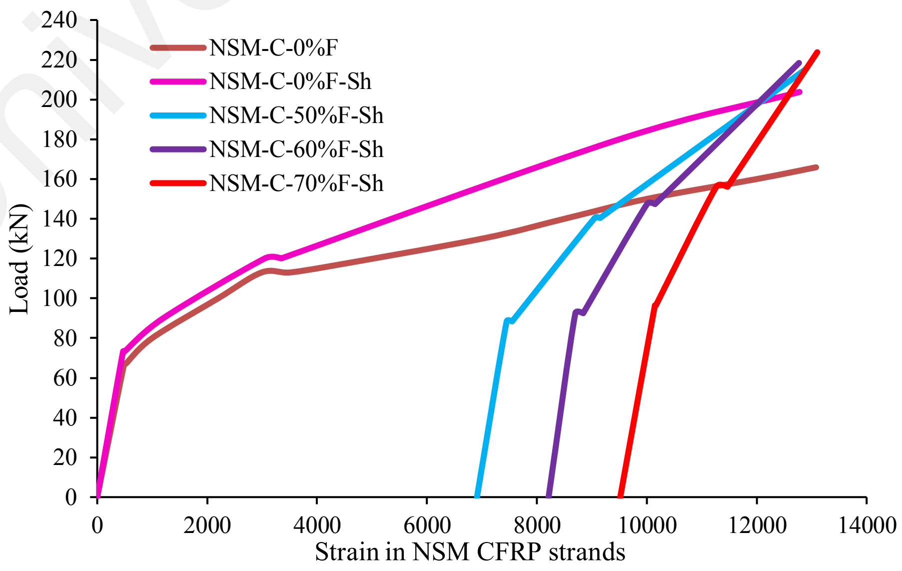

Figure 4.39: CFRP bar tensile strains in CEBPNSM beams with CFRP bars and CFRP sheet

The load versus tensile strain in CFRP bar at midspan is shown in Figure 4.39, where the initial strains due to prestressing are shown at zero load. The maximum tensile strains in the CFRP bars were 0.01308, 0.01278, 0.01290, 0.01277 and 0.01310 for the NSM, CEBNSM and 50%, 60% and 70% CEBPNSM beams, respectively. The maximum strain in the NSM strengthened beam may have been greater than the other beams as the tensile stress was shared between the CFRP bar and the internal steel strands only. Whereas in the CEBNSM and CEBPNSM beams the tensile stress was divided between the CFRP bar, internal steel strands and CFRP sheet, which reduced the tensile stress on the CFRP bar. The CEBPNSM strengthened beams showed the least increment in strain from load initiation until failure. Specifically, the CEBPNSM beam with 70% prestress showed the least increment in tensile CFRP bar strain, only 0.003585 (this disregards the initial strain from prestress). The addition of prestress and the consequent compression around the CFRP bar is the probable cause of this behavior.

4.5.8 Tensile Strains in CFRP Sheet

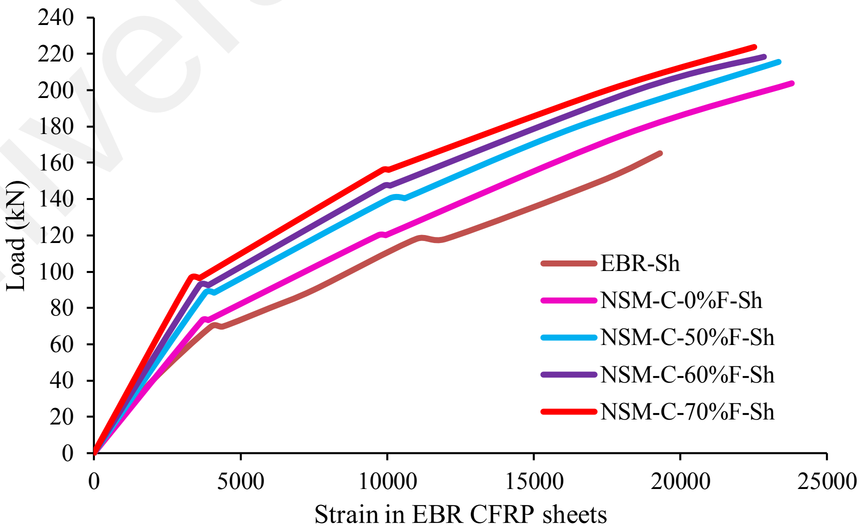

Figure 4.40: CFRP sheet tensile strains in CEBPNSM beams with CFRP bars and CFRP sheet

The relation between the loading and the tensile strains in the CFRP sheets at the midspan of the beam specimens is shown in Figure 4.40. The CEBNSM beam (without prestress) had an overall steeper CFRP sheet tensile strain curve than the EBR beam due to the additional CFRP bar, which enhanced strength and stiffness. In turn, the CEBPNSM beams had steeper curves than the CEBNSM beam and increasing the level of prestress further decreased the rate of tensile strain increment in the CFRP sheet. This can be attributed to the effect of prestress, which controls tensile strains. The maximum tensile strains measured in the CFRP sheets before failure of the strain gauges were 0.01931, 0.02380, 0.02335, 0.02285 and 0.02252 for the EBR, CEBNSM and 50%, 60% and 70% CEBPNSM beams, respectively. The maximum strains measured in the CEBNSM and CEBPNSM strengthened beams indicate that the full capacity of the CFRP sheet was utilized, which agrees with the observed failure mode of CFRP rupture and concrete crushing and confirms the full composite action of these strengthened beams.

4.5.9 Prestress Losses

Table 4.14: Prestress force and camber effect in CEBPNSM beams with CFRP bars and CFRP sheet

Beam ID	Applied Prestress Force		Effective Prestress Force		Negative camber at midspan (mm)
	(kN)	(%)	(kN)	(%)	
NSM-C-50%F-Sh	73	53	68.8	49.8	0.75
NSM-C-60%F-Sh	87	63	82.7	59.9	0.85
NSM-C-70%F-Sh	101	73	96.5	69.9	1.01

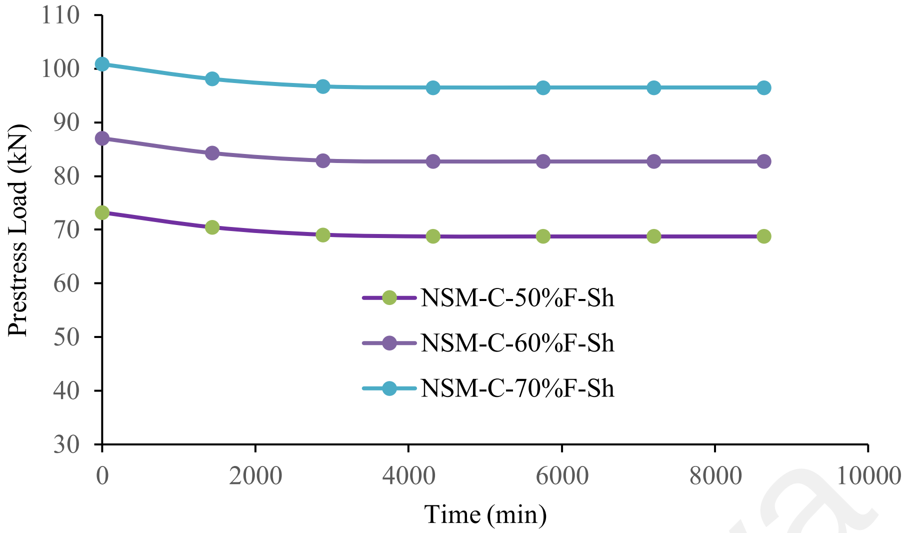

Figure 4.41: Prestress force in CFRP bars during curing period for CEBPNSM beams with CFRP bars and CFRP sheet

The prestressed CFRP bars in the CEBPNSM strengthened beams were monitored for losses in prestress from the time the prestress force was applied until the release of the prestress into the beams. The amount of force applied to prestress the 50%, 60% and 70% prestressed CEBPNSM strengthened beams were 73.22 kN, 87.04 kN and 100.86 kN, respectively, which were calculated based on the tensile strength of the CFRP bars, the desired prestress level and the estimated prestress loss to be covered (Table 4.14). The prestress force levels in the CFRP bars over the six-day curing period are shown in Figure 4.41. The actual loss in prestress force during this time was at about 4.32 kN to 4.47 kN. This loss was due to adhesive creep and anchor slip of the CFRP bars (Badawi et al. 2009). During prestress release, an LVDT was used to measure the negative camber at the midspan of the strengthened beams, which were found to be 0.75 mm, 0.85 mm and 1.01 mm for the 50%, 60% and 70% CEBPNSM beams, respectively.

4.5.10 Effect of Increasing Prestress Level

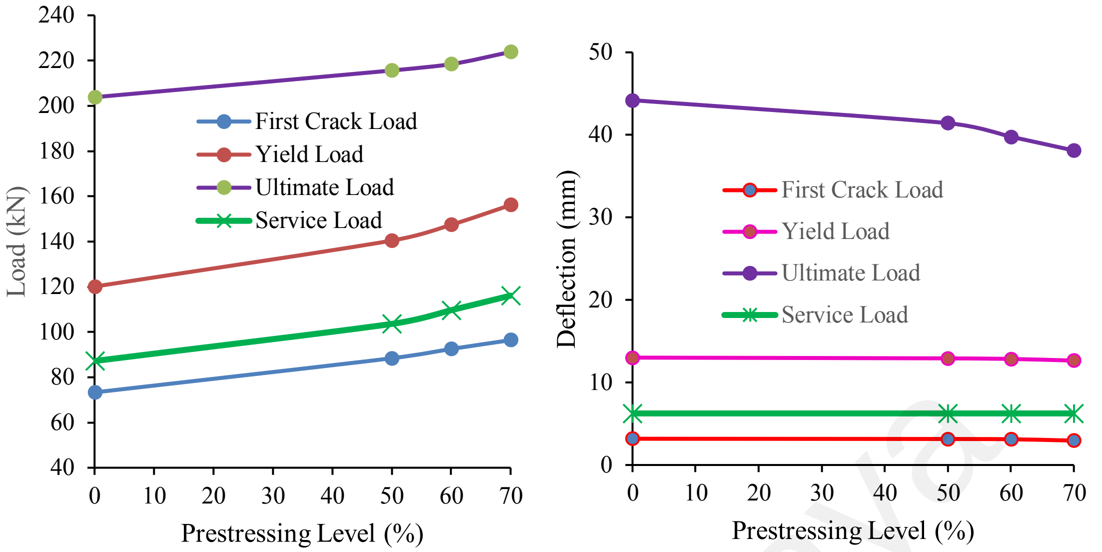

(a) Load vs level of prestressing force

(b) Deflection vs level of prestressing force

Figure 4.42: Effect of prestress level on CEBPNSM beams with CFRP bars and CFRP sheet

Prestressing the CFRP bar in the CEBPNSM strengthened beams had a significant effect on the flexural performance of the CEBPNSM beam specimens. Increasing the level of prestress force caused flexural performance to be further enhanced and the highest level prestress (70%) offered the greatest enhancement in flexural behavior. Overall, increasing the level of prestress enhanced flexural behavior by increasing flexural load capacity and reducing deflection, crack width, concrete compressive strains and tensile strains in the main steel, CFRP bar and CFRP sheet at any given load level. As can be seen from Figure 4.42 (a), the flexural load capacity of the beam at first crack, service, yield and ultimate was significantly improved by increasing the level of prestress, with yield load showing the most improvement. The 70% prestress level provided the highest loads at all stages. From Figure 4.42(b), it can be seen that the beams with prestress were able to maintain deflection at the same level as the beam without prestress despite the increases in load at first crack, service and yield. At ultimate, increasing the level of prestress significantly decreased deflection, with the 70% prestress level showing the smallest ultimate deflection. Increasing the level of prestress controlled concrete compressive strains and tensile strains in the main steel, NSM steel strand and CFRP sheet to significantly higher load levels. The rates at which these strains increased were significantly reduced. This can be seen in the strain graphs (Figure 4.37 – Figure 4.40). Increasing the level of prestress in the strengthened beams did not change the flexural failure mode of the CEBPNSM beams, which indicates that prestressing can help strengthened beams avoid premature debonding failure.

4.5.11 Assessment of FEM

Table 4.15: Experimental and FEM results at ultimate for CEBPNSM beams with CFRP bar and CFRP sheet

Beam specimen	Level of prestress (%)	Experimental		FEM		FEM/Experimental	
		Load (kN)	Deflection (mm)	Load (kN)	Deflection (mm)	Load (P_{FEM}/P_{exp})	Deflection ($\Delta_{FEM/}\ \Delta_{exp}$)
NSM-C-0%F-Sh	0	203.8	44.20	203.80	43.00	1.00	0.97
NSM-C-60%F-Sh	60	218.4	39.78	218.51	40.07	1.00	1.01
NSM-C-70%F-Sh	70	223.8	38.11	219.54	38.92	0.98	1.02

The experimental and FEM results for load and deflection at ultimate for the CEBNSM and 60% and 70% CEBPNSM strengthened beams are given in Table 4.15. The maximum percentage error between the experimental and numerical results was 2% for ultimate load and 3% for the corresponding deflection. Thus, the differences between the experimental data and FEM output were within the 10% acceptable limit and the agreement between the numerical model and the experimental results was good.

The load-deflection relationships generated by the numerical model and the experimental load-deflection curves are compared in Figure 4.43. The agreement between the numerical model and experimental data was extremely close.

The compressive and tensile concrete damage behaviors of the strengthened beams simulated by the FEM model were similar for all the beams. The damage behavior of the 70% CEBPNSM beam is shown in Figure 4.44. Experimentally, the strengthened beams displayed flexural cracks in the tension zone which were more developed at midspan and flexural failure occurred by concrete crushing in the compressive zone after yielding with simultaneous CFRP rupture. The numerical model was able to simulate the concrete damage behavior of the strengthened beams with reasonable accuracy compared to the experimental cracking and failure behavior.

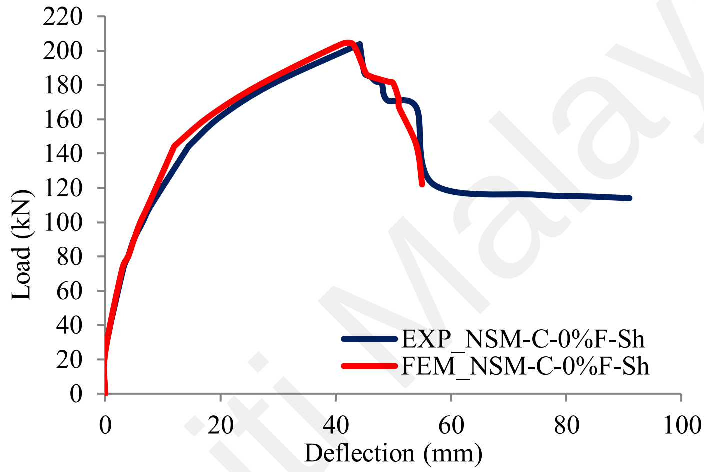

(a) Load Vs Deflection for NSM-C-0%F-Sh

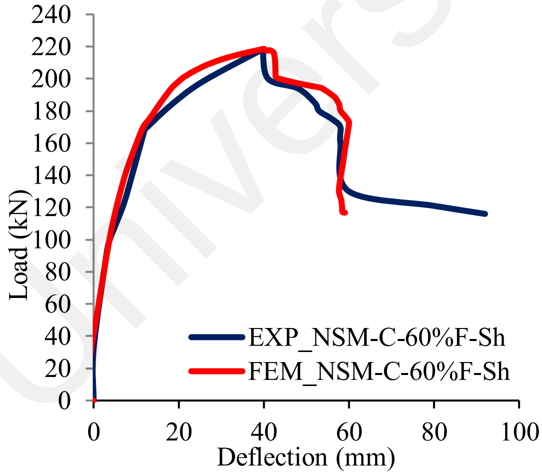

(b) Load Vs Deflection for NSM-C-60%F-Sh

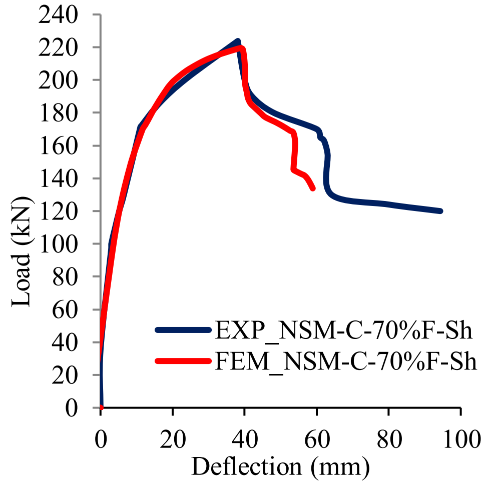

(c) Load Vs Deflection for NSM-C-70%F-Sh

Figure 4.43: FEM load-deflection for CEBPNSM beams with CFRP bar and CFRP sheet

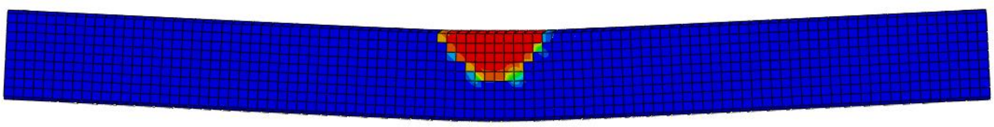

(a) Compressive damage behavior

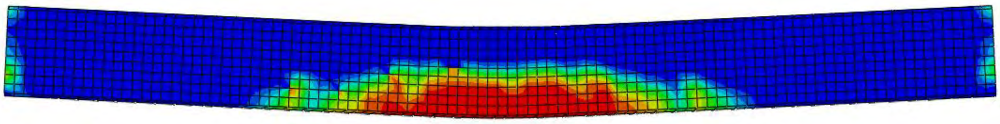

(b) Tensile damage behavior

Figure 4.44: FEM damage behavior of NSM-C-70%F-Sh

4.6 CEBPNSM Strengthened Beams Using Steel Strands and CFRP Sheet

4.6.1 Flexural Capacities

The flexural capacities in terms of first crack, serviceability, yield and ultimate loads of the CEBPNSM beams strengthened with a combination of steel strands and CFRP sheet are displayed in Table 4.16, along with the corresponding deflections. The load and deflection results of the control beam, the NSM steel strand strengthened beam, the EBR CFRP sheet strengthened beam and the CEBNSM beam strengthened with steel strands and CFRP sheet are also given for comparison purposes. Overall, the combination of strengthening materials and techniques enhanced the flexural capacities of the strengthened beams at all load stages, with the CEBPNSM strengthened beams with higher levels of prestress showing the greatest enhancement. The enhancements in the flexural load capacities of the strengthened beams are graphically presented in Figure 4.45 and Figure 4.46.

The ultimate load capacity was most significantly enhanced by CEBPNSM strengthening with steel strands and CFRP sheet. The CEBPNSM beams with 50%, 60% and 70% prestress improved by 65%, 68%, and 70%, respectively, over the control specimen. In comparison, the ultimate load of the NSM steel strand strengthened beam, the EBR CFRP sheet strengthened beam and the CEBNSM strengthened beam improved by 28%, 30% and 58%, respectively, over the control beam (Figure 4.45).

Table 4.16: Experimental load and deflection results of CEBPNSM beams strengthened with steel strands and CFRP sheet

Beam specimen	Level of prestress in NSM (%)	First crack (P_{cr})		Service (P_s) (kN)	Yield (P_y)		Ultimate (P_{ult})	
		Load (kN)	Deflection (mm)		Load (kN)	Deflection (mm)	Load (kN)	Deflection (mm)
UB	-	63	3.1	83	110	19.8	127	45.6
EBR-Sh	-	70 (10%)	3.2	93 (11%)	118 (7%)	9.7	165 (30%)	48.6
NSM-S-0%F	0	66 (5%)	3.2	92 (10%)	145 (32%)	23.5	162 (28%)	38.3
NSM-S-0%F-Sh	0	72 (14%)	3.2	98 (18%)	149 (35%)	14.5	200 (58%)	37.1
NSM-S-50%F-Sh	50	87 (38%)	3.1	113 (37%)	171 (55%)	13.5	210 (65%)	35.1
NSM-S-60%F-Sh	60	91 (45%)	3.1	116 (40%)	175 (59%)	13.0	213 (68%)	33.2
NSM-S-70%F-Sh	70	94 (49%)	2.5	122 (46%)	179 (62%)	12.7	216 (70%)	30.1
Note: Parentheses represent percentage increase over control beam								

The CEBPNSM strengthened beams also showed the greatest improvement in first crack load, service load and yield load when compared with the control beam, the NSM steel strand strengthened beam, the EBR CFRP sheet strengthened beam and the CEBNSM strengthened beam with steel strand and CFRP sheet.

The addition of prestress in the CEBPNSM technique significantly improved the flexural behavior of the strengthened beam specimens compared to the CEBNSM technique (without prestress). The CEBPNSM strengthened beam with the highest level of prestress (70%) showed the greatest improvement, with increases of 31% in first crack load, 24% in service load, 21% in yield load and 8% in ultimate load, over the CEBNSM strengthened beam (Figure 4.46).

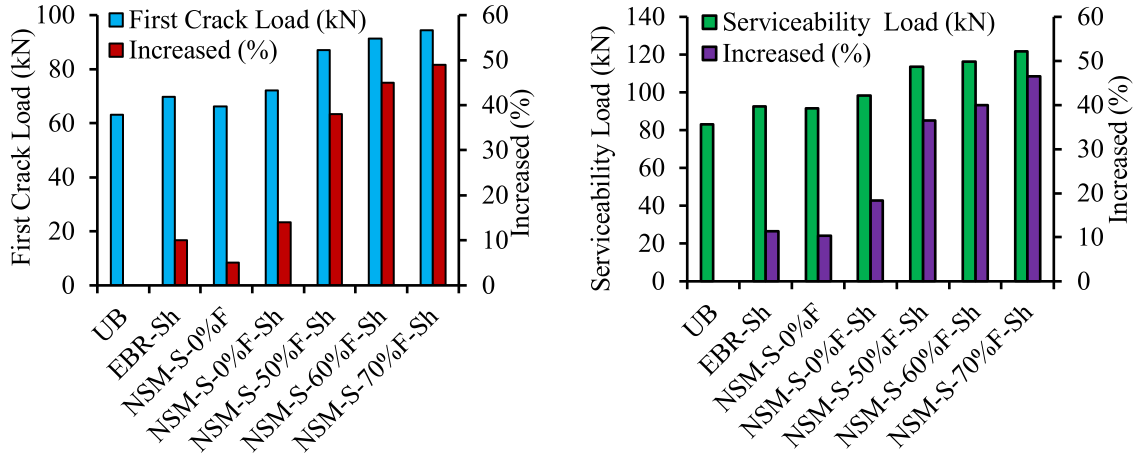

(a) First crack load (b) Service load

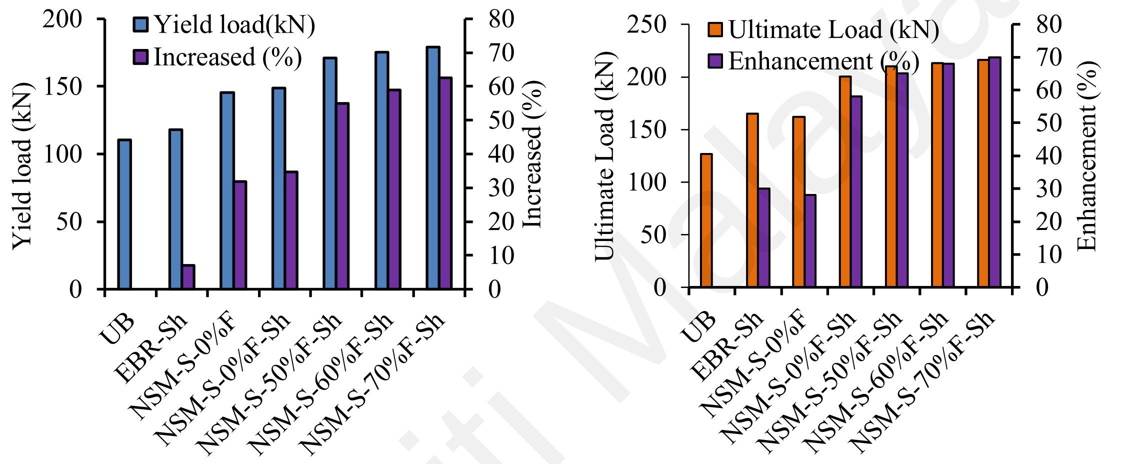

(c) Yield load (d) Ultimate load

Figure 4.45: Flexural load enhancements of EBR sheet and NSM steel strand strengthened beams over control beam

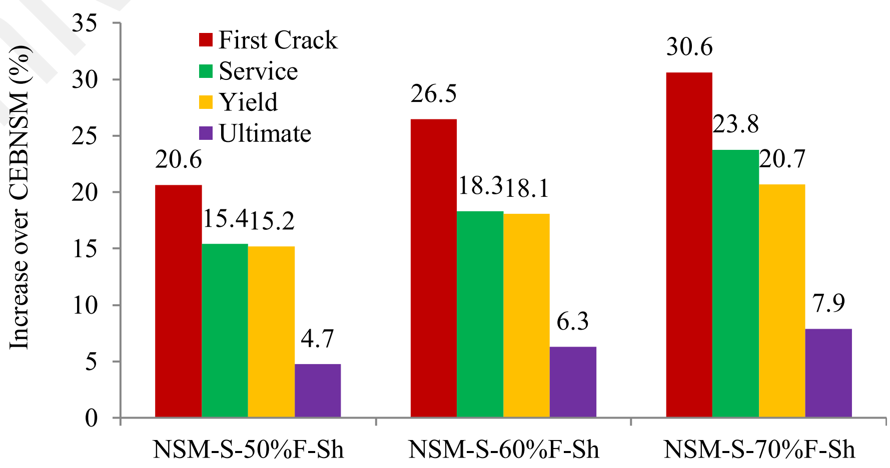

Figure 4.46: Percentile increment of CEBPNSM beam with CFRP sheet and steel strand over CEBNSM beam

4.6.2 Failure Modes

The failure modes of all of the beam specimens strengthened with a combination of steel strands and CFRP sheet are presented in Figure 4.47. The three CEBPNSM strengthened beams and the CEBNSM strengthened beam, all failed in a flexural manner. The beams failed by CFRP rupture in combination with concrete crushing after the main tension reinforcement yielded. Concrete crushing initiated before rupture of the CFRP sheet and continued after CFRP rupture. The rupture of the CFRP sheet occurred in stages at the maximum flexural zone and was accompanied by a loud sound. No debonding of the NSM steel strand or the CFRP sheet was observed. The failure behavior of the CEBPNSM and CEBNSM beams indicates the full composite action of the beams until failure and thus the full utilization of the tensile strength of the steel strand and CFRP sheet.

The debonding failure observed in the beam strengthened with EBR CFRP sheet only was eliminated when the EBR CFRP sheet was combined with NSM strengthening in the CEBNSM and CEBPNSM strengthened beams. This was most likely due to the increase in interface area between the strengthening materials, epoxy and concrete substrate. The prestressing of the steel strand in the CEBPNSM method may have provided a further deterrent to debonding of the CFRP sheet as the addition of prestress creates a cambering effect in the beam, which resists tensile strains during service (Shang et al. 2005).

Similar failure modes have been found in previous research. Darain et al. (2016) strengthened five RC beams using the CEBNSM technique with CFRP fabric and CFRP bars, and found that flexural failure by CFRP rupture was the dominant failure mode. However, other researchers also found premature debonding and concrete cover separation as failure modes for beams strengthened using a combination of EBR and NSM techniques (Rahman et al. 2014, Mathew and Prabhakaran 2018, Lim 2009).

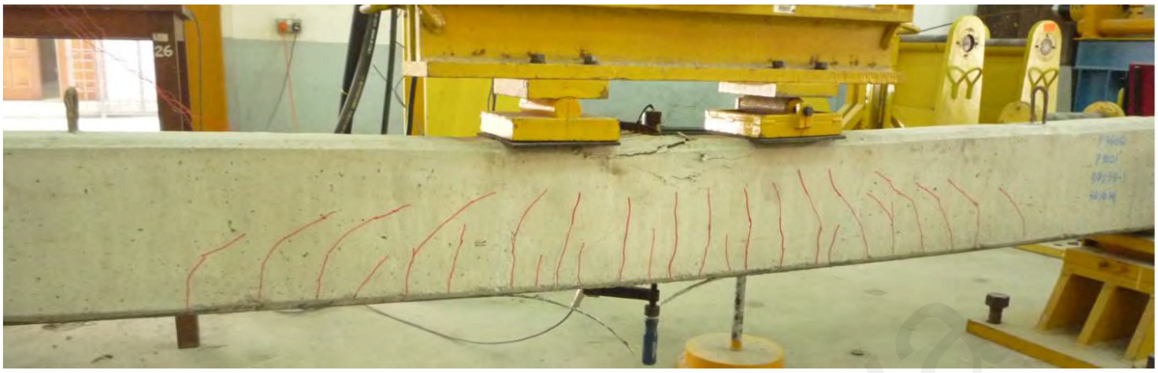

(a) NSM-S-0%F-Sh

(b) NSM-S-50%F-Sh

(c) NSM-S-60%F-Sh

(d) NSM-S-70%F-Sh

Figure 4.47: Failure modes of CEBPNSM beams strengthened with steel strands and CFRP sheet

4.6.3 Load-Deflection Behavior

The load-deflection behavior of the CEBPNSM beams with steel strands and CFRP sheet are graphically represented in Figure 4.48 with the exact deflection values at first crack, yield, ultimate and end point given in Table 4.16. The load-deflection behavior of the beam specimens was similar to that of the CEBPNSM beams with CFRP bar and CFRP sheet. Both groups displayed tri-linear load deflection curves characteristic of CFRP strengthened beams. However, the CEBPNSM beams with steel strands in this group displayed steeper load-deflection curves after yield. The ultimate deflections of these beams were smaller as can be seen from Table 4.13 and Table 4.16. This indicates that the steel strand was able to provide greater stiffness between yield and ultimate than the CFRP bar to the CEBPNSM strengthened beams. Another important difference can be seen in the deformation behavior after ultimate where the steel and CFRP sheet strengthened CEBPNSM beams displayed a slightly more ductile manner of failure with many small drops in load until loading reached the level of the strengthening steel strand. Whereas, the CEBPNSM beams with CFRP bar and CFRP sheet failed by two large drops in load until loading reached the level of the internal tension steel.

The CEBPNSM and CEBNSM strengthened beams in this group displayed similar tri-linear load-deflection responses. Compared to the EBR CFRP sheet strengthened beam and the NSM steel strand strengthened beam, first crack, yield and ultimate occurred at much higher loads and the load deflection response was much steeper at all stages, especially from yield to ultimate. This was due to the combined effect of the CFRP sheet and steel strand in the CEBPNSM and CEBNSM beam. The superior yield properties of steel greatly enhanced the yield point, while the high stiffness of CFRP reduced deflection. The increased amount of strengthening material also resulted in greater beam strength and stiffness, and thus a higher ultimate and less deflection. As can be seen in Table 4.16, the deflection at yield of the CEBPNSM and CEBNSM strengthened beams were less than the control beam and the NSM steel strengthened beam, but more than the EBR beam. This decrease in deflection over the control and NSM steel beam can be attributed to the stiffening effect of the CFRP sheet, while the increase in deflection over the EBR CFRP beam is due to the much higher load at which yield occurred. The first crack and ultimate deflections of the CEBPNSM and CEBNSM beams were also less than the EBR CFRP sheet and NSM steel strand beams.

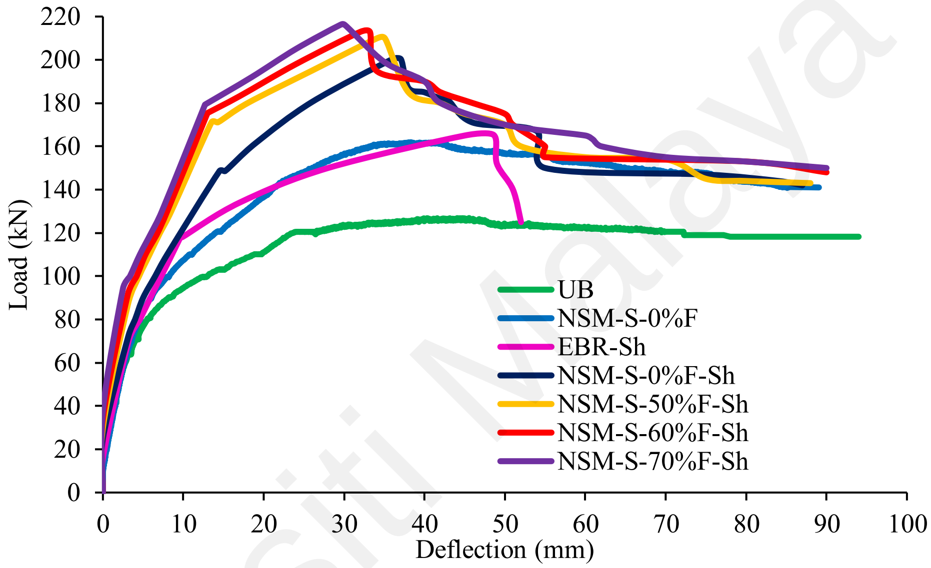

Figure 4.48: Load-deflection curves of CEBPNSM beams with steel strands and CFRP sheet

In comparison to the CEBNSM beam, the CEBPNSM beams had significantly steeper slopes at all stages until ultimate. This indicates the reduced deflection in the CEBPNSM strengthened beams, which was accompanied by increased load carrying capacity at each stage. Beam deflection was significantly controlled by increasing the level of prestress force in the steel strand, with higher levels of prestress resulting in corresponding decreases in deflection. This was probably because the additional prestress delayed the formation of cracks to a much higher load and acted as an opposing force to crack widening, thus increasing the stiffness of the beam specimens. At first crack, the use of prestress in the CEBPNSM beams was able to control deflection to the about same level as the control beam, and even reduce deflection at the highest level of prestress (70%), while at the same time greatly increasing the load at which the first crack occurred. At yield, the deflections of the CEBPNSM strengthened beams with 50%, 60% and 70% prestress were 13.5 mm, 13 mm and 12.7 mm, respectively, which when compared the CEBNSM strengthened beam (14.5 mm) shows that increasing the level of prestress in the CEBPNSM beams was able to provide corresponding reduction in beam deflection while simultaneously greatly increasing the yield load. At ultimate, a similar pattern of reduction in deflection with higher ultimate loads was seen in the CEBPNSM beams due to the increasing levels of prestress used in the steel strands.

The CEBPNSM strengthened beam with 70% prestress (NSM-S-70%F-Sh) showed the greatest enhancement in flexural response and reduction in deflection at all stages until ultimate. The load deflection response of the CEBPNSM beams is comparable to the findings of previous research in which similar load deflection responses were found in concrete beams strengthened with prestressed NSM CFRP strengthening (Badawi et al. 2009; El-Hacha & Gaafar 2011) and with combined strengthening techniques (Darain et al. 2016).

4.6.4 Cracking Behavior

The CEBPNSM beams strengthened with a combination of steel strands and CFRP sheet showed cracking behavior similar to that of the CEBPNSM beams strengthened with CFRP bar and CFRP sheet. Typical flexural crack patterns were observed, as can be seen in Figure 4.47. The crack pattern of both groups was very similar, with around 25 cracks uniformly distributed along the beam span, and greater crack development in the maximum moment zone. The first crack load for both groups was comparable, although the combination of steel strand with CFRP sheet was able to reduce crack widths and deflection at first crack slightly more than the CFRP bar and CFRP sheet combination. Overall, the cracking characteristics of the CEBPNSM strengthened beams in this group improved significantly in terms of first crack load, crack width, crack number and crack spacing.

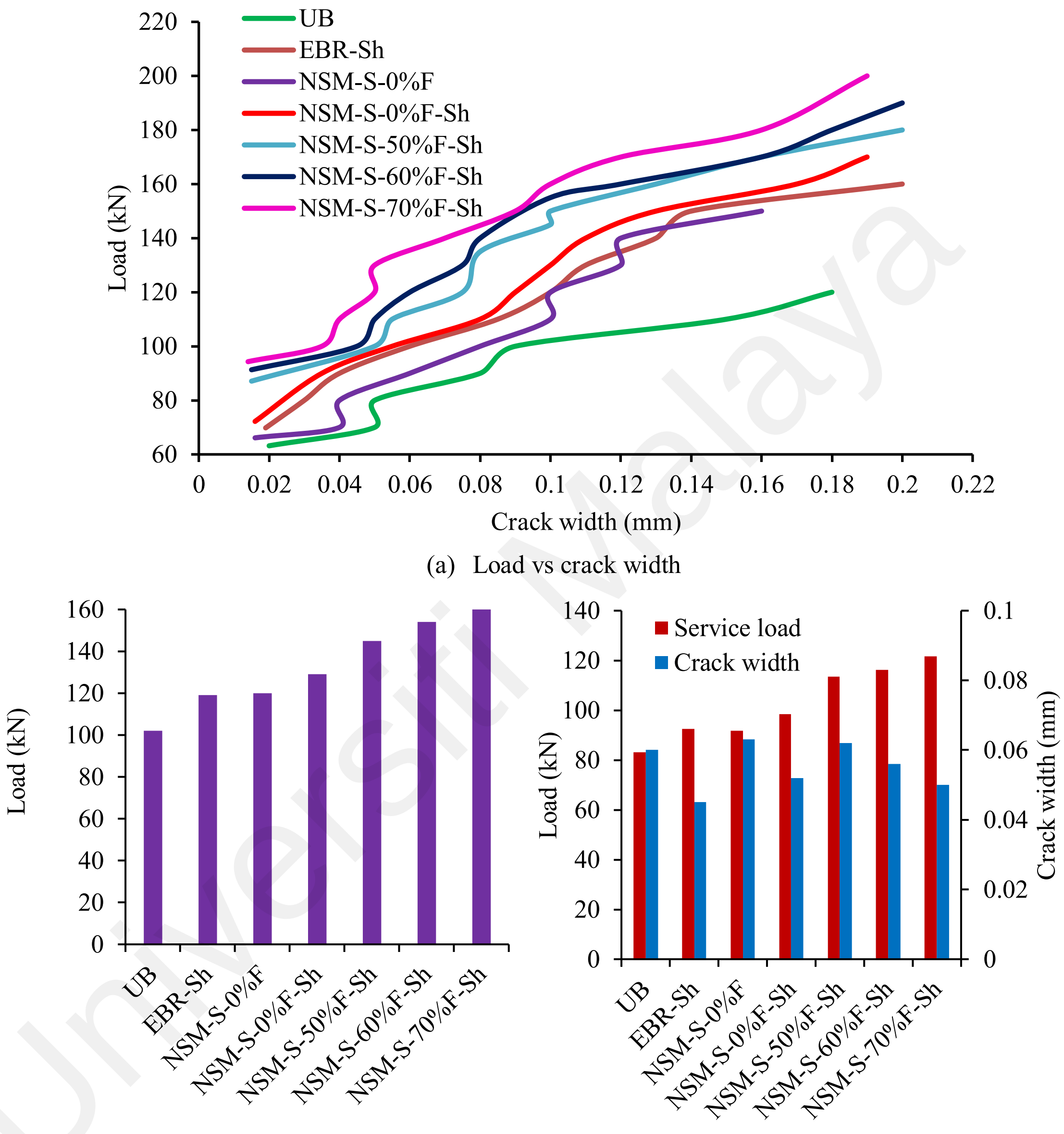

(a) Load vs crack width

(b) Load at 0.1 mm crack width

(c) Crack width at service load

Figure 4.49: Cracking behavior of CEBPNSM beams with steel strands and CFRP sheet

The first crack load and the corresponding deflection, as well as the increase in first crack load of the strengthened beams over the control beam are given in Table 4.16. The CEBPNSM strengthening technique was the most proficient at enhancing the first crack load compared to the EBR, NSM and CEBNSM strengthening techniques. This was due to the enhanced stiffness of the CEBPNSM beams in the pre-cracking stage (due to the effect of the combined strengthening materials and prestressing), which delayed crack initiation. The CEBPNSM strengthened beam with the highest level of prestress (70%) showed the greatest increase in first crack load, 49% over the control beam, while also greatly reducing the deflection at first crack.

The correlation between load and width of the main flexural crack of the specimens is shown in Figure 4.49 (a). Strengthening overall increased the load level for a given crack width, with the CEBPNSM beams showing the greatest increase. This can be seen in Figure 4.49 (b), where at 0.1 mm crack width, the CEBPNSM beam with 70% prestress carried a load of 160 kN, which was an increase of 56% over the control beam (102 kN), and an increase of 24% over the CEBNSM beam (129 kN). Crack width at the service stage is an important design consideration. As can be seen in Figure 4.49 (c), strengthening, especially CEBPNSM strengthening, was able to increase the service load while decreasing the crack width. The CEBPNSM beam with 70% prestress was able to increase the service load by 46% and decrease crack width at service by 17%, compared to the control beam. Overall, the CEBPNSM strengthening technique was able to control crack width significantly better than the EBR, NSM and CEBNSM techniques. The CEBPNSM strengthened beam with 70% prestress displayed the smallest crack widths among the strengthened specimens at any given load level.

The CEBPNSM technique was able to significantly improve the cracking characteristics of the PC beam by greatly increasing first crack load and reducing crack width, compared to the other strengthening techniques. Increasing the level of prestress in the CEBPNSM beams produced corresponding enhancements in cracking behavior. Improved cracking behavior is highly advantageous as it reduces deflections and crack widths, improving the serviceability and durability of structures. The greatest improvement was seen in the CEBPNSM strengthened beam with the highest level of prestress. This was due mainly to two reasons. Firstly, the combination of strengthening materials (steel and CFRP), increased the overall amount of strengthening reinforcement, which enhanced strength and stiffness, and the superior stiffness further controlled cracking. Secondly, the additional prestress force in the steel strand provided an opposing compressive force in the tensile region which significantly controlled the formation and widening of cracks.

4.6.5 Concrete Compressive Strains

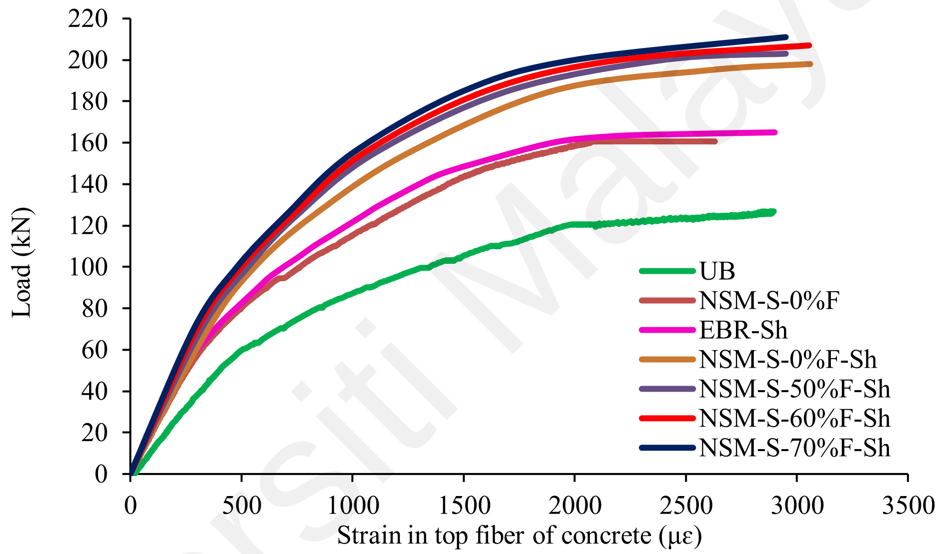

Figure 4.50: Concrete compressive strains in CEBPNSM beams with steel strands and CFRP sheet

The relation between the loading and the concrete compressive strain at midspan of the beam specimens is shown in Figure 4.50. The concrete load-strain behavior of all of the beams was linear at a steep incline until cracking and then mostly linear at a shallower slope until yield. After yield, the load-strain behavior was characterized by a curved gradient representing the increasing rate of strain increment. The reduction in the slope of the load-strain curve at each stage was due to the loss in beam stiffness due to cracking and yielding. The strengthened beams displayed markedly steeper concrete load-strain curves from the very onset of loading compared to the control beam, due to the increased stiffness of the strengthened beams. The CEBPNSM strengthened beams were able to control concrete strains to much higher load levels than the NSM, EBR and CEBNSM strengthened beams. The CEBPNSM strengthened beam with 70% prestress showed the greatest reduction in concrete compressive strain for a given load among the strengthened beams. This was due to the high level of prestress in the 70% beam which significantly enhanced the stiffness of the beam. The final strains measured in the beam specimens before the strain gauges were damaged by concrete crushing at failure were 0.00289, 0.00263, 0.00290, 0.00306, 0.00295, 0.00306 and 0.00295 in the control beam, NSM steel strand strengthened beam, EBR CFRP sheet strengthened beam, CEBNSM strengthened beam, and the 50%, 60% and 70% prestressed CEBPNSM strengthened beams, respectively. These final concrete strain values indicate that the full concrete strength of the beams was utilized, as concrete crushing occurs at a compressive strain value of around 0.003. This also indicates the full composite action of the strengthened beams until failure.

4.6.6 Tensile Strains in Main Steel Strands

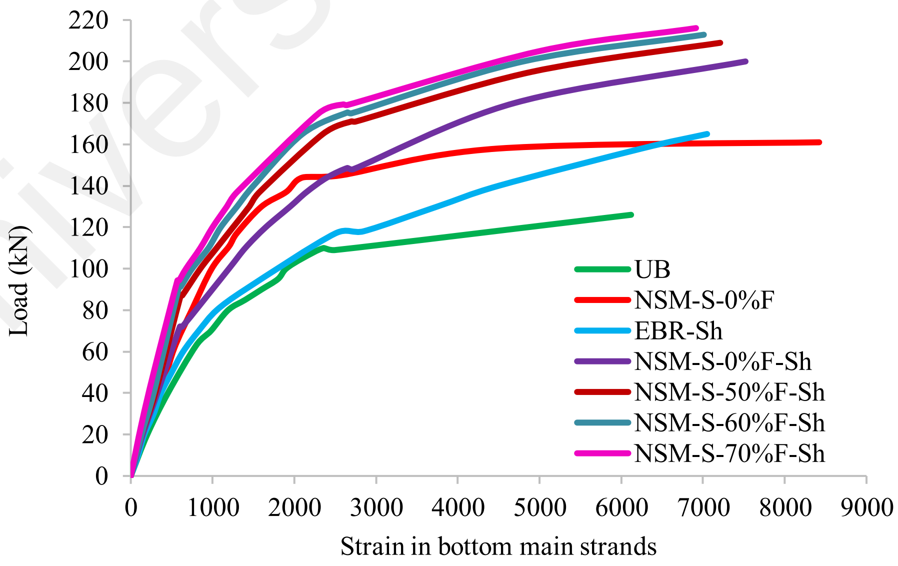

Figure 4.51: Main steel tensile strains in CEBPNSM beams with steel strands and CFRP sheet

The relation between loading and the tensile strain in the bottom main strands at midspan of the beam specimens is shown in Figure 4.51. Generally, all of the beams displayed the typical linear elastic followed by plastic tensile load-strain behavior seen in steel reinforced beams with some variations due to strengthening. The tensile steel load-strain behavior for all of the beams was linear at a slight incline until cracking, as the beams were at full strength and stiffness. After cracking, the initial stiffness of the beams was reduced and thus, the tensile load-strain curves of the bottom main strands deflected to a shallower, less linear slope until yield. After the yielding of the steel strands, the tensile load-strain behavior of the control beam and the NSM strengthened beam curved at a much gentler slope, indicating the increased rate of tensile strain increment in the strands due to the significant loss in strength and stiffness at yield, and the widening of cracks. For the EBR, CEBNSM and CEBPNSM strengthened beams, the tensile load strain behavior after yield was also less steep than before yield, but more steep than the control and NSM beam at this stage. This was due to the properties of CFRP which enhanced the stiffness and strength of the strengthened beams, especially from yield until ultimate.

The maximum tensile strain values measured in the bottom main steel strands before the strain gauges were damaged during beam failure were 0.00612, 0.00842, 0.00705, 0.00752, 0.00721, 0.00701 and 0.00691 for the control beam, NSM strengthened beam, EBR strengthened beam, CEBNSM strengthened beam, and the 50%, 60% and 70% prestressed CEBPNSM strengthened beams, respectively. The control beam had the lowest maximum tensile strain as it failed by concrete crushing at a much lower load level than the strengthened beams. The NSM strengthened beam measured a much higher maximum tensile strain before failure than the control beam due to the higher ultimate load and the tensile properties of the steel strands. However, the EBR strengthened beam measured a much lower maximum tensile strain in the main steel strands compared to the NSM strengthened beam, despite having a similar ultimate load. This was due to the superior tensile strength of the EBR CFRP sheet, which after yield carried a greater portion of the tensile strains in the beam. This strain sharing is indicative of the composite behavior of the beam. The CEBNSM strengthened beam displayed a maximum tensile strain value that was between the maximum tensile strain values of the NSM and EBR strengthened beams, indicating that the tensile strain was distributed between the main steel strands, the NSM steel strand and the CFRP sheet. The CEBPNSM strengthened beams with 50%, 60% and 70% prestress, displayed progressively lower maximum tensile strain values, due to the preexisting compressive strains introduced into the lower half of the beams by prestressing the NSM steel strand, which opposed the tensile strains created by loading. This is similar to the findings of El-Hacha and Gaafar (2011).

Strengthening was able to significantly reduce the tensile strains in the main steel strands at any given load level, and of all the strengthening techniques used, CEBPNSM strengthening was best able to control tensile steel strains. The CEBPNSM strengthened beam with the highest level of prestress (70%) displayed the steepest load-strain curve, indicating that tensile steel strains were controlled to much higher load levels. This was due to the combination of strengthening materials and the high level of prestress, which enhanced the strength and stiffness, as well as the strain sharing characteristics of the beam.

4.6.7 Tensile Strains in NSM Steel Strands

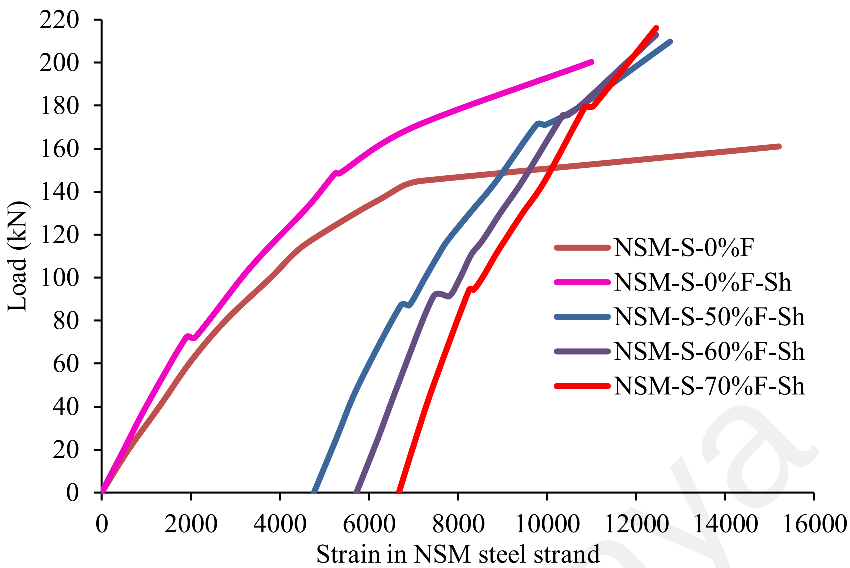

Figure 4.52: Steel strand tensile strains in CEBPNSM beams with steel strands and CFRP sheet

The relation between the loading and the tensile strains in the NSM steel strands at the midspan of the beam specimens is shown in Figure 4.52. Prestressing caused an initial strain in the prestressed NSM steel strands used in the CEBPNSM strengthened beams. This initial strain was calculated from the effective prestressing force and the load-tensile strain curves of the prestressed NSM strands were thus accordingly displaced at zero loading, as can be seen in the graph (Figure 4.52). When the first crack occurs in the beam specimens, the tensile stress shifts from the concrete beam section to the tensile reinforcements (steel strands and CFRP), which causes an abrupt increase in the tensile strain in these reinforcements. This can be seen as a small deflection at first crack load in the tensile strain graphs for the bottom main strands, the NSM steel strands and the CFRP sheet. A similar effect occurs at yield, as can be seen in the graphs, due to the shifting of much of the tensile stress from the steel reinforcements to the CFRP sheet. For the beams without CFRP, tensile stress is carried by the remaining strength in the steel reinforcements after yield, which causes the steel to elongate with increasing strains.

The load-tensile strain curve of the NSM steel strand in the NSM strengthened beam displayed the typical steel strain behavior of linear elastic until yield followed by plastic elongation until failure. The CEBNSM strengthened beam displayed linear elastic tensile strain behavior until yield at a slightly steeper slope than the NSM strengthened beam, and after yield the slope of the tensile strain curve was much steeper than the NSM strengthened beam, which indicates that tensile strain was significantly controlled. This was due to the effect of the superior tensile properties and stiffness of the CFRP sheet, which was able to control and carry the tensile strains to much higher loads. This same CFRP effect also played a part in the tensile behavior of the CEBPNSM strengthened beams. A similar linear elastic behavior until yield was seen in the CEBPNSM beams. However, the addition of prestress to these beams caused them to have much steeper load-strain curves and the strain curve after yield was markedly steeper than the CEBNSM beam, almost linear, which indicates that the rate of strain increment was significantly reduced. This was the effect of prestress, and the higher the level of prestress, the greater the reduction in strain increment was. This prestressing effect was due to the ability of the prestress to counteract tensile strains by introducing compressive strains into the surrounding beam area around the NSM strand.

The maximum tensile strains in the NSM steel strands were 0.01521, 0.01100, 0.01277, 0.01255 and 0.01245 for the NSM strengthened beam, the CEBNSM strengthened beam and the CEBPNSM beams with 50%, 60% and 70% prestress, respectively. The maximum tensile NSM steel strand strain in the NSM strengthened beam was much greater than the other beams as the tensile stress was shared between the NSM strand and the internal steel strands only. Whereas in the CEBNSM and CEBPNSM beams the tensile stress was divided between the NSM steel strand, internal steel strands and the CFRP sheet, which reduced the tensile strains in the NSM steel strand. The CEBPNSM strengthened beams showed the least increment in strain from load initiation until failure. Specifically, the CEBPNSM beam with 70% prestress showed the least increment in tensile NSM strand strain, only 0.00578 (this disregards the initial strain from prestress). The addition of prestress and the consequent compression around the NSM strand is the probable cause of this behavior.

4.6.8 Tensile Strains in CFRP Sheet

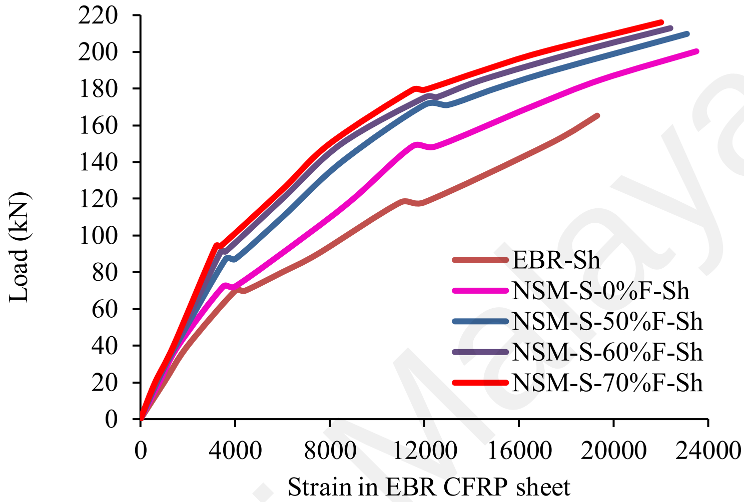

Figure 4.53: CFRP sheet tensile strain in CEBPNSM beams with steel strands and CFRP sheet

The relation between the loading and the tensile strains in the CFRP sheets at the midspan of the beam specimens is shown in Figure 4.53. Each of the beams showed similar tri-linear tensile strain development in the CFRP sheet, with first crack, yield and ultimate marking the end of each phase. After first crack and after yield, the strain increment increased slightly for all of the beams, as can be seen from the slightly lower slope of the load-strain curves after first crack and yield. The largest increments in the CFRP tensile strains were seen in the last phase from yield to failure for all of the beams, as at this phase the tensile stress was carried in large part by the CFRP. However, the CEBNSM beam had an overall steeper CFRP tensile strain curve than the EBR beam due to the additional NSM strand, which enhanced strength and stiffness. In turn, the CEBPNSM beams had steeper curves than the CEBNSM beam and increasing the level of prestress in the NSM strand further decreased the rate of tensile strain increment in the CFRP sheet. This can be attributed to the effect of prestress, which controls tensile strains.

The maximum tensile strains measured in the CFRP sheets before failure of the strain gauges were 0.01931, 0.02350, 0.02310, 0.02240 and 0.02201 for the EBR strengthened beam, CEBNSM strengthened beam and the CEBPNSM strengthened beams, respectively. The rupture strain for the CFRP sheet based on the manufacturer's specifications was 0.02130. The EBR strengthened beam had a lower maximum CFRP tensile strain as the CFRP sheet debonded at failure. The CEBNSM and CEBPNSM beams recorded tensile CFRP strains somewhat higher than the ultimate rupture strain provided by the manufacturer. This could be due to the local curvature of the CFRP at midspan, which may have caused the strain gauges to record higher strain values than those found in direct tensile tests (Rezazadeh et al. 2014). The maximum strains measured in the CEBNSM and CEBPNSM strengthened beams indicate that the full capacity of the CFRP sheet was utilized, which agrees with the observed failure mode of CFRP rupture and concrete crushing and confirms the full composite action of these strengthened beams.

4.6.9 Prestress Losses

The prestressed steel strands in the CEBPNSM strengthened beams were monitored for losses in prestress force from the time the prestress was applied until the release of the prestress into the beams. The amount of force applied to prestress the 50%, 60% and 70% CEBPNSM strengthened beams were 51.15 kN, 61.38 kN and 71.61 kN, respectively, which were calculated based on the tensile strength of the steel strands (Table 4.17). The prestress force levels in the steel strands over the six-day curing period are shown in Figure 4.54. The prestress losses were 0.47%, 0.54% and 0.36% in the 50%, 60% and 70% beams, respectively. The prestress force was released gradually into the beam around 20% at a time and no cracks were seen during or after prestress release. During prestress release, an LVDT was used to measure the negative cambers at the midspan of the strengthened beams, which were found to be 0.50 mm, 0.65 mm and 0.80 mm for the 50%, 60% and 70% CEBPNSM beams, respectively.

Table 4.17: Prestress force and camber effect in CEBPNSM beams with steel strands and CFRP sheet

Beam specimen	Applied prestress force		Effective prestress force		Negative camber at midspan
	(kN)	(%)	(kN)	(%)	(mm)
NSM-S-50%F-Sh	51	50	50.9	49.8	0.50
NSM-S-60%F-Sh	61	60	61.1	59.7	0.65
NSM-S-70%F-Sh	72	70	71.4	69.8	0.80

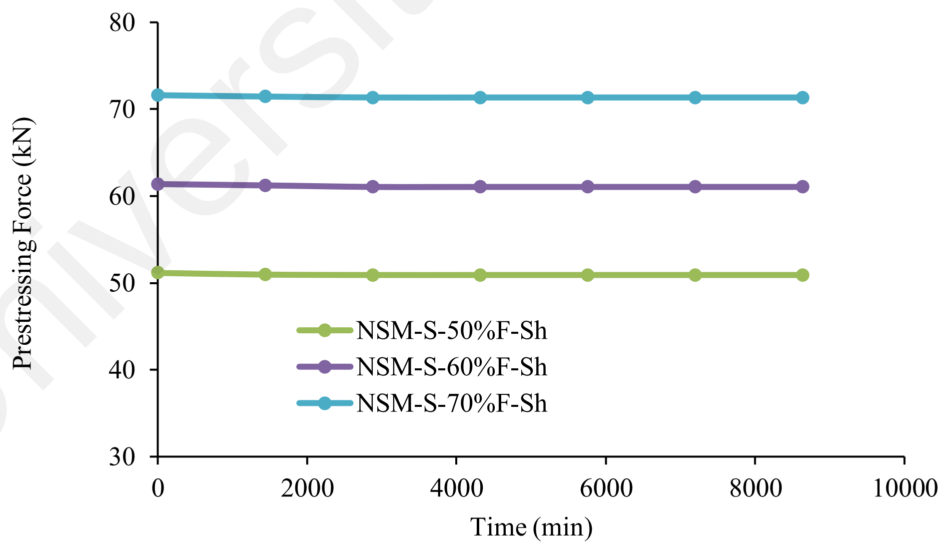

Figure 4.54: Prestress force in steel strands during curing period for CEBPNSM beams with steel strands and CFRP sheet

4.6.10 Effect of Increasing Prestress Level

Prestressing the steel strand in the CEBPNSM strengthened beams had a significant effect on the flexural performance of the CEBPNSM beam specimens. The prestressing effect was especially enhanced by increasing the level of prestress force and the highest level prestress force (70%) offered the greatest enhancement in flexural behavior. Overall, increasing the level of prestress enhanced flexural behavior by increasing flexural load capacity and reducing deflection, crack width, concrete compressive strains and tensile strains in the main steel, strengthening steel strands and CFRP sheet at any given load level. As can be seen from Figure 4.55(a), the flexural load capacity of the beam at first crack, service, yield and ultimate was significantly improved by increasing the level of prestress, with yield load especially showing the most improvement, and the 70% prestress level providing the highest loads at all stages. From Figure 4.55(b), it can be seen that the beams with prestress were able to maintain deflection at the same level as the beam without prestress despite the increases in load at first crack, service and yield. At ultimate, increasing the level of prestress significantly decreased deflection, with the 70% prestress level showing the smallest ultimate deflection. In Figure 4.55(c), it can be seen that at first crack, service, and ultimate, the beams with prestress were able to control crack width to the same level as the beam without prestress despite the increases in load at these stages. At yield, prestressing caused crack width to increase slightly, which may be due to the large increase in yield seen in the beams with prestress compared to the beam without prestress. Increasing the level of prestress was able to control concrete compressive strains and tensile strains in the main steel, NSM steel strand and CFRP sheet to significantly higher load levels. The rates at which these strains increased were significantly reduced. This can be seen in the strain graphs (Figure 4.50 – Figure 4.53). Increasing the level of prestress force in the strengthening steel strand improved the flexural behavior of the beams due to the increased compressive effect in tension region of the beams, which caused a corresponding increase in the stiffness of the beams, as well as an increase in the camber of the beams (Obaydullah et al. 2016).

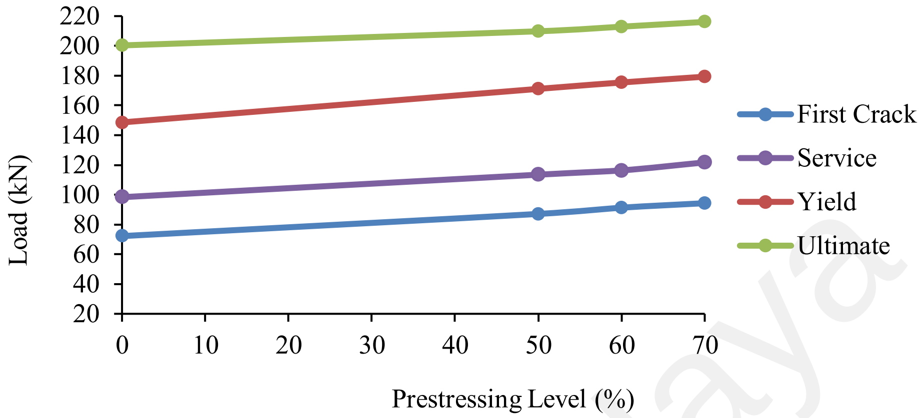

(a) Load vs level of prestressing force

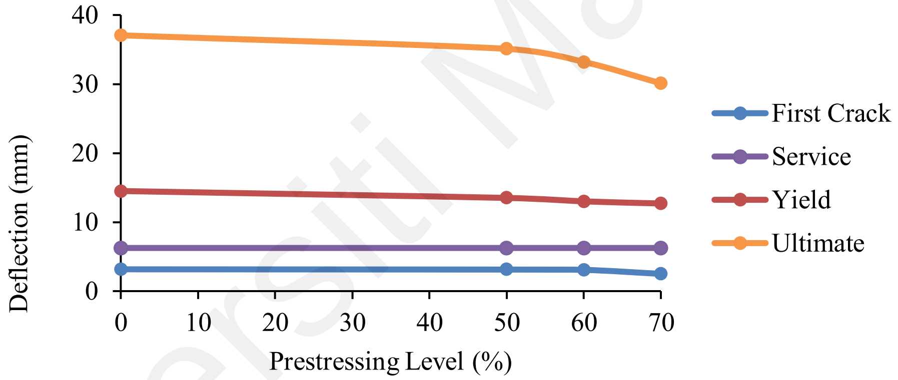

(b) Deflection vs level of prestressing force

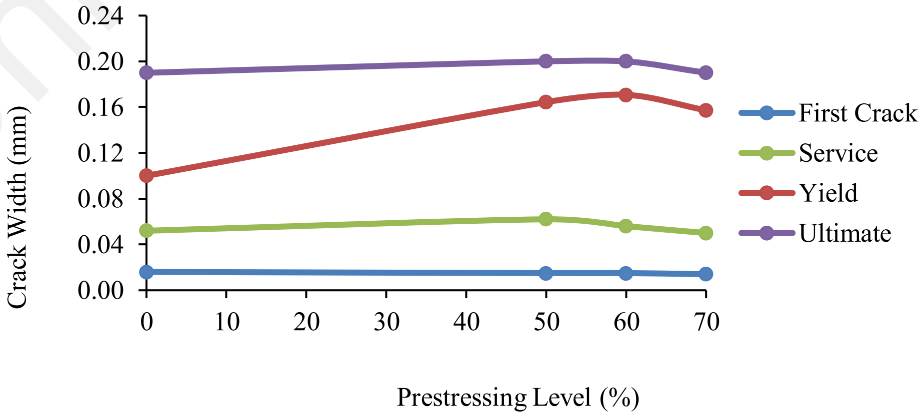

(c) Crack width vs level of prestressing force

Figure 4.55: Effect of prestress level in CEBPNSM beams with steel strands and CFRP sheet

4.6.11 Assessment of FEM

Table 4.18: Experimental and FEM results at ultimate for CEBPNSM beams with steel strands and CFRP sheet

Beam specimen	Level of Prestress (%)	Experimental		FEM		FEM/Experimental	
		Load (kN)	Deflection (mm)	Load (kN)	Deflection (mm)	Load (P_{FEM}/P_{exp})	Deflection ($\Delta_{FEM}/\Delta_{exp}$)
NSM-S-0%F-Sh	0	200.30	37.06	196.92	38.08	0.98	1.03
NSM-S-60%F-Sh	60	212.90	33.21	211.95	33.40	1.00	1.01
NSM-S-70%F-Sh	70	216.10	30.10	214.05	30.67	0.99	1.02

A comparison of the experimental and FEM results for the CEBNSM strengthened beam with steel and CFRP sheet, and the CEBPNSM strengthened beams with 60% and 70% prestressed steel strands and CFRP sheet are given in Table 4.18. The error between the experimental and numerical results reached a maximum of 2% for ultimate load and 3% for the corresponding deflections. Thus, the differences between the experimental and FEM output was within the acceptable limit (10%) (Kishi et al. 2005). The agreement between the load carrying capacity from numerical FEM model and the experimental output is satisfactory.

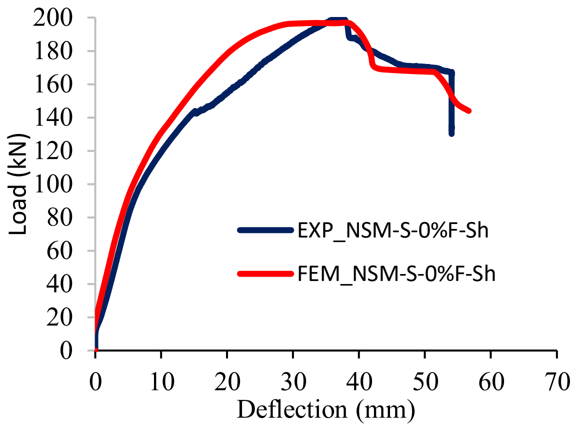

(d) Load Vs Deflection for NSM-S-0%F-Sh

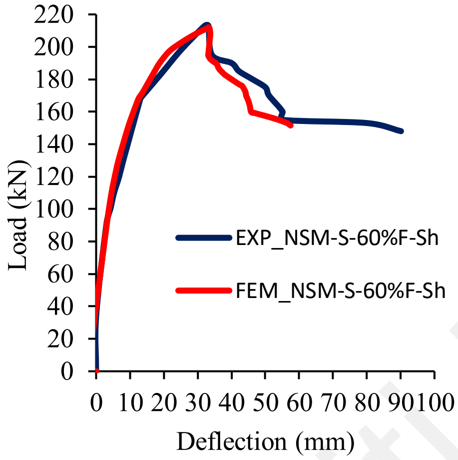

(e) Load Vs Deflection for NSM-S-60%F-Sh

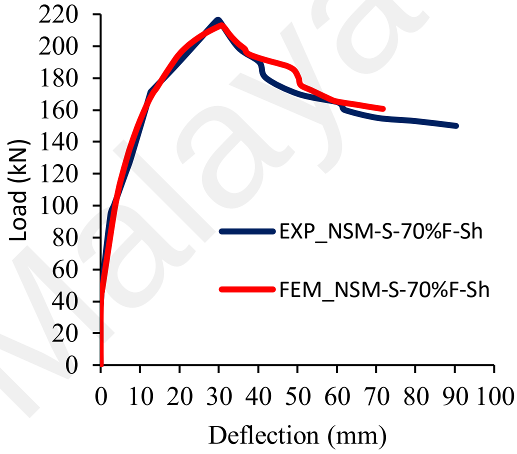

(f) Load Vs Deflection for NSM-S-70%F-Sh

Figure 4.56: FEM load-deflection for CEBPNSM beams using steel strands with CFRP sheet

The load-deflection relationships for the numerical prediction model and the experimental results are shown in Figure 4.56. It can be clearly observed that the correlation is reasonably good between the numerical results and experimental data.

The FEM concrete compressive damage behavior and concrete tensile damage behaviors for all simulated beams were almost similar and are shown in Figure 4.57. The compressive and tensile damage are displayed separately in ABAQUS. The experimental strengthened beams failed by concert crushing after steel yielding with simultaneous rupture of the CFRP sheet. Concrete crushing was the governing failure behavior as the beam failure initiated with concrete crushing. Thus, the FEM damage behaviors and the experimental failure behavior were similar.

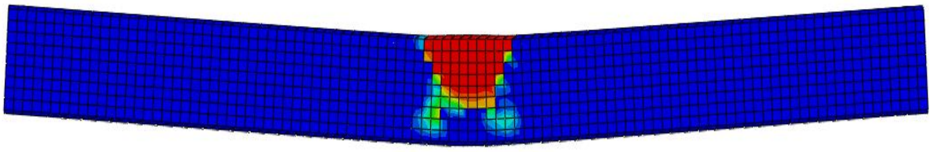

(a) Compressive damage behavior

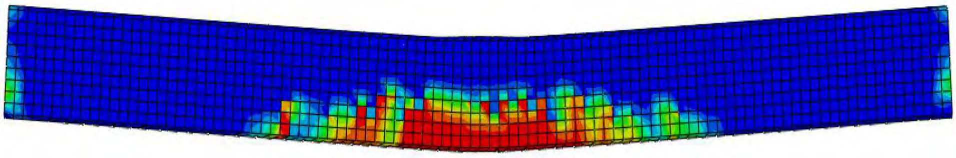

(c) Tensile damage behavior

Figure 4.57: Damage behavior of NSM-S-70%F-Sh

4.7 CEBPNSM Strengthened Beams Using CFRP Bars and CFRP Plate

4.7.1 Flexural Capacities

The experimental load and deflection results of the beams strengthened with the CEBPNSM technique using a combination of CFRP bars and CFRP plates are given in Table 4.22. The results of the control beam, the NSM CFRP bar strengthened beam, the EBR CFRP plate strengthened beams (with and without end anchors) and the CEBNSM beam strengthened with CFRP bar and CFRP plate are also given in the table for comparison purposes. As can be seen from the table, the use of the CEBPNSM technique gave results similar to those found for the CEBPNSM beams strengthened with other materials in the previous sections. The CEBPNSM strengthened beams were able to remarkably increase the first crack, service, yield and ultimate loads in comparison to the control beam and all of the other strengthening techniques. The CEBPNSM strengthened beams far outperformed the EBR and NSM strengthened beams mainly due to the increased quantity of strengthening reinforcement, as well as the effect of combining the two techniques and adding prestress. When compared to the CEBNSM beam, the effect of prestressing the NSM reinforcement becomes very clear, as in the previous groups of CEBPNSM strengthened beams. Increasing the level of prestress in the NSM reinforcement provided corresponding increases in load capacity at all stages for the CEBPNSM beams. In this group, the most significant increases in flexural load capacity were again seen in the beam with the highest amount of prestress (NSM-C-70%F-Pl-A). This beam, NSM-C-70%F-Pl-A, also had the highest first crack and ultimate loads recorded in this study, 99 kN and 230 kN, respectively. This 70% CEBPNSM beam was able to improve first crack, service, yield and ultimate loads by 32%, 28%, 45% and 7%, respectively, over the CEBNSM strengthened beam (NSM-C-0%F-Pl-A). This is similar to the findings in the previous CEBPNSM groups and thus it can be concluded that in comparison to other strengthening techniques, the CEBPNSM strengthening technique was able to enhance the flexural load performance of the beams most remarkably at the first crack, service and yield stages, as well as significantly enhancing ultimate load. The enhancements in the flexural load capacities of the strengthened beams are graphically represented in Figure 4.58 to Figure 4.60.

Table 4.19: Experimental load and deflection results of CEBPNSM beams with CFRP bar and CFRP plate

Beam specimen	Level of prestress (%)	First crack (P_{cr})		Service (Ps) (kN)	Yield (P_y)		Ultimate (P_{ult})	
		Load (kN)	Deflection (mm)		Load (kN)	Deflection (mm)	Load (kN)	Deflection (mm)
UB	-	63	3.1	83	110	19.8	127	45.6
EBR-Pl	-	71 (12%)	1.9	111 (33%)	118 (6%)	7.88	166 (30%)	27.4
EBR-Pl-A	-	71 (13%)	1.9	114 (37%)	125 (13%)	9.01	176 (39%)	31.2
NSM-C-0%F	0	67 (6%)	3.4	86 (3%)	113 (2%)	11.7	166 (31%)	40.1
NSM-C-0%F-Pl-A	0	75 (19%)	1.8	105 (26%)	127 (15%)	9.5	215 (69%)	37.2
NSM-C-50%F-Pl-A	50	90 (43%)	2.0	133 (60%)	147 (33%)	7.6	224 (77%)	34.4
NSM-C-60%F-Pl-A	60	95 (50%)	1.9	142 (71%)	154 (40%)	7.3	227 (79%)	32.8
NSM-C-70%F-Pl-A	70	99 (57%)	1.9	153 (84%)	163 (48%)	7.1	230 (81%)	31.1

Note: Parentheses represents percentage increase over control beam

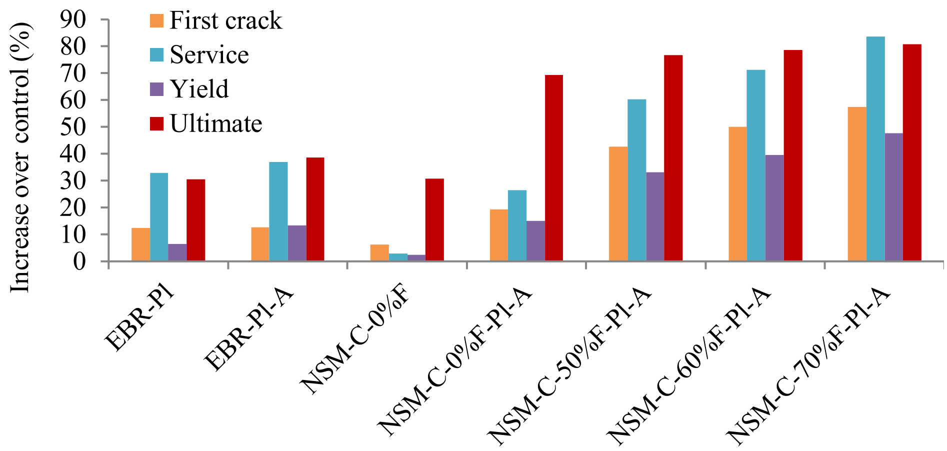

Figure 4.58: Percentile increment over control of CEBPNSM beams with CFRP bars and CFRP plate

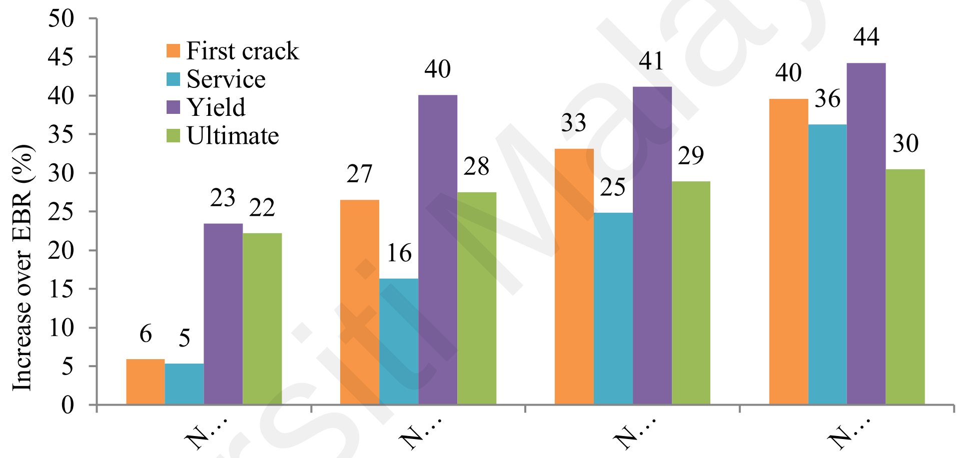

Figure 4.59: Percentile increment of CEBPNSM beams with CFRP bars and CFRP plate over end anchored EBR CFRP plate beam

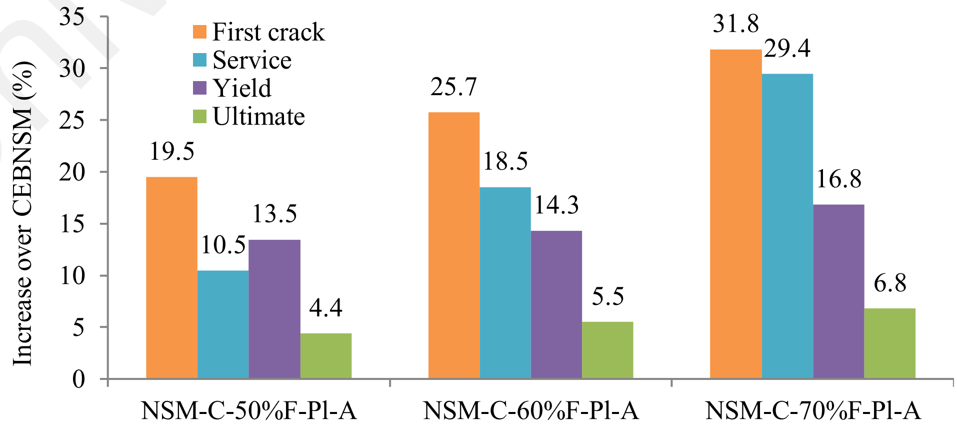

Figure 4.60: Percentile increment of CEBPNSM beams over CEBNSM beam (strengthened with CFRP bar and CFRP plate)

4.7.2 Failure Modes

The failure modes of the CEBPNSM and CEBNSM beams strengthened with CFRP bar and CFRP plate are shown in Figure 4.61. The failure mode of these beams was similar to the EBR CFRP plate strengthened beam with end anchors and the CEBPNSM beams strengthened with steel strands and CFRP plate. Failure occurred by concrete crushing after yielding of the internal steel reinforcement and was followed by debonding of the CFRP plate and rupture of the CFRP bar. The plate end anchors were able to effectively prevent the CFRP plate from debonding before the strengthened beam reached its full strength. As debonding of the plate occurred after concrete crushing initiated, this can be considered as a favorable failure mode as the full concrete strength of the beam was utilized and the full composite action of the strengthened beam was maintained until failure started. No debonding of the NSM CFRP bar was observed during testing. The CFRP bar is assumed to have ruptured immediately after the CFRP plate debonded, although no observable signs were seen from the outside of the beam. This assumption was made from the load deflection behavior of the beams where it can be clearly seen that the load capacity of the beams fell back in two sharp stages to the level of the internal steel reinforcement, indicating that both the CFRP plate and CFRP bar had failed and were no longer able to carry any loading.

(a) NSM-C-0%F-Pl-A

(b) NSM-C-50%F-Pl-A

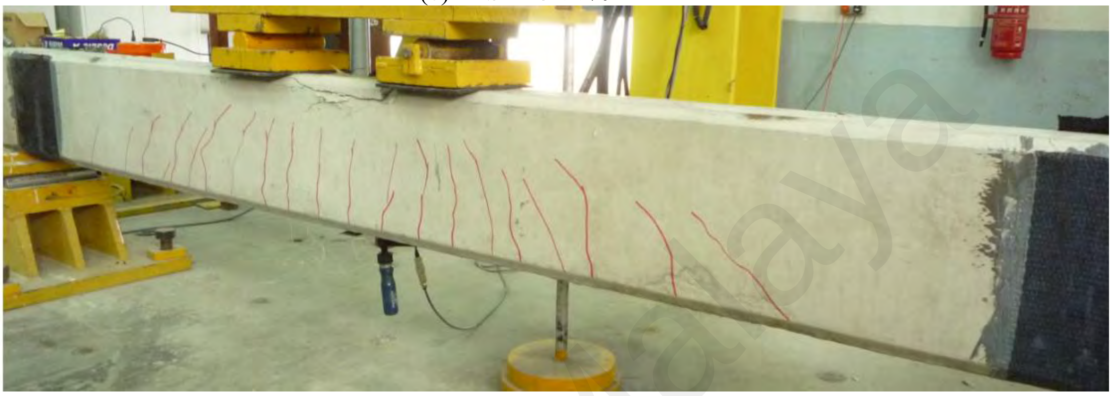

(c) NSM-C-60%F-Pl-A

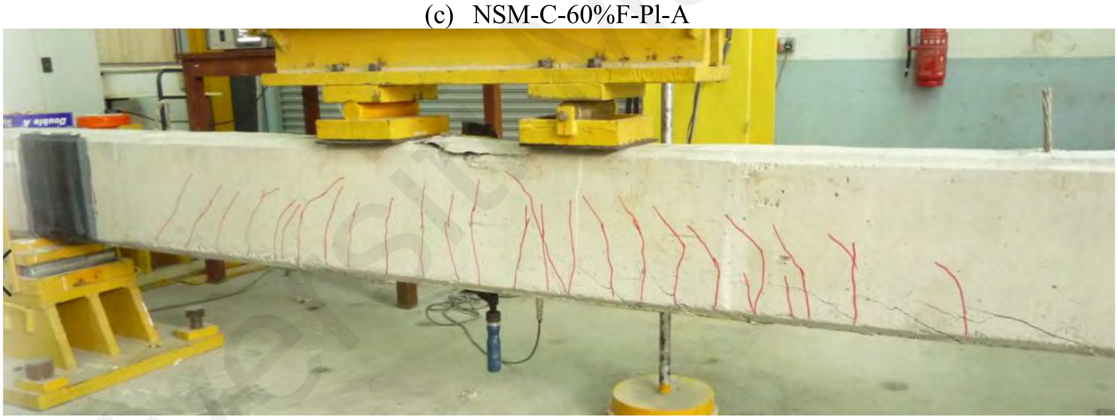

(d) NSM-C-70%F-Pl-A

Figure 4.61: Failure modes of CEBPNSM beams strengthened with CFRP bars and CFRP plate

4.7.3 Load-Deflection Behavior

The load-deflection curves of the CEBPNSM beams are presented in Figure 4.62 and the exact deflection values at first crack, yield, ultimate and end point are given in Table 4.19. The load-deflection responses of the strengthened beams were similar to the beams strengthened using any CFRP in the previous groups. The load-deflection responses were tri-linear from load initiation to ultimate, and the final phase after ultimate was characterized by two large and sharp drops in load capacity, which were due to the debonding of the CFRP plate and the rupture of the CFRP bar after beam failure initiated. The load capacity of the beams then returned to the level of the internal steel reinforcement.

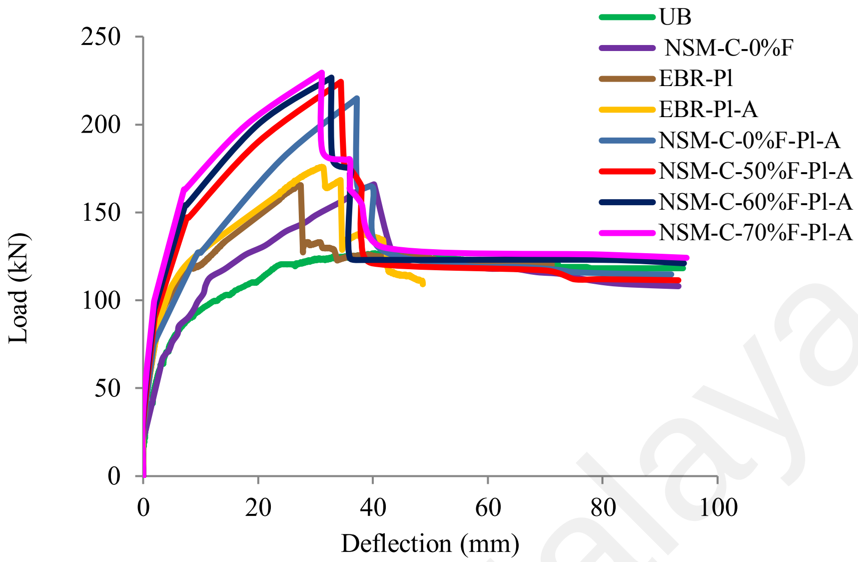

Figure 4.62: Load-deflection curves of CEBPNSM beams with CFRP bars and CFRP plate

In comparison to the NSM CFRP bar strengthened beam and the EBR CFRP plate strengthened beams, the use of CFRP bar and CFRP plate together resulted in much higher and steeper tri-linear load-deflection curves, with smaller deflections at any given load. At first crack, yield and ultimate, the deflections of the combined strengthened beams were significantly reduced compared to the control and the NSM CFRP bar strengthened beam. However, the EBR plate strengthened beams showed slightly smaller, though still comparable, deflections at first crack, yield and ultimate. This was probably due to the high stiffness properties of CFRP plate and greatly increased flexural loads achieved by the combined strengthened beams.

The addition of increasing levels of prestress force in the CEBPNSM beams enhanced the flexural response of the beams in a similar manner to the CEBPNSM beams in the previous groups. Increasing the levels of prestress resulted in correspondingly higher and steeper load-deflection curves and also produced corresponding reductions in deflection at first crack, yield and ultimate. In comparison to the CEBNSM beam, the deflections of the CEBPNSM beams were slightly elevated at first crack, but significantly reduced at yield and ultimate, similar to the deflections seen in the previous group. These effects can all be attributed to the ability of prestressed strengthening to greatly enhance load capacity while significantly reducing deflection. The beam with the greatest enhancement in load-deflection response in this group was, once again, the beam with the highest level of prestress (NSM-C-70%F-Pl-A). The deflections of NSM-C-70%F-Pl-A at first crack, yield and ultimate were only 1.9 mm, 8.2 mm and 31.1 mm, respectively. Figure 4.63 presents the percentage reduction in deflection of the CEBPNSM beams over other beams.

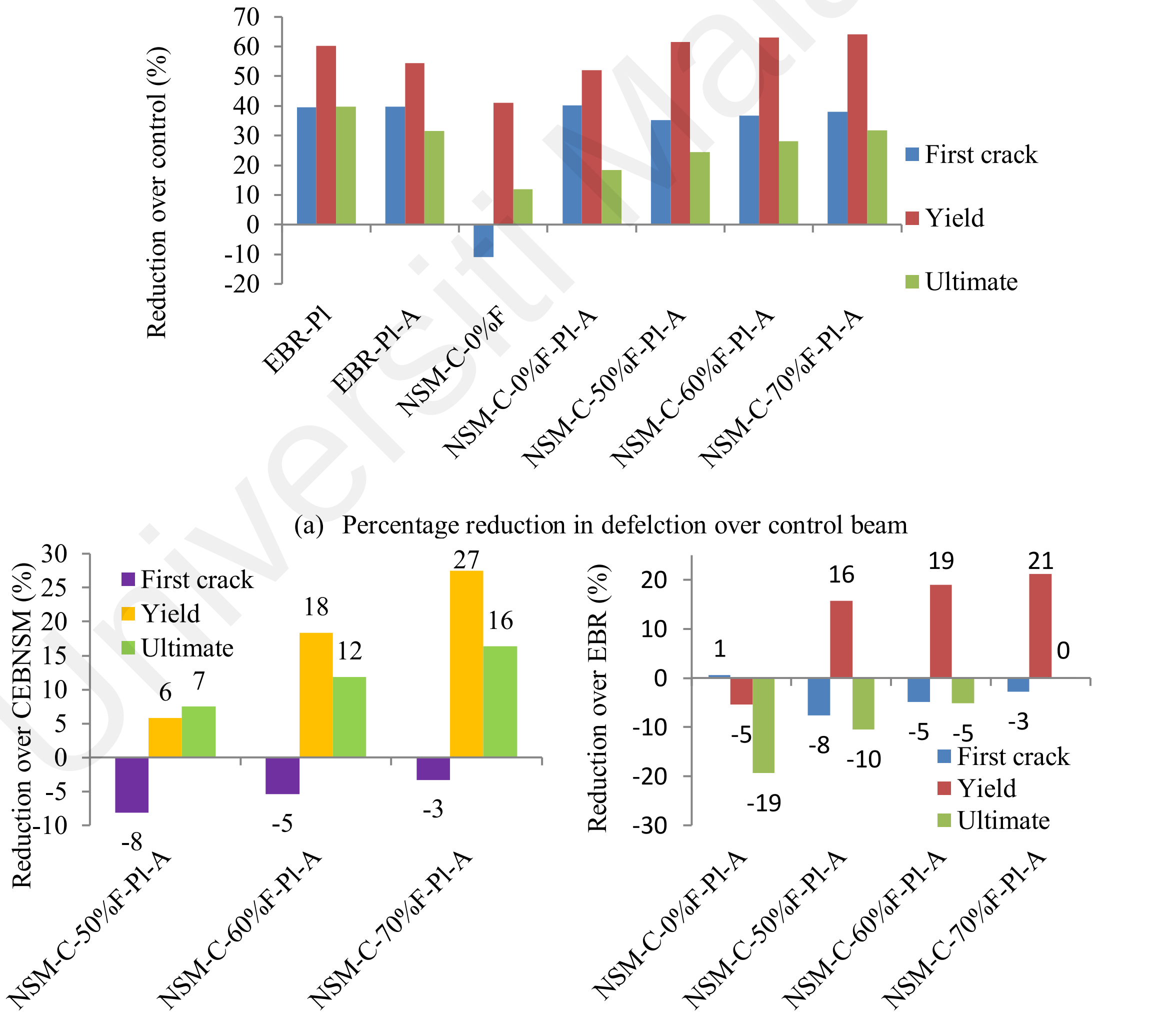

(b) Percentage reduction in deflection over CEBNSM beam

(c) Percentage reduction in deflection over EBR CFRP plate beam with end anchors

Figure 4.63: Percentage reduction in deflection of CEBPNSM beams with CFRP bars and CFRP plate

4.7.4 Cracking Behavior

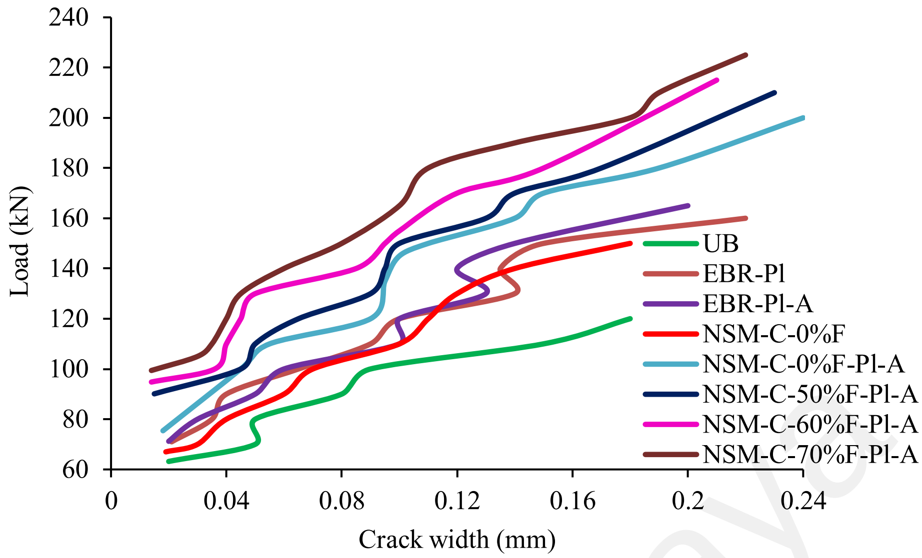

(a) Load vs crack width

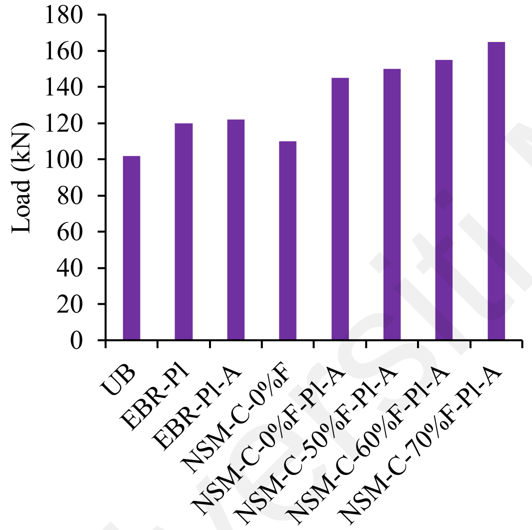

(b) Load at 0.1 mm crack width

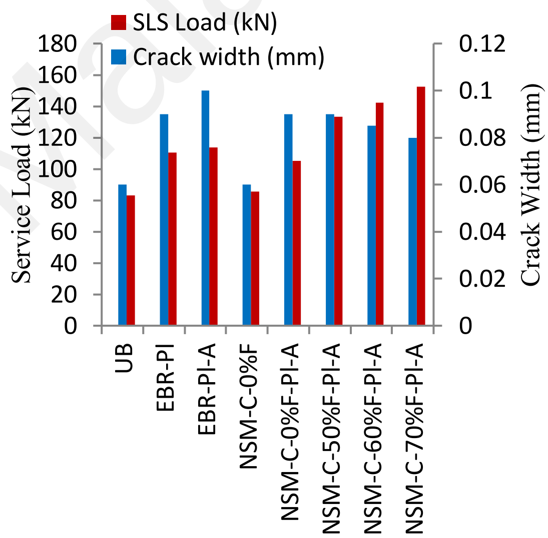

(c) Crack width at service load

Figure 4.64: Cracking behavior of CEBPNSM beams with CFRP bar and CFRP plate

The cracking behavior of the CEBPNSM strengthened beams in this group was similar to the other CEBPNSM strengthened beams in the previous groups. The crack behavior of the strengthened beams improved in terms of crack pattern, crack number, crack spacing, first crack load and crack width, compared to the control beam. The typical flexural crack patterns at ultimate failure of the strengthened beams are shown in Figure 4.61. The strengthened beams had around 21 to 27 cracks each, which were spaced evenly along the beam span. The increased number of cracks correlates to closer spacing and smaller crack widths. The beam with the highest level of prestress (70%) showed the greatest increase in first crack load in this study, 57% over the control beam, while also greatly reducing the deflection at first crack (Table 4.19).

The correlation between the load and crack width of the specimens is shown in Figure 4.64 (a). Strengthening overall increased the loading level at a given crack width, with the CEBPNSM beams showing the greatest increases, as can be seen in Figure 4.64 (b). At 0.1 mm crack width, the CEBPNSM beam with 70% prestress carried a load of 165 kN, which was an increase of 62% over the control beam (102 kN), and an increase of 14% over the CEBNSM beam (145 kN). Crack width at the serviceability stage is an important design consideration. As can be seen in Figure 4.64 (c), strengthening was generally able to increase the service load while decreasing the crack width. The CEBPNSM beam with 70% prestress was able to increase the service load by 84% (153kN) compared to the control beam and the corresponding crack width at service was only 0.08mm. The CEBPNSM strengthening technique was able to control crack width significantly better than the EBR, NSM and CEBNSM techniques, as can be seen in Figure 4.64.

Compared to the CEBPNSM strengthened beams in the previous groups (CFRP bar with CFRP sheet, and steel strand with CFRP sheet), the CEBPNSM beams in this group strengthened with CFRP bars and CFRP plate, displayed higher first crack loads, significantly less deflection at first crack, similar crack patterns, crack numbers and crack spacing, and smaller crack widths. The improvement in cracking behavior over the previous CEBPNSM beams can be attributed to the stiffening effect of the CFRP plate.

4.7.5 Concrete Compressive Strains

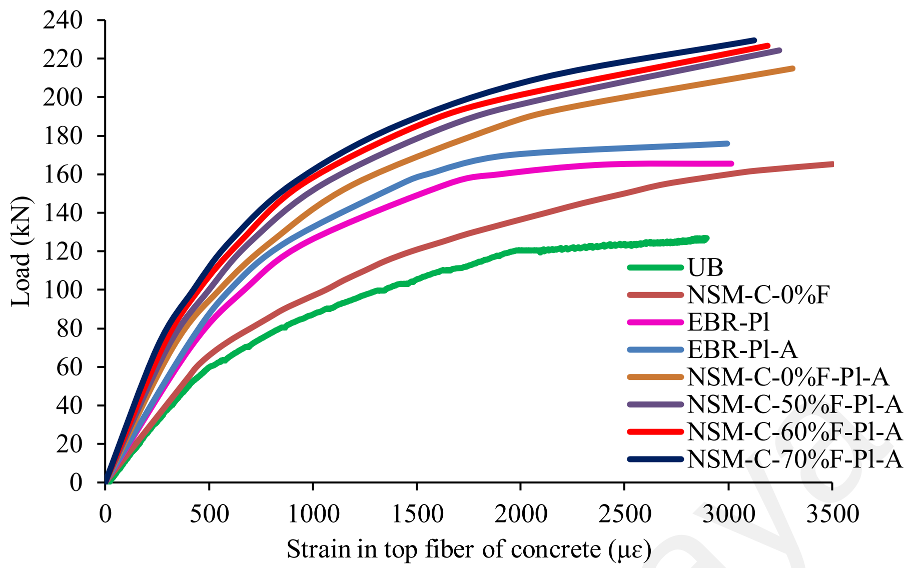

Figure 4.65: Concrete compressive strain of CEBPNSM beams with CFRP bar and CFRP plate

The relation between the loading and the concrete compressive strain at midspan of the beam specimens is shown in Figure 4.65. The strengthened beams displayed markedly steeper concrete load-strain curves from the very onset of loading compared to the control beam, due to the increased stiffness of the strengthened beams. The CEBPNSM strengthened beams were able to control concrete strains to much higher load levels than the NSM, EBR and CEBNSM strengthened beams. The CEBPNSM strengthened beam with 70% prestress showed the greatest reduction in concrete compressive strain for a given load among the strengthened beams. This was due to the high level of prestress in the 70% beam which significantly enhanced the stiffness of the beam. The final strains measured in the beam specimens before the strain gauges were damaged by concrete crushing at failure were 0.00289, 0.00301, 0.00299, 0.00350, 0.00331, 0.00325, 0.00319 and 0.00312 in the control beam, NSM strengthened beam, EBR without end anchorage beam, EBR with end anchorage beam, CEBNSM strengthened beam, and the 50%, 60% and 70% prestressed CEBPNSM strengthened beams, respectively. These final concrete strain values indicate that the full concrete strength of the beams was utilized, as concrete crushing occurs at a compressive strain value of around 0.003. This also indicates the full composite action of the strengthened beams until failure.

4.7.6 Tensile Strains in Main Steel Strands

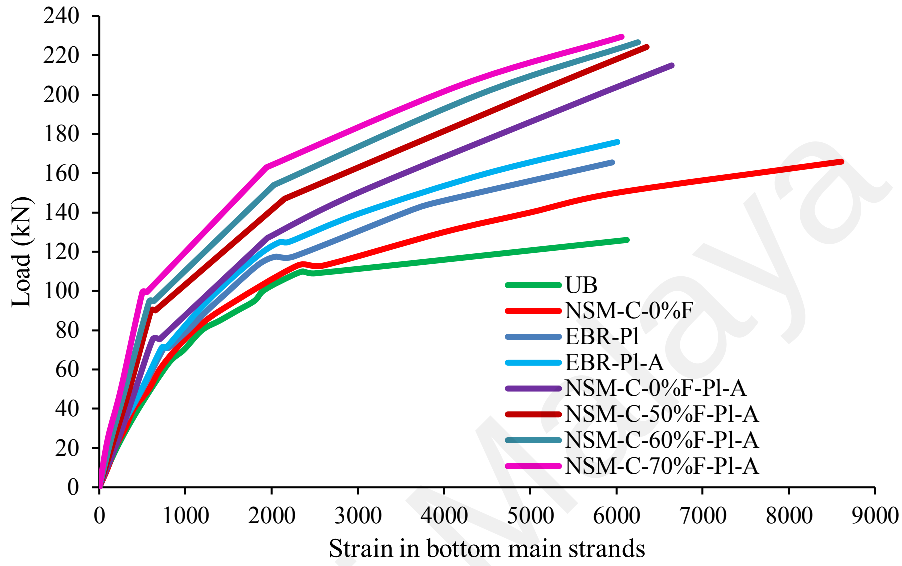

Figure 4.66: Main steel tensile strains of CEBPNSM beams with CFRP bar and CFRP plate

The tensile strains in the bottom main strands were measured at midspan during loading of the beams, and the results are shown in Figure 4.66. The maximum tensile strain values measured in the bottom main steel strands before the strain gauges were damaged during beam failure were 0.00612, 0.00842, 0.00595, 0.00601, 0.00664, 0.00635, 0.00625 and 0.00606 for the control beam, NSM strengthened beam, EBR beam without end anchorage, EBR beam with end anchorage, CEBNSM strengthened beam, and the 50%, 60% and 70% prestressed CEBPNSM strengthened beams, respectively. The CEBPNSM strengthened beams with 50%, 60% and 70% prestress, displayed progressively lower maximum tensile strain values, due to the preexisting compressive strains introduced into the lower half of the beams by prestressing the CFRP bar, which opposed the tensile strains created by loading. The CEBPNSM strengthened beam with the highest level of prestress (70%) displayed the steepest load-strain curve, indicating that tensile steel strains were controlled to much higher load levels. This was due to the combination of strengthening materials and the high level of prestress, which enhanced the strength and stiffness, as well as the strain sharing characteristics of the beam.

4.7.7 Tensile Strains in NSM Steel Strands

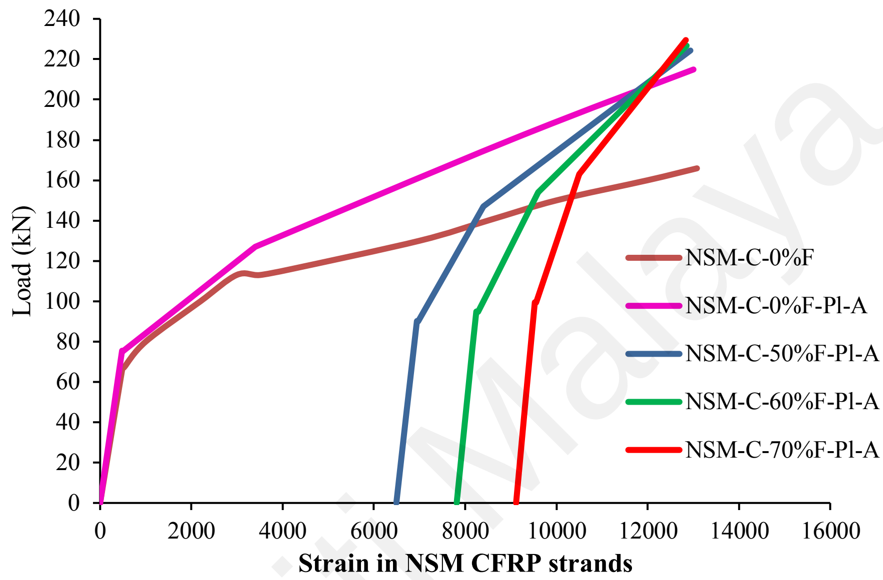

Figure 4.67: NSM CFRP bar tensile strains in CEBPNSM beams with CFRP bar and CFRP plate

The load versus NSM CFRP tensile strain at midspan is shown in Figure 4.67, where the initial strains due to prestressing are shown at zero load. The maximum tensile strains in the NSM CFRP bars were 0.01308, 0.01300, 0.01294, 0.01285 and 0.01283 for the NSM strengthened beam, the CEBNSM strengthened beam and the CEBPNSM beams with 50%, 60% and 70% prestress, respectively. These were the strain values just before the beams reached their ultimate point and failure occurred, damaging the strain gauges so no further readings could be taken. The maximum tensile CFRP bar strain in the NSM strengthened beam was greater than the other beams as the tensile stress was shared between the NSM bar and the internal steel strands only. Whereas in the CEBNSM and CEBPNSM beams the tensile stress was divided between the CFRP bar, internal steel strands and the CFRP sheet, which reduced the tensile strains in the CFRP bar. The CEBPNSM strengthened beams showed the least increment in strain from load initiation until failure. Specifically, the CEBPNSM beam with 70% prestress showed the least increment in tensile CFRP bar strain, only 0.00372 (this disregards the initial strain from prestress). The addition of prestress and the consequent compression around the CFRP is the probable cause of this behavior.

4.7.8 Tensile Strains in CFRP Plate

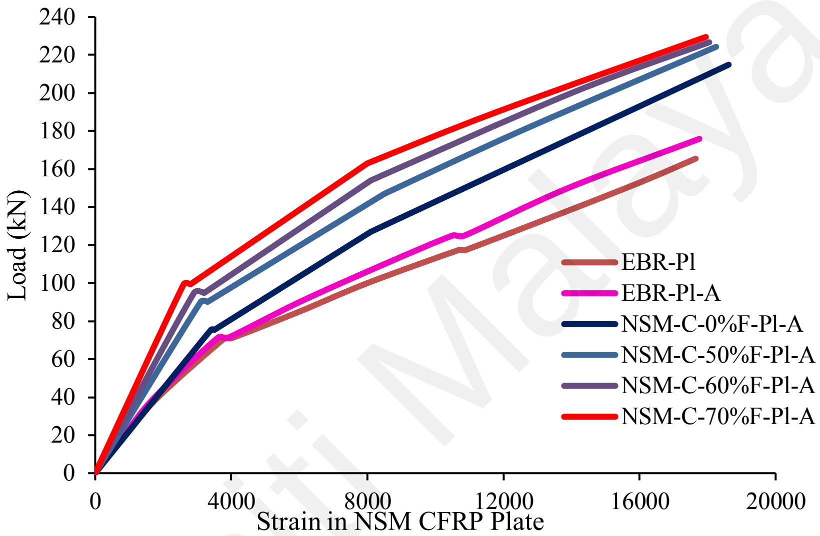

Figure 4.68: Load versus tensile strain in CFRP plate

Figure 4.68 presents the variations in tensile strain in the EBR CFRP plate of the beam specimens for increasing load levels during testing. The CEBNSM beam had an overall steeper CFRP tensile strain curve than the EBR beam due to the additional NSM bar, which enhanced strength and stiffness. In turn, the CEBPNSM beams had steeper curves than the CEBNSM beam and increasing the level of prestress in the NSM strands further decreased the rate of tensile strain increment in the CFRP plate. This can be attributed to the effect of prestress, which controls tensile strains. The maximum tensile strains measured in the CFRP plates before failure of the strain gauges were 0.01765, 0.01776, 0.01862, 0.01825, 0.01805 and 0.01795 for the EBR beam without end anchorage, EBR beam with end anchorage, CEBNSM strengthened beam and the CEBPNSM strengthened beams with 50%, 60% and 70% prestress, respectively. The maximum strains measured in the CEBNSM and CEBPNSM strengthened beams indicate that the full capacity of the CFRP plate was utilized, which agrees with the observed failure mode of concrete crushing and confirms the full composite action of these strengthened beams.

4.7.9 Prestress Losses

Table 4.20: Prestress force and camber effect in CEBPNSM beams with CFRP bar and CFRP plate

Beam ID	Applied Prestress Force		Effective Prestress Force		Negative camber at mid-section
	(kN)	(%)	(kN)	(%)	(mm)
NSM-C-50%F-Pl-A	73.36	53	68.80	49.80	0.80
NSM-C-60%F-Pl-A	87.04	63	82.81	59.94	0.85
NSM-C-70%F-Pl-A	100.72	73	96.61	69.93	1.10

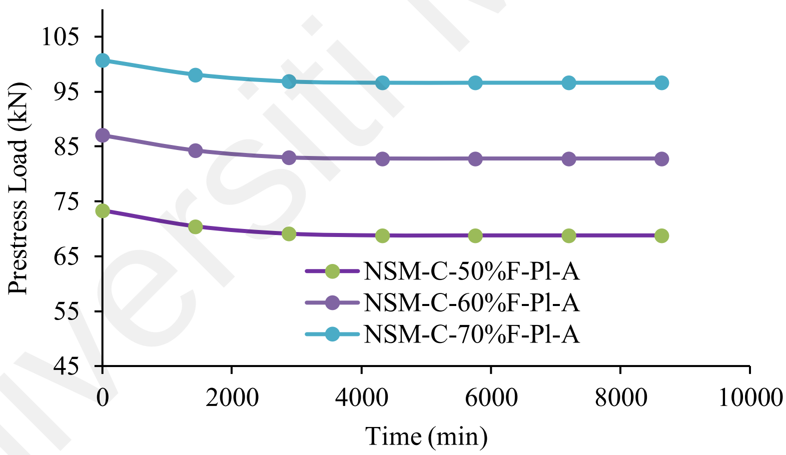

Figure 4.69: Prestress force in CFRP bars during curing period for CEBPNSM beams with CFRP bar and CFRP plate

The prestressed CFRP bars in the CEBPNSM strengthened beams were monitored for losses in prestress force from the time the prestress was applied until the release of the prestress into the beams. The amount of force applied to prestress the 50%, 60% and 70% prestressed CEBPNSM strengthened beams were 73 kN, 87 kN and 100 kN, respectively, which were calculated based on the tensile strength of the CFRP bars and the estimated prestress loss to be covered (Table 4.20). The prestressing force levels in the NSM bars over the six-day curing period are shown in Figure 4.69. The loss in prestressing force during this time was at about 4.1 kN to 4.6 kN. This loss was due to adhesive creep and anchor slip of the CFRP bars (Badawi et al. 2009). During prestress release, an LVDT was used to measure the negative camber at the midspan of the strengthened beams, which were found to be 0.80 mm, 0.85 mm and 1.10 mm for the 50%, 60% and 70% CEBPNSM beams, respectively.

4.7.10 Effect of Increasing Prestress Level

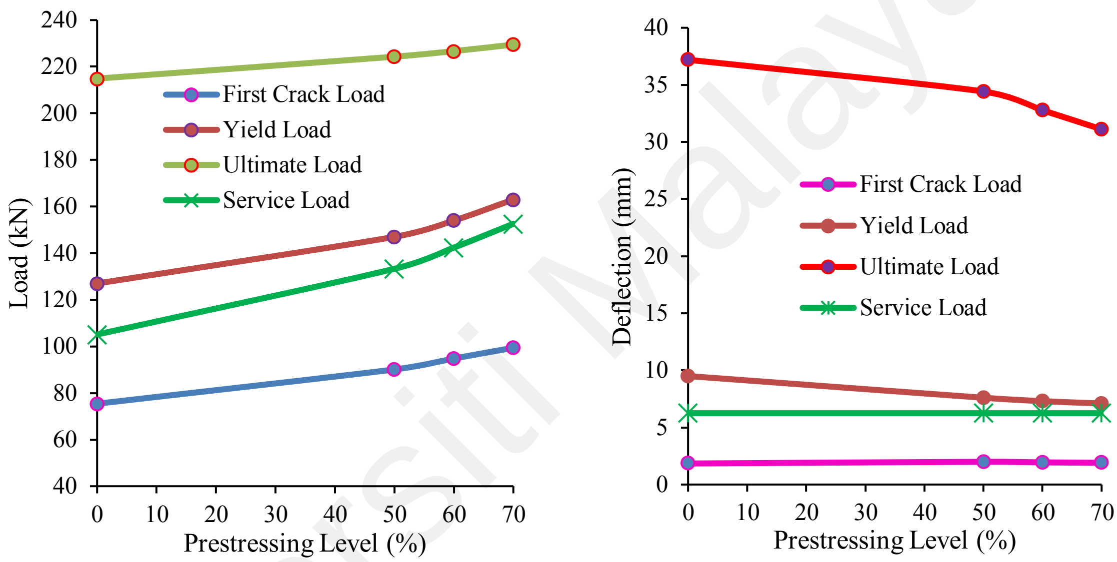

(a) Load vs level of prestressing force

(b) Deflection vs level of prestressing force

Figure 4.70: Effect of prestress level in CEBPNSM beams with CFRP bar and CFRP plate

Increasing the level of prestress in the CEBPNSM strengthened beams significantly enhanced flexural performance. The highest level of prestress force (70%) enhanced flexural performance the most among the CEBPNSM beams. The first crack, service, yield and ultimate loads of beam CEBPNSM with 70% prestress force increased by about 32%, 46%, 28% and 7%, respectively, over the CEBNSM beam (0% prestress), and by 10%, 15%, 11% and 3%, respectively, over the 50% CEBPNSM beam. The improvement in flexural load capacity, especially at service and yield, by increasing the level of prestress in the CEBPNSM beams can be seen from Figure 4.70 (a).

Increasing the level of prestress also reduced deflection, crack width, concrete compressive strains and tensile strains for any given load level. From Figure 4.70 (b), it can be seen that increasing the level of prestress in the beams did not negatively influence deflection at first crack and service, rather the beams were able to maintain the same level of deflection seen in the beam without prestress despite the significant increases in load at first crack and service. At ultimate and yield, increasing the level of prestress significantly decreased deflection and the 70% prestress level showed the smallest ultimate deflection among the strengthened beams. Increasing the level of prestress was able to reduce concrete compressive strains and tensile strains in the main reinforcement, steel strand and CFRP plate to for any given load level. The rates of strain increment were also significantly reduced by increasing prestress as can be seen in the strain graphs (Figure 4.65 – Figure 4.68).

4.7.11 Assessment of FEM

Table 4.21: Experimental and FEM results at ultimate for CEBPNSM beams with CFRP bars CFRP plate

Beam specimens	Level of Prestress (%)	Experimental		FEM		FEM/Experimental	
		Load (kN)	Deflection (mm)	Load (kN)	Deflection (mm)	Load (P_{FEM}/P_{exp})	Deflection ($\Delta_{FEM}/\Delta_{exp}$)
NSM-C-0%F-Pl-A	0	214.90	37.20	206.87	38.10	0.96	1.02
NSM-C-60%F-Pl-A	60	226.70	32.78	215.71	33.19	0.95	1.01
NSM-C-70%F-Pl-A	70	229.50	31.11	217.87	33.22	0.95	1.07

A comparison of the experimental and FEM results at ultimate for the strengthened beams is presented in Table 4.21. The difference between the experimental and numerical results reached a maximum of 5% for ultimate load and 7% for the corresponding deflection. The error difference was within the acceptable limit (10%)

(Darain et al. 2016; Kishi et al. 2005). The conformity between the experimental ultimate load and deflection and the FEM output was satisfactory.

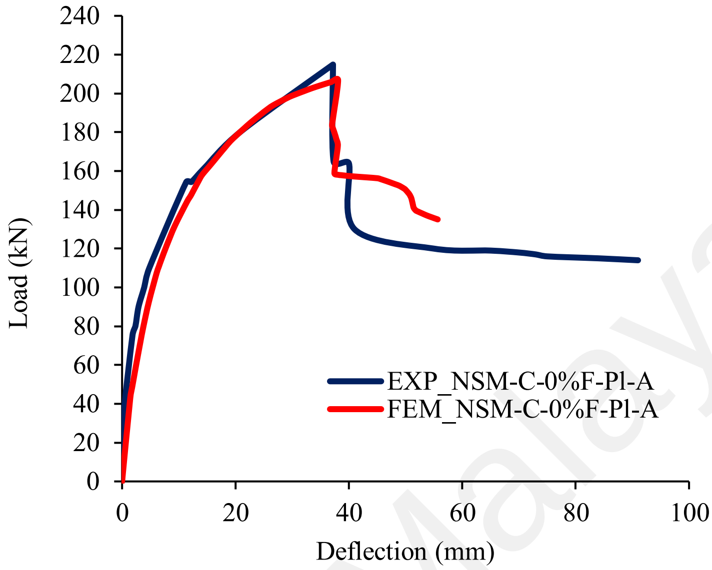

(a) Load Vs Deflection for NSM-C-0%F-Pl-A

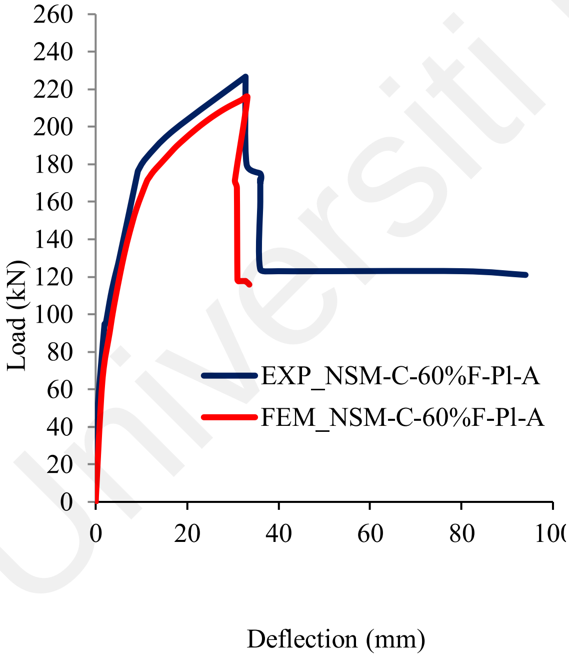

(b) Load Vs Deflection for NSM-C-60%F-Pl-A

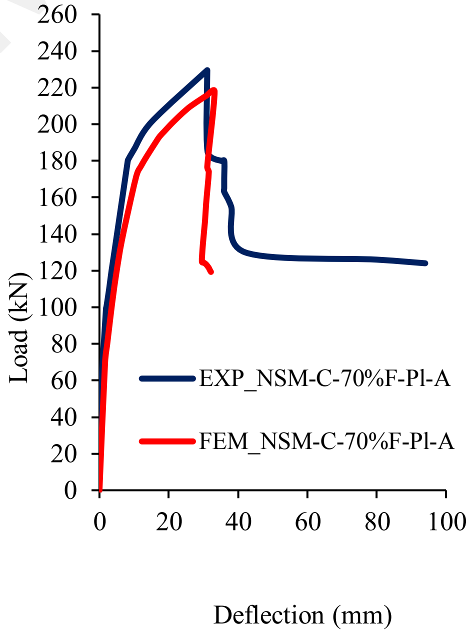

(c) Load Vs Deflection for NSM-C-70%F-Pl-A

Figure 4.71: FEM load-deflection for CEBPNSM beams with CFRP bar and CFRP plate

The numerical and the experimental load-deflection relationships are shown in Figure 4.71. As can be clearly observed from the figure, the correlation between the numerical results and experimental data is reasonably good.

The FEM compressive and tensile concrete damage behavior for all the beams were almost similar (Figure 4.72), with tensile damage spread along the tension span of the beam but more concentrated at midspan, and compressive damage at the top fiber at midspan. Experimentally, the strengthened beams all displayed flexural cracking along the tension zone which greater crack development at midspan and flexural failure by concrete crushing after yielding of the steel reinforcement with CFRP plate debonding and CFRP bar rupture. Concrete crushing initiated before and continued after CFRP plate debonding and CFRP bar rupture, indicating that concrete failure was the governing cause of failure. Thus, the damage behavior simulated by the FEM model agreed reasonably well with the cracking and failure behavior observed in the experimental beams.

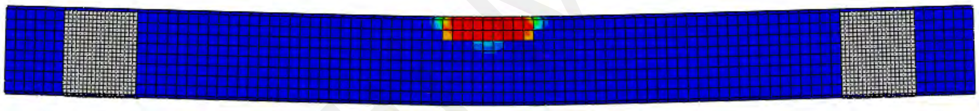

(d) Compressive damage behavior

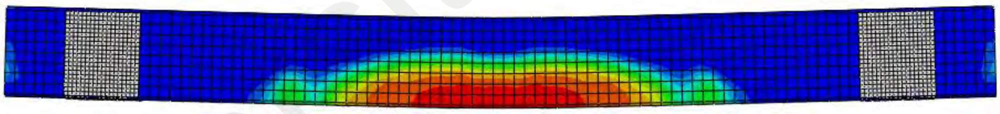

(e) Tensile damage behavior

Figure 4.72: FEM damage behavior of NSM-C-70%F-PL-A

4.8 CEBPNSM Strengthened Beams Using Steel Strands and CFRP Plate

4.8.1 Flexural Capacities

Table 4.19 presents the load and deflection results for the CEBPNSM beams strengthened with a combination of steel strands and CFRP plate. The percentage increases in load over the control beam are also given. The load and deflection results of the control beam, the NSM steel strand strengthened beam, the EBR CFRP plate strengthened beams (with and without end anchor) and the CEBPNSM beam strengthened with steel strands and CFRP plate are also given for comparison purposes. As can be seen from the table, the CEBPNSM strengthened beams displayed far greater load carrying capacity at all load stages than the beams strengthened with the other techniques, including the CEBNSM beam (without prestress). The greatest enhancement was seen in the CEBPNSM beam with 70% prestress, with the single greatest increase in this research seen at service load where a 100% increase over the control beam was recorded. This remarkable increase can be attributed to a number of factors - the combination of EBR CFRP plate and NSM steel strand, and the high prestress force in the steel strand, all of which remarkably increased the stiffness of the beam and reduced deflection, allowing the beam to reach a much higher service load. This 70% CEBPNSM strengthened beam also had the highest service and yield loads amongst all the beams tested in this study.

Table 4.22: Experimental load and deflection results of CEBPNSM beams with steel strands and CFRP plate

Beam specimen	Level of prestress (%)	First crack (P_{cr})		Service (P_s) (kN)	Yield (P_y)		Ultimate (P_{ult})	
		Load (kN)	Deflection (mm)		Load (kN)	Deflection (mm)	Load (kN)	Deflection (mm)
UB	-	63	3.1	83	110	19.8	127	45.6
EBR-Pl	-	71 (12%)	1.9	111 (33%)	118 (6%)	7.9	166 (30%)	27.4
EBR-Pl-A	-	71 (13%)	1.9	114 (37%)	125 (13%)	9.0	176 (39%)	31.2
NSM-S-0%F	0	66 (5%)	3.2	92 (10%)	145 (32%)	23.5	162 (28%)	38.3
NSM-S-0%F-Pl-A	0	75 (18%)	1.8	119 (43%)	148 (34%)	10.3	212 (67%)	29.0
NSM-S-50%F-Pl-A	50	89 (41%)	1.9	142 (71%)	175 (59%)	9.7	221 (74%)	28.1
NSM-S-60%F-Pl-A	60	92 (46%)	1.9	154 (86%)	179 (62%)	8.2	223 (76%)	26.5
NSM-S-70%F-Pl-A	70	97 (53%)	1.9	167 (100%)	182 (65%)	7.2	226 (78%)	24.1
Note: Parentheses represent percentage increase over control beam								

The addition of prestress significantly enhanced the flexural load capacities of the CEBPNSM beams with steel strands and CFRP plate in comparison to the CEBNSM beam. Increasing the level of prestress in the steel strand caused corresponding increases in enhancement. The highest level of prestress (70%) gave the greatest enhancement over the non-prestressed CEBNSM beam, with 29%, 40%, 23% and 7% increases in first crack, service, yield and ultimate loads, respectively. This can be attributed to the prestress effect, as has been elaborated in previous sections. The enhancements in the flexural load capacities of the strengthened beams are graphically presented in Figure 4.73 to Figure 4.75.

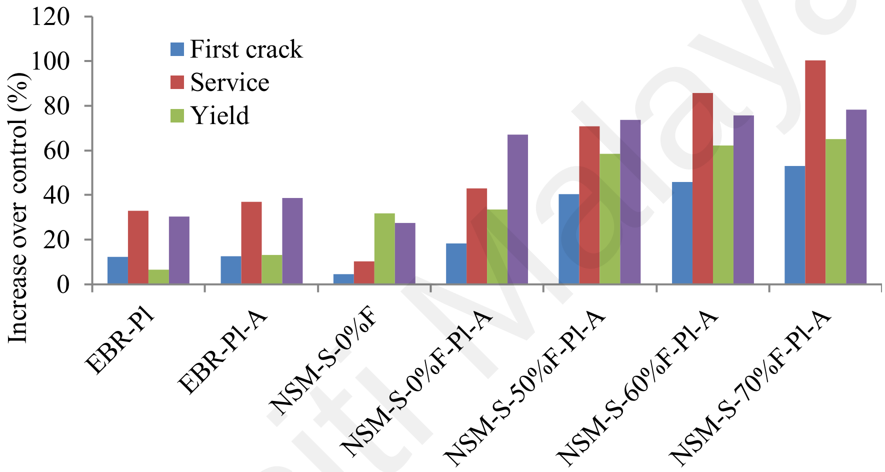

Figure 4.73: Percentile increment over control of beams strengthened with EBR CFRP plate and NSM steel strand

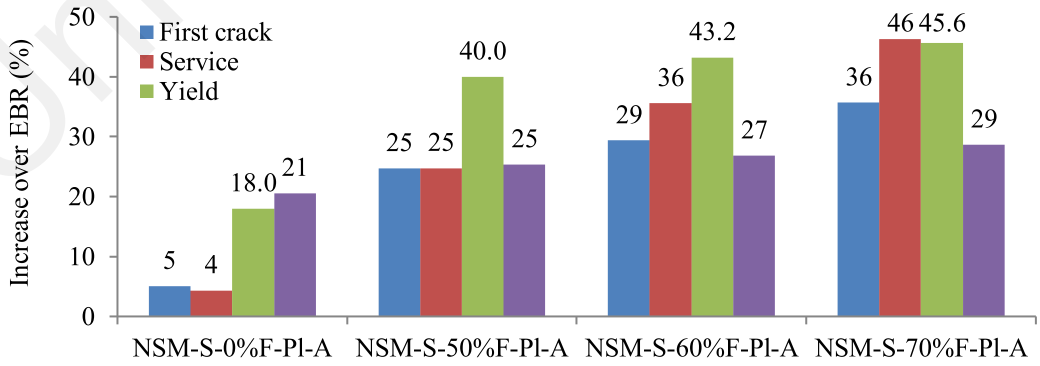

Figure 4.74: Percentile increment of beams strengthened with EBR CFRP plate and NSM steel strand over end anchored EBR CFRP plate beam

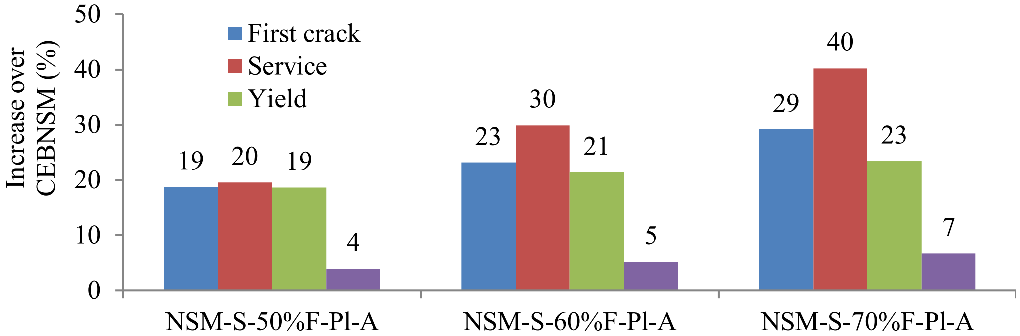

Figure 4.75: Percentile increment of CEBPNSM beams over CEBNSM beam (CFRP plate and steel strand)

4.8.2 Failure Modes

The failure modes of the beams strengthened with a combination of NSM steel strands and EBR CFRP plate are presented in Figure 4.76. The beams in this group all failed flexurally by concrete crushing followed by plate debonding, after yielding of the internal steel reinforcements, similar to the failure mode of the EBR CFRP plate strengthened beam with end anchors. Concrete crushing occurred at the top concrete face at midspan where the compression forces were greatest. As deflection increased due to beam softening, the CFRP plate lost full compatibility with the beam and suddenly debonded along the midspan with a loud sound. Concrete crushing continued to occur after plate debonding until testing was eventually discontinued. No debonding of the NSM steel strand was observed at any time during testing. As concrete crushing occurred before debonding of the plate, the strengthened beam is considered to have acted in a fully composite manner and reached its full design strength.

(a) NSM-S-0%F-Pl-A

(b) NSM-S-50%F-Pl-A

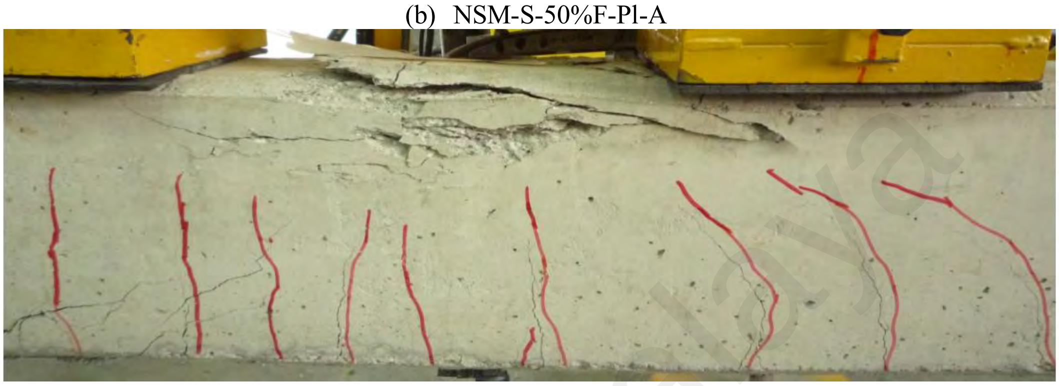

(c) NSM-S-60%F-Pl-A
2

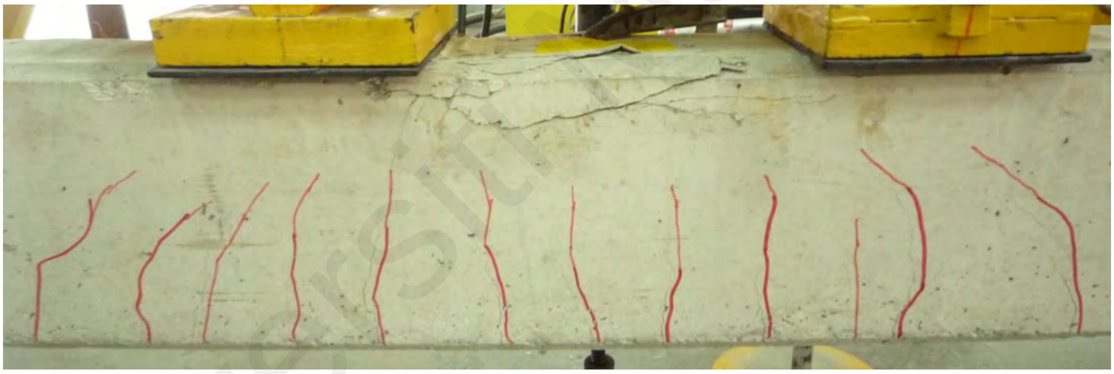

(d) NSM-S-70%F-Pl-A

Figure 4.76: Failure modes of CEBPNSM beams with steel strands and CFRP plate

4.8.3 Load-Deflection Behavior

The load-deflection behavior of the CEBPNSM beams strengthened with steel strands and CFRP plate are presented in Figure 4.77 and the exact deflection values at first crack, yield, ultimate and end point are given in Table 4.22. The load-deflection responses of the strengthened beams in this group were most similar to the beams strengthened using a combination of CFRP bars and CFRP plate. The expected CFRP tri-linear response was observed until ultimate, after which the debonding of the CFRP plate caused the loading to fall sharply back to the level of the combined NSM and internal steel reinforcements.

In comparison to the previous CEBPNSM group (CFRP bar and CFRP plate), the beams in this group (steel strands and CFRP plate) displayed stiffer load-deflection response, which can be seen from the load-deflection curves and from the deflection values at first crack, yield and ultimate. The increase in stiffness and resultant reduced deflections of this group of beams in comparison to the previous group can be attributed to the use of steel strands, instead of CFRP bar, as the NSM reinforcement. The steel strand had superior stiffness properties compared to the CFRP bar. The failure behavior after ultimate also differed slightly from the previous group (CFRP bar and CFRP plate), again due to the use of steel strands instead of CFRP bars. Whereas the beams in the previous group displayed two sharp drops (when the CFRP plate debonded and then the CFRP bar ruptured) all the way back to the level of the internal tension steel, the beams in this group showed a single sharp drop (when the CFRP plate debonded) back to the level of the NSM steel reinforcement.

Compared to the beams strengthened using combination techniques (CEBNSM and CEBPNSM) with various materials (steel strand, CFRP bar, CFRP sheet and CFRP plate) in the other groups in this study, the beams strengthened in this group with a combination of NSM steel strands and EBR CFRP plate had the stiffest load-deflection responses. This can be seen from the steepness of the load-deflection curves and also from the deflection values of the beams at first crack, yield and ultimate. Overall, the beams in this group had the smallest deflections in this study for any given load level, as well as at first crack, yield and ultimate. The stiff load-deflection response and greatly reduced deflection can be attributed to the CFRP plate and the steel strand, both of which have superior stiffness properties and as they were used in combination, the stiffness enhancement was even greater. Another significant difference can be seen in the failure behavior of the beams after ultimate where the CFRP plate debonds from the beam and causes a single large steep drop in load capacity back to the level of the NSM steel beam. The beams in the previous two groups which used CFRP sheet combined with NSM reinforcement displayed more gradual failure with several small drops in load spread out over a large deflection range. This difference is due to the difference in nature of CFRP plate and CFRP sheet. CFRP plate is extremely stiff and does not easily bend, whereas CFRP sheet is a more flexible, cloth-like material. At failure, CFRP plate debonds all at once, causing a sudden drop in the load capacity of the beam. Whereas, at failure, CFRP sheet ruptures one small portion at a time (in stages), which is why the load capacity of the beam falls more gradually in steps.

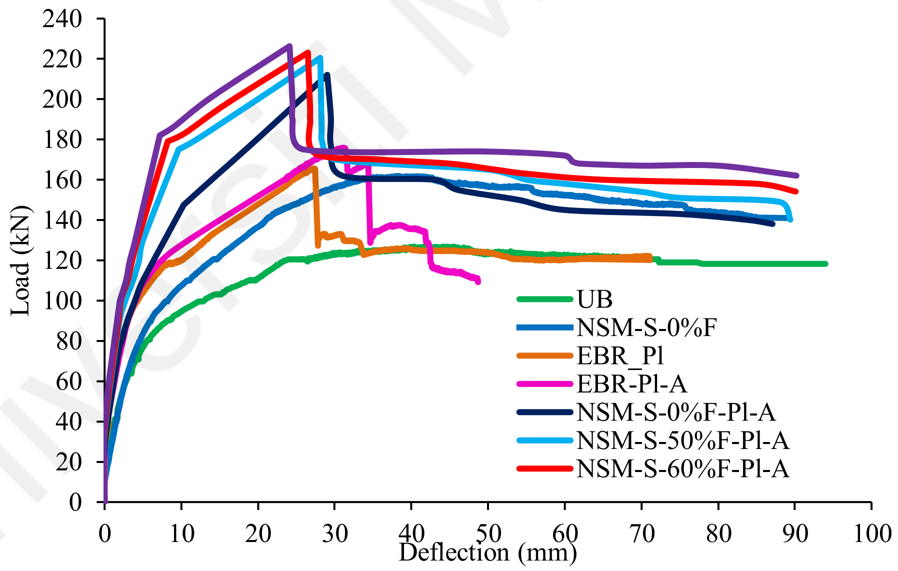

Figure 4.77: Load-deflection curves of CEBPNSM beams with steel strands and CFRP plate

In comparison to the NSM steel strand strengthened beam and the EBR CFRP plate strengthened beams, the use of NSM steel strand and EBR CFRP plate combined together resulted in much higher and steeper tri-linear load-deflection curves, with smaller deflections at any given load. At first crack, yield and ultimate, the deflections of the combined strengthened beams were comparable to the EBR plate strengthened beams and greatly reduced from the control and NSM steel strengthened beams, as can be seen in Table 4.22.

The effect of adding prestress to the steel strand in the combined technique (CEBPNSM) can be clearly seen from the load-deflection graph. The addition of prestress resulted in higher and steeper curves, and increasing the level of prestress further enhanced this effect. At first crack, the deflections of the CEBPNSM beams increased slightly over the CEBNSM beam, due to the significantly greater first crack loads. At yield and ultimate, the deflections of the CEBPNSM beams were significantly less than the CEBNSM beam, despite the substantial increases in yield and ultimate load, which indicates the remarkable ability of prestressed strengthening to reduce deflection. As can be seen in Table 4.22, increasing the level of prestress in the CEBPNSM beams produced corresponding decreases in deflection at all load stages (first crack, yield and ultimate). Similar to the previous groups, the beam with the greatest enhancement in load-deflection response in this group was the beam with the highest level of prestress (NSM-S-70%F-Pl-A), which was also the beam with greatest reduction in deflection at yield and ultimate among all the strengthened beams tested in this study. The deflections of NSM-S-70%F-Pl-A at first crack, yield and ultimate were only 1.9 mm, 7.2 mm and 24.1 mm, respectively.

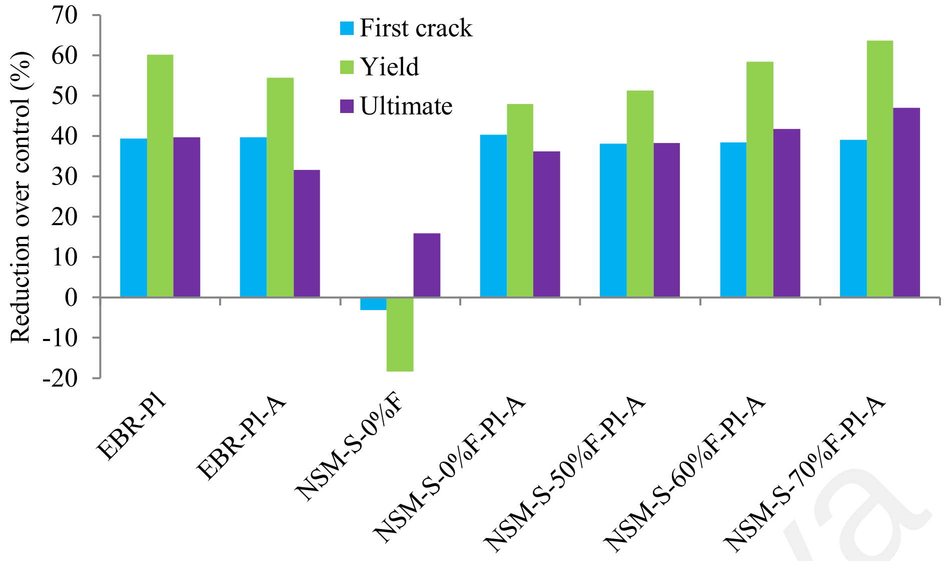

(a) Percentage reduction in defelction over control beam

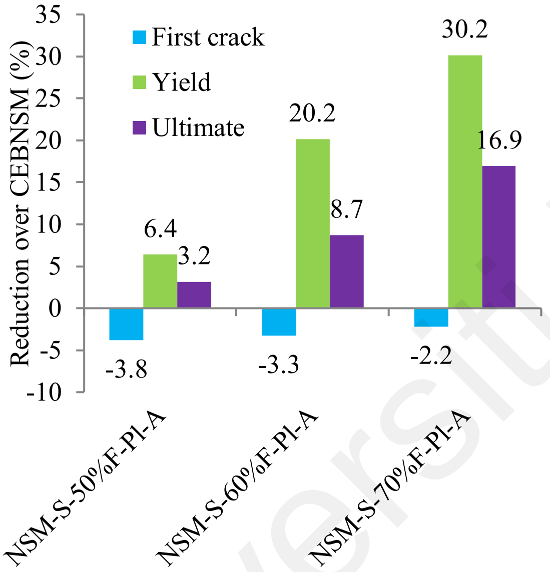

(b) Percentage reduction in deflection over CEBNSM beam

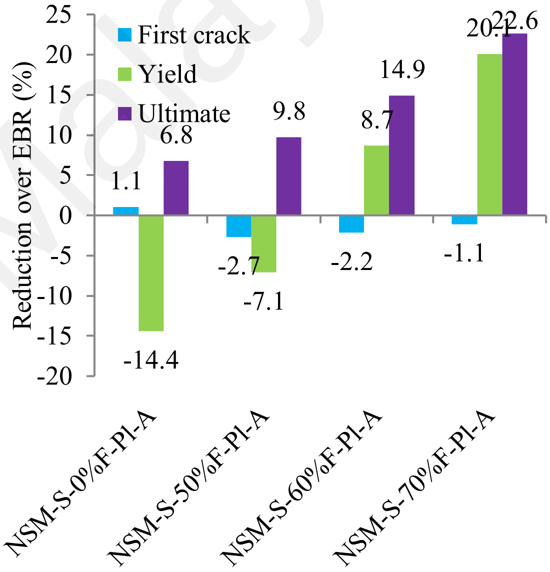

(c) Percentage reduction in deflection over EBR CFRP plate beam with end anchors

Figure 4.78: Percentage reduction in deflection of CEBPNSM beams with steel strands and CFRP plate

4.8.4 Cracking Behavior

The CEBPNSM beams strengthened with steel strands and CFRP plate displayed significantly better cracking behavior compared to the control, EBR, NSM and CEBNSM strengthened beams, in terms of first crack load, crack width, crack pattern, crack number and crack spacing. The general pattern of crack formation and crack widening was similar to that seen in the other CEBPNSM strengthened beams in this research.

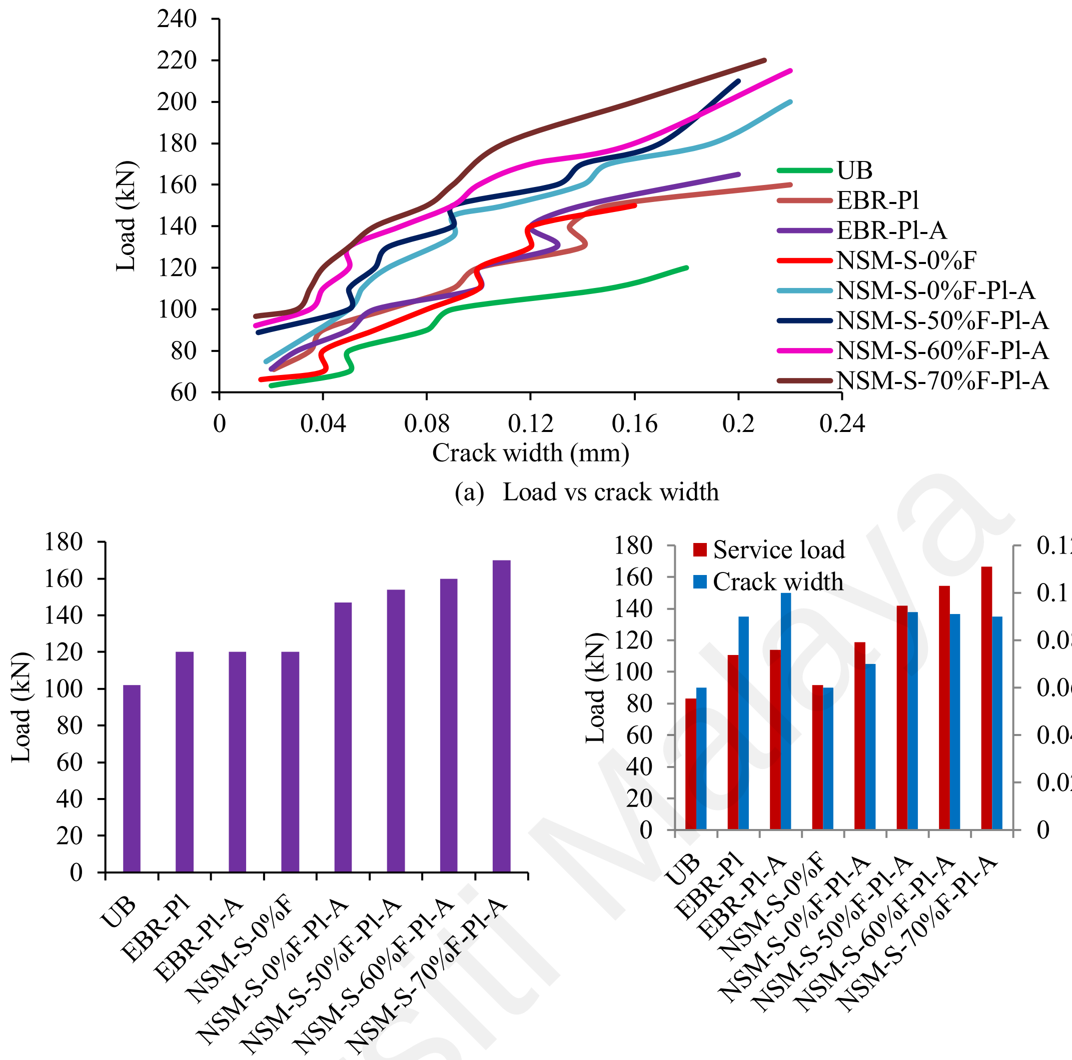

(b) Load at 0.1 mm crack width (c) Crack width at service load

Figure 4.79: Cracking behavior of CEBPNSM beams with steel strands and CFRP plate

The first crack load of the strengthened beams improved considerably over the control, EBR, NSM and CEBNSM strengthened beams (Table 4.22). Increasing the level of prestress caused the first crack load to increase further and the beam with the highest level of prestress (70%) showed the greatest increase in first crack load, while also greatly reducing the deflection at first crack. The 70% beam displayed a 53%, 36%, 46% and 29% improvement in first crack load over the control, EBR, NSM and CEBNSM strengthened beams.

The relation between load and crack width of the strengthened beams is shown in Figure 4.79 (a). The CEBPNSM beams showed the greatest increase in load for a given crack width. As can be seen in Figure 4.79 (b), at 0.1 mm crack width the CEBPNSM beam with 70% prestress carried a load of 170 kN, which was an increase of 67%, 42%, 42% and 16% over the control (102 kN), EBR (120 kN), NSM (120 kN) and CEBNSM (147 kN), respectively. Crack width at service is an important design consideration. In Figure 4.79 (c) it can be seen that increasing the level of prestress in the CEBPSNM beams significantly increased the service load while decreasing crack width. The 70% CEBPNSM beam was able to increase service load by 100% (167kN) compared to the control beam and corresponding crack width at service was only 0.09mm. The CEBPNSM strengthening technique was thus able to control crack width significantly better than the EBR, NSM and CEBNSM techniques.

The CEBPNSM strengthened beams displayed more flexural cracks with closer spacing, smaller crack widths and more uniform distribution compared to the control beam and the EBR beams. The CEBPNSM beams had around 22 to 27 cracks each, while the control beam had 15 cracks and the EBR beams around 17 cracks. The NSM and CEBNSM strengthened beams had 22 and 20 cracks each, with crack patterns similar to the CEBPNSM beams. The crack patterns at ultimate failure of the beams CEBPNSM beams strengthened with NSM steel strands and EBR CFRP plate are shown in Figure 4.76.

Compared to the CEBPNSM strengthened beams in the previous groups (CFRP bar with CFRP sheet, steel strand with CFRP sheet, CFRP bar and CFRP plate), the CEBPNSM beams in this group strengthened with steel strands and CFRP plate, displayed significantly smaller crack widths, significantly less deflection at first crack, similar crack patterns, crack numbers and crack spacing, and first crack load values comparable to the CFRP bar with CFRP plate CEBPNSM beams. The improvement in cracking behavior over the previous CEBPNSM beams, especially the reduced crack widths, can be attributed to the superior stiffening effect achieved by combining EBR CFRP plate with NSM steel strands.

4.8.5 Concrete Compressive Strains

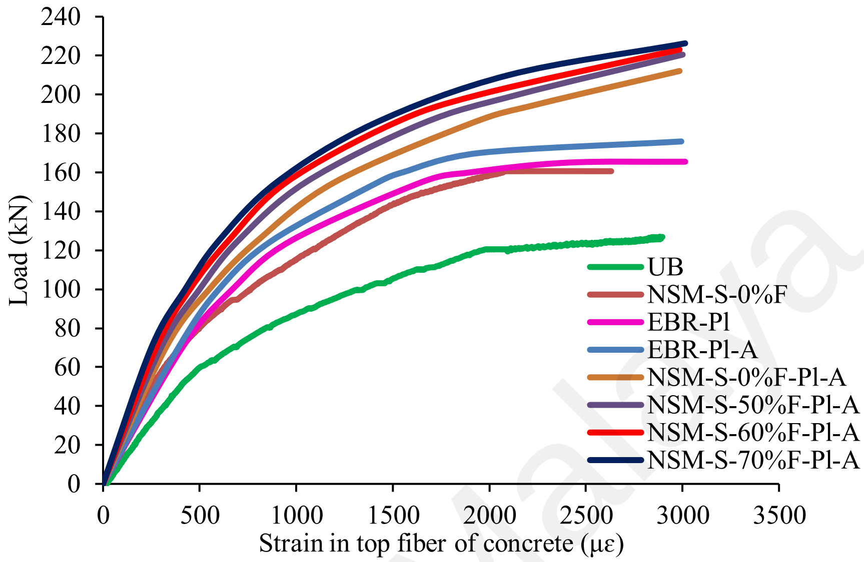

Figure 4.80: Concrete compressive strain of CEBPNSM beams with steel strands and CFRP plate

The variation of concrete compressive strain at midspan due to loading is shown in Figure 4.80. The concrete compressive strain increased in a linear manner with a steep slope at almost the same rate for all the beams until first crack. After first crack the control beam diverged to a shallower slope with a greater rate of increase in strain while the strengthened beams diverged less and had similar rates of increase in strain until yield. The rate of increment of the compressive strain was higher in this phase due the loss in stiffness after first crack. Overall, the compressive strains in the strengthened beams were significantly less than the strain in the control beam for a given load. The CEBPNSM strengthened beam with 70% prestress showed the greatest reduction in concrete compressive strain for a given load among the strengthened beams. Increasing the level of prestressed strengthening reduced compressive strains in the beams at higher load levels, especially after yield. The reduction in compressive strain was due to the increased stiffness of the prestressed strengthened beams. The maximum compressive strain values were last measured just before the ultimate loads were reached and for all of the beams maximum compressive strain was around 0.003, after which strain could not be measured as concrete crushing damaged the strain gauges.

4.8.6 Tensile Strains in Main Steel Strands

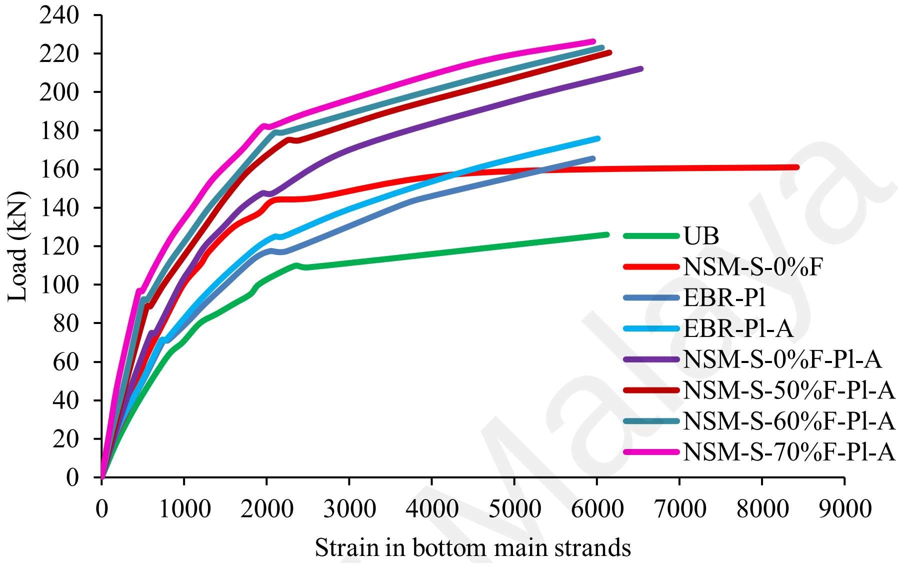

Figure 4.81: Main steel tensile strains in CEBPNSM beams with steel strands and CFRP plate

The tensile strains in the bottom main strands were measured at midspan during loading of the beams, and the results are shown in Figure 4.81. Generally, all of the beams displayed the typical linear elastic followed by plastic tensile load-strain behavior seen in steel reinforced beams with some variations due to strengthening. The maximum tensile strain values measured in the bottom main steel strands before the strain gauges were damaged during beam failure were 0.00612, 0.00842, 0.00595, 0.00601, 0.00653, 0.00615, 0.00606 and 0.00595 for the control beam, NSM strengthened beam, EBR beam without end anchorage, EBR beam with end anchorage, CEBNSM strengthened beam, and the 50%, 60% and 70% prestressed CEBPNSM strengthened beams, respectively. The CEBPNSM strengthened beams with 50%, 60% and 70% prestress, displayed progressively lower maximum tensile strain values, due to the preexisting compressive strains introduced into the lower half of the beams by prestressing the NSM CFRP bar, which opposed the tensile strains created by loading. The CEBPNSM strengthened beam with the highest level of prestress (70%) displayed the steepest load-strain curve, indicating that tensile steel strains were controlled to much higher load levels. This was due to the combination of strengthening materials and the high level of prestress, which enhanced the strength and stiffness, as well as the strain sharing characteristics of the beam.

4.8.7 Tensile Strains in NSM Steel Strands

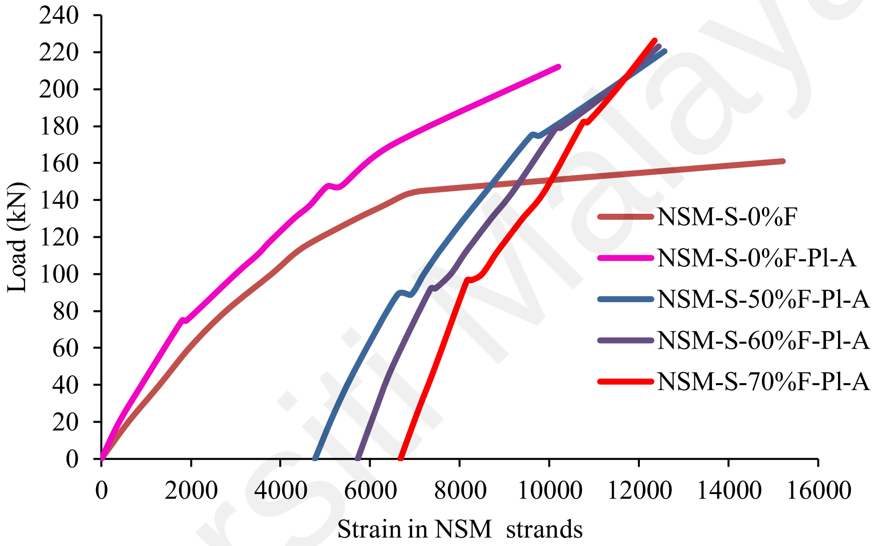

Figure 4.82: NSM steel strand tensile strains of CEBPNSM beams with steel strands and CFRP plate

The relation between the loading and the tensile strains in the NSM steel strands at the midspan of the beam specimens is shown in Figure 4.82. The load-tensile strain curve of the NSM steel strand in the NSM strengthened beam displayed the typical steel strain behavior of linear elastic until yield followed by plastic elongation until failure. The CEBNSM strengthened beam displayed linear elastic tensile strain behavior until yield at a slightly steeper slope than the NSM strengthened beam, and after yield the slope of the tensile strain curve was much steeper than the NSM strengthened beam, which indicates that tensile strain was significantly controlled. This was due to the effect of the superior tensile properties and stiffness of the CFRP plate, which was able to control and carry the tensile strains to much higher loads. This same CFRP effect also played a part in the tensile behavior of the CEBPNSM strengthened beams. A similar linear elastic behavior until yield was seen in the CEBPNSM beams. However, the addition of prestress to these beams caused them to have much steeper load-strain curves and the strain curve after yield was markedly steeper than the CEBNSM beam, almost linear, which indicates that the rate of strain increment was significantly reduced. Specifically, the CEBPNSM beam with 70% prestress showed the least increment in tensile NSM strain, only 0.00567 (this disregards the initial strain from prestress). This was the effect of prestress, and the higher the level of prestress, the greater the reduction in strain increment was. This prestressing effect was due to the ability of the prestress to counteract tensile strains by introducing compressive strains into the surrounding beam area around the NSM strand.

4.8.8 Tensile Strains in CFRP Plate

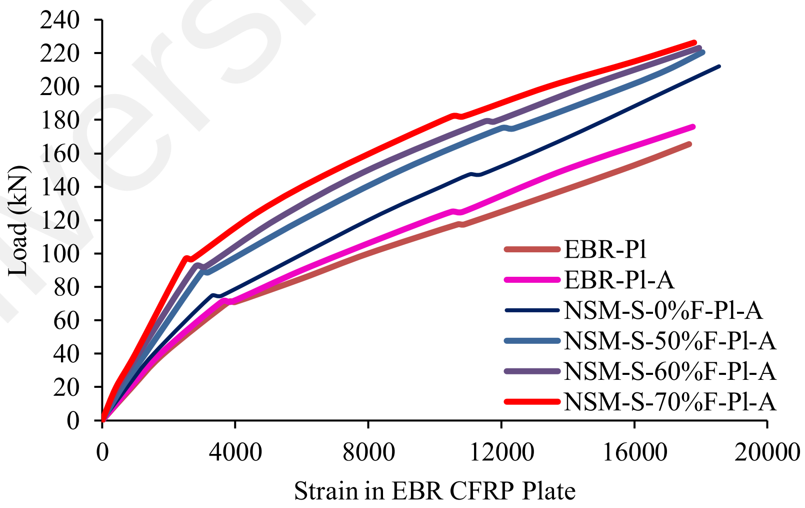

Figure 4.83: CFRP plate tensile strains in CEBPNSM beams with steel strands and CFRP plate

Figure 4.83 presents the variations in tensile strain in the CFRP plate of the beam specimens for increasing load levels during testing. The CEBNSM beam had an overall steeper CFRP tensile strain curve than the EBR beam due to the additional NSM strand, which enhanced strength and stiffness. In turn, the CEBPNSM beams had steeper curves than the CEBNSM beam and increasing the level of prestress in the NSM strands further decreased the rate of tensile strain increment in the CFRP plate. This can be attributed to the effect of prestress, which controls tensile strains. The maximum tensile strains measured in the CFRP plates before failure of the strain gauges were 0.01765, 0.01776, 0.01855, 0.01805, 0.01795 and 0.01780 for the EBR beam without end anchorage, EBR beam with end anchorage, CEBNSM strengthened beam and the CEBPNSM strengthened beams with 50%, 60% and 70% prestress, respectively. The ultimate strain for the CFRP plate based on the manufacturer's specifications was 0.01750 micro strain. The EBR beam without anchorage had a lower maximum CFRP tensile strain as the CFRP sheet debonded at failure. The maximum strains measured in the CEBNSM and CEBPNSM strengthened beams indicate that the full capacity of the CFRP plate was utilized, which agrees with the observed failure mode of concrete crushing and confirms the full composite action of these strengthened beams.

4.8.9 Prestress Losses

Table 4.23: Prestress force and camber effect in CEBPNSM beams with steel strands and CFRP plate

Beam Specimen	Applied Prestress Force		Effective Prestress Force		Negative camber at mid-section
	(kN)	(%)	(kN)	(%)	(mm)
NSM-S-50%F-Pl-A	51.18	50.00	50.95	49.80	0.60
NSM-S-60%F-Pl-A	61.44	60.00	61.15	59.78	0.75
NSM-S-70%F-Pl-A	71.71	70.00	71.37	69.77	0.85

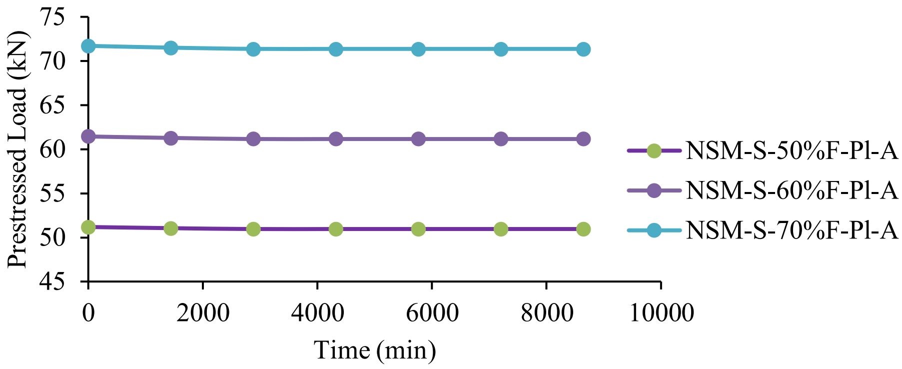

Figure 4.84: Prestress force in steel strands during curing period of CEBPNSM beams with steel strands and CFRP plate

The prestressed steel strands in the CEBPNSM strengthened beams were monitored for losses in prestress force from the time the prestress was applied until the release of the prestress into the beams. The amount of force applied to prestress the 50%, 60% and 70% prestressed CEBPNSM strengthened beams were 51.18 kN, 61.44 kN and 71.71 kN, respectively, which were calculated based on the tensile strength of the steel strands (Table 4.23). The prestressing force levels in the NSM strands over the six-day curing period are shown in Figure 4.84. The prestress losses were 0.45%, 0.47% and 0.48% in the 50%, 60% and 70% beams, respectively. During prestress release, an LVDT was used to measure the negative camber at the midspan of the strengthened beams, which were found to be 0.60 mm, 0.75 mm and 0.85 mm for the 50%, 60% and 70% CEBPNSM beams, respectively.

4.8.10 Effect of Increasing Prestress Level

Prestressing the steel strand in the CEBPNSM strengthened beams had a significant effect on the flexural performance of the CEBPNSM beam specimens. Increasing the level of prestress force further enhanced flexural performance and the highest level of prestress force (70%) offered the greatest enhancement in flexural behavior. Overall, increasing the level of prestress enhanced flexural behavior by increasing flexural load capacity and reducing deflection, crack width, concrete compressive strains and tensile strains in main reinforcement, steel strands and CFRP plate at any given load level.

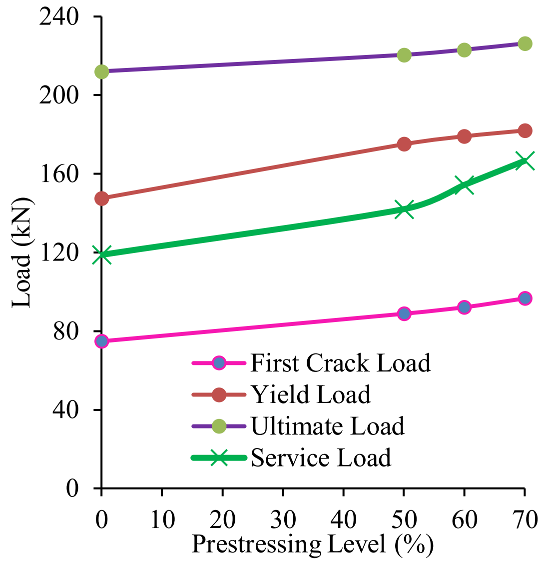

(a) Load vs prestress level

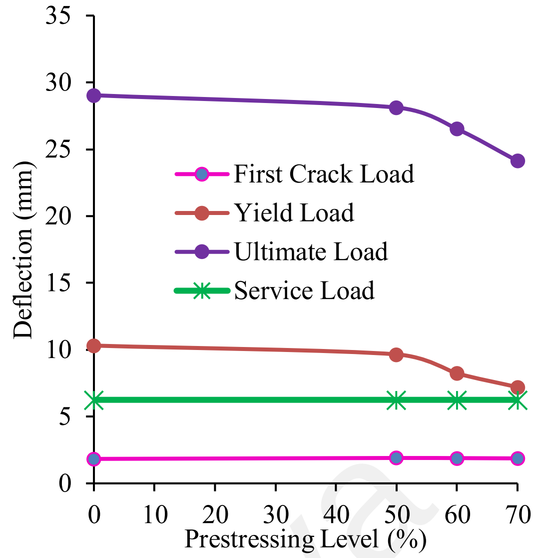

(b) Deflection vs prestress level

Figure 4.85: Effect prestress level on CEBPNSM beams with steel strands and CFRP plate

As can be seen from Figure 4.85 (a), the flexural load capacity of the beam at first crack, service, yield and ultimate was significantly improved by increasing the level of prestress, with yield load especially showing significant improvement. The 70% prestress level provided the highest loads at all stages. From Figure 4.85 (b), it can be seen that the beams with prestress were able to control deflection to the same level as the beam without prestress despite the significant increases in load at first crack, service and yield. At ultimate, increasing the level of prestress significantly decreased deflection, with the 70% prestress level showing the smallest ultimate deflection. Increasing the level of prestress was able to control concrete compressive strains and tensile strains in the main internal reinforcement, steel strand and CFRP plate to significantly higher load levels. The rates at which these strains increased were significantly reduced. This can be seen from the strain graphs (Figure 4.80 to Figure 4.83). Increasing the level of prestress force in the steel strand improved the flexural behavior of the CEBPNSM beams due to the increased compressive effect in tension region of the beams, which caused a corresponding increase in the stiffness of the beams, as well as an increase in the camber of the beams (El Hacha and Soudki, 2013; Obaydullah et al. 2016).

Failure occurred by concrete crushing after steel yielding and was then followed by plate debonding for all of the CEBPNSM beams, indicating that higher levels of prestressed strengthening did not adversely affect the composite behavior of the beams. Previous studies have suggested that prestressing may be able to reduce and even eliminate premature debonding failures in strengthened beams (El Hacha and Soudki, 2013). The results of this study can conclude that prestressing did not cause any premature debonding to occur in any of the strengthened beams, and for the scope of this study, premature failure was indeed eliminated by prestressed strengthening.

4.8.11 Assessment of FEM

By comparing the experimental and FEM ultimate load and deflection for the strengthened beams, it was found that the maximum percentage error for ultimate load and deflection was 5% and 3%, respectively. This was well within the acceptable 10% limit [20]. The agreement between the predicted load carrying capacity from numerical FEM model and the experimental output is satisfactory.

Table 4.24: Experimental and FEM results at ultimate for CEBPNSM beams with steel strands and CFRP plate

Beam specimens	Level of prestress (%)	Experimental		FEM		FEM/Experimental	
		Load (kN)	Deflection (mm)	Load (kN)	Deflection (mm)	Load (P_{FEM}/P_{exp})	Deflection ($\Delta_{FEM}/\Delta_{exp}$)
NSM-S-0%F-Pl-A	0	212	29.0	202	29.3	0.95	1.01
NSM-S-60%F-Pl-A	60	223	26.5	212.	27.4	0.95	1.03
NSM-S-70%F-Pl-A	70	226	24.1	215	24.7	0.95	1.03

The load-deflection relationships for the numerical model and the experimental results are shown in Figure 4.86. It can be clearly observed that the correlation between the numerical results and experimental data is reasonably good.

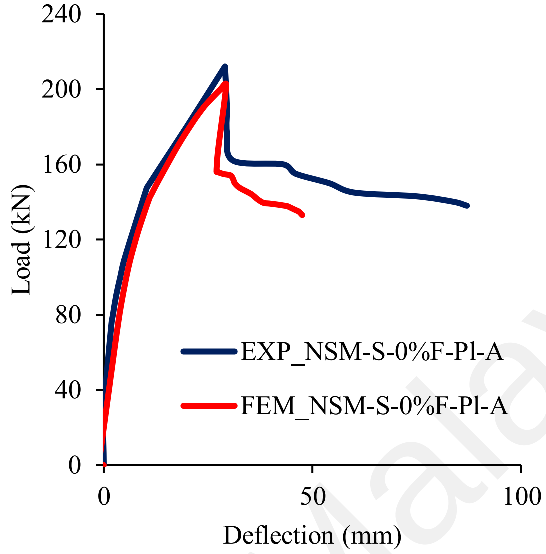

(a) NSM-S-0%F-Pl-A

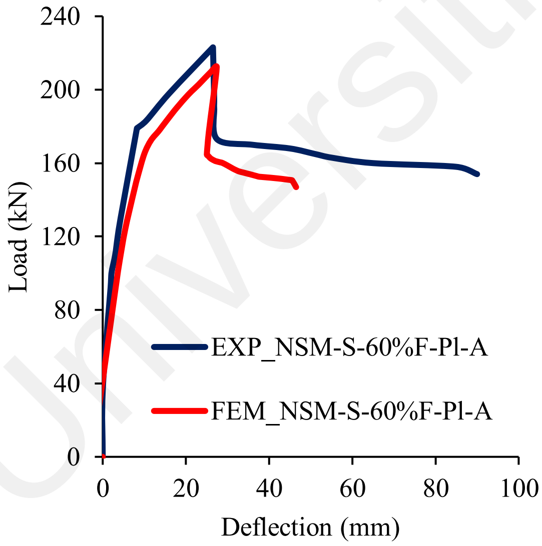

(b) NSM-S-60%F-Pl-A

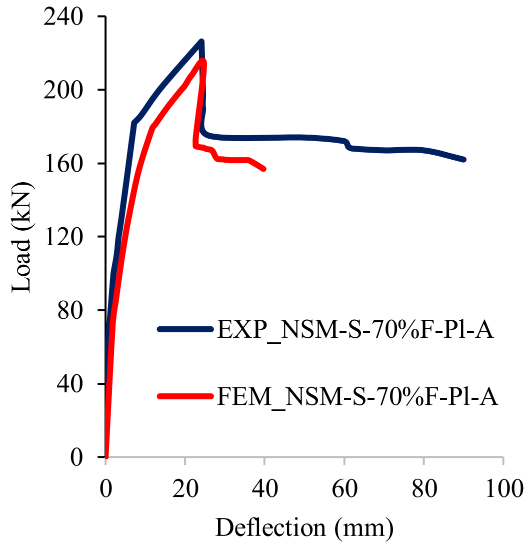

(c) NSM-S-70%F-Pl-A

Figure 4.86: FEM load-deflection for CEBPNSM beams with steel strands and CFRP Plate

The FEM compressive and tensile damage behaviors for all of the strengthened beams were almost similar (Figure 4.87). The experimental strengthened beams displayed flexural crack patterns and concrete crushing at failure, simialr to the simulated damage behavior from the numerical model. However, at failure the experimental beams displayed CFRP plate debonding after concrete crushing initiated, which was not simulated by the numerical model. Overall, the numerical damage behavior of the beams agreed reasonably well with the experimental crack patterns and failure modes.

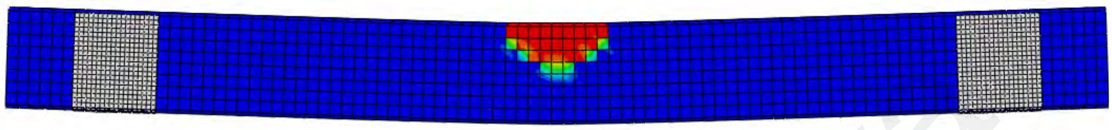

(d) Compressive damage behavior

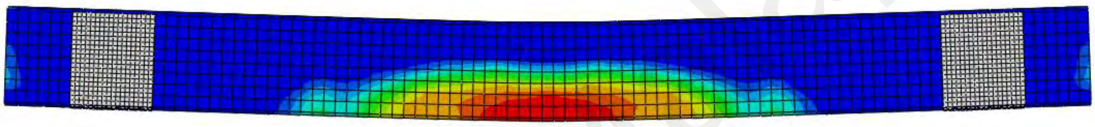

(e) Tensile damage behavior

Figure 4.87: FEM damage behavior of NSM-S-70%F-PL-A

4.9 Summary of Research Findings

A summary of the experimental results is presented in Table 4.25 and a brief assessment of how the objectives of this research were achieved is presented in Table 4.26.

Table 4.25: Experimental Load and Deflection Results for All Beams

No.	Beam specimen	Level of prestress in NSM (%)	First crack (P_{cr})		Service (P_s) (kN)	Yield (P_y)		Ultimate (P_{ult})		End point of test		Failure mode
			Load (kN)	Deflection (mm)		Load (kN)	Deflection (mm)	Load (kN)	Deflection (mm)	Load (kN)	Deflection (mm)	
1	UB	-	63	3.1	83	110	20	127	45.6	118	94	Concrete crushing
2	EBR-Sh	-	70 (10%)	3.2	93 (11%)	118 (7%)	9.67	165 (30%)	48.6	125	52	Concrete crushing
3	EBR-Pl	-	71 (12%)	1.9	111 (33%)	118 (6%)	7.88	166 (30%)	27.4	120	71	CFRP debonding
4	EBR-Pl-A	-	71 (13%)	1.9	114 (37%)	125 (13%)	9.01	176 (39%)	31.2	109	49	Concrete crushing
Group A: Beams strengthened with NSM CFRP bars												
5	NSM-C-0%F	0	67 (6%)	3.4	86 (3%)	113 (2%)	11.7	166 (31%)	40.1	108	93	CFRP rupture
6	NSM-C-30%F	30	77 (23%)	3.6	95 (14%)	122 (10%)	11.6	170 (34%)	38.6	111	89	CFRP rupture
7	NSM-C-40%F	40	79 (26%)	3.6	98 (17%)	124 (12%)	11.5	174 (37%)	38.1	118	96	CFRP rupture
8	NSM-C-50%F	50	82 (30%)	3.5	101 (22%)	133 (20%)	11.5	177 (40%)	37.1	102	97	CFRP rupture
9	NSM-C-60%F	60	86 (36%)	3.4	106 (28%)	140 (27%)	11.5	180 (42%)	36.5	108	96	CFRP rupture
10	NSM-C-70%F	70	90 (43%)	3.4	111 (34%)	149 (35%)	11.4	186 (46%)	35.1	103	96	CFRP rupture

No.	Beam specimen	Level of prestress in NSM (%)	First crack (P_{cr})		Service (P_s) (kN)	Yield (P_y)		Ultimate (P_{ult})		End point of test		Failure mode
			Load (kN)	Deflection (mm)		Load (kN)	Deflection (mm)	Load (kN)	Deflection (mm)	Load (kN)	Deflection (mm)	
Group B: Beams strengthened with NSM steel strands												
11	NSM-S-0%F	0	66 (5%)	3.2	92 (10%)	145 (32%)	23.5	162 (28%)	38.3	141	89	Concrete crushing
12	NSM-S-30%F	30	77 (21%)	3.4	103 (24%)	154 (39%)	23.2	165 (30%)	36.0	144	89	Concrete crushing
13	NSM-S-40%F	40	78 (24%)	3.5	111 (33%)	164 (48%)	19.9	169 (33%)	36.8	142	90	Concrete crushing
14	NSM-S-50%F	50	81 (28%)	3.1	111 (34%)	169 (53%)	19.1	172 (35%)	35.3	161	97	Concrete crushing
15	NSM-S-60%F	60	85 (34%)	3.1	118 (42%)	170 (54%)	18.9	174 (37%)	33.7	165	98	Concrete crushing
16	NSM-S-70%F	70	88 (40%)	2.5	134 (61%)	174 (57%)	18.7	178 (40%)	30.1	170	96	Concrete crushing
Group C: Beams strengthened with NSM CFRP bars and EBR CFRP sheet												
17	NSM-C-0%F-Sh	0	73 (16%)	3.2	87 (5%)	120 (9%)	13.0	204 (61%)	44.2	114	91	CFRP rupture
18	NSM-C-50%F-Sh	50	88 (40%)	3.2	104 (25%)	140 (27%)	12.9	216 (70%)	41.4	111	88	CFRP rupture
19	NSM-C-60%F-Sh	60	93 (46%)	3.1	110 (32%)	147 (34%)	12.9	218 (72%)	39.8	116	93	CFRP rupture
20	NSM-C-70%F-Sh	70	96 (53%)	3.0	116 (40%)	156 (41%)	12.7	224 (76%)	38.1	120	94	CFRP rupture

No.	Beam specimen	Level of prestress in NSM (%)	First crack (P_{cr})		Service (P_s) (kN)	Yield (P_y)		Ultimate (P_{ult})		End point of test		Failure mode
			Load (kN)	Deflection (mm)		Load (kN)	Deflection (mm)	Load (kN)	Deflection (mm)	Load (kN)	Deflection (mm)	
Group D: Beams strengthened with NSM steel strands and EBR CFRP sheet												
21	NSM-S-0%F-Sh	0	72 (14%)	3.2	98 (18%)	149 (35%)	14.5	200 (58%)	37.1	142	87	CFRP rupture
22	NSM-S-50%F-Sh	50	87 (38%)	3.1	113 (37%)	171 (55%)	13.5	210 (65%)	35.1	143	88	CFRP rupture
23	NSM-S-60%F-Sh	60	91 (45%)	3.1	116 (40%)	175 (59%)	13	213 (68%)	33.2	148	90	CFRP rupture
24	NSM-S-70%F-Sh	70	94 (49%)	2.5	122 (46%)	179 (62%)	12.7	216 (70%)	30.1	150	90	CFRP rupture
Group E: Beams strengthened with NSM CFRP bars and EBR CFRP plates												
25	NSM-C-0%F-Pl-A	0	75 (19%)	1.8	105 (26%)	127 (15%)	9.5	215 (69%)	37.2	115	92	Concrete crushing
26	NSM-C-50%F-Pl-A	50	90 (43%)	2.0	133 (60%)	147 (33%)	7.6	224 (77%)	34.4	111	93	Concrete crushing
27	NSM-C-60%F-Pl-A	60	95 (50%)	1.9	142 (71%)	154 (40%)	7.3	227 (79%)	32.8	121	94	Concrete crushing
28	NSM-C-70%F-Pl-A	70	99 (57%)	1.9	153 (84%)	163 (48%)	7.1	230 (81%)	31.1	124	95	Concrete crushing
Group F: Beams strengthened with NSM steel strands and EBR CFRP plates												
29	NSM-S-0%F-Pl-A	0	75 (18%)	1.8	119 (43%)	148 (34%)	10.3	212 (67%)	29.0	138	87	Concrete crushing
30	NSM-S-50%F-Pl-A	50	89 (41%)	1.9	142 (71%)	175 (59%)	9.7	221 (74%)	28.1	140	89	Concrete crushing
31	NSM-S-60%F-Pl-A	60	92 (46%)	1.9	154 (86%)	179 (62%)	8.2	223 (76%)	26.5	154	90	Concrete crushing
32	NSM-S-70%F-Pl-A	70	97 (53%)	1.9	167 (100%)	182 (65%)	7.2	226 (78%)	24.1	162	90	Concrete crushing

Table 4.26: Achievement of Objectives

No.	Objective	Beam No.	Method	Achievement
1	To investigate the structural behavior of prestressed beams strengthened using the NSM technique with prestressed steel strands and prestressed CFRP bars.	1-13 (13 beams)	Five beams strengthened using PNSM with steel strands and five beams strengthened using PNSM with CFRP bars were tested and compared with a control beam and one NSM steel strand strengthened beam and one NSM CFRP bar strengthened beam.	- The PNSM technique was able to greatly enhance the flexural performance of the PC beam compared to the control and non-prestressed NSM strengthened beams in terms of load carrying capacity at first crack, service, yield and ultimate, and reduced deflection, crack widths, compressive strains and tensile strains. Stiffness and energy absorption capacity also increased. - All the PNSM beams failed flexurally with no sign of premature debonding, indicating full composite behavior. - The PNSM steel strand beams and the PNSM CFRP bar beams had comparable first crack and ultimate loads. - PNSM steel strands increased service and yield loads, reduced deflection and crack widths, displayed ductile behavior, and enhanced stiffness and energy absorption, all considerably more than PNSM CFRP bars. - Both PNSM steel strands and PNSM CFRP bars are capable of fulfilling serviceability and ultimate requirements of PC structures.
2	To propose a new strengthening technique which combines EBR with prestressed NSM to enhance the flexural performance of prestressed beams.	18-20, 22-24, 26-28, 30-32 (12 beams)	Twelve beams were strengthened in this study using the newly proposed CEBPNSM technique	- The CEBPNSM technique was found to be an effective new strengthening technique capable of fulfilling the serviceability and ultimate requirements of prestressed concrete structures. - The CEBPNSM technique greatly enhanced the flexural performance of the PC beam in terms of increased load carrying capacity at first crack, service, yield and ultimate, and reduced deflection, crack widths, compressive strains and tensile strains.

3	To assess the structural performance of the proposed strengthening technique which combines EBR and prestressed NSM.	1, 2, 8, 14-32 (22 beams)	Twelve beams were strengthened with the CEBPNSM technique using four different combinations of strengthening materials and then compared with a control beam, three EBR strengthened beams, two NSM strengthened beams and four CEBNSM strengthened beams.	- CEBPNSM strengthening significantly improved flexural behavior compared to the EBR, NSM and CEBNSM techniques. - All the CEBPNSM strengthened beams failed flexurally with no sign of premature debonding, indicating full composite behavior. - All the four strengthening material combinations used with CEBPNSM were able to greatly enhance flexural performance. - The combination of PNSM steel strand and EBR CFRP plate for the CEBPNSM beams provided the most significant increase in load capacity at service and yield, as well as the greatest enhancement in stiffness and the largest reduction in deflection. - The combination of PNSM CFRP bar and EBR CFRP plate for the CEBPNSM beams provided the most significant increase in load capacity at first crack and ultimate.
4	To evaluate the effect of varying the level of prestress force in the prestressed NSM reinforcement on the prestressed beams strengthened using PNSM and CEBPNSM.	3-7, 9-13, 18-20, 22-24, 26-28, 30-32 (22 beams)	The prestress level was varied from 30% to 70% in the ten PNSM beams and from 50% to 70% in the twelve CEBPNSM beams.	- The higher the level of prestress, the greater the improvement in flexural behavior, with the highest level of prestress (70%) showing the greatest improvement. - Increasing the prestress level enhanced load capacity at first crack, service, yield and ultimate, and reduced deflection, crack width, and compressive and tensile strains at any applied load level. - Service load, cracking behavior and stiffness especially improved.
5	To simulate the structural behavior of the strengthened prestressed beams using finite element modeling and validate the experimental results.	1-2, 5-8, 11-13, 14, 16, 17, 19-21, 23-25, 27-29, 31-32 (23 beams)	A FEM model was developed for the control beam, two NSM beams, six PNSM beams, two EBR beams, four CEBNSM beams, and eight CEBPNSM beams.	- The developed FEM model produced ultimate load values for the beams with reasonable accuracy, with less than 5% error. - The simulated the load and deflection behavior of the beams were reasonably accurate with a percentage error of less than 8%. - The predicted damage behavior and failure modes of the strengthened beams were similar to the experimental results.

CHAPTER 5: CONCLUSIONS

The present study has proposed and investigated an innovative new strengthening technique, the Combined Externally Bonded and Prestressed Near Surface Mounted (CEBPNSM) technique. This CEBPNSM technique further develops the CEBNSM technique by using PNSM in the place of NSM. The main aim of this study was to develop the CEBPNSM technique as an effective new strengthening technique to overcome the limitations of NSM, EBR and CEBNSM, and provide a possible solution for structures that require higher levels of strengthening. This study also investigated the use of PNSM strengthening with steel strands and CFRP bars in order to explore the effectiveness of using steel strands as an alternative to CFRP bars. The effect of increasing the level of prestress in the PNSM reinforcement on the structural performance of the PNSM and CEBPNSM strengthening techniques was also evaluated.

Therefore, according to the test matrix described in Table 3.1, six groups of strengthened PC beams were tested along with one unstrengthened control beam. To achieve the objectives of this study, five strengthening techniques were investigated, namely NSM, PNSM, EBR, CEBNSM and CEBPNSM. Four different combinations of strengthening materials were investigated with the CEBPNSM technique.

A FEM model was also developed using ABAQUS to verify the flexural responses of the beam specimens. The simulated load, deflection and failure behavior corresponded well with the experimental results. The major findings of this study are summarized in the following sections.

5.1 PNSM Strengthening Technique

The PNSM strengthening technique was investigated in this research using two materials – steel strands and CFRP bars. The level of prestress in the PNSM strengthening reinforcement was varied from 30% to 70% for both groups. Both groups of strengthened beams demonstrated improved flexural performance compared to the control beam. Flexural failure was the common failure mode for all of the beams in both groups. The detailed conclusions from the investigation of the PNSM strengthening technique with steel strands and CFRP bars are as follows.

(i) PNSM strengthening with both steel strands and CFRP bars significantly improved structural performance compared to the control beam and the non-prestressed NSM strengthened beam in terms of higher first crack, service, yield, and ultimate loads, decreased deflections and reduced crack widths.

(ii) The use of steel strands with PNSM strengthening enhanced service and yield loads significantly more than CFRP bars.

(iii) However, the use of CFRP bars with PNSM strengthening provided slightly higher first crack and ultimate loads than the use of steel strands.

(iv) Deflection and crack width were reduced significantly more for any given load level by the use of steel strands with PNSM, compared to CFRP bars.

(v) Increasing the level of prestress in PNSM strengthening with both steel strands and CFRP bars further enhanced the flexural behavior of the PC beam. First crack, service and yield loads especially improved, and crack width and ultimate deflection were significantly reduced, especially at higher levels of prestress.

(vi) The use of CFRP with PNSM strengthening caused flexural failure to occur by CFRP rupture with simultaneous concrete crushing after yielding of the tension reinforcement. No debonding or separation of concrete cover was observed the indicating full composite action of the strengthened beams.

(vii) The use of steel strands with PNSM strengthening caused flexural failure to occur in the typical manner of reinforced concrete, which is by concrete crushing at the top fiber of the beam after yielding of the tension reinforcement. No debonding or separation of the concrete cover occurred indicating full composite behavior.

(viii) The use of steel strands with PNSM strengthening caused failure to occur in a ductile manner with high deformability, similar to an unstrengthened beam.

(ix) The use of CFRP bars with PNSM strengthening led to brittle failure behavior with less ductility as the rupture of the CFRP bar caused a large sudden fall in load capacity back to the level of the internal steel reinforcement.

(x) Both the use of CFRP bars and the use of steel strands with PNSM strengthening improved the energy absorption capacity of the PC beam. Additional prestress significantly enhanced energy absorption capacity.

(xi) However, steel strands provided significantly higher energy absorption capacity than CFRP bars with PNSM strengthening.

(xii) PNSM strengthening with both steel strands and CFRP bars improved the stiffness at service of the PC beam. Increasing the prestress level further enhanced stiffness.

(xiii) However, steel strands produced significantly greater increase in stiffness at service compared to CFRP bars, when used with PNSM strengthening.

Overall, this study found that PNSM strengthening when used with both steel strands and with CFRP bars was an effective strengthening technique capable of fulfilling the serviceability and ultimate requirements of reinforced concrete structures.

5.2 CEBPNSM Strengthening Technique

In this study the CEBPNSM strengthening technique was used with four different combinations of strengthening materials, namely PNSM steel strands with EBR CFRP sheet, PNSM CFRP bars with EBR CFRP sheet, PNSM steel strands with EBR CFRP plate, and PNSM CFRP bars with EBR CFRP plate. The level of prestress in the PNSM reinforcement was varied from 50% to 70% in all of the groups. All of the CEBPNSM strengthened beams demonstrated significant improvement in flexural performance and flexural failure was the common failure mode. The detailed conclusions drawn from the investigation on the CEBPNSM technique are described below.

(i) CEBPNSM strengthening greatly enhanced flexural performance of the PC beam in terms of increased load carrying capacity at first crack, service, yield and ultimate, and reduced deflection, crack widths, concrete compressive strains and tensile strains in internal reinforcements.

(ii) The CEBPNSM technique was able to significantly improve the flexural behavior of the PC beam compared to the existing EBR, NSM and CEBNSM techniques.

(iii) Compared to the CEBNSM technique, the CEBPNSM technique was able to especially enhance first crack, service and yield loads, and reduce deflection and crack width at all load levels.

(iv) Increasing the level of prestress used with CEBPNSM strengthening caused a corresponding enhancement in flexural performance.

(v) The use of CFRP plate with the CEBPNSM technique produced greater increases in load capacity than the use of CFRP sheet.

(vi) The use of steel strands in the CEBPNSM beams provided greater enhancement of load capacity at service and yield, compared to the use of CFRP bars. However, using CFRP bars with the CEBPNSM technique produced slightly higher ultimate loads than steel strands.

(vii) The use of a combination of steel strands with CFRP plate with the CEBPNSM technique provided the greatest increase in load capacity at service and yield among all the strengthened beams.

(viii) CEBPNSM strengthening shows trilinear load–deflection response with considerable reduction in deflection at all load levels.

(ix) CEBPNSM strengthening causes stiffness at service to increase significantly compared to EBR, NSM and CEBNSM strengthening.

(x) The use of CFRP plate with the CEBPNSM technique provided greater enhancement of stiffness and larger reductions in deflection, compared to the use of CFRP sheet.

(xi) The combination of steel strands and CFRP plate produced the greatest enhancement in stiffness and largest reductions in deflection, especially at the ultimate stage, among the CEBPNSM strengthened beams.

(xii) CEBPNSM strengthening eliminated premature debonding and concrete cover separation, with flexural failure after yielding as the common failure mode.

(xiii) The use of CFRP sheet with the CEBPNSM technique caused flexural failure to occur by CFRP rupture with simultaneous concrete crushing.

(xiv) The use of CFRP plate with the CEBPNSM technique caused flexural failure to occur by concrete crushing followed by plate debonding, which led to an abrupt and brittle manner of failure.

(xv) The use of steel strands with the CEBPNSM technique caused the load capacity of the strengthened beams to return to the level of the steel strand after failure.

(xvi) The use of CFRP bars with CEBPNSM technique caused the load capacity of the beams to return to the level of the internal tension steel after failure.

(xvii) The use of a combination of steel strands and CFRP sheet with the CEBPNSM technique caused the beam to fail in a somewhat more gradual manner than the CEBPNSM beams strengthened with other material combinations.

Over all this study found the CEBPNSM to be a highly effective new strengthening technique with certain advantages over other existing techniques. The CEBPNSM strengthening technique displayed significantly greater improvement in the flexural behavior of the PC beam compared to the existing EBR, NSM and CEBNSM strengthening techniques. The CEBPNSM strengthening technique was also able to completely eliminate failure by premature debonding. All of the CEBPNSM strengthened beams displayed flexural failure modes with no premature debonding observed indicating the full composite action of the strengthened beams. The potential flexural enhancement offered by the CEBPNSM technique is greater than the EBR, NSM and CEBNSM techniques as each of these techniques has certain limitations, such EBR strengthening cannot exceed a certain thickness without risking premature debonding failure, while NSM strengthening is often limited by the requirements for sufficient clear spacing and groove size, and the CEBNSM technique often fails to use the full tensile capacity of strengthening materials and also does not completely eliminate premature debonding. The CEBPNSM strengthening technique was able to address each of these limitations and provide a combined solution that exploits the advantages of each of these strengthening techniques while minimizing their weaknesses. By combining EBR with NSM, the thickness of the EBR reinforcement was reduced to within the allowable limits while still taking advantage of the superior stiffness and strength of EBR, and the restrictions on the NSM reinforcement dimensions no longer limited strengthening, as the necessary amount of strengthening reinforcement could be divided between the two strengthening systems. The addition of PNSM to this combination allowed the CEBPNSM technique to use the full tensile capacity of the NSM reinforcement and also eliminated the premature debonding seen in the CEBNSM technique due to the additional cambering effect. Another advantage of the CEBPNSM technique is the additional cover it provides to the PNSM reinforcement in the form of EBR reinforcement, which can protect steel strands used with the CEBPNSM technique from corrosion. This study has thus demonstrated that the CEBPNSM technique is an effective new strengthening technique to overcome the limitations of NSM, EBR and CEBNSM, and provide a possible solution for structures that require higher levels of strengthening.

5.3 Advantages of Steel Strands Over CFRP Bars

Prestressed steel strands offer a practical alternative strengthening material to CFRP bars as they are readily available and far more economical. The main problem with the use of steel as strengthening reinforcement is the tendency of steel to corrode over time when there is a lack of adequate cover. Although steel may be prone to corrosion when exposed, with adequate cover and proper maintenance it has been shown to have long term durability. Steel also displays greater ductility and good bonding performance. In this study, both steel strands and CFRP bars were used with the PNSM and the CEBPNSM strengthening techniques. The PNSM groove and epoxy filling provide protection to the steel strand from corrosion and in the CEBPNSM technique, the use of CFRP plate or CFRP sheet as EBR reinforcement provides an additional level of protection for the steel strand. In this study, the use of steel strands in the PNSM and CEBPNSM techniques for the strengthening of PC beams was proven to be effective. The detailed conclusions drawn from the investigation which demonstrate the effectiveness of prestressed steel strands as an alternative to CFRP bars are as follows:

(i) Prestress loss during application of prestress force to the steel strands was less than 1%. However, the prestress loss in the CFRP bars was about 5% due to greater slippage.

(ii) The service and yield loads of the steel strand strengthened beams were significantly greater than the CFRP bar strengthened beams, even at higher levels of prestress.

(iii) The ultimate capacities of the CEBPNSM and PNSM steel strand strengthened beams were comparable to the corresponding CFRP bar strengthened beams.

(iv) In terms of load-deflection behavior, the strengthened beams that used steel strands showed less deflection than the CFRP bar strengthened beams.

(v) Prestressed steel strands were able to reduce crack widths in the strengthened beam specimens more than CFRP bars.

(vi) Both the steel strand strengthened beams and CFRP bar strengthened beams displayed flexural failure modes and showed full composite behavior until failure.

(vii) The PNSM steel strand strengthened beams showed more ductility than the CFRP bar strengthened beams, with high deformability after ultimate similar to a typical concrete beam.

(viii) The CEBPNSM beam strengthened with steel strands and CFRP sheet displayed a somewhat more gradual manner of failure than the other CEBPNSM beams.

5.4 Effect of Increasing Prestress Level

The effect of increasing the level of prestress on the structural performance of the PNSM and CEBPNSM strengthened beams was also evaluated. The level of prestress in the PNSM strengthened beams was varied from 30% to 70% and in the CEBPNSM beams from 50% to 70%. Prestressing created an initial compressive force in the tension region and a corresponding tensile force in the top fiber, which generated a negative camber in the beams. This cambering effect led to an increase in the flexural performance of the strengthened beams and increasing the level of prestress caused a likewise increase in camber. The detailed conclusions are as follows:

(i) Each increase in the level of prestress produced a corresponding enhancement in flexural performance. The highest level of prestress (70%) produced the greatest flexural enhancement.

(ii) Increasing the prestress level improved the load capacity of the strengthened beams at first crack, service, yield and ultimate.

(iii) The service load was especially improved by increasing the level of prestress in the NSM reinforcement.

(iv) Increasing the level of prestress in the strengthened beams significantly reduced deflection at all load levels.

(v) Increasing the prestress level improved cracking behavior by significantly delaying crack initiation and controlling crack widths, which also reduced overall deflection.

(vi) Concrete compressive strains and tensile reinforcement strains were also reduced for any given load level by increasing the level of prestress in the strengthened beams.

(vii) Increasing the prestress level in the NSM reinforcement significantly increased the stiffness of the strengthened beams.

5.5 FEM Modelling

The load-deflection behavior and damage behavior produced by the FEM model had reasonably good correlation to the experimental results. The detailed conclusions are as follows:

(i) The FEM model produced ultimate load values for the beam specimens that were in decent agreement with the experimental results, with only a maximum of 5% error.

(ii) The simulated load-deflection behavior of the strengthened beams was reasonable accurate with a percentage error of less than 8% between the model and the experimental values.

(iii) The predicted damage behavior and failure modes of the strengthened beams were similar to the experimental results.

5.6 Recommendations

The following recommendations for future research work are offered by the present researcher to further explore the PNSM and CEBPNSM strengthening techniques.

i. Assessment of the response of structures strengthened using the CEBPNSM technique under repeated loading.
ii. Evaluation of the residual capacity of pre-cracked PC structures and assessment of their structural performance after applying the CEBPNSM strengthening technique.
iii. Investigation of the bond performance between the PNSM reinforcement, the epoxy adhesive and concrete substrate when reinforcement size and prestress level are varied.
iv. Determination of the minimum required spacing between multiple PNSM grooves to avoid premature failure due to overlapping stresses from the prestress forces.
v. Application of CEBPNSM and PNSM to PC structural elements in real field situations with structural health monitoring (SHM) systems in order to assess structural performance in field practice.
vi. Investigation of the long-term prestress losses in CEBPNSM and PNSM strengthened structures.
vii. Development of design guidelines for the CEBPNSM technique with appropriate consideration of safety factors.

REFERENCES

ACI 318-99. (1999). Building Code Requirements for Structural Concrete (ACI 318-99) and Commentary (318R-99), Farmington Hills, Mich.

ACI-Committee-318., Building Code Requirements for Reinforced Concrete. Detroit: American Concrete Institute. 2011.

ACI 440. (2006). Guide for the Design and Construction of Concrete Reinforced with FRP Bars (ACI 440.1 R-06). American Concrete Institute, Detroit, Michigan.

ACI 440.2R-08. (2008). Guide for the design and construction of externally bonded FRP systems for strengthening concrete structures, Farmington Mills, MI.

ACI. (2002). Guide for the design and construction of externally bonded FRP systems for strengthening concrete structures. ACI 440.2R-02, ACI, Farmington Hills, Michigan.

Aïtcin, P.-C., & Mehta, P. K. (1990). Effect of coarse aggregate characteristics on mechanical properties of high-strength concrete. Materials Journal, 87(2), 103-107.

Akbarzadeh, H., & Maghsoudi, A.A. (2010). Experimental and analytical investigation of reinforced high strength concrete continuous beams strengthened with fiber reinforced polymer. Materials & Design, Volume 31, Issue 3, Pages 1130-1147

Akmaluddin, A. (2011). Effect of Tensile Reinforcement Ratio on the Effective Moment of Inertia of Reinforced Lightweight Concrete Beams for Short Term Deflection Calculation. Journal of Engineering and Technological Sciences, 43(3), 209-226.

Al-Emrani, M., Haghani, R., Höglind, J., & Björklund, A. (2007). The effect of plate end tapering on the interfacial stresses in adhesively bonded composite elements. Paper presented at the The third international conference on structural engineering, mechanics and computation. Cape Town, South Africa, 10-12 September 2007.

Al-Mahmoud, F., Castel, A., Francois, R., & Tourneur, C. (2009). Strengthening of RC members with near-surface mounted CFRP rods. Composite Structures, 91(2), 138-147. doi: 10.1016/j.compstruct.2009.04.040

Al-Mahmoud, F., Castel, A., Francois, R., & Tourneur, C. (2011). Anchorage and tension-stiffening effect between near-surface-mounted CFRP rods and concrete. Cement & Concrete Composites, 33(2), 346-352. doi: 10.1016/j.cemconcomp.2010.10.016

Al-Mahmoud, F., Castel, A., François, R., & Tourneur, C. (2009). Strengthening of RC members with near-surface mounted CFRP rods. Composite Structures, 91(2), 138-147.

Al-Mahmoud, F., Castel, A., François, R., & Tourneur, C. (2011). Anchorage and tension-stiffening effect between near-surface-mounted CFRP rods and concrete. Cement and Concrete Composites, 33(2), 346-352.

Alam, M. A., & Jumaat, M. Z. (2012). Experimental Investigations on U- and L-Shaped End Anchored CFRP Laminate Strengthened Reinforced Concrete Beams. Arabian Journal for Science and Engineering, 37(4), 905-919. doi: DOI 10.1007/s13369-012-0213-6

Ali, M., Oehlers, D. J., & Park, S. M. (2001). Comparison between FRP and steel plating of reinforced concrete beams. Composites Part A: Applied Science and Manufacturing, 32(9), 1319-1328.

Ali, M. S. M., Oehlers, D. J., & Griffith, M. C. (2008). Shear transfer across cracks in FRP strengthened RC members. Journal of Composites for Construction, 12(4), 416-424. doi: 10.1061/(asce)1090-0268(2008)12:4(416)

Allam, S. M., Shoukry, M. S., Rashad, G. E., & Hassan, A. S. (2012). Crack width evaluation for flexural RC members. Alexandria engineering journal, 51(3), 211-220.

Almusallam, T. H., Elsanadedy, H. M., Al-Salloum, Y. A., & Alsayed, S. H. (2013). Experimental and numerical investigation for the flexural strengthening of RC beams using near-surface mounted steel or GFRP bars. Construction and Building Materials, 40, 145-161. doi: 10.1016/j.conbuildmat.2012.09.107

Amarasinghe, N.A., and Gamage, J.C. (2015). Experimental study on integrated method of NSM and EBR techniques for flexural strengthening of Concrete Beams using CFRP. International Conference on Structural Engineering and Construction Management 2015, Kandy, Sri Lanka, 11th-13th December 2015

Ashour, A. F. (2006). Flexural and shear capacities of concrete beams reinforced with GFRP bars. Construction and Building Materials, 20(10), 1005-1015. doi: 10.1016/j.conbuildmat.2005.06.023

Aslam, M., Shafigh, P., Jumaat, M.Z. (2015). Strengthening of RC beams using prestressed fiber reinforced polymers–A review. 2015. 82: p. 235-256.

Asplund, S.O. (1949). Strengthening bridge slabs with grouted reinforcement. Journal of the American Concrete Institue, 1949. Vol. 45, p. 397-406.

Attari, N., S. Amziane, and M. Chemrouk, Flexural strengthening of concrete beams using CFRP, GFRP and hybrid FRP sheets. Construction and Building Materials, 2012. 37: p. 746-757.

ASTM. (2014). Standard Test Method for Compressive Strength of Cylindrical Concrete Specimens ASTM C39/C39M-14. USA: American Society for Testing and Materials (ASTM) International.

Aydin, K., & Kisi, O. (2014). Applicability of a Fuzzy Genetic System for Crack Diagnosis in Timoshenko Beams. Journal of Computing in Civil Engineering, 29(5), 04014073.

Babaeidarabad, S., Loreto, G., & Nanni, A. (2014). Flexural strengthening of RC beams with an externally bonded fabric-reinforced cementitious matrix. Journal of Composites for Construction, 18(5), 04014009.

Badawi, M. & Soudki, K. (2009). Flexural strengthening of RC beams with prestressed NSM CFRP rods–experimental and analytical investigation. Construction and Building Materials, 23(10): p. 3292-3300.

Badawi, M. A. (2007). Monotonic and fatigue flexural behaviour of RC beams strengthened with prestressed NSM CFRP rods. (PhD thesis), University of Waterloo.

Badawi, M. & Soudki. K. (2006). Strengthening of RC beams with prestressed near surface mounted CFRP rods. in Proceeding of the 3rd International Conference on FRP Composites in Civil Engineering (CICE 2006), Miami, Florida, USA.

Barris, C., Torres, L., Comas, J., & Mias, C. (2013). Cracking and deflections in GFRP RC beams: an experimental study. Composites Part B: Engineering, 55, 580-590.

Barros, J. A., Ferreira, D., Fortes, A. S., & Dias, S. J. E. (2005). Assessing the effectiveness of embedding CFRP laminates in the near surface for structural strengthening. Construction and Building Materials, 20(7), 478-491. doi: 10.1016/j.conbuildmat.2005.01.030

Beber, A., Fihlo, A., & Campagnolo, J. (2001, December 12-15). CFRP in the strengthening of reinforced concrete beams. Paper presented at the FRP Composites in Civil Engineering. Proceedings of the International Conference on FRP composites in Civil Engineering, Hong Kong, China.

Bilotta, A., Ceroni, F., Nigro, E., & Pecce, M. (2015). Efficiency of CFRP NSM strips and EBR plates for flexural strengthening of RC beams and loading pattern influence. Composite Structures, 124: p. 163-175.

Bizindavyi, L., & Neale, K. (1999). Transfer lengths and bond strengths for composites bonded to concrete. Journal of Composites for Construction, 3(4), 153-160.

Blaschko, M., & Zilch, K. (1999, July). Rehabilitation of concrete structures with CFRP strips glued into slits. In Proceedings of the twelfth international conference of composite materials, ICCM (Vol. 12).

Blaschko, M. (2003). Bond behaviour of CFRP strips glued into slits. Paper presented at the 6th International Symposium on FRP Reinforcement for Concrete Structures (FRPRCS-6).

Bouchikhi, A., Lousdad, A., & Megueni, A. (2010). On the reduce of interfacial shear stresses in fiber reinforced polymer plate retrofitted concrete beams. Materials & Design, 31(3), 1508-1515.

Breña, S. F., & Macri, B. M. (2004). Effect of carbon-fiber-reinforced polymer laminate configuration on the behavior of strengthened reinforced concrete beams. Journal of Composites for Construction, 8(3), 229-240.

Casadei, P., Galati, N., Boschetto, G., Tan, K.Y., Nanni, A., Galecki, G. (2006). Strengthening of impacted prestressed concrete bridge I-girder using prestressed near surface mounted C-FRP bars, in: Proceedings of 2nd International Fib Congress, Naples, Italy, (CD-ROM, paper ID 10–76).

Ceroni, F. (2010). Experimental performances of RC beams strengthened with FRP materials. Construction and Building Materials, 24(9), 1547-1559. doi: 10.1016/j.conbuildmat.2010.03.008

Ceroni, F., & Pecce, M. (2009). Design provisions for crack spacing and width in RC elements externally bonded with FRP. Composites Part B: Engineering, 40(1), 17-28.

Cevik, A. (2011). Modeling strength enhancement of FRP confined concrete cylinders using soft computing. Expert Systems with Applications, 38(5), 5662-5673.

Chaallal, O., Mofidi, A., Benmokrane, B., & Neale, K. (2011). Embedded through-section FRP rod method for shear strengthening of RC beams: Performance and comparison with existing techniques. Journal of Composites for Construction, 15(3), 374-383.

Chajes, M. J., Finch, W. W., Januszka, T. F., & Thomson, T. A. (1996). Bond and force transfer of composite material plates bonded to concrete. ACI Structural Journal, 93(2), 208-217.

Charkas, H., Rasheed, H. A., & Melhem, H. (2003). Rigorous procedure for calculating deflections of Fiber-Reinforced Polymer-Strengthened reinforced concrete beams. ACI Structural Journal, 100(4).

Chen, J., & Teng, J. (2001). Anchorage strength models for FRP and steel plates bonded to concrete. Journal of Structural Engineering, 127(7), 784-791.

Chicoine, T. (1997). Conception et analyse d'ancrages sur les poutres renforcées en flexion à l'aide de matériaux composites. Mémoire de maîtrise, Département de génie civil, Université de Sherbrooke, Canada.

Choi HT, West JS, Soudki KA. (2010). Effect of partial unbonding on prestressed near surface-mounted CFRP-strengthened concrete T-Beams. Journal of Composites for Construction,15(1):93–102.

CNR. (2006). Guide for the design and construction of concrete structures reinforced with fiber-reinforced polymer bars. CNR-DT 203/2006. Rome, Italy: Italian National Research Council (CNR).

Coelho, M.R., J.M. Sena-Cruz, and L.A. (2015). Neves, A review on the bond behavior of FRP NSM systems in concrete. Construction and Building Materials, 2015. 93: p. 1157-1169.

Committee, A. (2011). Building code requirements for structural concrete (318-11) and commentary-(318R-11). Detroit Mich. Am. Concr. Inst.

Darain, K.M. (2016). Strengthening performance of reinforced concrete beam using combined externally bonded and near surface mounted techniques. (PhD thesis), Faculty of Engineering, University of Malaya Kuala Lumpur, Malaysia

Darain, K. M., Jumaat, M. Z., Hossain, M. A., Hosen, M. A., Obaydullah, M., Huda, M. N., & Hossain, I. (2015). Automated serviceability prediction of NSM strengthened structure using a fuzzy logic expert system. Expert Systems with Applications, 42(1), 376-389.

Darain, K. M., Jumaat, M. Z., Shukri, A. A., Obaydullah, M., Huda, M. N., Hosen, M. A., & Hoque, N. (2016). Strengthening of RC Beams Using Externally Bonded Reinforcement Combined with Near-Surface Mounted Technique. Polymers, 8(7), 261.

De Lorenzis, L. (2002). Strengthening of RC structures with near surface mounted FRP rods. (PhD Thesis), University of Lecce, Italy.

De Lorenzis, L., & Nanni, A. (2001a). Characterization of FRP rods as near-surface mounted reinforcement. Journal of Composites for Construction, 5(2), 114-121.

De Lorenzis, L., & Nanni, A. (2001b). Shear strengthening of reinforced concrete beams with near-surface mounted fiber-reinforced polymer rods. ACI Structural Journal, 98(1), 60-68.

De Lorenzis, L., & Nanni, A. (2002). Bond between near-surface mounted fiber-reinforced polymer rods and concrete in structural strengthening. ACI Structural Journal, 99(2), 123-132.

De Lorenzis, L., & Teng, J. G. (2007). Near-surface mounted FRP reinforcement: An emerging technique for strengthening structures. Composites Part B: Engineering, 38(2), 119-143.

Dias, S.J.E., Barros, J.A.O., & Janwaen, W. (2018). Behavior of RC beams flexurally strengthened with NSM CFRP laminates. Composite Structures, Volume 201, 1 October 2018, Pages 363-376

Dong, J., Wang, Q. & Guan, Z. (2013).Structural behaviour of RC beams with external flexural and flexural–shear strengthening by FRP sheets. Composites Part B: Engineering, Volume 44, Issue 1, Pages 604-612

El-Hacha, R. and Soudki, K. (2013). Prestressed near-surface mounted fibre reinforced polymer reinforcement for concrete structures—a review 1. Canadian Journal of Civil Engineering, 40(11): p. 1127-1139.

El-Hacha, R., & Gaafar, M. (2011). Flexural strengthening of reinforced concrete beams using prestressed, near-surface-mounted CFRP bars. Pci Journal, 134-151.

El-Hacha, R., & Rizkalla, S. H. (2004). Near-surface-mounted fiber-reinforced polymer reinforcements for flexural strengthening of concrete structures. ACI Structural Journal, 101(5), 717-726.

El-Hacha, R., Wight, R., and Green, M. (2001). Prestressed fibre-reinforced polymer laminates for strengthening structures. Progress in Structural Engineering and Materials, 3(2): p. 111-121.

El-Maaddawy, T. & Soudki, K. (2005). Carbon-Fiber-Reinforced Polymer Repair to Extend Service Life of Corroded Reinforced Concrete Beams. Journal of Composites for Construction. Volume 9 Issue 2

El-Mihilmy, M. T., & Tedesco, J. W. (2000). Deflection of reinforced concrete beams strengthened with fiber-reinforced polymer (FRP) plates. ACI Structural Journal, 97(5).

EN, B. (2009). 12390-5:2009. Flexural Strength of Test Specimens. Testing Hardened Concrete, 1-14.

Esfahani, M.R., Kianoush, M.R., & Tajaria, A.R. (2007). Flexural behaviour of reinforced concrete beams strengthened by CFRP sheets. Engineering Structures, Volume 29, Issue 10, Pages 2428-2444

Eshwar, N., Nanni, A., & Ibell, T. J. (2008). Performance of two anchor systems of externally bonded fiber-reinforced polymer laminates. ACI Materials Journal, 105(1), 72-80.

Euro Code 2. (2004). Eurocode 2: Design of Concrete Structures: Part 1-1: General Rules and Rules for Buildings: British Standards Institution.

Fanning, P. J., & Kelly, O. (2001). Ultimate response of RC beams strengthened with CFRP plates. Journal of Composites for Construction, 5(2), 122-127.

Ferrier, E., Larbi, A. S., Georgin, J., & Ambroise, J. (2012). New hybrid cement-based composite material externally bonded to control RC beam cracking. Construction and Building Materials, 36, 36-45.

Fib. (2001). Externally bonded FRP reinforcement for RC structures Bulletin (Vol. 14, pp. 138). Switzerland: fédération internationale du béton (fib).

Frosch, R. J. (1999). Another look at cracking and crack control in reinforced concrete. ACI Structural Journal, 96, 437-442.

GangaRao, H. V. S., Vijay, P. V., & Taly, N. (2006). Frequently Asked Questions about Composite Materials *Reinforced Concrete Design with FRP Composites* (pp. 1-18): CRC Press.

Gao, D., Benmokrane, B., & Masmoudi, R. (1998). A Calculating Method for Flexural Properties of FRP-reinforced Concrete Beam: Department of Civil Engineering, Faculty of Engineering, University of Sherbrooke.

Gao, P., Gu, X., & Mosallam, A.S. (2016). Flexural behavior of preloaded reinforced concrete beams strengthened by prestressed CFRP laminates. Composite Structures, Volume 157, Pages 33-50

Garden, H., Hollaway, L., & Thorne, A. (1997). A preliminary evaluation of carbon fibre reinforced polymer plates for strengthening reinforced concrete members. Proceedings of the Institution of Civil Engineers. Structures and buildings, 122(2), 127-142.

Garden, H., Hollaway, L., & Thorne, A. (1998). The strengthening and deformation behaviour of reinforced concrete beams upgraded using prestressed composite plates. Mat. Struct. 31, 247–258

Gergely, P., & Lutz, L. A. (1973). Maximum crack width in reinforced concrete flexural members. ACI Special Publication, 20, pp. 87-117.

Godat, A., L'hady, A., Chaallal, O., & Neale, K. (2012). Bond Behavior of the ETS FRP Bar Shear-Strengthening Method. Journal of Composites for Construction, 16(5), 529-539.

Gopalaratnam, V. S., & Gettu, R. (1995). On the characterization of flexural toughness in fiber reinforced concretes. Cement and Concrete Composites, 17(3), 239-254.

Grelle, S. V., & Sneed, L. H. (2013). Review of anchorage systems for externally bonded FRP laminates. International Journal of Concrete Structures and Materials, 7(1), 17-33.

Güler, K., Demir, F., & Pakdamar, F. (2012). Stress–strain modelling of high strength concrete by fuzzy logic approach. Construction and Building Materials, 37, 680-684.

Haghani, R., Al-Emrani, M., & Kliger, R. (2008). Effect of tapering on interfacial stresses in adhesive joints without adhesive fillet. Paper presented at the Fourth International Conference on FRP Composites in Civil Engineering (CICE 2008).

Hajihashemi A, Mostofinejad D, Azhari M. Investigation of RC beams strengthened with prestressed NSM CFRP laminates. Journal of Composites for Construction, 2011;15(6):887–95.

Hassan, T. (2002). *Flexural performance and bond characteristics of FRP strengthening techniques for concrete structures.* PhD thesis, University of Manitoba, Winnipeg, Manitoba, Canada.

Hassan, T., & Rizkalla, S. (2002). Flexural strengthening of prestressed bridge slabs with FRP systems. Pci Journal, 47(1), 76-93.

Hassan, T., & Rizkalla, S. (2003). Investigation of bond in concrete structures strengthened with near surface mounted carbon fiber reinforced polymer strips. Journal of Composites for Construction.

Hassan, T. K., & Rizkalla, S. H. (2004). Bond mechanism of near-surface-mounted fiber-reinforced polymer bars for flexural strengthening of concrete structures. ACI Structural Journal, 101(6), 830-839.

Hassanen, M. A., & Raoof, M. (2001). Design against premature peeling failure of RC beams with externally bonded steel or FRP plates. Magazine of Concrete Research, 53(4), 251-262.

Hassoun, M. N. (1984). Design of reinforced concrete structures. USA: PWS Engineering.

Hawileh, R. A., Rasheed, H. A., Abdalla, J. A., & Al-Tamimi, A. K. (2014). Behavior of reinforced concrete beams strengthened with externally bonded hybrid fiber reinforced polymer systems. Materials & Design, 53, 972-982.

Hillerborg, A., Modéer, M., & Petersson, P.-E. (1976). Analysis of crack formation and crack growth in concrete by means of fracture mechanics and finite elements. Cement and concrete research, 6(6), 773-781.

Hawileh, R. A., Abdalla, J. A., Tanarslan, M. H., & Naser, M. Z. (2011). Modeling of nonlinear cyclic response of shear-deficient RC T-beams strengthened with side bonded CFRP fabric strips. Computers & Concrete, 8(3), 193-206.

Hollaway, L. (2010). A review of the present and future utilisation of FRP composites in the civil infrastructure with reference to their important in-service properties. Construction and Building Materials, 24(12), 2419-2445.

Hollaway, L. C., & Leeming, M. (1999). Strengthening of reinforced concrete structures: Using externally-bonded FRP composites in structural and civil engineering: Elsevier.

Hollaway, L. C., & Teng, J.-G. (2008). Strengthening and rehabilitation of civil infrastructures using fibre-reinforced polymer (FRP) composites: Elsevier.

Hong, S. & Sun-Kyu Park, S. (2016). Effect of prestress and transverse grooves on reinforced concrete beams prestressed with near-surface-mounted carbon fiber-reinforced polymer plates. Composites Part B 91- pp 640-650

Hosen, M. A. (2019). Effective side near surafce mounting techniques for strengthening of reinforced concrete beams. . (PhD thesis), Faculty of Engineering, University of Malaya Kuala Lumpur, Malaysia

Hosen, M. A., Jumaat, M. Z., Alengaram, U. J., Islam, A., & bin Hashim, H. (2016). Near Surface Mounted Composites for Flexural Strengthening of Reinforced Concrete Beams. Polymers, 8(3), 67.

Hosen, M. A., Jumaat, M. Z., Darain, K. M. U., Obaydullah, M., & Islam, A. S. (2014). *Flexural Strengthening of RC Beams with NSM Steel Bars*. Paper presented at the IICBE International Conference, Kuala Lumpur, Malaysia. www.iicbe.org

Hosen, M. A., Jumaat, M. Z., & Islam, A. (2015). Inclusion of CFRP-Epoxy Composite for End Anchorage in NSM-Epoxy Strengthened Beams. Advances in Materials Science and Engineering, 2015.

Hossain, A., Rahman, A., & Mohiuddin, A. (2012). Fuzzy evaluation for an intelligent air-cushion tracked vehicle performance investigation. Journal of Terramechanics, 49(2), 73-80.

Hu, H.-T., Lin, F.-M., & Jan, Y.-Y. (2004). Nonlinear finite element analysis of reinforced concrete beams strengthened by fiber-reinforced plastics. Composite Structures, 63(3), 271-281.

Irani, Z., & Kamal, M. M. (2014). Intelligent systems research in the construction industry. Expert Systems with Applications, 41(4), 934-950.

Jalali, M., Sharbatdar, M. K., Chen, J.-F., & Alaee, F. J. (2012). Shear strengthening of RC beams using innovative manually made NSM FRP bars. Construction and Building Materials, 36, 990-1000.

Jeong, S.-M. (1994). Evaluation of ductility in prestressed concrete beams using fiber reinforced plastic tendons: University of Michigan.

Jung, W., Park, J., Kang, J. & Park, Y. (2017). Flexural Behaviour of RC Beams Strengthened with Prestressed CFRP NSM Tendon Using New Prestressing System. International Journal of Polymer Science. Volume 2017 |Article ID 1497349

Jung, W. T., Park, Y. H., Park, J. S., Kang, J. Y., & You, Y. J. (2005). Experimental investigation on flexural behavior of RC beams strengthened by NSM CFRP reinforcements. in Proceedings of the 7th International Symposium on Fiber Reinforced Polymer Reinforcement for Reinforced Concrete Structures (FRPRCS-7). 2005.

Kalayci, A. S., Yalim, B., & Mirmiran, A. (2010). Construction tolerances and design parameters for NSM FRP reinforcement in concrete beams. Construction and Building Materials, 24(10), 1821-1829. doi: 10.1016/j.conbuildmat.2010.04.022

Kalfat, R., Al-Mahaidi, R., & Smith, S. T. (2011). Anchorage devices used to improve the performance of reinforced concrete beams retrofitted with FRP composites: State-of-the-art review. Journal of Composites for Construction, 17(1), 14-33.

Kaur, A., & Kaur, A. (2012). Comparison of Mamdani-Type and Sugeno-Type Fuzzy Inference System for Air Conditioning System. International Journal of Soft Computing and Engineering, 2(2), 2231-2307.

Kim, Y. J., Shi, C., & Green, M. F. (2008). Ductility and cracking behavior of prestressed concrete beams strengthened with prestressed CFRP sheets. Journal of composites for construction, 12(3), 274-283.

Kishi, N., Mikami, H., Kurihashi, Y., & Sawada, S. (2005, December). Flexural behaviour of RC beams reinforced with NSM AFRP rods. In Proceedings of the International Symposium on Bond Behaviour of FRP in structures (BBFS 2005) (pp. 337-342).

Klaiber, F.W., Wipf, T.J. & Kempers, B.J. (2003). Repair of Damaged Prestressed Concrete Bridges Using CFRP. Proceedings of the 2003 Mid-Continent Transportation Research Symposium, Ames, Iowa, August 2003. © 2003 by Iowa State University, USA.

Kotynia, R. (2012). Bond between FRP and concrete in reinforced concrete beams strengthened with near surface mounted and externally bonded reinforcement. Construction and Building Materials, 32, 41-54.

Kotynia, R., Abdel Baky, H., Neale, K. W., & Ebead, U. A. (2008). Flexural strengthening of RC beams with externally bonded CFRP systems: Test results and 3D nonlinear FE analysis. Journal of Composites for Construction, 12(2), 190-201.

Kupfer, H., Hilsdorf, H. K., & Rusch, H. (1969). Behavior of concrete under biaxial stresses. Paper presented at the ACI Journal proceedings.

Larson, K.H., Peterman, R.J. & Rasheed H.A. (2005). Strength-Fatigue Behavior of Fiber Reinforced Polymer Strengthened Prestressed Concrete T-Beams. ASCE. Journal of Composites for Construction, Volume 9 Issue 4 - August 2005.

Lee, H.Y., Jung, W.T. & Chung, W.J.C.S. (2017). Flexural strengthening of reinforced concrete beams with pre-stressed near surface mounted CFRP systems. 163: p. 1-12.

Leung, C.K., & Tung, W.K. (2006). Three-Parameter Model for Debonding of FRP Plate from Concrete Substrate. Journal of Engineering Mechanics, Volume 132 Issue 5.

Lim, D. H. (2009). Combinations of NSM and EB CFRP strips for flexural strengthening of concrete structures. Magazine of Concrete Research, 61(8), 633-643. doi: 10.1680/macr.2008.61.8.633

Lim, D. H. (2010). Shear behaviour of RC beams strengthened with NSM and EB CFRP strips. Magazine of Concrete Research, 62(3), 211-220. doi: 10.1680/macr.2010.62.3.211

Lousdad, A., Megueni, A., & Bouchikhi, A. (2010). Geometric edge shape based optimization for interfacial shear stress reduction in fiber reinforced polymer plate retrofitted concrete beams. Computational Materials Science, 47(4), 911-918.

Lu, X., Teng, J., Ye, L., & Jiang, J. (2007). Intermediate crack debonding in FRP-strengthened RC beams: FE analysis and strength model. Journal of Composites for Construction, 11(2), 161-174.

Maalej, M., & Bian, Y. (2001). Interfacial shear stress concentration in FRP-strengthened beams. Composite Structures, 54(4), 417-426.

Maruyama, K., & Ueda, T. (2001). JSCE design recommendations for upgrading of RC members by FRP sheet. Proc. FRPRCS-5—Fibre-Reinforced Plastics for Reinforced Concrete Structures, 441-446.

Mathew, M. J., & Prabhakaran, P. (2018). Combined EBR and NSMR for Flexural Strengthening of RC beam. International Research Journal of Engineering and Technology (IRJET). Volume: 05 Issue: 04; p-ISSN: 2395-0072

Meier, U., & Kaiser, H. (1991). Strengthening of structures with CFRP laminates. Paper presented at the Advanced composites materials in civil engineering structures.

Mohamed Ali, M. S., Oehlers, D. J., & Seracino, R. (2006). Vertical shear interaction model between external FRP transverse plates and internal steel stirrups. Engineering Structures, 28(3), 381-389. doi: http://dx.doi.org/10.1016/j.engstruct.2005.08.010

Mohammadhassani, M., Jumaat, M. Z., Jameel, M., Badiee, H., & Arumugam, A. M. (2012). Ductility and performance assessment of high strength self compacting concrete (HSSCC) deep beams: An experimental investigation. Nuclear Engineering and Design, 250, 116-124.

Morais, M., & Burgoyne, C. (2001, September). Energy dissipation in sections prestressed with FRP tendons. In Proceedings of the composite in construction International conference CCC 2001 (pp. 421-426). Balkema/Lisse The Netherlands.

Mostofinejad, D., & Shameli, S. M. (2013). Externally bonded reinforcement in grooves (EBRIG) technique to postpone debonding of FRP sheets in strengthened concrete beams. Construction and Building Materials, 38, 751-758.

Motavalli, M., & Czaderski, C. (2007). FRP composites for retrofitting of existing civil structures in Europe: state-of-the-art review. Paper presented at the International Conference of Composites & Polycon., American Composites Manufacturers Association. Tampa, FL, USA.

Muhamad, R., Mohamed Ali, M., Oehlers, D., & Griffith, M. (2010). The tension stiffening mechanism in reinforced concrete prisms. Int J Adv Struct Eng, submitted for publication.

Nardone, F., Lignola, G. P., Prota, A., Manfredi, G., & Nanni, A. (2011). Modeling of flexural behavior of RC beams strengthened with mechanically fastened FRP strips. Composite Structures, 93(8), 1973-1985.

Nasrollahzadeh, K., & Basiri, M. M. (2014). Prediction of shear strength of FRP reinforced concrete beams using fuzzy inference system. Expert Systems with Applications, 41(4), 1006-1020.

Nawy, E.G. (2005). Reinforced Concrete a Fundamental Approach, Prentice Hall, New Jersey, United States.

Nayak, A.N., Kumari, A., & Swain, R.B. (2018). Strengthening of RC Beams Using Externally Bonded Fibre Reinforced Polymer Composites. Structures, Volume 14, Pages 137-152

Nilson, A. H. (1982). State-of-the-art report on finite element analysis of reinforced concrete. New York, NY: American Society of Civil Engineers: Task Committee on Finite Element Analysis of Reinforced Concrete Structures of the Structural Division Committee on Concrete and Masonry Structures, ASCE.

Nordin, H., & Täljsten, B. (2006). Concrete beams strengthened with prestressed near surface mounted CFRP. Journal of Composites for Construction, 10(1), 60-68.

Obaidat, Y. (2011). Structural retrofitting of concrete beams using FRP-debonding issues. Lund University.

Obaydullah M., Jumaat M. Z., Alengaram U. J., ud Darain K. H., Huda M. N., Hosen M. A. (2016) Prestressing of NSM steel strands to enhance the structural performance of prestressed concrete beams. Construction and Building Materials 2016;129:289–301.

Oehlers, D. J. (1992). Reinforced concrete beams with plates glued to their soffits. Journal of Structural Engineering, 118(8), 2023-2038.

Oehlers, D. J., Mohamed Ali, M., Haskett, M., Lucas, W., Muhamad, R., & Visintin, P. (2010). FRP-Reinforced concrete beams: unified approach based on IC theory. Journal of Composites for Construction, 15(3), 293-303.

Oller, E., Cobo, D., & Mari, A. (2011). Laminate debonding process of FRP-strengthened beams. Structure and Infrastructure Engineering, 7(1-2), 131-146.

Oudah F. and El-Hacha R. Analytical fatigue prediction model of RC beams strengthened in flexure using prestressed FRP reinforcement. Eng Struct 2013;46:173–83

Oudah, F., & El-Hacha, R. (2012). A new ductility model of reinforced concrete beams strengthened using Fiber Reinforced Polymer reinforcement. Composites Part B-Engineering, 43(8), 3338-3347. doi: 10.1016/j.compositesb.2012.01.071

Oudah, F., & El-Hacha, R. (2012). A new ductility model of reinforced concrete beams strengthened using Fiber Reinforced Polymer reinforcement. Composites Part B: Engineering, 43(8), 3338-3347. doi: 10.1016/j.compositesb.2012.01.071

Pantelides, C.P., Reaveley, L.D. & Burningham C.A. (2010). Repair of prestressed concrete girder ends and girder collision repair. Transportation research board (TRB). http://www.udot.utah.gov/main/uconowner.gf?n=13262517291499267

Parretti, R., & Nanni, A. (2004). Strengthening of RC members using near-surface mounted FRP composites: Design overview. Advances in Structural Engineering, 7(6), 469-483. doi: 10.1260/1369433042863198

Patel J.R., Patel M.R., Tank T.G., Vasanwala S.A., Modhera C.D. (2019) Flexural Strengthening of RC Beams Using NSM Technique. Advances in Intelligent Systems and Computing, vol 757. Springer, Singapore

Peng, H., Zhang, J., & Cai, C.S. (2014). An-experimental-study-on-reinforced-concrete-beams-strengthened-with-prestressed-near-surface-mounted-CFRP-strips. Engineering Structures, 2014; 79:222-233

Quantrill, R.J., & Hollaway, L.C. (1998). The flexural rehabilitation of reinforced concrete beams by the use of prestressed advanced composite plates. Composites Science and Technology, Volume 58, Issue 8, Pages 1259-1275

Rahal, K. N., & Rumaih, H. A. (2011). Tests on reinforced concrete beams strengthened in shear using near surface mounted CFRP and steel bars. Engineering Structures, 33(1), 53-62. doi: 10.1016/j.engstruct.2010.09.017

Rahimi, H., & Hutchinson, A. (2001). Concrete beams strengthened with externally bonded FRP plates. Journal of Composites for Construction, 5(1), 44-56.

Rahman, M. M. (2016). Hybridization and optimization of structural strengthening system. (PhD thesis), Faculty of Engineering 2016, University of Malaya Kuala Lumpur, Malaysia

Rahman, M. M., Jumaat, M. Z., Rahman, M. A., & Qeshta, I. M. (2015). Innovative hybrid bonding method for strengthening reinforced concrete beam in flexure. Construction and Building Materials, 79, 370-378.

Rasheed, H. A., Harrison, R. R., Peterman, R. J., & Alkhrdaji, T. (2010). Ductile strengthening using externally bonded and near surface mounted composite systems. Composite Structures, 92(10), 2379-2390. doi: 10.1016/j.compstruct.2010.03.009

Razaqpur, A. G., Shedid, M., & Petrina, D. (2011). Behavior of beams strengthened with novel self-anchored near-surface-mounted CFRP bars. Journal of Composites for Construction, 15(4), 625-634. doi: 10.1061/(ASCE)CC.1943-5614.0000183

Rezazadeh, M., Costa, I. & Barros, J.J.C.S. (2014). Influence of prestress level on NSM CFRP laminates for the flexural strengthening of RC beams. Composite Structures. 116: p. 489-500.

Reed, M. W., Barnes, R. W., Schindler, A. K., & Lee, H.-W. (2005). Fiber-reinforced polymer strengthening of concrete bridges that remain open to traffic. ACI Structural Journal, 102(6), 823.

Reza Aram, M., Czaderski, C., & Motavalli, M. (2008). Effects of gradually anchored prestressed CFRP strips bonded on prestressed concrete beams. Journal of Composites for Construction, 12(1), 25-34.

Ritchie, P. A., Thomas, D. A., Lu, L.-W., & Conelly, G. M. (1991). External reinforcement of concrete beams using fiber reinforced plastics. ACI Structural Journal, 88(4).

Ritchie, P. A., Thomas, D. A., Lu, L.-W., & Connelly, G. M. (1990). External reinforcement of concrete beams using fiber-reinforced plastics.

Rizkalla, S., & Hassan, T. (2001). Various FRP strengthening techniques for retrofitting concrete structures. Paper presented at the CICE 2001 Conference proceedings.

Rosenboom, O., & Rizkalla, S. (2006). Behavior of prestressed concrete strengthened with various CFRP systems subjected to fatigue loading. Journal of Composites for Construction, 10(6), 492-502.

Saxena, P., Toutanji, H., & Noumowe, A. (2008). Failure analysis of FRP-strengthened RC beams. Journal of Composites for Construction, 12(1), 2-14.

Sena-Cruz, J. (2005). Strengthening of concrete structures with near-surface mounted CFRP laminate strips.

Sena-Cruz, J., & Barros, J. A. (2004). Modeling of bond between near-surface mounted CFRP laminate strips and concrete.

Sena-Cruz, J. M., Barros, J. A. O., Coelho, M. R. F., & Silva, L. F. F. T. (2012). Efficiency of different techniques in flexural strengthening of RC beams under monotonic and fatigue loading. Construction and Building Materials, 29, 175-182. doi: 10.1016/j.conbuildmat.2011.10.044

Shang, S., Zou, P. X., Peng, H., & Wang, H. (2005, December). Avoiding de-bonding in FRP strengthened reinforced concrete beams using prestressing techniques. In Proceedings of the international symposium on Bond behaviour of FRP in structures (BBFS). Hong Kong, China (pp. 321-28).

Sharaky, I., L. Torres, and H. Sallam,. (2015). Experimental and analytical investigation into the flexural performance of RC beams with partially and fully bonded NSM FRP bars/strips. Composite Structures, 2015. 122: p. 113-126.

Sharaky, I. A., Torres, L., Baena, M., & Vilanova, I. (2013). Effect of different material and construction details on the bond behaviour of NSM FRP bars in concrete. Construction and Building Materials, 38, 890-902. doi: 10.1016/j.conbuildmat.2012.09.015

Shehata, I., Cerqueira, E., Pinto, C., & Shehata, L. (2001). Strengthening of RC beams in flexure and shear using CFRP laminate. Thomas Tetford London, 97-106.

Sikadur®-30. Product Data Sheet-Adhesive for bonding reinforcement. Retrieved May 21, 2016, from: <https://mys.sika.com/dms/...get/...e6dc.../Sikadur-30%202011-10_1.pdf>.

Singh, S.B., Reddy, A.L., & Khatri, C.P. (2014). Experimental and Parametric Investigation of Response of NSM CFRP-Strengthened RC Beams. Journal of Composites for Construction, Volume 18 Issue 1.

Smith, S. T., & Teng, J. (2002a). FRP-strengthened RC beams. I: review of debonding strength models. Engineering Structures, 24(4), 385-395.

Smith, S. T., & Teng, J. (2002b). FRP-strengthened RC beams. II: assessment of debonding strength models. Engineering Structures, 24(4), 397-417.

Soliman, S. M., El-Salakawy, E., & Benmokrane, B. (2010). Flexural behaviour of concrete beams strengthened with near surface mounted fibre reinforced polymer bars. Canadian Journal of Civil Engineering, 37(10), 1371-1382.

Spadea, G., Bencardino, F., & Swamy, R. (2015). Structural effectiveness of FRP materials in strengthening RC beams. Engineering Structures, Volume 99, Pages 631-641

Spadea, G., Bencardino, F., & Swamy, R. (1998). Structural behavior of composite RC beams with externally bonded CFRP. Journal of Composites for Construction, 2(3), 132-137.

Sun, Z., Wu, G., Wu, Z., & Luo, Y. (2011). Flexural strengthening of concrete beams with near-surface mounted steel-fiber-reinforced polymer composite bars. Journal of Reinforced Plastics and Composites, 0731684411427209.

Swamy, R., Jones, R., & Bloxham, J. (1987). Structural behaviour of reinforced concrete beams strengthened by epoxy-bonded steel plates. Structural Engineer. Part A, 65, 59-68.

Täljsten, B., Carolin, A., & Nordin, H. (2003). Concrete Structures Strengthened with near Surface Mounted Reinforcement of CFRP. Advances in Structural Engineering. Vol 6, Issue 3.

Tanarslan, H.M., Alver, N., Jahangiri, R. (2017). Flexural strengthening of RC beams using UHPFRC laminates: Bonding techniques and rebar addition. Construction and Building Materials, Volume 155, Pages 45-55

Tehrani, B.N., Mostofinejad, D. & Hosseini, A.M. (2019). Experimental and analytical study on flexural strengthening of RC beams via prestressed EBROG CFRP plates. Engineering Structures, Volume 197, 109395

Teng, J., De Lorenzis, L., Wang, B., Li, R., Wong, T., & Lam, L. (2006). Debonding failures of RC beams strengthened with near surface mounted CFRP strips. Journal of Composites for Construction, 10(2), 92-105.

Teng, J., Smith, S. T., Yao, J., & Chen, J. (2003). Intermediate crack-induced debonding in RC beams and slabs. Construction and Building Materials, 17(6), 447-462.

Thomsen, H., Spacone, E., Limkatanyu, S., & Camata, G. (2004). Failure mode analyses of reinforced concrete beams strengthened in flexure with externally bonded fiber-reinforced polymers. Journal of Composites for Construction, 8(2), 123-131.

Toutanji, H., Zhao, L., & Zhang, Y. (2006). Flexural behavior of reinforced concrete beams externally strengthened with CFRP sheets bonded with an inorganic matrix. Engineering Structures, 28(4), 557-566.

Traplsi, A. M. (2013). Combined NSM bars and externally bonded GFRP in strengthening T-beams. (PhD Thesis). College of Engineering, Al-Mergab University, Al-khoms, Libya

Triantafyllou, G.G., Rousakis, T.C., & Karabinis, A.I. (2018). Effect of patch repair and strengthening with EBR and NSM CFRP laminates for RC beams with low, medium and heavy corrosion. Composites Part B: Engineering, Volume 133, Pages 101-111

Triantafillou, T. C. & Deskovic, N. (1991). Innovative prestressing with FRP sheets: mechanics of short-term behavior. Journal of Engineering Mechanics,Volume 117 Issue 7

Triantafillou, T. C. (1998). Shear strengthening of reinforced concrete beams using epoxy-bonded FRP composites. ACI Structural Journal, 95(2).

Triantafillou, T. C., & Plevris, N. (1992). Strengthening of RC beams with epoxy-bonded fibre-composite materials. Materials and Structures, 25(4), 201-211.

Tsai, M., & Morton, J. (1995). The effect of a spew fillet on adhesive stress distributions in laminated composite single-lap joints. Composite Structures, 32(1), 123-131.

Ulaga, T., Vogel, T., & Meier, U. (2003). Bilinear stress-slip bond model: theoretical background and significance. FRPRCS-6-Fibre-reinforced polymer reinforcement for concrete structures.

Van Gemert, D. (1980). Force transfer in epoxy bonded steel/concrete joints. International Journal of Adhesion and Adhesives, 1(2), 67-72.

Wahab, N., Soudki, K. A., & Topper, T. (2010). Mechanism of bond behavior of concrete beams strengthened with near-surface-mounted CFRP rods. Journal of Composites for Construction, 15(1), 85-92.

Wang, C., & Salmon, C. (1992). Reinforced concrete design, 5, 1992: Harper and Row, New York.

Wight, R., Green, M., & Erki, M. (2001). Prestressed FRP sheets for poststrengthening reinforced concrete beams. Journal of Composites for Construction, 5(4), 214-220.

Wu, G., Wu, Z.-S., Luo, Y.-B., Sun, Z.-Y., & Hu, X.-Q. (2010). Mechanical properties of steel-FRP composite bar under uniaxial and cyclic tensile loads. Journal of Materials in Civil Engineering, 22(10), 1056-1066.

Yost, J. R., Gross, S. P., Dinehart, D. W., & Mildenberg, J. J. (2007). Flexural behavior of concrete beams strengthened with near-surface-mounted CFRP strips. ACI Structural Journal, 104(4).

Yost, J. R., Gross, S. P., Dinehart, D. W., & Mildenberg, J. J. (2007). Flexural behavior of concrete becams strengthened with near-surface-mounted CFRP strips. ACI Structural Journal, 104(4), 430-437.

Zhang, S. S., & Teng, J. G. (2013). Interaction forces in RC beams strengthened with near-surface mounted rectangular bars and strips. Composites Part B: Engineering, 45(1), 697-709.

Zhang C., Zhang M. and Ding Y. (2011). Experiment on the deformation of the reinforced concrete beam NSM prestressed steel spiral ribs. Applied Mechanics and Materials, Vols 94-96, pp 1278-1285

Ziraba, Y., Baluch, M., Basunbul, I., Sharif, A., Azad, A., & Al-Sulaimani, G. (1994). Guidelines toward the design of reinforced concrete (RC) beams with external plates. Structural Journal, 91(6), 639-646.